



## **Deliverable D2.5: Experiments and numerical model studies on interfaces**

Work Package [ACED](#)

The project leading to this application has received funding from the European Union's Horizon 2020 research and innovation programme under grant agreement No 847593.



## Document information

Project Acronym	<b>EURAD</b>
Project Title	<b>European Joint Programme on Radioactive Waste Management</b>
Project Type	<b>European Joint Programme (EJP)</b>
EC grant agreement No.	<b>847593</b>
Project starting / end date	<b>1<sup>st</sup> June 2019 – 30 May 2024</b>
Work Package No.	<b>2</b>
Work Package Title	<b>Assessment of Chemical Evolution of ILW and HLW Disposal Cells</b>
Work Package Acronym	<b>ACED</b>
Deliverable No.	<b>D2.5</b>
Deliverable Title	<b>Experiments and numerical model studies on interfaces</b>
Lead Beneficiary	<b>FZJ</b>
Contractual Delivery Date	<b>M5</b>
Actual Delivery Date	<b>12/05/2021</b>
Type	<b>Report</b>
Dissemination level	<b>PU</b>
Authors	<b>Guido Deissmann (FZJ), Naila Ait Mouheb (FZJ), Christelle Martin (Andra), Maria J. Turrero (CIEMAT), Elena Torres (CIEMAT), Bruno Kursten (SCK CEN), Eef Weetjens (SCK CEN), Diederik Jacques (SCK CEN), Jaime Cuevas (UAM), Javier Samper (UDC), Luis Montenegro (UDC), Markku Leivo (VTT), Mervi Somervuori (VTT), Leena Carpen (VTT)</b>

### To be cited as:

Deissmann G., Ait Mouheb N., Martin C., Turrero, M.J., Torres, E., Kursten, B., Weetjens, E., Jacques, D., Cuevas, J., Samper, J., Montenegro, L., Leivo, M., Somervuori, M., Carpen, L. (2021): Experiments and numerical model studies on interfaces. Final version as of 12.05.2021 of deliverable D2.5 of the HORIZON 2020 project EURAD. EC Grant agreement no: 847593.

### Disclaimer

All information in this document is provided "as is" and no guarantee or warranty is given that the information is fit for any particular purpose. The user, therefore, uses the information at its sole risk and liability. For the avoidance of all doubts, the European Commission has no liability in respect of this document, which is merely representing the authors' view.

### Acknowledgement

This document is a deliverable of the European Joint Programme on Radioactive Waste Management (EURAD). EURAD has received funding from the European Union's Horizon 2020 research and innovation programme under grant agreement No 847593.

Status of deliverable		
	By	Date
Delivered (Lead Beneficiary)	G. Deissmann (FZJ)	2021-04-01
Verified and reviewed (WP Leader)	D. Jacques (SCK CEN)	2021-05-11
Approved (PMO)	L. Théodon (Andra)	2021-05-11
Submitted to EC (Coordinator)	Andra	2021-05-12

## Executive Summary

The main objective of the EURAD work package (WP) ACED (Assessment of Chemical Evolution of ILW and HLW Disposal Cells) is to improve methodologies to obtain multi-scale quantitative models for the description of the chemical evolution at the disposal cell scale and to derive robust mathematical models including the most relevant processes. The WP seeks to compile and integrate the process level knowledge and description of reactivity at the interfaces between materials relevant for ILW and HLW disposal cells and evaluates how process level knowledge can be incorporated in models describing chemical evolution between waste forms (e.g. glass or cemented waste) and the near field materials to assess the evolution of the buffer, container and waste matrix accounting for transport of reactive species and/or other drivers for geochemical alterations. During repository evolution, a significant chemical/geochemical evolution of near field interfaces will occur due to steep chemical gradients, and, for HLW disposal cells, thermal gradients in the first hundreds to thousand years.

Within ACED, we start from the knowledge available at the scale of interfaces between two materials in order to build models for assessing the chemical evolution at the cell disposal scale. This deliverable describes the existing knowledge on the relevant processes and transients occurring at the interfaces between materials, focussing on materials combinations relevant for the chemical evolution ILW and HLW disposal cells in European repository concepts. It addresses the following interfaces as basis for the work to be performed in ACED tasks 2 to 4:

- glass-steel,
- cement/mortar-granite,
- cement/concrete-clay,
- steel/iron-bentonite,
- steel/iron-cement/concrete, and
- steel/iron-granite.

This deliverable provides a structured overview on i) existing (experimental) data on relevant processes occurring at the interfaces, ii) information on natural/archaeological/industrial analogues that provide insight/data for long-term processes relevant to the chemical evolution at the interfaces not accessible in short-term (laboratory) experiments, and iii) conceptual and mathematical models used to describe the processes occurring at the different interfaces. This information forms the basis for conceptualisation of the chemical evolution at these interfaces in the ACED tasks 2 to 4 and will be used to support model validation and parametrisation of models.

## Table of content

Executive Summary.....	4
Table of content.....	5
List of Figures.....	7
List of Tables.....	11
Abbreviations.....	12
1. Introduction.....	14
1.1 Aims and scope.....	14
1.2 Structure of the report.....	15
1.3 References.....	15
2. Interface "glass – steel".....	16
2.1 Processes at the interface.....	16
2.2 Evidence from experiments and analogues.....	18
2.2.1 Nature of the iron/steel corrosion products.....	18
2.2.2 Studies of glass/iron (or CPs) interactions: experimental approach.....	19
2.2.3 Glass alteration in the presence of iron or corrosion products.....	20
2.2.4 Mechanisms.....	26
2.3 Application of conceptual and mathematical models.....	36
2.3.1 Sorption models.....	36
2.3.2 Precipitation of iron silicates.....	38
2.4 Resume.....	39
2.5 References.....	40
3. Interface "cement/mortar – granite".....	45
3.1 Processes at the interface.....	45
3.1.1 Concrete.....	45
3.1.2 Granite.....	47
3.2 Evidence from experiments and analogues.....	48
3.2.1 Concrete.....	48
3.2.2 Granite.....	50
3.3 Application of conceptual and mathematical models.....	52
3.3.1 Concrete.....	52
3.3.2 Granite.....	54
3.4 Resume.....	54
3.5 References.....	55
4. Interface "cement/concrete – clay".....	58

4.1	Processes at the interface .....	58
4.2	Evidence from experiments and analogues .....	60
4.3	Application of conceptual and mathematical models .....	66
4.4	Resume .....	71
4.5	References .....	71
5.	Interface "steel/iron – bentonite" .....	80
5.1	Processes at the interface .....	80
5.2	Evidence from experiments and analogues .....	82
5.2.1	Laboratory experiments .....	83
5.2.2	Mock-up and field scale experiments .....	96
5.2.3	Natural/Archaeological/Industrial analogues .....	101
5.3	Application of conceptual and mathematical models .....	105
5.4	Resume .....	112
5.5	References .....	113
6.	Interface "steel/iron – cement/concrete" .....	126
6.1	Processes at the interface .....	126
6.1.1	Description .....	126
6.1.2	Factors influencing the corrosion rate in a cementitious environment .....	128
6.1.3	Consequence of corrosion on concrete properties .....	139
6.2	Evidence from experiments and analogues .....	140
6.2.1	Experiments .....	140
6.2.2	Analogues .....	142
6.3	Application of conceptual and mathematical models .....	142
6.4	Resume .....	145
6.5	References .....	145
7.	Interface "steel/iron – granite" .....	152
7.1	Processes at the interface .....	152
7.2	Evidence from experiments and analogues .....	152
7.3	Application of conceptual and mathematical models .....	157
7.4	Resume .....	157
7.5	References .....	157
8.	Concluding remarks .....	160

## List of Figures

Figure 2-1 – Stages of nuclear glass corrosion and related potential rate-limiting mechanisms (Gin et al., 2013).....	16
Figure 2-2 – Diagram showing a glass package in its environment following disposal container failure. ....	17
Figure 2-3 – Photographs of the machined brick of argillite, the glass/iron mock-up, and the three specimens inserted in the brick: the glass/iron mock-up studied by Schlegel et al. (2016) in the centre, the gold specimen at the top, and the Armco iron specimen studied by Schlegel et al. (2014) at the bottom.....	20
Figure 2-4 – Example of reactors used by Rébiscoul et al. (2015) for leaching tests in set-up: i) homogeneous system and ii) systems in which glass and magnetite are kept physically separated... 21	
Figure 2-5 – Evolution of normalized mass losses of boron during the alteration of SON68 glass powder (63-125 $\mu\text{m}$ ) in COx water (at 50°C, S/V = 74 $\text{cm}^{-1}$ ) in configuration i) (absence of magnetite (G), presence of 10 g (GM1) or 20 g (GM2) magnetite) and in configuration ii) (presence of 10 g magnetite physically separated from glass powder (GSM1)) (Rébiscoul et al., 2015). ....	21
Figure 2-6 – Evolution of pH and Si concentration ( $\text{mg L}^{-1}$ ) during the alteration of SON68 glass powder (63-125 $\mu\text{m}$ ) in in COx water (at 50°C, S/V = 74 $\text{cm}^{-1}$ ) in the different experiments G, GM1, GM2 and GSM1 (see Figure 2-5, Rébiscoul et al., 2015). ....	22
Figure 2-7 – Evolution of normalized lithium mass losses NL(Li) during different experiments in which claystone, glass, magnetite or iron powder or a drilled iron sheet are stacked in successive layers (left diagram). (CEA data partially published in Burger et al., 2013). ....	22
Figure 2-8 – SEM/ TEM images and elemental maps of cross-sections of glass grains located in different zones (Zone 1: directly above the iron sheet; Zone 2: in a notch on the iron sheet, partly filled with iron beads) (Burger et al., 2013). ....	23
Figure 2-9 – Variability in the thickness (minimal, maximal and average) of altered glass measured through the length of a modelled crack from analysis of SEM-FEG images: empty (blue); containing siderite (purple); containing iron (red). Comparison with the thickness of glass altered as per the initial rate regime (green) (Michelin et al., 2013a). Note: bearing in mind the extreme variability in the thickness of glass altered in the presence of iron, the average thickness is not shown. ....	24
Figure 2-10 – Analysis of altered glass thickness in cracks in blast-furnace slag (Michelin et al., 2015). ....	24
Figure 2-11 – Thickness of alteration layer measured on one side of the crack after around 6 months of alteration at 50°C in COx water: empty (E), containing synthetic corrosion products (SCP), archaeological corrosion products (ACP) and an iron sheet (IS) (Dillmann et al., 2016). ....	25
Figure 2-12 – SEM photographs of the glass/argillite and glass/iron interfaces of the ArCorr 2008 set-up. Top: overview of each of the interfaces made up of SEM photographs; bottom: detailed images of the glass/argillite interface (left) and the glass/iron interface (right) (Schlegel et al., 2015). ....	26
Figure 2-13 – Sorption of silicon on goethite, magnetite and siderite as a function of pH at 20 °C (Philippini et al., 2006). ....	28
Figure 2-14 – TEM observations of the centre of the crack formed by two samples of synthetic archaeological glass and initially containing an iron sheet, after 20 months of alteration (at 50 °C, in clayey water from the Glinet site) (Michelin et al., 2013a). ....	29
Figure 2-15 – Elemental distribution maps (Si, Fe, O) on a FIB section sampled from the centre of the crack formed by two samples of SON68 glass and initially containing a sheet of iron, after 6 months of	

alteration (at 50 °C, groundwater). STXM spectra at the Si edge (green) and Fe edge (blue) characteristic of iron silicates formed near corrosion products (Dillmann et al., 2016)..... 31

Figure 2-16 – Top: High-resolution SEM observations of the alteration layer on an <sup>29</sup>Si- and <sup>57</sup>Fe-doped SON68 glass monolith altered for 31 months at 50 °C in an argillite core sample saturated with CO<sub>x</sub> water in the presence of a foil of corroded iron sampled from an archaeological nail from the Glinet site. Bottom: FIB foil and high-resolution SEM observations of corrosion products formed at the surface of an iron foil opposite a SON68 glass sample composing a stack of 4 steel plates of different grades and of glass altered in a reactor at 90 °C, under anoxic conditions, in synthesised CO<sub>x</sub> water for approx. 2.5 years (Carrière, 2017). ..... 32

Figure 2-17 – Evolution of mass losses for different alteration solutions in the presence and absence of iron (McVay and Buckwalter, 1983). ..... 33

Figure 2-18 – Electron Diffraction Spectrum on nano-crystals formed inside the gel during alteration of a crack formed by two samples of SON68 glass and initially containing a sheet of iron, after 6 months of alteration (at 50 °C, groundwater) (Dillmann et al., 2016)..... 34

Figure 2-19 – SEM observations of a FIB foil sampled from the surface of grains of glass altered in contact with an iron powder at 50 °C by the CO<sub>x</sub> water in a vertical borehole at the Bure underground research laboratory (MVE in-situ "transient phase" test) for ~24 months (CEA Data)..... 34

Figure 2-20 – SEM and TEM observations of blast-furnace slag: network of cracks and cavities filled with corrosion products (left); corrosion facies in a crack (right) (Michelin, 2011) ..... 35

Figure 2-21 – Optical microscope image and elemental distribution maps of iron and deuterium on a cross-section of blast-furnace slag block after being immersed in D<sub>2</sub>O for one week (Michelin et al., 2015)..... 35

Figure 2-22 – Comparison of the evolution of experimental and simulated boron concentrations by taking into account the sorption of Si on magnetite and the precipitation of magnesium silicates during alteration of SON68 glass powder in the presence of magnetite in CO<sub>x</sub> water at 50 °C (Case 1: 10 g of magnetite, Case 2: 20 g of magnetite). All this is compared to glass alteration in CO<sub>x</sub> water, only..... 38

Figure 2-23 – Comparison of the evolution of experimental and simulated concentrations of boron by taking into account Si sorption on magnetite and the precipitation of an iron silicate (nontronite Na<sub>0.33</sub>Fe<sub>2</sub>(Si<sub>3.67</sub>Al<sub>0.33</sub>)OH<sub>14.68</sub>, Si/Fe = 1.835) during alteration of a glass powder in the presence of magnetite in CO<sub>x</sub> water at 50 °C (Case 1: 10 g of magnetite, Case 2: 20 g of magnetite). All this is compared to glass alteration in CO<sub>x</sub> water, only (Godon et al., 2013). ..... 39

Figure 3-1 – Generic “zones” formed in cementitious materials through ingress of sulphate ions (Alexander et al., 2013). ..... 46

Figure 3-2 – Schematic evolution of pore solution pH during leaching of Portland cement-based materials by pure water (Berner, 1992; Snelman and Vieno, 2005; Cau Dit Coumes et.al., 2006)..... 47

Figure 3-3 – Strength development during 12.5 years of monitoring. .... 49

Figure 3-4 – Chloride profiles for all concretes in solution L5. .... 49

Figure 3-5 – Chloride profiles for all concretes in solution L6. .... 49

Figure 3-6 – Effects of an alkaline plume in granitic host rocks (POSIVA 2012, from Savage, 1996). 51

Figure 3-7 – Illustrative example for modelling of leaching of cementitious materials in the groundwater environment (Ferreira et al., 2014). ..... 52

Figure 3-8 – Illustration of diffusion controlled simultaneous leaching of portlandite and CSH-gel in concrete. The blue line corresponds to a concentration gradient for the case of pure phase portlandite, green and red lines correspond to concentration gradients in the presence of both portlandite and C-S-H phases (Höglund, 2014)..... 53

Figure 3-9 – Diffusion controlled leaching of concrete showing the calculated depth of depletion of portlandite or C-S-H-gel for different cases (Höglund, 2014)..... 53

Figure 3-10 – Comparison of simulated scenarios for quartz only and quartz with K-feldspar: a SiO<sub>2</sub>; b pH (Chen et al., 2015). ..... 54

Figure 4-1 – Schematic diagram of the potential sequence of secondary mineral forming as consequence of the migration of hyperalkaline pore fluids through bentonite (Savage and Benbow, 2007; Bamforth et al., 2012). Na/K phases may be replaced by more Ca-rich ones as the composition of cementitious pore fluids evolves with time. .... 59

Figure 5-1 – Approximate evolution of temperature and relative humidity at the canister surface (from Landolt et al 2009)..... 83

Figure 5-2 – Elemental transfers at the Fe–clay corroded interface reacted at 90 °C and 50 bars during 8 months (iDPL: internal dense product layer; eDPL: external dense product layer; TML: transformed medium layer (from Schlegel et al., 2008)..... 93

Figure 5-3 – (a) Elemental transfers at the massive iron rod–clay (Callovo-oxfordian) interface reacted at 90 °C during 2 years. (b) Idem at the model overpack-clay (Callovo-oxfordian) interface. (iDPL: internal dense product layer; eDPL: external dense product layer; TML: transformed medium layer (from Schlegel et al., 2014)..... 101

Figure 5-4 – Raman distribution map at the metal-corrosion interface of nails cross-sections (figure from Leon et al., 2014)..... 103

Figure 6-1 – Evolution of corrosion potential as predicted by the Mixed Potential Model (MPM) (Engelhardt et al., 2014). ..... 127

Figure 6-2 – Effect of temperature on the anaerobic corrosion rate of carbon steel in various alkaline solutions. The anaerobic corrosion rate is plotted as a function of reciprocal temperature (highest temperature: left side of the graph; lowest temperature: right side of the graph) (adapted from Smart et al., 2004)..... 129

Figure 6-3 – Effect of temperature on the anaerobic corrosion rate and hydrogen gas evolution rate of carbon steel in saturated Ca(OH)<sub>2</sub> solutions (pH = 12.8) and in mortar-equilibrated water (pH = 12.6). (a) plot of hydrogen gas generation versus exposure time (Fujisawa et al., 1999), (b) plot of the corrosion rate versus reciprocal of temperature (1/T) (Fujisawa et al., 1997). ..... 130

Figure 6-4 – Effect of temperature on the long-term (t > 365 days) uniform corrosion rate of carbon steel exposed to alkaline and anoxic environments. Closed symbols represent tests conducted in solutions; open symbols represent tests conducted in cement. .... 131

Figure 6-5 – Evolution of the corrosion rate as a function of (a) the relative humidity (Vu, 2011; adapted from Tuutti, 1982), (b) the saturation degree of a carbonated CEM I Portland cement paste for different cover depths (Chitty et al., 2008)..... 132

Figure 6-6 – Relationship between chloride threshold concentration and the pH of the concrete pore solution (Bentur et al., 1997). ..... 133

Figure 6-7 – Evolution of the corrosion rate of carbon steel in saturated Ca(OH)<sub>2</sub>+0.2 N KOH solution at 21 °C as a function of chloride addition (adapted from Goñi and Andrade (1990)). (a) Chlorides added as NaCl salt, (b) chlorides added as CaCl<sub>2</sub> salt. .... 134

Figure 6-8 – Corrosion rate versus exposure time for carbon steel immersed in a 1.85 g L<sup>-1</sup> Ca(OH)<sub>2</sub> solution with increasing NaCl concentrations (days 1-2: chloride-free sat. Ca(OH)<sub>2</sub>; days 3-4: sat. Ca(OH)<sub>2</sub> + 0.67 g L<sup>-1</sup> NaCl; days 5-6: sat. Ca(OH)<sub>2</sub> + 35 g L<sup>-1</sup> NaCl) (Deshpande et al., 2000). Conversion factor: 1 mpy ~25.4 μm yr<sup>-1</sup>..... 134

Figure 6-9 – Plot of current density (determined potentiostatically) as a function of chloride content versus time for A615 grade carbon steel in saturated  $\text{Ca}(\text{OH})_2$  solution at 25 °C (Hurley and Scully, 2002)..... 135

Figure 6-10 – Evolution of the corrosion potential and corrosion rate (expressed as a corrosion current density) of carbon steel in saturated  $\text{Ca}(\text{OH})_2$  solution as a function of chloride addition (Zhang, et al, 2009)..... 136

Figure 6-11 – Compilation of uniform corrosion rates (reported in the non-nuclear industrial and nuclear waste management literature) of carbon steel in anoxic and alkaline chloride-free solutions (pH ~ 12–13.5)..... 137

Figure 6-12 – Compilation of uniform corrosion rates (reported in the non-nuclear industrial and nuclear waste management literature) of carbon steel in anoxic and alkaline solutions (pH ~ 12-13.5) containing various chloride concentrations up to 20,000 mg L<sup>-1</sup>..... 138

Figure 6-13 – Top: SEM image from the surface of carbon steel wire specimen after 13,600h in YCW at 80 °C. Bottom: EDX spectrum from “crystalline” material formed on the wire surface at the indicated location. (Figure 105 from Smart et al. (2019)..... 141

Figure 6-14 – Film growth model for carbon steel in alkaline conditions according to the Point Defect Model (PDM) (McDonald, 2011)..... 143

Figure 6-15 – Film growth model for carbon steel in alkaline conditions according to the Diffusion Poisson Coupled Model (DPCM) (Bataillon et al., 2010). ..... 144

## List of Tables

<i>Table 2-1 – Example of corrosion products identified during corrosion tests of carbon steel in anaerobic conditions.</i>	18
<i>Table 2-2 – Example of corrosion products identified during corrosion tests of carbon steel in anaerobic conditions.</i>	25
<i>Table 2-3 – Specific surface area and sorption capacity of three corrosion products: commercial goethite, commercial magnetite and synthesized siderite (Philippini et al., 2006).</i>	27
<i>Table 2-4 – Different types of iron/magnesium silicate precipitates observed in experiments on glass leaching in the presence of iron and CPs in the laboratory.</i>	30
<i>Table 2-5 – Some examples of iron silicates of interest.</i>	32
<i>Table 2-6 – pH values measured in leachates in different laboratory leaching tests at 50 °C (CEA data).</i>	36
<i>Table 3-1 – Composition of test solutions.</i>	49
<i>Table 4-1 – Summary of laboratory and in situ experiments addressing cement/clay interactions using cementitious materials in contact with clay materials (modified after Dautères, 2016).</i>	61
<i>Table 4-2 – Summary of simulation studies addressing i) laboratory and in situ experiments and ii) long-term predictions of cement/clay interactions.</i>	69
<i>Table 5-1 – Summary of clay transformation from laboratory experiments considering high temperature and transient from aerobic to anaerobic conditions.</i>	88
<i>Table 5-2 – Influence of exposure time (months) on the average uniform corrosion rate (<math>V_{corr}</math>), maximum depth of pitting attack (<math>D_{max}</math>), average pit depths (<math>D_{aver}</math>) and pitting factor calculated for the fine-grained carbon steel TStE355 exposed to saturated FEBEX bentonite at different temperatures (25, 50, 75 and 100 °C) (based on Madina et al., 2002; Azcárate et al., 2004).</i>	90
<i>Table 5-3 – Average corrosion rates determined by the UK AEA, JNC, SCK-CEN, NAGRA and CEA in different clays and with various water chemistries (Kursten et al., 2004a).</i>	90
<i>Table 5-4 – Summary of corrosion products and clay transformation from laboratory experiments made under anaerobic conditions and temperature <math>\leq 100</math> °C.</i>	95
<i>Table 5-5 – Calculated average uniform corrosion rates (<math>V_{corr}</math>) and maximum pit depths (<math>D_{max}</math>) of the carbon steel samples obtained from in situ corrosion experiments (from Debruyne et al., 1990; Cornelis and Van Iseghem, 1993; Kursten et al., 1997, 1999).</i>	96
<i>Table 5-6 – Comparison of the recent reactive transport models at the disposal scale (modified from Bildstein et al., 2019).</i>	110
<i>Table 7-1 – Analyses of water from drill holes in the TVO repository area (Carpén et al., 2012b).</i>	154
<i>Table 7-2 – Water composition in the long-term exposure experiments (Rajala et al., 2019).</i>	156

## Abbreviations

AAR	Alkali aggregate reaction
C-A-S-H	Calcium aluminium silicate hydrates
CDZ	Chemical disturbed zone
CEC	Cation exchange capacity
CH	Calcium hydroxide (portlandite)
COx	Callovo-Oxfordian
CP	Corrosion product
CRH	Critical relative humidity
C-S-H	Calcium silicate hydrates
DDC	Dormant desiccated cells
DEF	Delayed ettringite formation
DGR	Deep geological repository
DPCM	Diffusion Poisson coupled model
EBS	Engineered barrier system
EDX	Energy-dispersive X-ray fluorescence spectroscopy
FEBEX	Full-scale engineered barrier experiment
FEG	Field emission gun
FIB	Focussed ion beam
GGE	Gas generation experiment
GR	Green rust
GTS	Grimsel Test Site
HLW	High level waste
HPF	Hyperalkaline plume in fractured rock
ILW	Intermediate level waste
IRB	Iron reducing bacteria
ISG	International simple glass
LAC	Low alkali cement
LCS	Long-term cement studies
LLW	Low level waste
MIC	Microbiological induced corrosion
M-S-H	Magnesium silicate hydrates
OPA	Opalinus clay
OPC	ordinary Portland cement
PDM	Point defect model

RH	Relative humidity
RT	Room temperature
SEM	Scanning electron microscope
SF	Spent fuel
SRB	Sulphate reducing bacteria
SCC	Stress corrosion cracking
SSC	Sulphide stress cracking
STXM	Scanning Transmission X-ray Microscope
TEM	Transmission electron microscope
THMC	Thermal-hydraulical-mechanical-chemical
ThRB	Thiosulphate reducing bacteria
URL	Underground Research Laboratory
WP	Workpackage

## 1. Introduction

The chemical evolution of a disposal cell in a geological repository for nuclear waste, i.e., waste packages and their immediate surroundings such as other waste packages and/or near field components, forms an important input for the repository evolution and the assessment of safety- and performance related aspects. A better conceptual and mathematical representation of this evolution enhances the assessment and quantification of generic safety functions as isolation and immobility of waste constituents, the reduction of conservatism and uncertainty and the definition of requirements on materials.

The objective of EURAD WP ACED is the assessment of the chemical evolution at the disposal cell scale involving interacting components/materials and thermal, hydraulic and/or chemical gradients by considering intermediate-level waste (ILW) and high-level waste (HLW) disposal concepts representative for different concepts throughout Europe (see Neeft et al., 2020). The study of disposal cells ranges from micro-scale processes at interfaces between different materials up to interactions of waste packages with their immediate surrounding near field environment and the host rock.

Regarding, the interface scale WP ACED aims at compiling and integrating the process level knowledge and description of reactivity at the interfaces between materials relevant for ILW and HLW disposal cells. The focus of the interface scale in ACED task 2 is in particular on steel/material interfaces. However, other interfaces (e.g., glass/steel, concrete clay or concrete/granite) are important within ACED tasks 3 (Waste package scale) or 4 (Disposal cell scale), to provide geochemical and coupled reactive transport models to simulate relevant (long-term) processes acting under different environmental gradients as basis for up-scaled representations of interfaces at the waste package scale. The upscaling approach is defined in terms of information exchange from relatively small-scale processes at interface scale to more complex systems at waste package scale and further to full disposal cell scale. The exchange information can take different forms such as identified critical processes, abstracted process representation, up-scaled parameter values, or simplified representation of features.

### 1.1 Aims and scope

An important basis for the work to be performed within ACED is the state-of-the-art scientific knowledge and experimental evidence on chemical processes acting at the interface between various materials in HLW and ILW disposal cells, which in consequence could also alter transport-relevant properties of the materials. This report D2.5 serves as input for the desk-top studies on the state-of-the-art (D2.1) that contains descriptions of the relevant processes and transients that influence the chemical evolution of HLW and ILW disposal cells. Thus D2.5 aims at providing a structured overview of existing (experimental) data on relevant processes occurring at the following six interfaces, relevant for the work to be performed in ACED tasks 2 to 4:

- glass-steel,
- cement/mortar-granite,
- cement/concrete-clay,
- steel/iron-bentonite,
- steel/iron-cement/concrete, and
- steel/iron-granite.

This includes also information on natural/archaeological analogues that may provide insight/data for long-term processes relevant to the chemical evolution at the interfaces not accessible in short-term (laboratory) experiments. Moreover, an overview on conceptual and mathematical models used to describe the processes at the interface is provided. The information summarised in D2.5 should contribute to the conceptualisation of the chemical evolution at these interfaces in the ACED tasks 2 to 4 and will be used to support model validation and parametrisation of models.

Thus D2.5 provides for each interface considered:

- a concise listing of processes deemed relevant at the respective interface with respect to disposal cell evolution;
- an overview on laboratory/field scale experiments addressing these processes as well as evidence from natural/archaeological/technical analogues;
- an overview about conceptual and mathematical models that have been and are used to describe these processes at the respective interfaces and their parametrisation; and
- an evaluation regarding the availability of data/information and the applicability of existing models.

## 1.2 Structure of the report

The structure of deliverable D2.5 closely follows the systematic approach and rationale outlined above. In each of the following chapters 2 to 7 one specific interface is addressed, namely in chapter 2: interface glass-steel, in chapter 3: interface cement/mortar-granite, in chapter 4: interface cement/concrete-clay, in chapter 5: interface steel/iron-bentonite, in chapter 6: interface steel/iron-cement/concrete, and in chapter 7: interface steel/iron-granite. The main conclusions drawn from these chapters with respect to the current state of knowledge on the processes occurring at the respective interfaces, the availability of experimental data and evidence, as well as modelling approaches to describe processes at the interfaces are summarized in chapter 8.

## 1.3 References

Neeft, E., Weetjens, E., Vokal, A., Leivo, M., Cochepin, B., Martin, C., Munier, I., Deissmann, G., Montoya, V., Poskas, P., Grigaliuniene, D., Narkukniene, A., Garcia, E., Samper, J., Montenegro, L., Mon, A. 2020. Treatment of chemical evolution in National Programmes. D2.4 of the HORIZON 2020 project EURAD.

## 2. Interface "glass – steel"

Christelle Martin (Andra)

### 2.1 Processes at the interface

The aim of this chapter is to examine how the materials in the environment surrounding the glass influence its alteration. These materials are the metal containers (according to the concept: stainless steel containers, non-alloy steel disposal containers and sleeves) and the host rock.

The alteration and dissolution of nuclear waste glass in contact with water is controlled by several inter-related processes at the glass surface. Based on extensive studies on the dissolution of nuclear waste glasses and in particular simulated HLW borosilicate glasses, a general picture on the typical dissolution behaviour of HLW borosilicate glasses under conditions representative for geological disposal environments has been established (Figure 2-1, cf. van Iseghem et al., 2006; Gin et al., 2013; Gin, 2014).

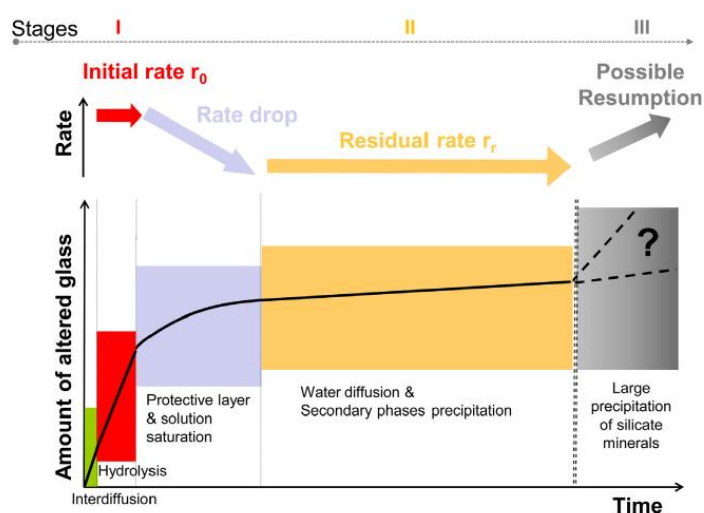


Figure 2-1 – Stages of nuclear glass corrosion and related potential rate-limiting mechanisms (Gin et al., 2013).

Glass alteration by water only starts after the container loses its integrity, due to corrosion processes and to lithostatic pressure. For this reason, the corrosion products from the metal containers are included as surrounding materials whose influence are examined as well.

Understanding the glass/steel interactions and their consequences on nuclear glass long-term behaviour requires knowing the main processes underpinning aqueous alteration of glass. According to literature (Vienna, 2013; Gin et al., 2015a), glass alteration is due to the formation and dissolution of an alteration film layer, which is likely to incorporate chemical elements from the solution and to act as a diffusion barrier for reactive species. How effective this barrier is depends primarily on the concentration of silicon in solution in the vicinity of the glass.

The influence of the surrounding materials on glass alteration (Figure 2-2) can then be divided into four main categories of phenomena, all of which are related to the phenomenology of a coupled chemistry-transport model:

- the materials in the surrounding environment may modify the composition of the solution that alters the glass (pH, redox, ionic strength, concentrations of elements, etc.), mainly through their buffering capacity and their sorption capacity, and may thereby affect the kinetics of glass alteration (e.g., sorption of silicon);
- the materials in the surrounding environment may also act as media for secondary phase nucleation and growth; this then implies issues with the kinetics, thermodynamics and stoichiometry of such phase formation, as well as the advance of the precipitation front in the

porous medium. The fact that the solution becomes depleted in silicon as a result of this precipitation may help to sustain glass alteration;

- the materials in the surrounding environment may also restrict the transport of species involved in glass alteration, especially in the case of water, depending on the transport properties of the host rock and the corrosion products. The formation of secondary phases mentioned above may also clog porosity, thus changing the transport properties of the medium;
- last, it has been shown that some elements in the glass may stabilise (in the case of calcium (Paul, 1977; Gin et al., 2012) or destabilise (in the case of magnesium (Arena et al., 2016)) the hydrated glass layer. It has also been shown that the same effects can be expected when these elements come from the aqueous phase (Chave et al., 2011).

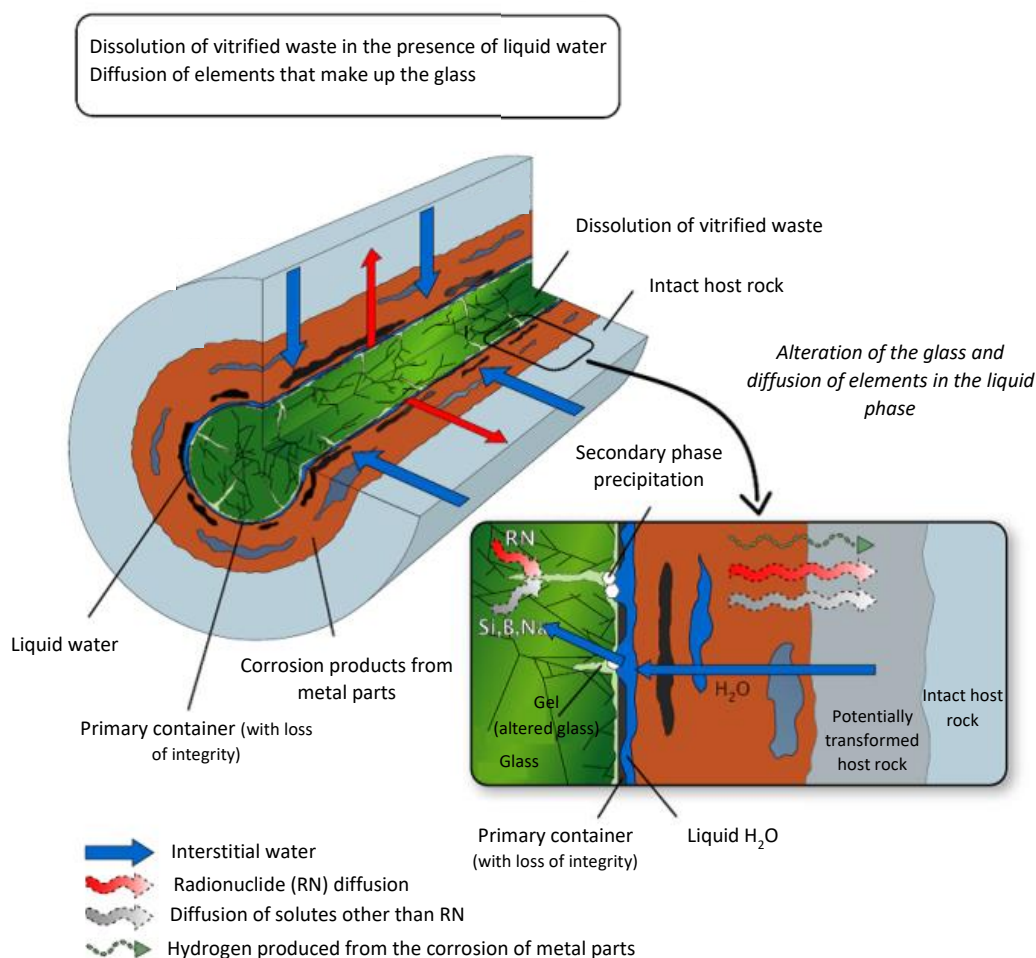


Figure 2-2 – Diagram showing a glass package in its environment following disposal container failure.

Note: Most of this review is based on glass/steel interactions in a clay medium. Of course, some disposal concepts (e.g., in Belgium) are based on a cementitious environment. In such alkaline conditions, glass/steel interactions are not the key issue and the different studies dealing with nuclear glass alteration available in literature are more focused on the influence of cementitious porewater on glass alteration (e.g., Ferrand et al. 2011, 2013; Utton et al., 2012, 2013a, 2013b; Depierre, 2013; Depierre et al., 2013; Corkhill et al., 2013; Fournier, 2015; Gin et al., 2015b; Liu et al., 2015; Maraghechi et al., 2016; Suzuki-Muresan et al., 2018).

## 2.2 Evidence from experiments and analogues

### 2.2.1 Nature of the iron/steel corrosion products

Several experimental programmes have been launched since the mid-1980s by various countries (e.g., UK, Switzerland, Belgium, France, Japan) studying the possibility of a HLW repository in a granitic environment with an engineered clay barrier or in a clay environment, and considering the use of a non-alloy (carbon) steel container, or even cast iron, for HLW packaging.

According to the Table 2-1, corrosion products (CPs) from a low-alloy steel disposal container are mainly composed of iron oxides such as magnetite ( $\text{Fe}_3\text{O}_4$ ), or iron carbonates such as siderite ( $\text{FeCO}_3$ ) or chukanovite ( $\text{Fe}_2(\text{OH})_2\text{CO}_3$ ). In some cases,  $\text{Fe}^{\text{III}}$  oxy-hydroxides were detected; they may have formed during the initial period of the corrosion test with remaining traces of oxygen.

Table 2-1 – Example of corrosion products identified during corrosion tests of carbon steel in anaerobic conditions.

Temperature (°C)	Duration (years)	Nature of leaching solution	Nature of corrosion products	Reference
90	1.30 2.28	Granitic	$\text{Fe}_3\text{O}_4$ $\text{Fe}_3\text{O}_4$	(Marsh and Taylor, 1988)
16 90 90 170	4.8 2 7 4.8	Clay (Mol)	$\text{Fe}_3\text{O}_4$ , $\text{SiO}_2$ , $\text{Fe}_2\text{O}_3$ ? $\text{Fe}_3\text{O}_4$ , $\text{SiO}_2$ , $\text{Fe}_2\text{O}_3$ $\text{Fe}_3\text{O}_4$ , $\text{SiO}_2$ , $\text{Fe}_2\text{O}_3$ ? $\text{Fe}_3\text{O}_4$ , $\text{SiO}_2$ , $\text{Fe}_2\text{O}_3$	(Debruyne et al., 1991) (Kurstner, Van Iseghem, 1998, 1999)
50 to 150 50 to 150 80 80	0.25 0.25 0.5 0.5	Distilled water Sea water Distilled water Sea water	$\text{Fe}_3\text{O}_4$ $\text{FeCO}_3$ $\text{Fe}_3\text{O}_4$ $\text{FeCO}_3$	(Honda et al., 1991)
50 and 80	1 to 4	Representative groundwater	$\text{FeCO}_3$ , $\text{Fe}_{1-x}\text{Ca}_x\text{CO}_3$ , $\text{Fe}_2(\text{OH})_2\text{CO}_3$	(Taniguchi et al., 2004)
30 and 50	2.27 to 2.5	Carbonated chloride water (pH ~ 10,4)	$\text{Fe}_3\text{O}_4$	(Carlson et al., 2007)
90	2	Synthetic Callovo-Oxfordian porewater + compacted claystone Slurry (3% MX80 bentonite + Synthetic Callovo-Oxfordian porewater)	$\text{Fe}_3\text{O}_4$ maghemite $\gamma\text{-Fe}_2\text{O}_3$ $\text{FeCO}_3$ $\text{Fe}_{1-x}(\text{Ca}, \text{Mg})_x\text{CO}_3$ Fe-silicates	(Leon et al., 2017)

Iron corrosion products formed *in situ* in the presence of claystone are typically iron silicates and carbonates and, more rarely, iron sulphides (De Combarieu et al., 2007; Schlegel et al., 2014).

Magnetite is not always detected. When it is detected, it is often present in small quantities and localised on the inner surface of the CPs. It has, however, been observed in some surface laboratory experiments as the predominant CP (Burger et al., 2013). Localised variations in pH and in concentrations of carbonates may favour the formation of the one or other CP (Michelin et al., 2015). Models developed by Ngo et al. (2015) also show that the nature of the corrosion products is heavily dependent on the concentration of silicates: depending on silicate content, magnetite may be formed, or chukanovite, before transforming into iron silicates. Studies conducted by Azoulay et al. (2012) on iron corrosion products (other than iron silicates) also confirm the metastable nature of chukanovite which evolves into siderite.

Iron carbonates (siderite, chukanovite) have been observed on archaeological analogues (Michelin, 2011; Michelin et al., 2015). The latter appears to be stable when placed back in Callovo-Oxfordian (COx) water, with the formation of a new layer of corrosion products (siderite/calcite) on the surface. Note that measurements taken by the CEA/CNRS on these archaeological corrosion products give a specific surface area ( $\sim 23.7 \text{ m}^2\text{g}^{-1}$ ) and a silicon sorption capacity ( $\geq 160 \text{ } \mu\text{mol Si g}^{-1}$ ) higher than those measured on artificial corrosion products, which could be explained by certain experimental artefacts (measurements taken on powders sampled at the surface of archaeological artefacts, desorption of silicon found when measuring sorption capacity in spite of rinsing a number of times). Dillmann et al. (2016) also showed that the reactivity of these corrosion products with regard to the glass was limited (see section 2.2.3).

In the glass/iron/claystone system, the formation of these phases is accompanied by a destabilisation in the interstratified illite/smectite, and the formation of new iron-rich argillaceous phases, such as smectites and serpentines (De Combarieu et al., 2006, 2007).

In addition, a distinction needs to be made between a primary phase, in which the steel container or overpack corrodes in the groundwater until its mechanical failure: the CPs formed in this phase are characteristic of corrosion in the host rock medium and some residual metallic iron remains in the system. In a subsequent phase, the disposal container continues to corrode in parallel to the alteration of the glass. The nature of the CPs forming may then be influenced by the solution chemistry at the glass/iron interface, including elements released by the glass (see section 2.2.3).

## 2.2.2 Studies of glass/iron (or CPs) interactions: experimental approach

In the literature, studies designed to investigate the effect of CPs on glass alteration are mainly based on two kinds of experiments:

- i. where the authors wanted to study the direct effect of CPs on glass alteration, the CPs were simulated using model compounds. Using such simplified systems makes it possible to distinguish between the influence of the different phases. For these studies, the CPs are primarily simulated by magnetite (Grambow, 1987a; Grambow, 1987b; Bart et al., 1987; Godon et al., 2013), which has long been thought to be the main corrosion product likely to be produced under geological disposal conditions (McKinley, 1985; Grauer, 1984), but also goethite (Bart et al., 1987; Grambow, 1987a; Grambow, 1987b) or haematite (Shanggeng et al., 1985), or even additions of  $\text{FeCl}_2/\text{FeCl}_3$  in solution (Pan et al., 2003; Aréna, 2017; Aréna et al., 2018). Recent studies have also included the results of CP characterisation and studied iron carbonates (Michelin et al., 2013a). Other experiments found in the literature also include CPs obtained from the dissolution of stainless steel from the container in aqua regia or by precipitation in a sodium hydroxide solution: the representativeness of CPs obtained by these ways is more debatable;
- ii. where the authors wanted to study the effect of the *in situ* formation of CPs on glass alteration, they have used integral experiments that provide data on the system as a whole thanks to the presence of glass and metallic iron (McVay and Buckwalter, 1983; De Combarieu et al., 2007; De Combarieu et al., 2011; Michelin et al., 2013a; Reiser et al., 2015). In these studies, iron alteration also produces corrosion products such as magnetite or siderite, as well as forming hydrogen.

The impact of iron or CPs on glass alteration heavily depends on how the tests are set up. Various leaching tests can be found in the literature:

- homogeneous systems, in which the glass and iron or CPs are placed in the cell in the form of intimately-mixed powders (Rébiscoul et al., 2015);
- systems in which the glass and iron or CPs are kept physically separate, for example, by a membrane or sinter (Rébiscoul et al., 2015);
- the different materials are stacked in successive layers (glass, iron or CPs), placed in the cell in monolith or powder form. In this type of set-up, the leachate recovered at the end of the test and removed from the cell is the product of exchanges with the different layers (Burger et al., 2013);

- the different materials are stacked in concentric layers. This set-up is similar to the stacked set-up, but is more representative of that expected in the repository conditions;
- leaching tests on a crack formed by two glass monoliths in which iron or CPs, or vice versa, have been placed (Michelin et al., 2013a);
- tests carried out *in situ*, where glass alteration is monitored directly in the disposal environment, in contact with the water from the geological formation, and in the presence of iron (and the CPs formed *in situ*) (Carrière et al., 2019).

While the interactions between glass and host rock, glass and iron or glass and corrosion products have been widely studied, experiments that consider all three materials together, glass and iron or corrosion products and clay or cement, are less common. One such study was the European NF-PRO project (Grambow et al., 2008), in which various experiments were conducted using an argillaceous fraction of MX-80 (Volclay) bentonite, magnetite and, in some other cases, with silica additives (Godon and Vernaz, 1990; Godon et al., 1991; Mitsui and Aoki, 2001). These tests confirmed that glass alteration is governed by the interactions between silicon released during glass alteration and magnetite and the clay, and also confirmed the beneficial effect of silica additives on glass alteration. According to Grambow et al. (2008), it was essential to improve our understanding of these systems by means of more in-depth knowledge of how the pH evolves in the vicinity of the glass, of the interactions between silicon and materials in the surrounding environment (secondary phase precipitation to be taken into consideration in addition to sorption) etc. Studies on glass/iron/corrosion products/claystone interactions started in 2007 with studies carried out by De Combarieu (2007). As for the study of interactions between glass and corrosion products, these tests have often been initially carried out by using magnetite. Nonetheless, some experiments have also been carried out by using iron, to specify interactions between glass and iron when iron corrosion and glass alteration are concomitant, and, in particular, the nature of the corrosion products formed *in situ* in contact with the host rock. Tests carried out *in situ* in Underground Research Laboratories (e.g., the Meuse/Haute-Marne URL) but also more complex experiments including microcontainer mock-ups (Figure 2-3) have given also further information during the last years.



Figure 2-3 – Photographs of the machined brick of argillite, the glass/iron mock-up, and the three specimens inserted in the brick: the glass/iron mock-up studied by Schlegel et al. (2016) in the centre, the gold specimen at the top, and the Armco iron specimen studied by Schlegel et al. (2014) at the bottom.

Studies on archaeological analogues (slag from a former ironworks, altered over 400 years in an anoxic and iron-rich medium) also helped to improve our understanding of glass/iron/clay interactions (Michelin, 2011; Michelin et al., 2013b; Michelin et al., 2015).

### 2.2.3 Glass alteration in the presence of iron or corrosion products

The effect of magnetite on glass alteration was compared by Rébiscoul et al. (2015) in two configurations (configurations i) and ii) described in section 2.2.2) (Figure 2-4). A first series of experiments was focused on the effect of various amounts of magnetite by mixing and altering glass and magnetite powders. In a second series of experiments, magnetite was separated from the glass by a diffusive barrier in order to slow down the transport of aqueous species.

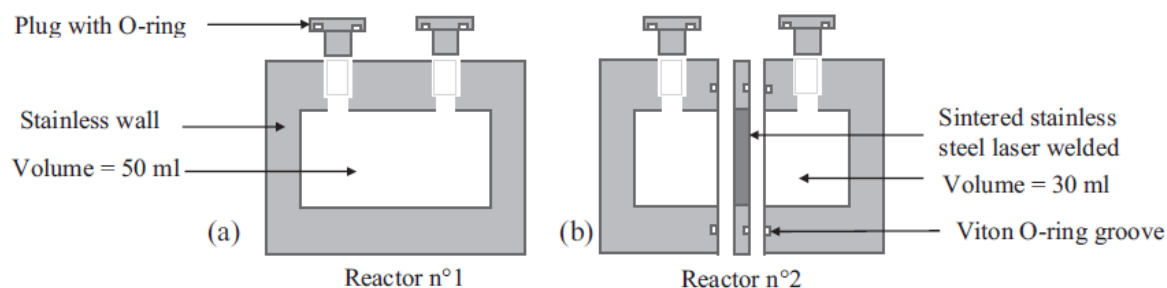


Figure 2-4 – Example of reactors used by Rébiscoul et al. (2015) for leaching tests in set-up: i) homogeneous system and ii) systems in which glass and magnetite are kept physically separated.

Using these set-ups, total glass alteration increased in the presence of magnetite. This increased alteration was not caused by an increase of the glass alteration rate, but by maintaining an alteration rate close to the initial rate for a longer period. Nonetheless, this effect seems to be transient and does not prevent the rate from dropping progressively over time (Figure 2-5).

Diffusion cell experiments (set-up ii), GSM1 experiment in Figure 2-5 have been designed to quantify the impact of a diffusive barrier between glass and magnetite. These tests have confirmed that limitation of transport results in reduced alteration of the glass, linked to a slower consumption of the silicon combined with a pH effect (Figure 2 6).

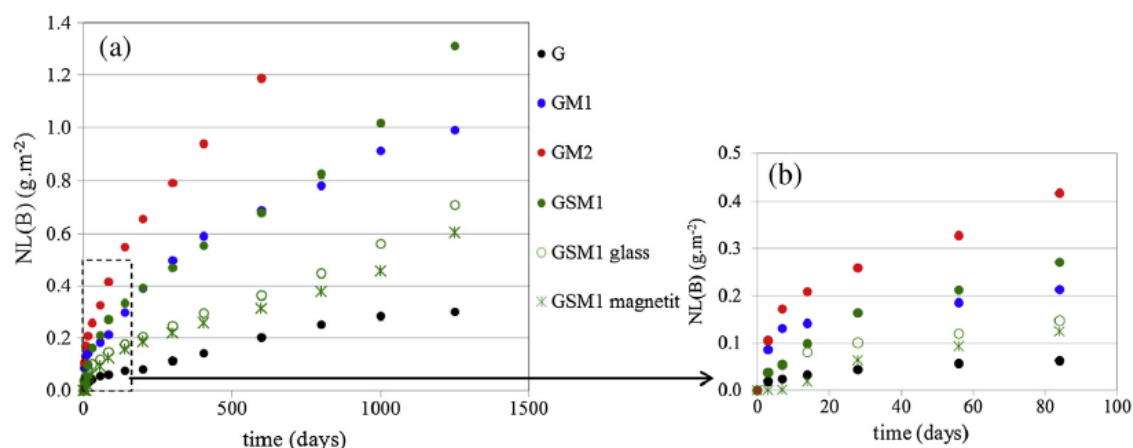


Figure 2-5 – Evolution of normalized mass losses of boron during the alteration of SON68 glass powder (63-125  $\mu\text{m}$ ) in  $\text{CO}_x$  water (at  $50^\circ\text{C}$ ,  $S/V = 74 \text{ cm}^{-1}$ ) in configuration i) (absence of magnetite (G), presence of 10 g (GM1) or 20 g (GM2) magnetite) and in configuration ii) (presence of 10 g magnetite physically separated from glass powder (GSM1)) (Rébiscoul et al., 2015).

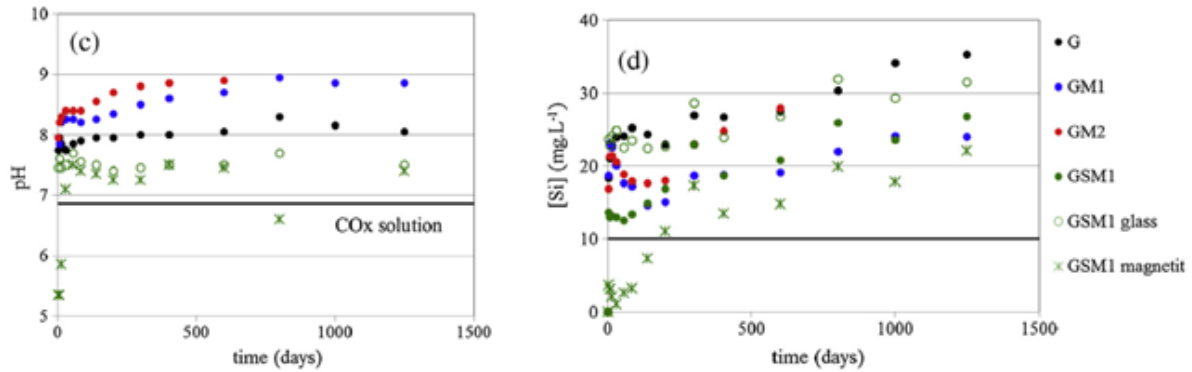


Figure 2-6 – Evolution of pH and Si concentration ( $\text{mg L}^{-1}$ ) during the alteration of SON68 glass powder ( $63\text{-}125\ \mu\text{m}$ ) in in  $\text{CO}_x$  water (at  $50^\circ\text{C}$ ,  $S/V = 74\ \text{cm}^{-1}$ ) in the different experiments G, GM1, GM2 and GSM1 (see Figure 2-5, Rébiscoul et al., 2015).

In the case of systems where the materials are stacked in successive layers (set-up iii) in section 2.2.2), the alteration kinetics at the overall scale determined using the concentrations of tracer elements in solution (B, Li) do not seem to be influenced by the presence or absence of either magnetite or iron, at least not initially (Figure 2-7).

Indeed, the CEA's results obtained at a low flow rate ( $2.5\ \text{mL month}^{-1}$ ) show quite similar alteration rates, even though the quantities of altered glass in the presence of magnetite, iron powder, and of a drilled sheet of iron are significantly different after two years of testing (Figure 2-7). Apart from the nature of the iron source (magnetite, iron powder, drilled sheet of iron), fluctuations in flow rates, probably due to the release of  $\text{H}_2$  during iron corrosion, before stabilising at  $2.5\ \text{mL month}^{-1}$  may have affected glass alteration during the first few months. More generally, the low flow rate ( $2.5\ \text{mL month}^{-1}$ ) and the chosen "stack" set-up led, at the end of the test, to very similar alteration rates.

However, Burger et al. (2013) characterised one of these experiments, involving SON68 glass powder in contact with a drilled sheet of iron (Figure 2-8). They found altered glass layers of different thicknesses for the glass grains close to the holes filled with iron beads (after 800 days, altered thickness  $\sim 1.5\text{-}2\ \mu\text{m}$ ) and the glass grains above the iron sheet ( $\sim 1.2\ \mu\text{m}$ ). Glass alteration a few millimetres from the iron source was 2 to 5 times less extensive than that found close to the iron.

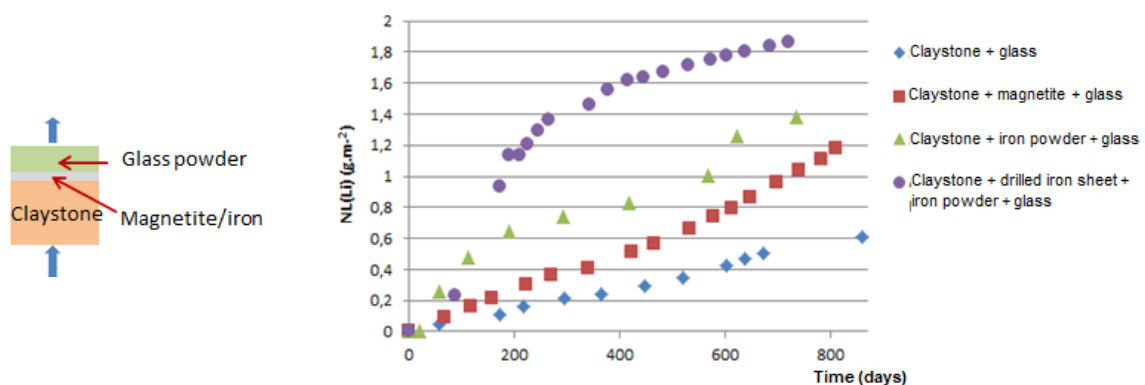


Figure 2-7 – Evolution of normalized lithium mass losses  $NL(\text{Li})$  during different experiments in which claystone, glass, magnetite or iron powder or a drilled iron sheet are stacked in successive layers (left diagram). (CEA data partially published in Burger et al., 2013).

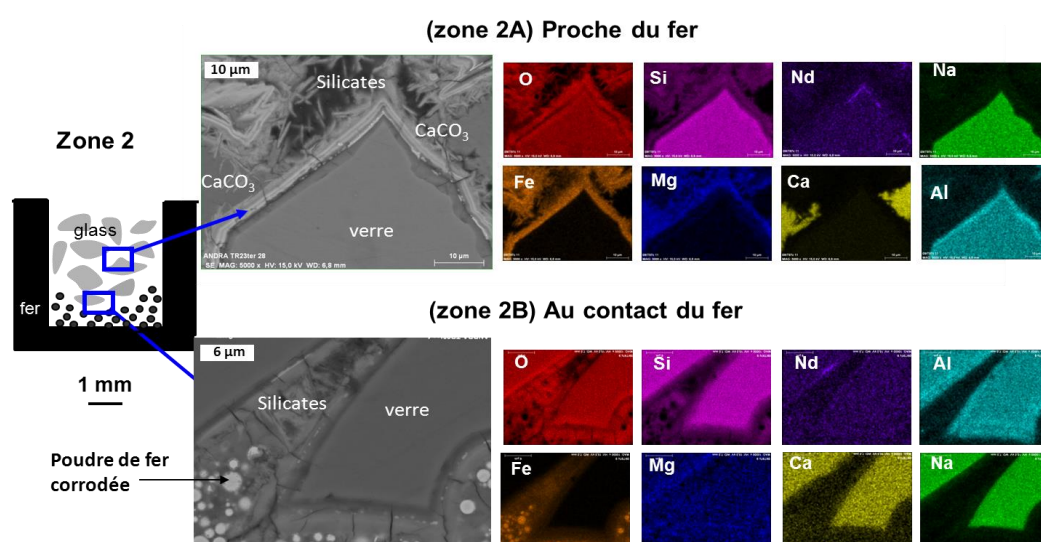
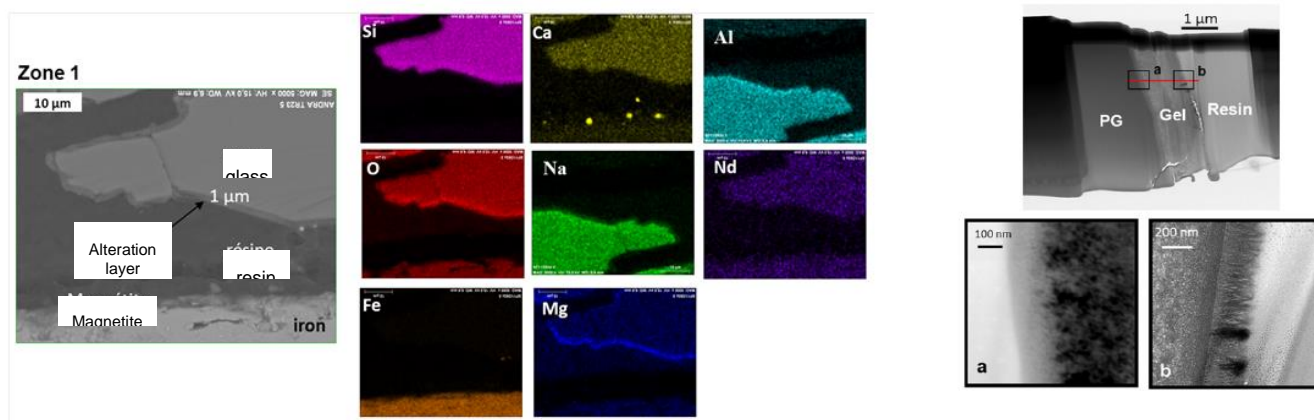


Figure 2-8 – SEM / TEM images and elemental maps of cross-sections of glass grains located in different zones (Zone 1: directly above the iron sheet; Zone 2: in a notch on the iron sheet, partly filled with iron beads) (Burger et al., 2013).

Set-up (v) studied mainly by Michelin et al. (2013a) and Dillmann et al. (2016) focuses on the coupling between chemistry and transport in a crack in the glass matrix. Michelin et al. (2013a) clearly showed a significant effect due to siderite and iron on alteration of a ferro-calcium silicate glass<sup>1</sup>, but which differed at the centre and at the edges of the crack (Figure 2-9). They attributed this difference to a transport effect, by which the solution reaches silicon saturation faster at the centre of the crack than at the edges, which favours the formation of a protective gel. The recent work performed by De Echave et al. (2019) led to the same conclusions.

<sup>1</sup> Michelin et al. (2011, 2013b, 2015) studied blast-furnace slag buried in an argillaceous medium at the archaeological site of Glinet (Normandy). Michelin et al. (2011, 2013a) also studied a synthetic ferro-calcium silicate glass with the same composition as the vitreous matrix of blast-furnace slag.

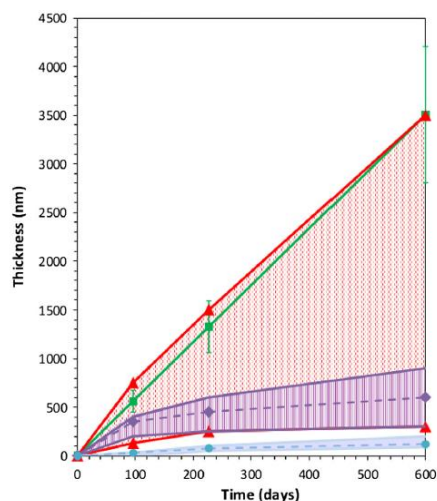


Figure 2-9 – Variability in the thickness (minimal, maximal and average) of altered glass measured through the length of a modelled crack from analysis of SEM-FEG images: empty (blue); containing siderite (purple); containing iron (red). Comparison with the thickness of glass altered as per the initial rate regime (green) (Michelin et al., 2013a). Note: bearing in mind the extreme variability in the thickness of glass altered in the presence of iron, the average thickness is not shown.

These observations can be compared to studies carried out on archaeological analogues: in-depth analysis of the crack network in several samples of blast-furnace slag (Michelin et al., 2015) found more extensive alteration (by a factor of 2 to 4) of the glassy matrix at the edges of the samples where cracks emerge (Figure 2-10). This phenomenon is very localised and disappears a few hundred micrometres below the surface. This result supports observations made on other archaeological analogues by Chomat (2008), and on cracks formed by two samples of glass: the chemistry-transport coupling has a determining influence on the alteration of the glassy matrix.

Michelin et al. (2015) also compared the alteration rates determined in laboratory tests inside model cracks and the altered glass thickness measured on the slag. Even if the iron beads present in the slag have a significant impact on alteration of the glassy matrix, the altered thickness measured on archaeological analogues is lower than the altered glass thickness extrapolated over 400 years from alteration rates measured inside model cracks containing iron (Table 2-2), suggesting a drop in the alteration rate within the archaeological sample. De Echave et al. (2019) also observed that the glass/steel interactions may delay but not prevent the glass alteration rate from decreasing with time.

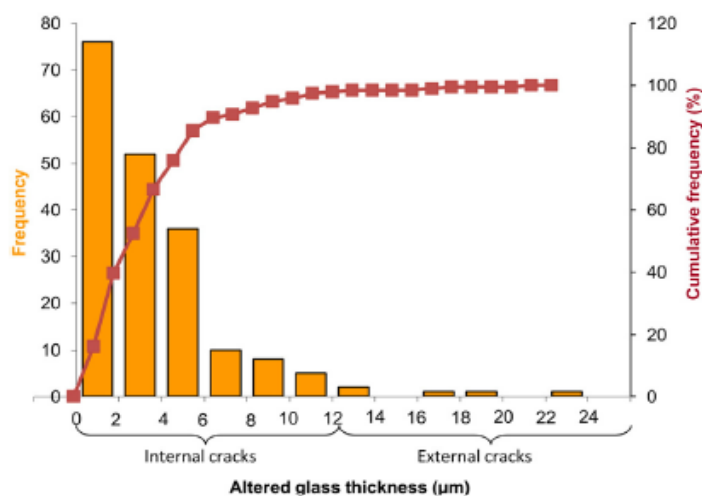


Figure 2-10 – Analysis of altered glass thickness in cracks in blast-furnace slag (Michelin et al., 2015).

Table 2-2 – Example of corrosion products identified during corrosion tests of carbon steel in anaerobic conditions.

Type of sample	Thickness altered over 400 years
Archaeological analogues	< 6 μm (85% of the cracks) Max ~ 24 μm
Model crack with no iron	0.3 – 1 μm
Model crack with iron	17 - 54 μm

Apart from the chemistry-transport effect at the centre of the crack, Dillman et al. (2016) also used the set-up (v) to focus more specifically on the difference in reactivity between CPs obtained by corrosion of an iron foil in a synthetic Callovo-Oxfordian groundwater and CPs sampled from nails buried 400 years ago in an argillaceous medium. The nature of these different CPs is characteristic of CPs products formed in an anoxic argillaceous medium: siderite, chukanovite and magnetite. However, they present a very different reactivity towards glass (Figure 2-11). The CPs from the archaeological site, already in equilibrium with a silicon-rich argillaceous medium, prove to be much less reactive than the synthetic CPs, but nonetheless they have a slight effect on the glass alteration kinetics. De Echave et al (2019) carried out a similar study by comparing the reactivity of a pristine and a pre-corroded iron foil: in the tested conditions (14 days of alteration in confined environment), there is no clear difference between the two systems: pre-corrosion seems not to have any influence on glass/steel interaction within a crack, suggesting that in spite of the existence of a corrosion layer, the iron flux remains sufficient to impact glass alteration. De Echave et al (2019) points out that the pre-corrosion leads to a slightly stronger alteration on external sides of the glass sample, probably due to a pH effect.

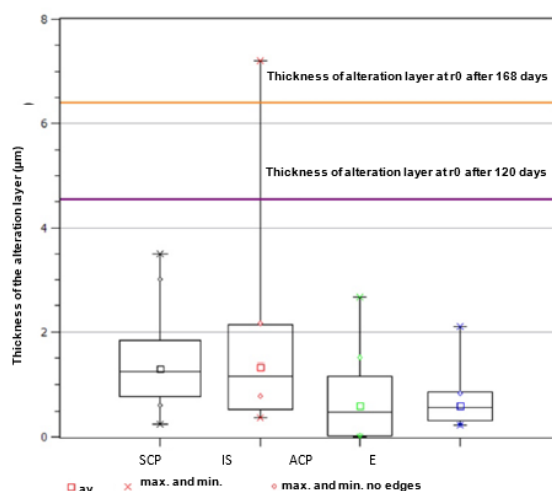


Figure 2-11 – Thickness of alteration layer measured on one side of the crack after around 6 months of alteration at 50°C in COx water: empty (E), containing synthetic corrosion products (SCP), archaeological corrosion products (ACP) and an iron sheet (IS) (Dillmann et al., 2016).

So-called "mock-up" samples in the form of microcontainers containing a block of glass or crushed glass were also altered in specific tests (e.g. the ArCorr 2008 mock-up experiment, Figure 2-3). Characterisation of the ArCorr 2008 set-up (Schlegel et al., 2016) once again confirmed that very different reactivities exist at the glass/claystone and glass/iron interfaces. Although glass alteration is clearly visible at the glass/claystone interface, it is hard to distinguish the alteration layer at the glass/iron interface (Figure 2-12 top):

- The maximum alteration thickness measured at the glass/claystone interface (140-150 μm) is consistent with a mean alteration rate close to the initial glass alteration rate  $r_0$  (around  $r_0/3$ ).

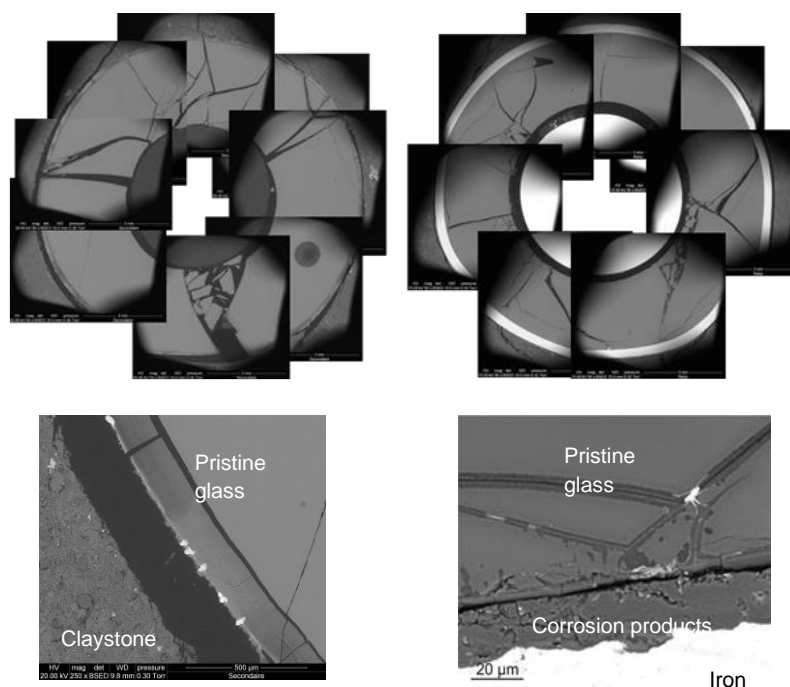


Figure 2-12 – SEM photographs of the glass/argillite and glass/iron interfaces of the ArCorr 2008 set-up. Top: overview of each of the interfaces made up of SEM photographs; bottom: detailed images of the glass/argillite interface (left) and the glass/iron interface (right) (Schlegel et al., 2015).

- The glass alteration thickness measured at the glass/iron interface and inside cracks (4 - 7 µm) is consistent with a much lower mean alteration rate than the initial rate. As stated by Schlegel et al. (2016), a phase of alteration at a rate close to  $r_0$  for a few dozen of days followed by a significant rate drop cannot be ruled out.

In addition to the configuration of the different materials in the system, the test dimensioning is another significant parameter that affects glass/iron reactivity. Thus, for homogeneous mixes of glass and iron, the glass surface-to-solution volume ratio (S/V) and the glass surface-to-iron surface ratio are determining factors. Moreover, the effect of CPs on glass alteration depends on the conditions used in the tests, especially on redox conditions in the surrounding medium. Studies on glass/magnetite systems, carried out in an oxidising or reducing medium, show that, even though an increase of glass alteration is seen in both cases, there is more alteration in oxidising conditions. Inagaki et al. (1996) linked this to the instability of magnetite in oxidising conditions and to the formation of maghemite ( $\gamma$ -Fe<sub>2</sub>O<sub>3</sub>) which increases silicon sorption capacity.

#### 2.2.4 Mechanisms

Iron and corrosion products increase glass alteration by maintaining high alteration rates over longer periods than in the same leaching solution without iron or CPs. However, this impact is only perceptible at local scale, and seems to be significantly attenuated as the distance between glass and the iron source increases. To study the underlying mechanisms impacting the glass alteration (Figure 2-1), it is possible to use homogeneous systems, for which the slowing of transport is kept to the minimum, or to use in-depth characterisations of altered materials (on cross-sections) at the (sub-) microscopic scale. If we group together existing studies in the literature, we find four possible mechanisms (Rébiscoul et al., 2015):

- silicon sorption at surface sites of corrosion products, or even silica precipitation at the iron source;
- iron silicates precipitation;
- the retention of iron in the gel, which could modify its structure and its protective properties;
- an indirect effect due to the pH, which seems to increase in the presence of iron.

The first two mechanisms (sorption and precipitation) have similar consequences. They both lead to the consumption of cross-linking elements of the glass by CPs, mainly silicon, but also, to a lesser degree, aluminium and calcium. Depending on whether it starts as soon as glass alteration starts or with a delay – linked, for example, to a large distance between the glass and the iron – this consumption can have two consequences (Lemmens, 2001): (i) a depletion of the concentration of silicon in solution, which increases glass dissolution, or (ii) the formation of a gel depleted in silicon which is, therefore, less protective.

These effects both work to the detriment of the formation of a protective layer, delaying saturation of the aqueous solution needed for its formation. In the first case, the effect works by making the initial rate phase ( $r_0$ ) last longer, and, in the second case, by slowing down the rate drop (cf. Figure 2-1).

In the following sections, we will describe each of these mechanisms in detail, based on existing leaching studies in the literature.

#### 2.2.4.1 Sorption of silicon on corrosion products

The first of these mechanisms that can delay the start of a rate drop is the sorption of species produced by glass alteration on corrosion products in the surrounding environment. This effect has been demonstrated in the presence of magnetite (Grambow, 1987a; Grambow, 1987b; Bart et al., 1987), goethite (Bart et al., 1987; Grambow, 1987a; Grambow, 1987b), and siderite (Michelin et al., 2013a).

Whatever the number of surface sites available for sorption, their number is finite. Sorption therefore lasts for a period that is proportional to the sorption capacity of the CPs. The higher the sorption capacity of the CPs (dependent on the quantity of CPs and their specific surface), the longer it takes to reach silicon saturation in solution. This can be seen in Figure 2 5; in all cases, the presence of magnetite leads to an increase of glass alteration. The more magnetite there is (GM1 and GM2 in Figure 2-5) or the larger its specific surface area is, the greater is the release of boron (tracer of glass alteration) into solution.

However, the results from different glass alteration experiments carried out in the presence of corrosion products seems to indicate that silicon/CP interactions do not prevent a slowing of the alteration rate over time (Figure 2-5 and Figure 2-9).

#### *Sorption capacity*

To predict and quantify the impact of silicon sorption by CPs on glass alteration, it is necessary to evaluate their sorption capacity and their specific surface area. A number of studies have been carried out to this end. One such study was carried out by EDF on three reference compounds: magnetite, goethite and siderite. This study shows that maximum sorption occurs at pH values between 6 and 9 (Philippini et al., 2006), but tends to fall in very acidic or very basic pH (Figure 2-13). The results obtained at pH 8.5 are given in Table 2-3. These values seem to indicate that silicon sorption by CPs will be maintained for a very short period of time with regard to the time scales relevant for geological disposal (Philippini et al., 2006 and 2007).

*Table 2-3 – Specific surface area and sorption capacity of three corrosion products: commercial goethite, commercial magnetite and synthesized siderite (Philippini et al., 2006).*

	<b>Goethite <math>\alpha</math>-FeOOH</b>	<b>Magnetite Fe<sub>3</sub>O<sub>4</sub></b>	<b>Siderite FeCO<sub>3</sub></b>
Specific surface area / (m <sup>2</sup> .g <sup>-1</sup> )	20 ± 2	1.8 ± 0.2	0.45 ± 0.02
Silicon consumption (mg <sub>Si</sub> .g <sup>-1</sup> )	2.2 ± 0.6	0.5 ± 0.4	0.6 ± 0.2
Silicon consumption (mg <sub>Si</sub> .m <sup>-2</sup> )	0.11	0.28	0.33

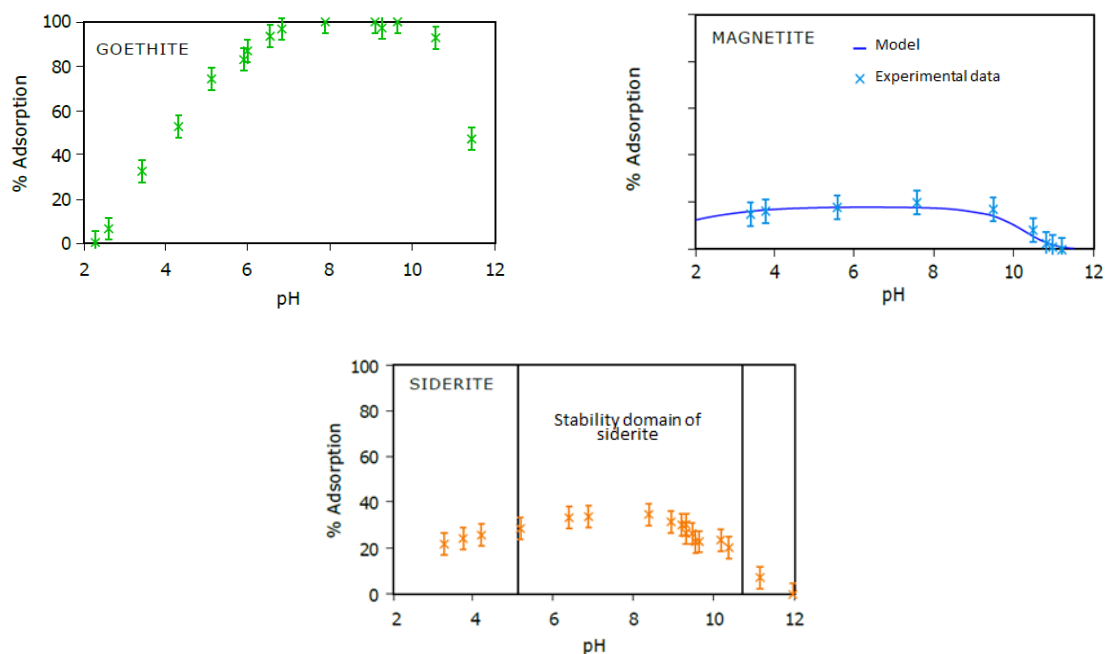


Figure 2-13 – Sorption of silicon on goethite, magnetite and siderite as a function of pH at 20 °C (Philippini et al., 2006).

Furthermore, potentiometric measurements performed on dispersed and compacted magnetite showed comparable site densities, varying between 2.2 and 4.4 nm<sup>-2</sup>. These results show that compacting has no impact on the sorption capacity of magnetite; the sorption models (see below) are, therefore, still applicable (Mayant et al., 2008; Mayant et al., 2009).

To conclude, note that this sorption phenomenon is highly reversible: 27.1 %, 40.1 % and 49.2 % of the silicic acid is released in solution after one, two and three desorption stages, respectively (Grambow, 1987a; Grambow, 1987b).

#### 2.2.4.2 Precipitation of iron silicates

Sorption of silicon on CPs on its own seems to be not sufficient to explain the quantities of altered glass during experimental tests (see section 2.3.1): even after saturation of the CPs' sorption sites, alteration rates remained higher than the residual rate  $r_r$  observed in pure water, over longer periods. Thus, in the longer term, other mechanisms may prolong the consumption of silicon: silicate phase precipitation and/or transformation of the alteration layer.

The scale and the rates of reaction related to these two mechanisms (sorption and precipitation) are quite different. First, sorption is limited by the specific surface area of the CPs, and it is maintained for relatively short periods of time in comparison to the time scales taken into account for geological disposal. The precipitation of ferrosilicates, on the other hand, may be less extensive in the short term but, potentially, more significant in the long term.

Most authors suggest the formation of ferrosilicates (Grambow, 1987a; Grambow, 1987b; Werme et al., 1990; McVay and Buckwalter, 1983; Shade et al., 1983; Shangeng et al., 1995; Kim et al., 1997; Björner et al., 1989; Godon et al., 2013; Michelin et al., 2013a; Dillmann et al., 2016), sometimes in nano-colloidal form. Only Inagaki et al. (1996) considered the formation of amorphous silica. Michelin et al. (2013a) also suggested that, given the heterogeneous CPs interface observed by TEM (Figure 2-14), ferrosilicates may form to the detriment of siderite, the CP observed in their experimental system.

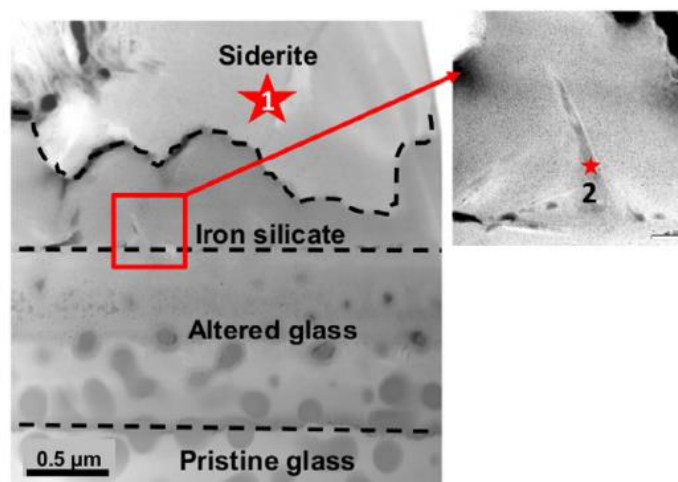


Figure 2-14 – TEM observations of the centre of the crack formed by two samples of synthetic archaeological glass and initially containing an iron sheet, after 20 months of alteration (at 50 °C, in clayey water from the Glinet site) (Michelin et al., 2013a).

Table 2-4 gives the different types of compounds observed in glass leaching tests in the presence of iron or CPs. Note that the precipitates formed may incorporate other elements in addition to iron and oxygen, such as magnesium, aluminium, sodium and calcium. In particular, the characterisation of glass samples altered in "glass/iron/claystone" systems also revealed the formation of both iron and magnesium silicates (Burger et al., 2013; Figure 2-8). Burger et al. (2013) observed many iron and magnesium silicates in lamellar structure located near the iron beads (Zone 2 in Figure 2-8), although the latter were only present in small quantities in the zones directly above the iron sheet (Zone 1), visible only by TEM. The (Fe+Mg)/Si ratio of the silicates formed can vary, especially depending on the distance from the iron source. Thus, in the system studied by Burger et al. (2013), it varies between 1:3 and 3:2.

The nature of precipitated silicates highly depends on local pH: iron/magnesium silicates can only be precipitated above a certain pH, which is a function of the silicon activity imposed by glass alteration. Moreover, when the precipitation of silicates is thermodynamically possible; then, it leads to a pH decrease: the precipitation of silicate minerals is a self-limited process that stops when the pH reaches a threshold value. In leaching experiments carried out using CO<sub>x</sub> water, the pH threshold below which magnesium will not precipitate in the form of secondary silicate phases is around 8.3 to 8.4 at 50 °C, 7.5 ± 0.1 at 70 °C, and 7.0 at 90 °C (Fleury, 2013). Aréna et al. (2018) also pointed out the key role of pH in leaching experiments performed in FeCl<sub>2</sub>/MgCl<sub>2</sub> solutions at 50 °C with different pH threshold values for magnesium silicates (~7.8) and iron silicates (~6.2).

Table 2-4 – Different types of iron/magnesium silicate precipitates observed in experiments on glass leaching in the presence of iron and CPs in the laboratory.

Reference	Glass	Environment	Water	T°	S/V (m <sup>-1</sup> )	Redox	Phases observed
(McVay, Buckwalter, 1983)	PNL 76-68 monolith	Fe	Deionised, basaltic, tuff water	90 °C	10	aerated	after 28 days: amorphous, colloidal compounds in suspension
(Shade et al., 1983)	MCC 76-68 monolith	Fe	Deionised water, saturated with NaCl	50-150 °C	?	aerated	sepiolite, talc
(Kim et al., 1997)	Borosilicate glass	Fe	Deionised water	72 °C	?	aerated and anoxic (N <sub>2</sub> )	after 25 days: nanocolloidal iron silicates
(Mitsui, Aoki, 2001)	P0798	Fe; Fe <sub>3</sub> O <sub>4</sub>	?	30 °C	?	anoxic	?
(Björner et al., 1989)	JSS-A	Fe <sub>3</sub> O <sub>4</sub>	?	?	1,100 and 4,000	?	after 91 days, colloids retaining Pu and Am
(Shangeng et al., 1995)	HLW monolith	Fe <sub>2</sub> O <sub>3</sub>	Deionised water; Groundwater	?	?	aerated	iron silicates rich in Ti, Ca, U
(Godon et al., 2013)	SON68	Fe <sub>3</sub> O <sub>4</sub>	Groundwater	50 °C	7,400	anoxic (Ar/H <sub>2</sub> /CO <sub>2</sub> )	probably too small a quantity to be detected
(Michelin et al., 2013a)	Synthetic archaeological glass	Fe	Synthetic clayey water (Glinet site)	50 °C		anoxic (N <sub>2</sub> /CO <sub>2</sub> )	iron silicates (Fe(II)/Fe(III) mix)
(Dillmann et al., 2016)	SON68	Fe Archaeological/synthetic corrosion products	Groundwater	50 °C		anoxic (Ar/H <sub>2</sub> /CO <sub>2</sub> )	iron silicates (Fe(II)/Fe(III) mix) e.g. nontronite and greenalite
Aréna et al. (2017, 2018)	ISG	FeCl <sub>2</sub> or FeCl <sub>2</sub> / MCl <sub>2</sub> (M = Mg and/or Ca)	Deionised water	50 °C	20,000	anoxic (N <sub>2</sub> )	iron silicates (trioctahedral smectites Si/Fe ~1.36)

Note also that the formation of the phases reported in Table 2-4 is rare and occurs on a very small scale in experiments carried out directly in the presence of iron CPs. There are only two studies which mention this in such a set-up: one on experiments on a glass/haematite model system (Shangeng et al., 1995) and one study on glass/magnetite (Björner et al., 1989).

However, the same is not the case in the presence of metallic iron in which iron silicates may be seen from the start of alteration. Therefore, the formation of corrosion products *in situ* at the same time as glass alteration seems to modify the predominant mechanisms, and causes more precipitation of secondary silicate phases. Dillmann et al. (2016) explained the difference in reactivity by a more or less significant iron flux induced by iron corrosion or the solubility of the CPs.

Identifying the iron silicates (or iron/magnesium silicates) formed remains tricky, all the more that several phases can precipitate with different Fe/Si ratios: De Echave et al. (2019) observed two different iron silicates, one containing a Fe/Si ratio of 1.1 and another with a Fe/Si ratio of 1.8. As part of a more systematic study, Aréna et al. (Aréna et al., 2016; Aréna, 2017; Aréna et al., 2017; Aréna et al., 2018) recently also studied silicates that form at 50 °C during the alteration of ISG glass in simplified solutions such as  $XCl_2$  (where  $X = Zn, Mg, Ni, Co, Fe, \text{etc.}$ ). It appears that the phases formed are trioctahedral smectites with a similar X/Si ratio (~0.6 to 0.7), no matter what X is, including in the case of uptake of several X elements in solution ( $XaCl_2 + XbCl_2$ ). Based on these analyses, Aréna et al. (2017) determined the stoichiometry of the silicates formed in the presence of iron and/or magnesium:  $(Fe+Mg)/Si = 0.71 \pm 0.2$ .

Dillmann et al. (2016) identified a phase enriched in Fe(III) compared to the other corrosion products (siderite, chukanovite) present in their experimental system initially containing iron, which presented structural similarities with nontronite (Figure 2-15). This initial analysis has been refined as part of the characterisation of glass/iron/claystone samples (Carrière, 2017) based primarily on a broader range of reference spectra that included other iron silicates, which cannot *a priori* be excluded, such as serpentines (berthierine), or smectites (saponite).

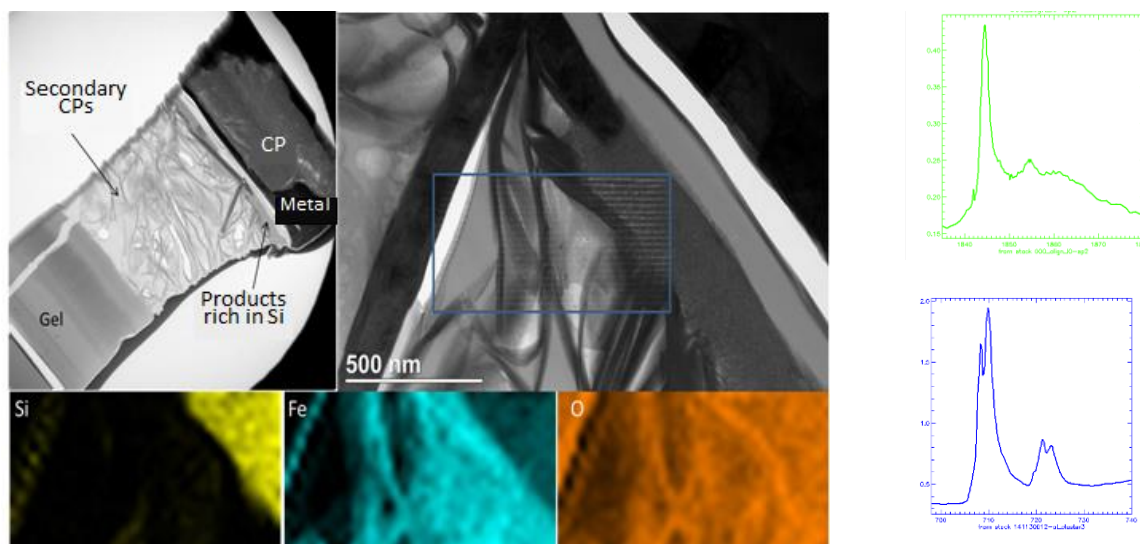


Figure 2-15 – Elemental distribution maps (Si, Fe, O) on a FIB section sampled from the centre of the crack formed by two samples of SON68 glass and initially containing a sheet of iron, after 6 months of alteration (at 50 °C, groundwater). STXM spectra at the Si edge (green) and Fe edge (blue) characteristic of iron silicates formed near corrosion products (Dillmann et al., 2016).

Carrière (2017) highlighted the influence of temperature in laboratory experiments, usually at 50 °C or 90 °C, which may favour the formation of one phase or another one depending on their stability domains (Figure 2-16). Thus, at high temperature (90 °C) serpentines will be the main phases that form until they reach their stability limit, at around 50-60 °C. Below 50 °C, serpentines will be partly or completely destabilised in favour of smectites (Table 2-5). Characterisation of experiments conducted at 50 °C and 90 °C seem to support this and find nontronite in systems altered at 50 °C and serpentines in an experiment at 90 °C. Furthermore, given that the nature of the phases formed depends on the pH conditions, among other things, Carrière (2017) linked the absence of magnesium silicates and trioctahedral smectites rich in iron in the systems studied to a local pH below 8, close to the altered glass, thus stopping the formation of these secondary phases. The formation of Fe(III)-rich nontronite in experimental systems that are anoxic and in which iron corrosion results in the release of Fe(II) in solution raises the question of the related reaction mechanisms, which have yet to be specified. In-depth characterisation of the alteration layer also found the presence of other types of iron silicates, such as greenalite (see Section 2.2.4.3).

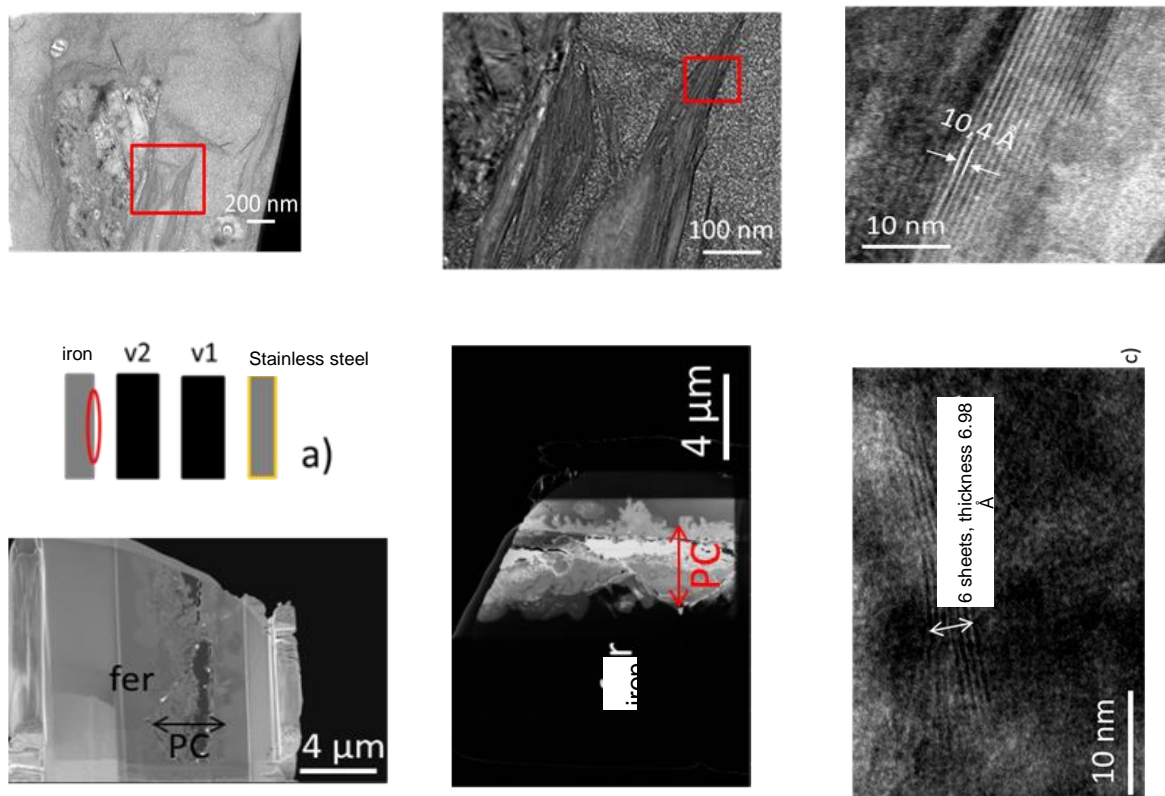


Figure 2-16 – Top: High-resolution SEM observations of the alteration layer on an  $^{29}\text{Si}$ - and  $^{57}\text{Fe}$ -doped SON68 glass monolith altered for 31 months at 50 °C in an argillite core sample saturated with  $\text{CO}_x$  water in the presence of a foil of corroded iron sampled from an archaeological nail from the Glinet site. Bottom: FIB foil and high-resolution SEM observations of corrosion products formed at the surface of an iron foil opposite a SON68 glass sample composing a stack of 4 steel plates of different grades and of glass altered in a reactor at 90 °C, under anoxic conditions, in synthesised  $\text{CO}_x$  water for approx. 2.5 years (Carrière, 2017).

Table 2-5 – Some examples of iron silicates of interest.

Families	Compounds (toroidal formulae)	Fe : Si
Trioctahedral serpentines	Greenalite $\text{Fe(II)}_{2-3}\text{Fe(III)}_{0.5}\text{Si}_{2.2}\text{O}_5(\text{OH})_{3.3}$	~3:2
	Berthierine $(\text{Fe(II)}, \text{Fe(III)}, \text{Al}, \text{Mg})_{2-3}(\text{Si}, \text{Al})_2\text{O}_5(\text{OH})_4$	≤ 3:2
	Cronstedtite $\text{Fe(II)}_2\text{Fe(III)}_2\text{SiO}_5(\text{OH})_4$	4:1
Trioctahedral smectites	Hectorite $\text{Na}_{0.3}(\text{Mg}, \text{Li})\text{Si}_4\text{O}_{10}(\text{OH})_2$	-
	Saponite $(\text{Ca}, \text{Na})_{0.3}(\text{Mg}, \text{Fe(II)}, \text{Fe(III)})_3(\text{Si}, \text{Al})_4\text{O}_{10}(\text{OH})_2 \cdot 4(\text{H}_2\text{O})$	≤ 3:4
Diocahedral smectites	Nontronite $(\text{Na}, \text{Ca}, \text{K})_{0.5}(\text{Si}_7\text{Al}_{0.8}\text{Fe}_{0.2})(\text{Fe}_{3.5}\text{Al}_{0.4}\text{Mg}_{0.1})\text{O}_{20}(\text{OH})_4$	~1:2
	Montmorillonite	

Precipitation of iron silicates always correlates to more extensive glass alteration; near these phases, the gel on the surface of the glass is always more developed than when they are absent. These ferrosilicates thus have the same effect as other secondary phases, such as zeolites, which consume silicon and inhibit the effects of solution saturation, except that their formation is conditioned by the flux of iron released in solution. That means that it depends on the quantity of iron remaining, and on its solubility. Note also that the influence of iron on glass alteration is predominant compared to the influence of the altering solution (McVay and Buckwalter, 1983) (Figure 2-17). When glass is leached in the absence of iron, it has been demonstrated that the initial composition of the altering solutions affects the alteration: solutions simulating basaltic water or tuff water do not lead to such a large release of species into solution as deionised water, since such solutions are charged with elements, i.e. that they are close to saturation. In the presence of iron, this effect is eliminated since the formation of iron silicates consumes the elements present in solution; all solutions rapidly become equivalent to deionised water and the glasses are altered at the same rate in different media.

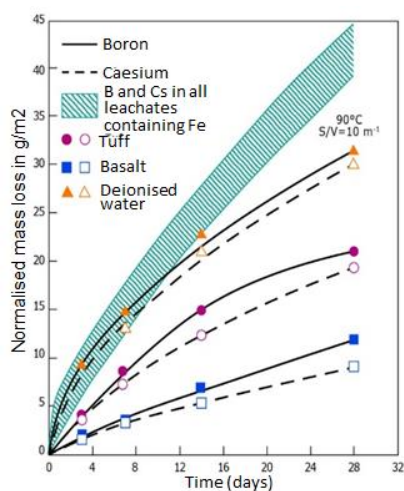


Figure 2-17 – Evolution of mass losses for different alteration solutions in the presence and absence of iron (McVay and Buckwalter, 1983).

#### 2.2.4.3 The influence of CPs on the morphology and structure of the gel layer

The interactions between silicon and CPs, playing the role of “silicon sink”, could act to the detriment of the gel's protective properties, reducing its content of cross-linking elements (Si, Al, etc.). This change in the chemical composition of the gel layer may have a direct impact on its morphology (porosity), and may also affect its structure (local environments).

After close observation of the alteration layers on SON68 glass, a number of studies found that the appearance of the gel seems to be affected by the presence of iron. De Combarieu et al. (2011) suggested that the major alteration of glass in the presence of iron is due to the gel layer having a greater porosity, thus reducing its protective nature. Rébiscoul et al. (2015), Reiser et al. (2017) and De Echave et al. (2019) also found that the gel layer was enriched in iron during glass alteration in the presence of magnetite or iron. When iron corrodes at the same time as the glass is altered, a large quantity of iron is dissolved, from the first stage of hydrolysis at  $t_0$  (Figure 2-1). In this case, as the gel becomes depleted in silicon (relative to pristine glass) it also retains iron; according to Reiser et al. (2017), this enrichment may only affect part of the gel. A number of in-depth examinations of alteration gels developed in glass-iron-clay systems confirm this phenomenon, as the one carried out by Dillmann et al. (2016). They found that the gel was enriched in iron during glass alteration in the presence of iron or of synthetic corrosion products, but not of archaeological corrosion products. Electron diffraction patterns reveal the presence of structural nano-crystals similar to greenalite ( $\text{Fe}_{2-3}\text{Si}_2\text{O}_5(\text{OH})_4$ ) (Figure 2-18), possibly precipitated thanks to a highly porous structure of the gel layer.

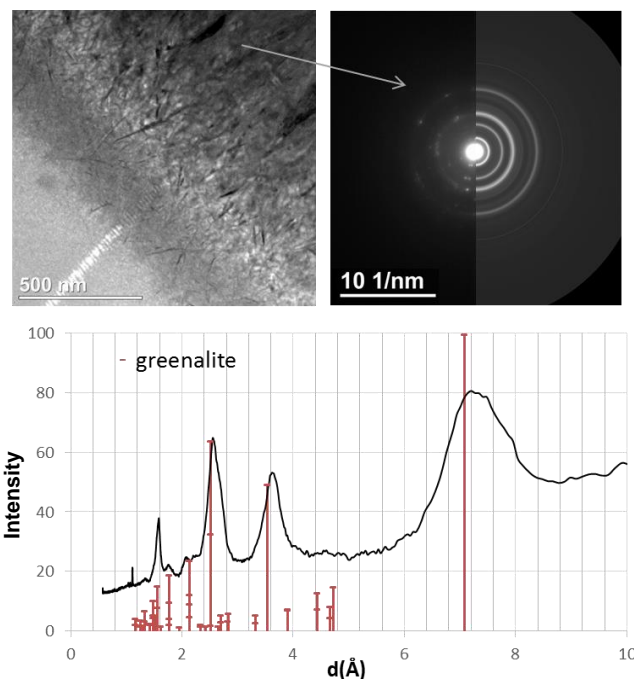


Figure 2-18 – Electron Diffraction Spectrum on nano-crystals formed inside the gel during alteration of a crack formed by two samples of SON68 glass and initially containing a sheet of iron, after 6 months of alteration (at 50 °C, groundwater) (Dillmann et al., 2016).

Further studies, on the characterisation of glass – iron interfaces in glass – iron – claystone systems using STXM (Scanning Transmission X-ray Microscope), a technique used to probe the structural environment of iron at nanometric scale, were able to identify the speciation of iron in iron corrosion and glass alteration products. These studies were conducted i) on ferro-calcium silicate glass as part of the investigation on archaeological analogues (slag from a former ironworks, altered over 400 years in an iron-rich and anoxic environment) (Michelin, 2011; Michelin et al., 2013a; b), and ii) on SON68 glass altered at 50 °C in the presence of iron and claystone (Burger et al., 2013; Carrière, 2017).

The gel formed close to iron contains significant quantities of iron (between 15% and 35% of its mass). It seems that iron is incorporated in the form of a mix of Fe(II) and Fe(III), which has a similar absorption signal to ferrosilicates precipitated close to the alteration layer (Michelin, 2011; Michelin et al., 2013a; b; Burger et al., 2013; Carrière, 2017).

Burger et al. (2013) used STXM analysis to find that iron is in the form of an Fe(II)/Fe(III) mix (in a ratio of between 1:1.92 and 1:1.66) similar to that which is characteristic of iron silicates formed in surface tests: the hypothesis put forward is that the dissolved iron reacts with the silicon released from the glass to form nano-crystalline iron silicates within the amorphous gel. This hypothesis now seems to be backed up by the characterisation of certain samples of altered glass (cf. Figure 2-16 and Figure 2-19).

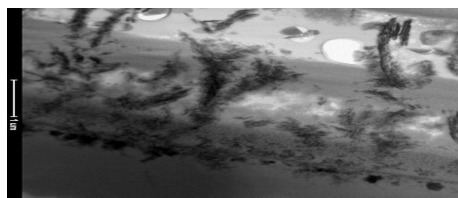


Figure 2-19 – SEM observations of a FIB foil sampled from the surface of grains of glass altered in contact with an iron powder at 50 °C by the CO<sub>x</sub> water in a vertical borehole at the Bure underground research laboratory (MVE in-situ "transient phase" test) for ~24 months (CEA Data).

The impact that these nano-crystalline phases may have on the properties of the gel has not yet been clearly assessed. The presence of iron changes the equilibrium between the glass and the solution, and alters the stoichiometry of the gel. Furthermore, the iron precipitating in the form of ferrosilicates may influence the depolymerisation of the silicate network.

Burger et al. (2013) suggest a possible clogging of porosity and, as a result, a decrease in the diffusion coefficient of the reactive species, but point out that the alterations observed on analogues suggest that this effect does not seem to be predominant. Indeed, Michelin et al. (2015), who carried out a detailed study on blast-furnace slag, detected deuterium diffusion inside cracks that were nonetheless filled with alteration products (Figure 2-20 and Figure 2-21).

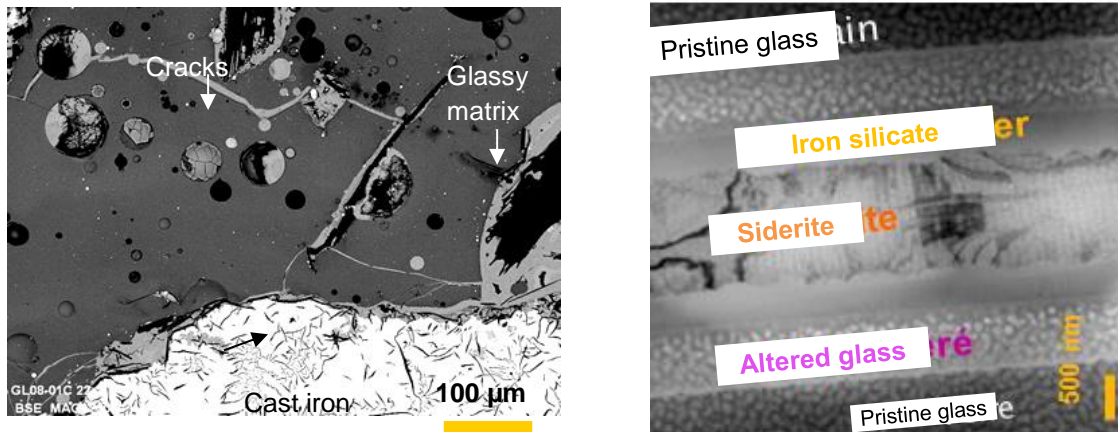


Figure 2-20 – SEM and TEM observations of blast-furnace slag: network of cracks and cavities filled with corrosion products (left); corrosion facies in a crack (right) (Michelin, 2011)

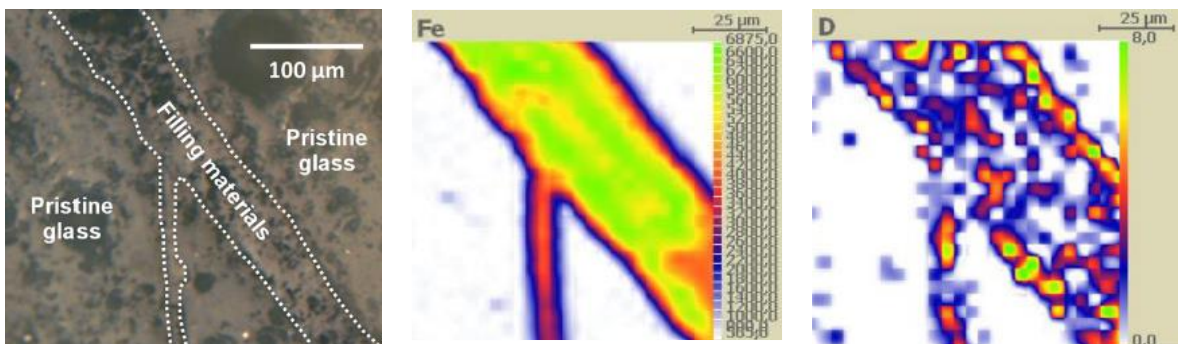


Figure 2-21 – Optical microscope image and elemental distribution maps of iron and deuterium on a cross-section of blast-furnace slag block after being immersed in D<sub>2</sub>O for one week (Michelin et al., 2015)

#### 2.2.4.4 Impact of corrosion *in situ* on pH

In addition to the consumption of silicon, the iron corrosion reaction also affects the pH of the solution. The formation of iron CPs, when it occurs at the same time as glass alteration, tends to raise the pH (Bildstein et al., 2007), thereby favouring glass alteration and the formation of magnesium silicates. For information, the table below (Table 2 5) gives some pH values measured at 50 °C during leaching tests in the laboratory (CEA data). The pH values range between 7.5 and 8.7 in the absence of iron (it would appear that the pH in these experiments was governed by the presence of the glass), and between 8 and 9.7 in the presence of metallic iron.

Table 2-6 – pH values measured in leachates in different laboratory leaching tests at 50 °C (CEA data).

System	pH in the absence of iron	pH in the presence of iron
glass in CO <sub>x</sub> water (static)	8.3	9-9.2
glass in CO <sub>x</sub> water (dynamic)	8.2-8.7	8-9.7

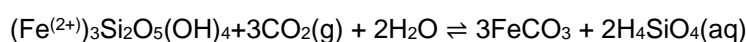
This increase in the pH is due to the formation of hydroxyl ions OH<sup>-</sup> which accompanies the anoxic corrosion of iron in an aqueous medium (the buffer effect of the glass is then no longer strong enough to regulate the pH), expressed by:



The pH is also higher in glass alteration tests in presence of magnetite (8.2 < pH < 9.0 at 50 °C) than in leaching tests on glass alone (see Figure 2-6). This rise in pH is thus the result of a larger quantity of altered glass, i.e. of a greater quantity of alkaline species being released. Tests in diffusion cells in which glass and magnetite are separated by a material that slows down transport sufficiently (two sintered filters) also found this CPs effect on pH (see Figure 2-6).

This variation in the pH may be localised depending on the test set-up and may, potentially, impact on the nature of the corrosion products formed. In addition, studies carried out by Dillmann et al. (2016) suggest that the nature of the iron silicates may vary in glass-iron systems, even at very short distances: they thus observed greenalite inside the gel at the surface of the altered glass and a structural phase similar to nontronite in proximity to iron corrosion products.

The nature and the crystallinity of these phases thus seem to be highly dependent on the local concentrations of iron and silicon, on the pH, and even on the partial pressure of gaseous CO<sub>2</sub> if we take into account the stability of greenalite compared to siderite (Dillmann et al., 2016):



## 2.3 Application of conceptual and mathematical models

Among the different mechanisms involved in glass/steel interactions, some specific models have been developed in order to take into account silicon sorption on CPs (section 2.3.1).

Taking into account the potential formation of iron silicates requires to identify the neoformed phases (section 2.3.2) and include them into the thermodynamic databases associated to the reactive transport model used in modelling exercises. Their formation will depend on the evolution of chemical conditions (pH) in the surrounding of glass that will depend, among other things, on glass alteration and corrosion kinetics.

As mentioned in section 2.2.4.3, the impact of the enrichment of gel in iron, with the potential formation of nano-crystalline iron silicate phases, has not yet been clearly assessed. Consequently, the current description of the gel that forms at the glass surface, e.g., in the GRAAL model (CEA model of nuclear glass alteration), does not include iron incorporation in the gel structure, yet.

### 2.3.1 Sorption models

To date, three models have been developed to simulate the impact of CPs on glass alteration. These include: (i) a model developed at Subatech (Grambow, 1987a; Grambow, 1987b; Mayant et al., 2008, 2009); (ii) a model developed in 2006 by EDF (Philippini et al., 2006; De Windt et al., 2006); and (iii) a study led by Andra (Jordan et al., 2007; Jordan et al., 2009). Some of these models have been used, as part of the European programme, NF-PRO, to incorporate the effect of corrosion products in the computation codes for modelling the coupling between chemistry and transport (PHREEQC (Ribet and Grambow, 2007) and HYTEC (Bildstein et al., 2007)).

The basic hypotheses on which these models are based have many things in common. In all these models, CPs are primarily simulated by magnetite (and occasionally by siderite or goethite). The hypothesis is that sorption of silicon occurs on the CPs surface. Sorption is simulated using a surface complexation model, in which surface sites are thought of as complexing ligands in solution. Saturation of the solution in silicon only occurs once all the sorption sites are occupied. Thus, in these models, the effect of the CPs is directly dependent on the specific surface area.

However, while they are based on these common hypotheses, the three models differ in various ways:

- the choice of the type of complexes formed (stoichiometry of Si-based compounds);
- the choice of parameters related to CPs (surface density, specific surface area);
- the choice of thermodynamic constants: acidity constants (protonation/deprotonation reaction), surface complexation constant.

The first model developed by Subatech was originally based on the hypothesis that silicon is adsorbed in a mono-molecular layer (Grambow, 1987a; Grambow, 1987b). Compared with experimental data, this hypothesis proved consistent for short time periods (around 1 year), but, for longer periods, provides a more significant rate drop than observed in experiments (Grambow, 1987a; Grambow, 1987b). To explain this difference, the hypothesis that silicon is sorbed in multiple layers seems to have been widely accepted since then (Grambow, 1987a; Grambow, 1987b; Mayant et al., 2008; Mayant, 2009; Jordan et al., 2007; Jordan et al., 2008; Jordan et al., 2009) (even if the precipitation of a silicate phase, extending the consumption of silicon, cannot be excluded). This new hypothesis is also proposed in two studies (Jordan, 2008, confirmed by Mayant, 2009). Based on electrochemical titration, these studies showed that the magnetite's capacity to sorb silicon seems to exceed proton adsorption capacity, and seems to reveal a process whereby silicon is sorbed on magnetite in two stages: the first resulting in a mono-molecular layer of silicon, and the second in a multi-molecular layer of silicon on the surface. Observations made by Rébiscoul et al. (2015), finding silicon enrichment at the surface of magnetite at a thickness of 10 to 60 nm, seem to confirm this approach, and even indicate the precipitation of SiO<sub>2</sub>.

In a second model developed by EDF (Philippini, et al., 2006), adsorption is simulated by bidentate complexes (an approach that proves more reliable than taking monodentate complexes<sup>2</sup> into consideration), by taking into account only neutral species, according to the following reaction:



The parameters related to the sorption capacity of CPs and to thermodynamic constants are determined by experiment (acidity constants logK<sub>a1</sub> and logK<sub>a2</sub> of -3.87 and -8.89, respectively). This model gives a reduction in sorption as the pH rises (> 10). This desorption of silica is related to the fact that the OH<sup>-</sup> sorption sites are favoured at these pH values.

The third model, developed by Jordan et al., (2007, 2008), takes into account, in addition to neutral sites, sorption at negatively charged sites, through two silicon surface complexes on magnetite:  $\equiv\text{FeH}_3\text{SiO}_4$  and  $\equiv\text{FeH}_2\text{SiO}_4^-$ . Three surface complexation models were tested (i.e. Non Electrostatic Model (NEM), Constant Capacitance Model (CCM), Diffuse Double Layer Model (DDLm)). The model that proved most consistent with experimental data was the DDLm, which gives the following constants:



So, silicon adsorption on magnetite can be modelled using a bidentate complex,  $(\equiv\text{SO})_2\text{Si}(\text{OH})_2$ , or two monodentate complexes,  $\equiv\text{SH}_3\text{SiO}_4$  and  $\equiv\text{SH}_2\text{SiO}_4^-$ .

<sup>2</sup> The link between total density of surface sites and those surface sites interacting with silicon was made as a result of a number of tests based on acid–base titration of oxide surfaces. The number of sites accessible to silicic acid represents between 25 and 100 % of the density of proton-active sites. The most reliable silicon sorption model therefore seems to be the one that takes bidentate complexes into account (Philippini et al., 2006).

The CEA has modelled some of its tests by coupling the GRAAL model with a model of silicon sorption on magnetite based on the work of Ribet and Grambow (2007) and Jordan et al. (2007). The results show that the sorption process does indeed account for glass alteration in the first few dozen days (Figure 2-22). However, in the longer term, beyond a certain saturation point on the magnetite sorption sites, it seems that some other process is at work. Two hypotheses have been proposed (Godon et al., 2013; Rébiscoul et al., 2015):

- as previously observed by Inagaki et al. (1996), the partial transformation of magnetite into another iron oxide (goethite under the experimental conditions investigated by the CEA) with a higher sorption capacity than magnetite;
- silica could lead (in addition to the formation of multi-layers), with the Fe<sup>2+</sup> released by the slow dissolution of magnetite, to the precipitation of iron silicates, as suggested by Grambow (1987b) and Jordan (2008).

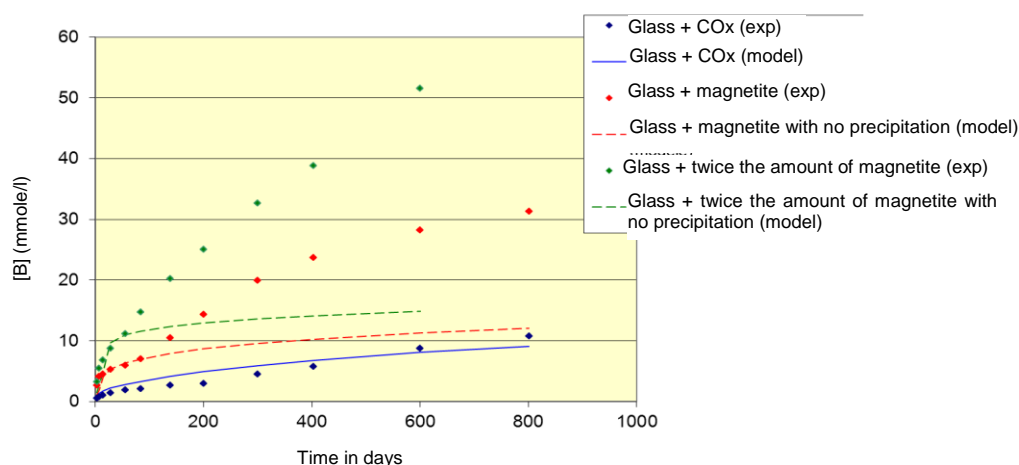


Figure 2-22 – Comparison of the evolution of experimental and simulated boron concentrations by taking into account the sorption of Si on magnetite and the precipitation of magnesium silicates during alteration of SON68 glass powder in the presence of magnetite in CO<sub>x</sub> water at 50 °C (Case 1: 10 g of magnetite, Case 2: 20 g of magnetite). All this is compared to glass alteration in CO<sub>x</sub> water, only.

### 2.3.2 Precipitation of iron silicates

For a better description of the impact of CPs on glass alteration, the CEA coupled the mechanism of silicon sorption on magnetite with precipitation of iron silicates in its models. Since no neoformed phases were found by experiment, most probably because they were only present in very small quantities, these silicates were initially assimilated with Na-nontronite ( $\text{Na}_{0.33}\text{Fe}_2(\text{Si}_{3.67}\text{Al}_{0.33})\text{OH}_{14.68}$ , Si/Fe ratio = 1.835). Thanks to this coupling, it was possible to model the quantities of glass altered over the duration of the experiment (Figure 2-23). These results do not exclude the possibility of magnetite being transformed into goethite or hematite, for example, phases which are thermodynamically more stable and which have greater sorption capacities than magnetite.

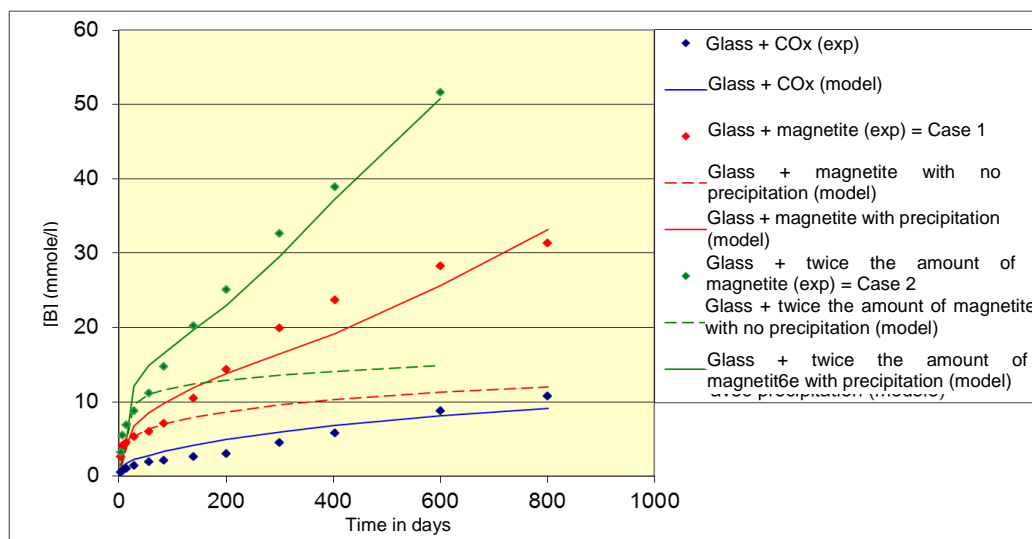


Figure 2-23 – Comparison of the evolution of experimental and simulated concentrations of boron by taking into account Si sorption on magnetite and the precipitation of an iron silicate (nontronite  $\text{Na}_{0.33}\text{Fe}_2(\text{Si}_{3.67}\text{Al}_{0.33})\text{OH}_{14.68}$ ,  $\text{Si}/\text{Fe} = 1.835$ ) during alteration of a glass powder in the presence of magnetite in  $\text{CO}_x$  water at 50 °C (Case 1: 10 g of magnetite, Case 2: 20 g of magnetite). All this is compared to glass alteration in  $\text{CO}_x$  water, only (Godon et al., 2013).

## 2.4 Resume

The interactions between silicon released during glass alteration and iron or CPs influence the glass dissolution kinetics. The main phenomenon related to this is the consumption of silicon (and other cross-linking elements such as Al and Ca), which act to the detriment of the formation of a protective gel: it delays reaching the conditions of saturation required for the formation of a passivating gel, which leads to faster alteration rates than in the absence of iron or corrosion products. Nonetheless, the impact of CPs is conditioned by the transport of elements, mainly iron and silicon, in solution, and seems to be significantly weaker when the glass is far from the iron source (corrosion products or iron).

Two mechanisms may be involved in this consumption: (i) sorption of these elements on the surface sites of the CPs, and (ii) precipitation of ferrosilicates. These two processes occur at quite different scales. The impact of sorption is easy to quantify if the nature of the CPs is known: the time of sorption is proportional to CP sorption capacity. Secondly, sorption is maintained for a very short period of time relative to the time scales considered for geological disposal. The precipitation of ferrosilicates, on the other hand, may be less extensive in the short-term but, potentially, not insignificant in the long term. Last, in direct proximity to an iron source, the gel that forms at the glass surface may also be highly enriched in iron, due to the precipitation of nano-crystalline phases within the gel. This retention of iron in the gel may also impact on the structure of the gel and, therefore, on its protective properties.

In general, the impact of these different mechanisms is highly dependent on the geometry of the system: how the different materials are configured (in stacks or as a homogeneous mix) and their dimensions (glass surface-to-solution volume ratio, glass surface-to-iron surface ratio). For those tests carried out in the laboratory with a stack geometry, the impact of iron is only seen locally, close to the iron (within a few micrometres). Given that iron has a very localised sphere of influence in this type of test set-up, the impact of CPs on glass alteration is hidden at the overall scale. Consequently, the concentrations measured in solution during alteration experiments reflect the total alteration of the glass sample and do not necessarily reveal the influence of iron.

These observations also reveal that the precipitation of iron silicates is conditioned by the fluxes of dissolved iron and silicon. The greater the distance from the iron, the less ferrosilicates there are and the less the grains of glass are altered. Furthermore, while the glass is always altered more locally in

proximity to iron, some authors also note a reciprocal effect: when glass and iron are placed together, McVay and Buckwalter (1983) also observed increased corrosion of the iron.

The silicon released during glass alteration can also interact with other elements transported in the groundwater such as magnesium, whence a distribution/competition between iron silicates and magnesium silicates.

To conclude, assessing the impact of CPs on glass alteration requires an understanding of the nature of the CPs, their position in relation to the glass, and the transport conditions within the system investigated, bearing in mind the influence of physical and chemical conditions (properties of the host rock, composition of the porewater, redox conditions, pH) and hydrodynamics on glass alteration processes. Glass/iron/claystone interactions occur as a result of very localised conditions which depend on the dissolution rates of iron and glass, and on the transport of different elements (including Fe, Si and Mg) in solution.

## 2.5 References

Aréna, H., Godon, N., Rébiscoul, D., Podor, R., Garcès, E., Cabie, M., Mestre, J.-P. 2016. Impact of Zn, Mg, Ni and Co elements on glass alteration: additive effects. *Journal of Nuclear Materials* 470, 55-67.

Aréna, H., 2017. Effets cumulatifs et compétitifs des éléments chimiques sur l'altération des verres nucléaires. Thèse de l'Université de Montpellier, rapport CEA-R-6450, Montpellier, France.

Aréna, H., Godon, N., Rébiscoul, D., Frugier, P., Podor, R., Garcès, E., Cabie, M., Mestre, J.-P., 2017. Impact of iron and magnesium on glass alteration: characterization of the secondary phases and determination of their solubility constants. *Applied Geochemistry* 82, 119-133.

Aréna, H., Rébiscoul, D., Podor, R., Garcès, E., Cabie, M., Mestre, J.-P., Godon, N., 2018. Impact of Fe, Mg and Ca elements on glass alteration: interconnected processes. *Geochimica Cosmochimica Acta* 239, 420-445.

Azoulay, I., Rémazeilles, C., Refait, P., 2012. Determination of standard Gibbs free energy of formation of chukanovite and Pourbaix diagrams of iron in carbonated media. *Corrosion Science* 58, 229-236.

Bart, G., Zwicky, H.U., Aerne, E.T., Graber, T.H., Z'Berg, D., Tokiwai, M., 1987. Borosilicate glass corrosion in the presence of steel corrosion products. *Materials Research Society Symposium Proceedings* 84, 459-470.

Bildstein, O., Trotignon, L., Pozo, C., Jullien, M., 2007. Modelling glass alteration in an altered argillaceous environment. *Journal of Nuclear Materials* 362, 493-501.

Björner, I.K., Christensen, H., Hermansson, H.P., Tsukamo, M., Werme, L., 1989. Corrosion of radioactive, crushed waste glass. *Materials Research Society Symposium Proceedings* 127, 113-120.

Carlson, L., Karnland, O., Oversby, V.M., Rance, A.P., Smart, N.R., Snellman, M., Vähänen, M., Werme, L.O., 2007. Experimental studies of the interactions between anaerobically corroding iron and bentonite. *Physics and Chemistry of the Earth* 32, 334-345.

Carrière, C., 2017. Influence de la corrosion du fer sur les processus d'altération du verre: approche analytique multi-échelle, Thèse de l'Université Pierre et Marie Curie, Paris, France.

Carrière, C., Dillmann, P., Foy, E., Neff, D., Dynes, J.J., Linard, Y., Michau, N., Martin, C., 2019. Use of nanoprobe to identify iron-silicates in a glass/iron/argillite system in deep geological disposal. *Corrosion Science* 158, 108104.

Chave, T., Frugier, P., Gin, S., Ayrat, A., 2011. Glass-water interphase reactivity with calcium rich solutions. *Geochimica Cosmochimica Acta* 75, 4125-4139.

Chomat, L., 2008. Compréhension de l'altération à long terme des colis de verre R7/T7: étude du couplage chimie transport dans un milieu fissuré. Thèse de l'Université Paris VI, Paris, France.

Corkhill, C.L., Cassingham, N.J., Heath, P.G., Hyatt, N.C., 2013. Dissolution of UK High-level waste glass under simulated hyperalkaline conditions of a collocated geological disposal facility. *International Journal of Applied Glass Science*, 4, 341-356.

De Combarieu, G., Neff, D., Foy, E., Gin, S., Barboux, P., 2006. Micro-beam analyses of glass and iron corrosion layers in clayey rock. *Goldschmidt Conference Abstracts*.

De Combarieu, G., 2007. Altération du verre de confinement de déchets type R7/T7 en conditions de stockage géologique. Thèse de l'Université Paris XI – Orsay, Paris, France.

De Combarieu, G., Barboux, P., Minet, Y., 2007. Iron corrosion in Callovo-Oxfordian argillite: from experiments to thermodynamic/kinetic modeling. *Physics and Chemistry of the Earth* 32, 346-358.

De Combarieu, G., Schlegel, M., Neff, D., Foy, E., Vantelon, D., Barboux, P., Gin, S., 2011. Glass–iron–clay interactions in a radioactive waste geological disposal: an integrated laboratory scale experiment. *Applied Geochemistry* 26, 65-79.

De Echave, T., Tribet, M., Gin, S., Jégou, C., 2019. Influence of iron on the alteration of the SON68 nuclear glass in the Callovo-Oxfordian groundwater. *Applied Geochemistry* 100, 268-278.

De Windt, L., Leclercq, S., van der Lee, J., 2006. Assessing the durability of nuclear glass with respect to silica controlling processes in a clayey underground disposal. *Materials Research Society Symposium Proceedings* 932, 313-320.

Debruyne, W., Dresselaers, J., Vermeiren, Ph., Kelchtermans, J., Tas, H., 1991. Corrosion of container and infrastructure materials under clay repository conditions. *Rapport CEC EUR-13667*.

Depierre, S., 2013. Etude des mécanismes d'altération du verre par des eaux cimentaires. Thèse de l'Université de Montpellier II, Rapport CEA-R-6336, Montpellier, France.

Depierre, S., Angeli, F., Frizon, F., Gin, S., 2013. Antagonist effects of calcium on borosilicate glass alteration. *Journal of Nuclear Materials* 441, 402-410.

Dillmann, P., Gin, S., Neff, D., Gentaz, L., Rébiscoul, D., 2016. Effect of natural and synthetic iron corrosion products on silicate glass alteration processes. *Geochimica Cosmochimica Acta* 172, 287-305.

Ferrand, K., Lemmens, K., Depierre, S., 2011. The interaction between nuclear waste glass and cement. *NUWCEM 2011 - 1st International Symposium on Cement-based Materials for Nuclear Wastes*, Avignon, France.

Ferrand, K., Liu, S., Lemmens, K., 2013. The interaction between nuclear waste glass and ordinary Portland cement. *International Journal of Applied Glass Science* 4, 328-340.

Fleury, B., 2013. Etude de la sensibilité de la vitesse résiduelle d'altération et de ses paramètres de modélisation à la composition des verres. Thèse de L'Université de Montpellier II, Montpellier, France.

Fournier, M., 2015. Etude des mécanismes à l'origine des reprises d'altération. Modélisation et évaluation de l'impact sur les verres de confinement, Thèse de l'Université Montpellier, Montpellier, France.

Gin, S., Beaudoux, X., Angéli, F., Jégou, C., Godon, N., 2012. Effect of composition on the short-term and long-term dissolution rates of ten borosilicate glasses of increasing complexity from 3 to 30 oxides. *Journal of Non-Crystalline Solids* 358, 2559-2570.

Gin, S., Abdelouas, A., Criscenti, L.J., Ebert, W.L., Ferrand, K., Geisler, T., Harrison, M.T., Inagaki, Y., Mitsui, S., Mueller, K.T., Marra, J.C., Pantano, C.G., Pierce, E.M., Ryan, J.V., Schofield, J.M., Steefel, C.I., Vienna, J.D., 2013. An international initiative on long-term behaviour of high-level nuclear waste glass. *Materials Today* 16, 243-248.

Gin, S., 2014. Open scientific questions about glass corrosion. *Procedia Materials Sciences* 7, 163-171.

- Gin, S., Jollivet, P., Fournier, M., Angéli, F., Frugier, P., Charpentier, T., 2015a. Origin and consequences of silicate glass passivation by surface layers. *Nature Communication* 6.
- Gin, S., Jollivet, P., Fournier, M., Berthon, C., Wang, Z., Mitroshkov, A., Zhu, Z., Ryan, J.V., 2015b. The fate of silicon during glass corrosion under alkaline conditions: a mechanistic and kinetic study with the International Simple Glass. *Geochimica Cosmochimica Acta* 151, 68-85.
- Godon, N., Vernaz, E. 1990. R7/T7 nuclear waste glass behavior in moist clay: role of the clay mass/glass surface area ratio. *Materials Research Society Symposium Proceedings* 176, 319-326.
- Godon, N., Adriambololona, Z., Vernaz, E., 1991. Effect of a siliceous additive in a clay engineered barrier on aqueous corrosion of R7/T7 nuclear waste glass. *Materials Research Society Symposium Proceedings* 257, 135-141.
- Godon, N., Gin, S., Rébiscoul, D., Frugier, P., 2013. SON68 glass alteration enhanced by magnetite, *Procedia Earth and Planetary Sciences* 7, 300-303.
- Grambow, B., 1987a. Nuclear waste glass dissolution: Mechanism, model and experiment. Report to JSS Project Phase IV. Report No. JSS-87-02.
- Grambow, B., Zwicky, H.U., Bart, G., Björner, I.K., Werme, L.O., 1987b. Modeling the effect of iron corrosion products on nuclear glass performance. *Materials Research Society Symposium Proceedings* 84, 471-481.
- Grambow, B., Lemmens, K., Minet, Y., Poinssot, C., Spahiu, K., Bosbach, D., Cachoir, C., Casas, I., Clarens, F., Christiansen, B., de Pablo, J., Ferry, C., Giménez, J., Gin, S., Glatz, J.P., Gago, J.A., Gonzalez Robles, E., Hyatt, N.C., Inglesias, E., Kienzler, B., Luckscheiter, B., Martinez-Esparza, A., Metz, V., Ödegaard-Jensen, A., Ollila, K., Quiñones, J., Rey, A., Ribet, S., Rondinella, V.V., Skarnemark, G., Wegen, D., Serrano-Purroy, D., Wiss, T., 2008. NF-PRO Final Synthesis Report RTD Component 1: Dissolution and release from the waste matrix.
- Grauer, R., 1984. Behältermaterialien für die Endlagerung hochradioaktiver Abfälle: Korrosionschemische Aspekte. EIR-Bericht Nr.523, Würenlingen, Switzerland.
- Honda, A., Teshima, T., Tsurudome, K., Ishikawa, H., Yusa, Y., Sasaki, N., 1991. Effect of compacted bentonite on the corrosion behavior of carbon steel as geological isolation overpack material. *Materials Research Society Symposium Proceedings* 212, 287-294.
- Inagaki, Y., Ogata, A., Furuya, H., Idemitsu, K., Banba, T., Maeda, T., 1996. Effects of redox condition on waste glass corrosion in the presence of magnetite. *Materials Research Society Symposium Proceedings* 412, 257-264.
- Jordan, N., Marmier, N., Lomenech, C., Giffaut, E., Ehrhart, J., 2007. Sorption of silicates on goethite, hematite, and magnetite: experiments and modelling. *Journal of Colloid and Interface Sciences* 312, 224-229.
- Jordan, N., 2008. Influence de l'acide silicique sur la rétention du sélénium (IV) sur des oxydes de fer. Thèse de l'Université de Nice Sophia-Antipolis, Nice, France.
- Jordan, N., Lomenech, C., Marmier, N., Giffaut, E., Ehrhart, J., 2009. Sorption of selenium(IV) onto magnetite in the presence of silicic acid. *Journal of Colloid and Interface Sciences* 329, 17-23.
- Kim, S.S., Lee, J.G., Choi, J.K., Lee, G.H., Chun, K.S., 1997. Effects of metals, metal oxides and metal hydroxide on the leaching of simulated nuclear waste glass. *Radiochimica Acta* 79, 199-205.
- Kursten, B., Van Iseghem, P., 1998. Geological disposal conditioned high-level and long lived radioactive waste. In situ experiments, Rapport SCK-CEN R-3247, SCK CEN, Mol, Belgium.
- Kursten, B., Van Iseghem, P., 1999. In situ corrosion studies on candidate container materials for the underground disposal of high-level radioactive waste in Boom clay. Congrès Corrosion Nace, communication n°473, San Antonio.

- Lemmens, K., 2001. The effect of clay on the dissolution of nuclear waste glass. *Journal of Nuclear Materials* 298, 11-18.
- Leon, Y., Dillmann, P., Neff, D., Schlegel, M., Foy, E., Dynes, J.J., 2017. Interfacial layers at a nanometre scale on iron corroded in carbonated anoxic environments. *RSC Advances* 7, 20101.
- Liu, S., Ferrand, K., Lemmens, K., 2015. Transport- and surface reaction-controlled SON68 glass dissolution at 30 °C and 70 °C and pH = 13.7. *Applied Geochemistry* 61, 302-311.
- Maraghechi, H., Rajabipour, F., Pantano, C.G., Burgos, W.D., 2016. Effect of calcium on dissolution and precipitation reactions of amorphous silica at high alkalinity. *Cement and Concrete Research* 87, 1-13.
- Marsh, G.P., Taylor, K.J., 1988. An assessment of carbon steel containers for radioactive waste disposal. *Corrosion Science* 28, 289-320.
- Mayant, C., 2009. Étude des propriétés de rétention et de transport de la magnétite dans un état compacté. Thèse de l'Université de Nantes, Nantes, France.
- Mayant, C., Grambow, B., Abdelouas, A., Ribet, S., Leclercq, S., 2008. Surface site density, silicic acid retention and transport properties of compacted magnetite powder. *Physics and Chemistry of the Earth* 33, 991-999.
- McKinley, I.G., 1985. The Geochemistry of the Near Field. Nagra Technical Report NTB 84-48, Nagra, Baden, Switzerland.
- McVay, G.L., Buckwalter, C.Q., 1983. Effect of iron on waste-glass leaching. *Journal of the American Ceramic Society* 66, 170-174.
- Michelin, A., 2011. Altération pluriséculaire des systèmes verre/fer en milieu anoxique: rapport des analogues archéologiques à la compréhension des mécanismes. Thèse de l'Université Paris VI, Paris, France.
- Michelin, A., Burger, E., Leroy, E., Foy, E., Neff, D., Benzerara, K., Dillmann, P., Gin, S., 2013a. Effect of iron metal and siderite on the durability of simulated archeological glassy material. *Corrosion Science* 76, 403-414.
- Michelin, A., Burger, E., Rébiscoul, D., Neff, D., Bruguier, F., Drouet, E., Dillmann, P., Gin, S., 2013b. Silicate glass alteration enhanced by iron: origin and long-term implications. *Environmental Science and Technology* 47, 750-756.
- Michelin, A., Leroy, E., Neff, D., Dynes, J.J., Dillmann, P., Gin, S., 2015. Archaeological slag from Glinet: an example of silicate glass altered in an anoxic iron-rich environment. *Chemical Geology* 413, 28-43.
- Mitsui, S., Aoki, R., 2001. Effect of a siliceous additive on aqueous alteration of waste glass with engineered barrier materials. *Journal of Nuclear Materials* 298, 184-191.
- Ngo, V.V., Clément, A., Michau, N., Fritz, B., 2015. Kinetic modeling of interactions between iron, clay and water: comparison with data from batch experiments. *Applied Geochemistry* 53, 13-26.
- Pan, Y.M., Jain, V., Pensado, O., 2003. Degradation of high-level waste glass under simulated repository conditions. *Journal of Non-Crystalline Solids* 319, 74-88.
- Paul, A., 1977. Chemical durability of glasses; a thermodynamic approach. *Journal of Materials Science* 12, 2246-2268.
- Philippini, V., Naveau, A., Catalette, H., Leclercq, S., 2006. Sorption of silicon on magnetite and other corrosion products of iron. *Journal of Nuclear Materials* 348, 60-69.
- Philippini, V., Naveau, A., Catalette, H., Leclercq, S., 2007. Erratum to "Sorption of silicon on magnetite and other corrosion products of iron". *Journal of Nuclear Materials* 362, 139.

Rébiscoul, D., Tormos, V., Godon, N., Mestre, J.-P., Cabie, M., Amiard, G., Foy, E., Frugier, P., Gin, S., 2015. Reactive transport processes occurring during nuclear glass alteration in presence of magnetite. *Applied Geochemistry* 58, 26-37.

Reiser, J., Neill, L., Weaver, J., Parruzot, B., Musa, C., Neeway, J., Ryan, J.V., Qafoku, N., Gin, S., Wall, N.A., 2015. Glass corrosion in the presence of iron-bearing materials and potential corrosion suppressors. *Materials Research Society Symposium Proceedings* 1744, 139-144.

Ribet, S., Grambow, B., 2007. Modelling of corrosion, sorption and diffusion processes in the near field. *NF-Pro Deliverable (D-N: 1.3.4)*.

Shade, J.W., Pederson, L.R., McVay, G.L., 1983. Waste glass-metal interactions in brines. In: Wicks, G.G., Ross, W.A. (eds.) *Advances in Ceramics VIII, Nuclear Waste Management*, American Ceramic Society, 358-367.

Schlegel, M.L., Martin, C., Brucker, F., Bataillon, C., Blanc, C., Chorro, M., Jollivet, P., 2016. Alteration of nuclear glass in contact with iron and claystone at 90 °C under anoxic conditions: characterization of the alteration products after two years of interaction. *Applied Geochemistry* 70, 27-42.

Shanggeng, L., Zhaoguang, W.U., Delu, L., 1995. Study of media effect on glass surface. *Materials Research Society Symposium Proceedings* 353, 63-71.

Suzuki-Muresan, T., Abdelouas, A., Landesman, C., Ait-Chaou, A., El Medili, Y., Ribet, S., Perrigaud, K., Shitara, D., Martin, C., Bourbon, X., 2018. Alteration of vitrified intermediate level nuclear waste in alkaline media: effect of cementitious materials, pH and temperature. *RSC Advances* 8, 37665-37680.

Taniguchi, N., Kawasaki, M., Kawakami, S., Kubota, M., 2004. Corrosion behaviour of carbon steel in contact with bentonite under anaerobic condition. *Proceedings of the 2<sup>nd</sup> International Workshop "Prediction of Long Term Corrosion Behaviour in Nuclear Waste Systems"*, Publication Andra, Science and Technology Series, ISBN 2-9510108-6-9.

Utton, C.A., Swanton, S.W., Schofield, J., Hand, R.J., Clacher, A., Hyatt, N.C., 2012. Chemical durability of vitrified wasteforms: effects of pH and solution composition. *Mineralogical Magazine* 76, 2919-2930.

Utton, C.A., Hand, R.J., Bingham, P.A., Hyatt, N.C., Swanton, S.W., Williams, S.J., 2013a. Dissolution of vitrified wastes in a high-pH calcium-rich solution. *Journal of Nuclear Materials* 435, 112-122.

Utton, C.A., Hand, R.J., Hyatt, N.C., Swanton, S.W., Williams, S.J., 2013b. Formation of alteration products during dissolution of vitrified ILW in a high-pH calcium-rich solution. *Journal of Nuclear Materials* 442, 33-45.

Van Iseghem, P., Lemmens, K., Aertsens, M., Gin, S., Ribet, I., Grambow, B., Crovisier, J.L., Del Nero, M., Curti, E., Schwyn, B., Luckscheiter, B., McMennamin, T., 2006. Chemical durability of high-level waste glass in repository environment: main conclusions and remaining uncertainties from the GLASTAB and GLAMOR projects. *Materials Research Society Symposium Proceedings* 932, 293-304.

Vienna, J.D., Ryan, J.V., 2013. Current understanding and remaining challenges in modeling long-term degradation of borosilicate nuclear waste glasses. *International Journal of Applied Glass Science* 4, 283-294.

Werme, L., Björner, I.K., Bart, G., Zwicky, U., Grambow, B., Lutze, W., Ewing, R.C., Magrabi, C., 1990. Chemical corrosion of highly radioactive borosilicate nuclear waste glass under simulated repository conditions. *Journal of Materials Research* 5, 1130-1146.

### 3. Interface "cement/mortar – granite"

Markku Leivo (VTT)

#### 3.1 Processes at the interface

In crystalline rocks the tunnels are sealed with concrete end plugs to ensure mechanical and hydrological isolation of the compartments. In the Finish final HLW repository, several thousand tons of ordinary Portland cement (OPC)–based grouts, shotcrete and rock bolt mortars will be present with bentonite in structural applications. In Finland LLW repository no bentonite is used in the engineered barrier system. Isolation is achieved by cementitious barriers and bedrock. The processes occurring at the interface of cement/mortar – granite can change both the properties of the cementitious material and the granite properties at the interface.

##### 3.1.1 Concrete

Concrete can be an extremely durable material if it is properly designed and produced for the environment in which it has to perform. If either the design and/or production are inadequate, concrete may deteriorate prematurely. For concrete to fulfil the service life, its design must take into account the deterioration process (and rates) affecting the concrete for the given environmental conditions. The rate of deterioration will depend on the type of chemical and/or physical processes that occur simultaneously. Coupled deterioration mechanisms of concrete most often have synergetic effect on the degradation.

Cement-based materials are fundamentally unstable in a long-term perspective. With time the concrete will change properties both as a consequence of recrystallisation and chemical interaction with the environment. The hydration products are stabilized by the high pH within the concrete. Thus, when the cement paste has equilibrated with the environment new phases will form (Lagerblad and Trägårdh, 1994).

Concrete is a multiphase composite material that is porous and strongly basic. The pH of the pore solution is approximately 13 for young hydrated Portland cement concrete. As a result of this, concrete is naturally not in equilibrium with its environment – reacting with the environment has to be seen as normal and not exceptional phenomena. The characteristics of the pore network, dimensions and connectivity of the capillary porosity in particular, determine the processes inside the hydrated cement paste matrix. The two main transport mechanisms for submerged concrete are characterised by diffusion (concentration gradient) and advection (pressure gradient). However, the chemical nature of the cement matrix is also a determining factor of the resistance of concrete to aggressive environments. The chemical composition of the hydrated phases of Portland cement and their proportions inside the matrix – which depend mainly on the composition of the binder (cement and supplementary cementitious materials) – mostly determine the chemical stability of the hydrated cement paste matrix (Alexander et al., 2013).

Water plays a key role in the durability performance of concrete – it is a driving force and an essential part in the chemical reactions between the aggressive substances and the hydrated cement phases. The chemical reactions that occur within concrete are of two types: the dissolution of the hydrated and anhydrous cement phases; and/or the precipitation of newly formed reaction products (Alexander et al., 2013). These reactions often start on the surface of the concrete and progress inwards with time, creating a reacted (deteriorated) layer in the process. The properties of the reacted layer are generally inferior (physical and mechanical characteristics in particular) than those of the unreacted inner concrete. Furthermore, the formation of new reaction products can in some particular cases induce new additional deterioration to the hydrated cement matrix.

##### *Chloride ingress*

Corrosion due to chloride penetration is one of the main causes of concrete degradation worldwide. Concrete itself is not affected by chloride ingress but the steel reinforcement and other steel material inside concrete is corroded due to chlorides. The transport and distribution of chlorides in a concrete

structure are very much a function of the environmental exposure, mainly of the concentration and duration of the solutions in contact with the concrete surface. The conditions vary significantly according to the exposure situations.

### Carbonation

Carbonation occurs when  $\text{CO}_2$  dissolves in the pore solution of cement paste, producing  $\text{CO}_3^{2-}$ , which will react with  $\text{Ca}^{2+}$  and produce  $\text{CaCO}_3$  (calcite). Later, when the CH is consumed, C-S-H is first decalcified and later decomposed. The AFm and AFt phases react with the carbonate anion and form special carbonate species. If pH is lowered even further by additions of more carbon dioxide, these initially formed carbonate species will decompose. The residues from complete carbonation are calcite, amorphous silica, hydrocarboaluminates and different Al- and Fe-hydroxides. The pH value of the carbonated cement paste first drops to around 10 when all the CH is consumed and later to a pH around 8 when the other phases are decomposed. These carbonation reactions are mostly happening in slow rate and only when carbon dioxide is present. This is especially happening when repository is in operation and open in air and also if waste forms  $\text{CO}_2$  as it decomposed.

### Sulphate attack

Sulphate attack in concrete originates mainly from its exterior, but it can also occur internally by a mechanism termed delayed ettringite formation. External attack often arises from an increased sulphate concentration in the service environment. Portland cement concrete is attacked by solutions containing sulphate, such as some natural or polluted ground waters. The damage to concrete structures resulting from external sulphate attack is related to the following factors:

- Transport of ions to the interior of the concrete through the pore system.
- Chemical reactions between sulphate and the solid hydration products of cement.
- Generation of stress in the interior of the concrete as a result of the formation of expansive products.
- Mechanical response of the bulk material resulting from these stresses, such as cracking.
- Characteristics of the concrete components and their proportions.

Expansion is generally related to the formation of ettringite. The overall phase changes occurring as sulphate ions penetrate into cementitious material are well characterised (Figure 3-1).

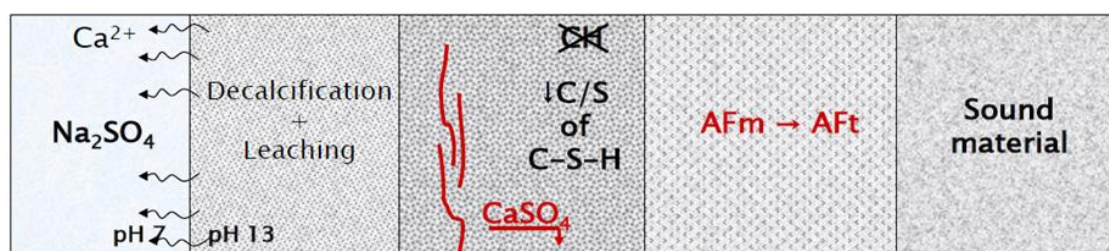


Figure 3-1 – Generic “zones” formed in cementitious materials through ingress of sulphate ions (Alexander et al., 2013).

### Delayed ettringite formation (DEF)

This term is used here to denote the formation of ettringite in concrete, mortar or paste that has been subjected to a temperature high enough to destroy any that was earlier present. The effect can cause expansion or cracking. It has been held partly or wholly responsible for delayed damage in railway sleepers and other precast concrete products. It could also occur in concrete that has been adventitiously heated by the energy evolved in hydration, or by an external source during service.

### Magnesium attack

The attack by Mg ion is particularly dangerous for concrete, as it can cause a complete disintegration of the C-S-H in the long term. However, in environments with high content of chlorides, such as in

seawater, there are some differences in the mechanism of magnesium attack as opposed to a typical sulphate attack.

### *Leaching of cementitious materials*

Leaching causes deterioration of many physical and mechanical properties of cement-based materials such as porosity, elastic modulus, compressive strength, internal friction angle and creep. Moreover, most studies carried out for the investigation of the safety of radioactive waste disposal concrete facilities involve tests and simulations based on attack by pure water. This is a very severe scenario that is implemented, notably to model the long-term behaviour of the concrete exposed to subterranean waters.

Leaching of concrete by percolating or flowing water has sometimes caused severe damage, e.g., in dams, pipes or conduits, and is potentially important for the long-term disposal of nuclear wastes. Pure water may be expected to remove alkali hydroxides, dissolve CH and decompose the hydrated silicate and aluminate phases. For practical purposes, the ultimate residue will consist essentially of hydrous forms of silica, alumina and iron oxide, while all CaO will be lost. By this stage, the cement paste will be disintegrated. The equilibria also suggest that CH will be dissolved before the other phases are attacked, but in practice attack is likely to take place simultaneously, because of the greater specific surface areas of the hydrated silicate and aluminate phases. The schematic evolution of pore solution pH during leaching of OPC based materials by pure water is presented in Figure 3-2.

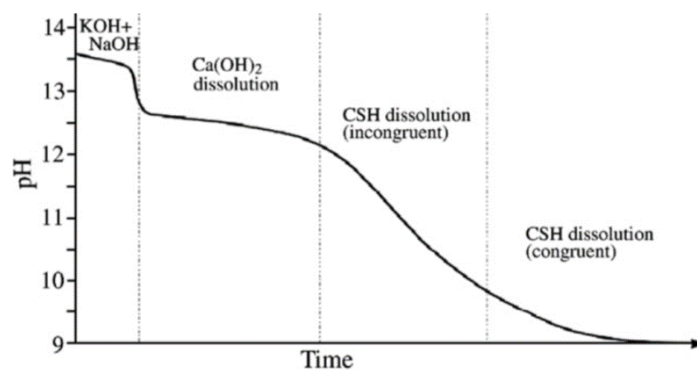


Figure 3-2 – Schematic evolution of pore solution pH during leaching of Portland cement-based materials by pure water (Berner, 1992; Snelman and Vieno, 2005; Cau Dit Coumes et al., 2006).

### *Alkali aggregate reactions (AAR)*

Alkali-aggregate reactions, commonly known as AAR, are chemical reactions that occur between certain types of aggregate minerals and alkali ( $\text{Na}^+$  and  $\text{K}^+$ ) and hydroxyl ( $\text{OH}^-$ ) ions present in the interstitial solution of cement paste in concrete. These dissolution reactions occur due to the high solubility of certain amorphous, disordered or poorly crystallized forms of silica in very alkaline solutions and lead to formation of a hygroscopic alkaline gel.

In general, these reactions are expansive in nature, resulting in internal stresses in concrete and consequently cracking. It is often accompanied by the appearance of efflorescence and exudations on the surface of the concrete. Normally these reactions are not the primary cause of collapse of a structure. However, they significantly decrease the durability of concrete as a result of cracking favouring other processes of deterioration, particularly in the cases of carbonation or chloride penetration resulting in reinforcement corrosion.

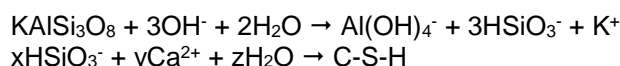
### 3.1.2 Granite

Alkaline ground water will develop at concrete/granite interfaces from alteration of concrete. This alkaline pore water may cause degradation of silicates around the repository and precipitation further along fractures, where more neutral pH conditions prevail (Baker et al., 2002). Interactions between the cement leachate and the rock are a potentially important factor for altering flow in the near-field rock, for example, clogging of fractures and/or formation of secondary minerals has been suggested. Similarly,

during the period of radiogenic heating, calcite may be precipitated in the near-field rock because it has lower solubility at higher temperatures (POSIVA 2012).

Initially, dissolution of KOH and NaOH within the cement will form a leachate of pH ~13. The leachate pH will then decrease to ~12.5 where it will be buffered by equilibration with portlandite (Ca(OH)<sub>2</sub>). The leachate will remain at this pH until all the Ca(OH)<sub>2</sub> has dissolved, after which, pH will be controlled by equilibrium with calcium silicate hydrate (C–S–H) gel and will decrease to ~10.5. The leachate will form a chemically disturbed zone (CDZ) (Moyce et.al., 2014)

Numerous studies have been taken in this subject. Findings are in granite normally that silicate mineral dissolution is followed by secondary solid phase (e.g., C–S–H) formation, with subsequent transformation of C–S–H to feldspars and zeolites over time. These reactions are very slow and highly dependent on pH, temperature and groundwater composition. Examples of the proposed reactions are presented in equations 3-1 and 3-2.



Most of the research on the effects of alkaline plumes is connected to clay materials both bentonite and host rock clay formations. This is dealt with in detail in section 4 of this report, but similarities for granitic host rock do exist.

## 3.2 Evidence from experiments and analogues

### 3.2.1 Concrete

Concrete degradation in waste repositories is under intensive research. As an example for this research, the interaction of concrete with real groundwater has been studied at VTT in projects financed by the Finnish Research Programme on Nuclear Waste Management (KYT). Studies have also been made in cooperation with Finnish Nuclear Power Companies (TVO and Fortum). First 12.5 years of this research program have been reported (Ferreira et. al., 2014).

Power companies initiated in 1997 a study to realistically assess the long-term durability of concrete subject to the erosion of the operating conditions in similar rock groundwater as found in final repository conditions. In particular they wanted to assess the performance of best concrete compositions that can fulfil the 500-year service life requirement. An important step toward the development of concrete that performs well in aggressive underground environments is the understanding of the deterioration mechanisms of concrete by these aggressive media.

Three types of binders were used in these investigations with three different water-binder ratios (0.35, 0.425 and 0.50). These concrete types were placed in nine different aggressive solutions (Table 3-1). These solutions correspond to groundwater chemistry in repository locations and elevated aggressiveness.

Table 3-1 – Composition of test solutions.

Solution code	Chemical compound	Aggressive component (mg L <sup>-1</sup> )
L1	Na <sub>2</sub> SO <sub>4</sub>	SO <sub>4</sub> - 20
L2	Na <sub>2</sub> SO <sub>4</sub>	SO <sub>4</sub> - 500
L3	Na <sub>2</sub> SO <sub>4</sub>	SO <sub>4</sub> - 1000
L4	NaCl	Cl - 50
L5	NaCl	Cl - 1,000
L6	NaCl	Cl - 10,000
L7	Na <sub>2</sub> SO <sub>4</sub> +NaCl+MgCl <sub>2</sub> ·6H <sub>2</sub> O	SO <sub>4</sub> - 20, Cl - 50, Mg - 5
L8	Na <sub>2</sub> SO <sub>4</sub> +NaCl+MgCl <sub>2</sub> ·6H <sub>2</sub> O	SO <sub>4</sub> - 500, Cl - 1,000, Mg - 100
L9	Na <sub>2</sub> SO <sub>4</sub> +NaCl+MgCl <sub>2</sub> ·6H <sub>2</sub> O	SO <sub>4</sub> - 1,000, Cl - 10,000, Mg - 300

Concrete samples were in solutions for years and the chemical and mechanical properties development was followed. In Figure 3-3, strength development during the 12.5 years monitoring time is presented. As it can be seen, no major strength loss has happened during this time yet.

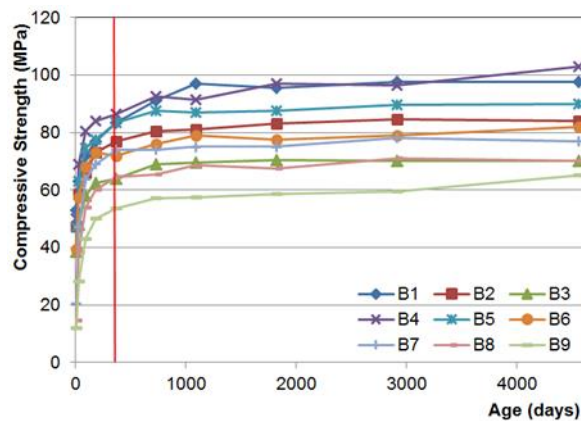


Figure 3-3 – Strength development during 12.5 years of monitoring.

In Figures 3-4 and 3-5, chloride ingress into the concrete is presented. In Figure 3-4 the chloride level in simulated groundwater was 1,000 mg L<sup>-1</sup> and in Figure 3-5 case 10,000 mg L<sup>-1</sup>. Effect of chloride concentration is evident. During the test in lower chloride content groundwater, the chloride diffusion into the concrete was almost negligible. In higher chloride content groundwater penetration was already some tens of millimetres.

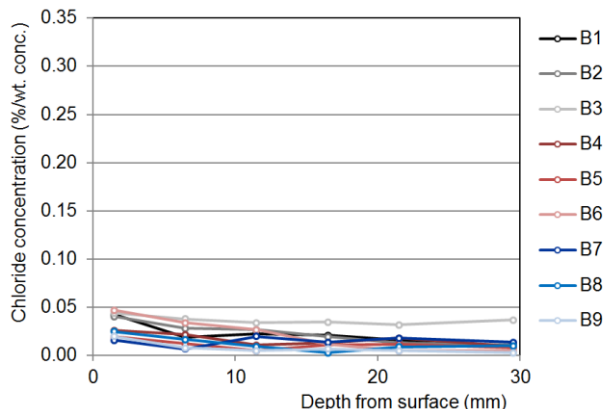


Figure 3-4 – Chloride profiles for all concretes in solution L5.

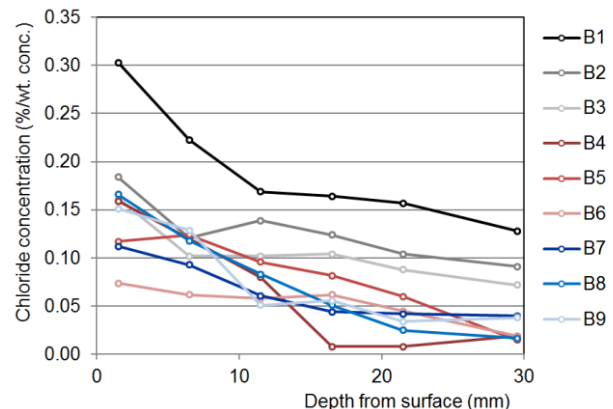


Figure 3-5 – Chloride profiles for all concretes in solution L6.

In these tests, also sulphate, magnesium and sulphur profiles were analysed. The element distributions in the concrete samples on a general level were determined by using an energy dispersive X-ray spectrometer (EDS) that was connected to the SEM. Most of these show how only the surface of the concrete had been affected with the simulated groundwater.

### *Analogues*

The ancient and medieval concretes and mortars do not give much information. In general, they are heavily carbonated due to the contact with the atmosphere. However, the data indicate that if the concrete is protected and not subjected to the atmosphere, C-S-H and the other hydration products may remain for at least a couple of thousand years.

Samples from the early 20<sup>th</sup> century demonstrate that when concrete is kept wet it remains durable and strong for a very long time. The concrete will at least to some extent reequilibrate and form secondary larger crystals. Moreover, the cement paste will react with some components from the aggregate. If the water cannot penetrate the cement paste, this will strengthen the concrete and make it more impermeable. Samples from a historic water tank indicate that the rate of dissolution of calcium hydroxide is small (Lagerblad and Trägårdh, 1994).

Natural analogues to alkaline cements have been extensively studied at the alkaline springs in Maqarin in northern Jordan (Pitty and Alexander, 2011; Smellie, 1998; Savage, 2018). The Maqarin natural analogue site is considered to be a good representation of the processes occurring in a cementitious repository during portlandite and C-S-H-gel phase dissolution (cf. chapter 4.2). Three different stages of concrete degradation have been identified:

1. An early, hyperalkaline stage dominated by leaching of sodium and potassium hydroxides.
2. An intermediate stage with a slightly lower pH determined by dissolution of portlandite.
3. A late and less active stage with a lower pH, dominated by dissolution of silica.

C-S-H-gel has been reported to be persistent in nature over periods of 10,000 years, despite it being metastable with respect to crystalline phases such as tobermorite and jennite (Stronach and Glasser, 1997). Very old gels have been reported in natural cements from Scawt Hill, Northern Ireland and Maqarin, Jordan (Milodowski et al., 1989, 1998). These are up to 2 Ma old in Jordan (Pitty and Alexander, 2011) and possibly more than 100 Ma old in Northern Ireland and appear to have survived as they have been isolated from groundwaters (Höglund, 2014).

### 3.2.2 Granite

The production of alkaline leachates (high-pH plume, Figure 3-6) due to the degradation of cement has been recognised as a potentially detrimental factor for the long-term performance of waste repositories for more than 20 years. There is a general consensus on what the dominant mineral alteration is expected to be (Ca–Si–(Al)-hydrates, Mg–(Si)-hydroxides, calcite, clays, zeolites) and that in several laboratory experiments and also in a natural analogue case a trend towards self-sealing of flow paths is observed (cf. Alexander, 2012). For instance, in the HPF Project (Hyperalkaline Plume in Fractured Rock; Mäder et al., 2006), a remarkable fracture sealing was observed due to this interaction. However, there are still a number of uncertainties associated with this sealing of fractures due to the formation of secondary minerals (Savage, 2018). It has been stated that these effects cannot be taken into account in the safety case because they cannot be quantified (e.g., Pastina et al., 2012; Koskinen, 2014).

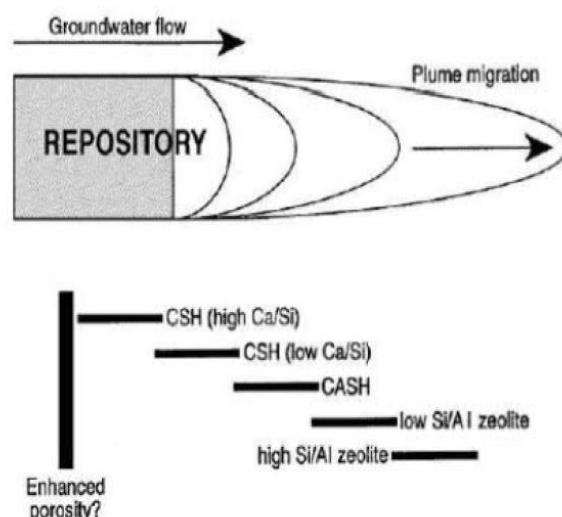


Figure 3-6 – Effects of an alkaline plume in granitic host rocks (POSIVA 2012, from Savage, 1996).

Among the earliest experiments conducted on the interaction of cementitious leachates with crystalline rocks (e.g., Avrö granite and Borrowdale Volcanic Group ‘fault rock’) were those of Bateman et al. (1999). The chemical interaction with the rocks in experiments conducted at 70 °C resulted in the development of one or more secondary phases such as C-S-H, C-A-S-H, C-K-S-H and C-K-(A)-S-H, leading to a decrease in overall porosity and an increase in surface area. Mäder et al. (2006) performed a hyperalkaline fluid core infiltration experiment for nine months, using a core from a fracture in Nagra’s Grimsel Test Site (GTS), where the fault gouge had been preserved *in situ*. The gradual decrease in flow rate by a factor of 25 was attributed to clogging of the flow paths in the fracture due to the formation of secondary C-S-H precipitates as consequence of the reaction of the rock with the hyperalkaline fluids.

Moreover, in the frame of the HPF project at the GTS, a long-term field experiment was carried out by injecting hyperalkaline fluids into a water-conducting shear zone along (Mäder et al., 2006). The hyperalkaline fluids caused a significant dissolution of the primary minerals, leading to the precipitation of secondary minerals that induce changes to the flow field including self-sealing. It was found that the conceptual model (cf. Alexander and Smellie, 1998) for the likely evolution of a hyperalkaline plume in crystalline (and other) host rocks was valid. Further *in situ* experiments in the natural flow regime at the GTS were performed using static cementitious materials (both liquid grouts and pre-hardened cements placed in boreholes) as source for hyperalkaline fluids within the frame of the LCS (Long-term cement studies) project (cf. Lanyon, 2015; Watson et al., 2017).

Recently, Szabó-Krausz et al. (2021) evaluated the geochemical interactions occurring at the granite-concrete interface in the operating LLW/ILW repository at Bataapáti, Hungary. Shotcrete made from OPC and containing sand and gravel (including granitic rock fragments) as aggregate was used for mechanical support. Core samples were drilled across the granite-concrete interface 1 to 15 months after the shotcrete installation. The mineral composition of the granite (predominantly monzogranite) was found to be quite heterogeneous with quartz, K-feldspar, plagioclase, mica and chlorite as the main phases and some muscovite, amphibole and calcite. The main secondary phases observed at the interface were the Ca-carbonates calcite and vaterite. Calcite veins occurred along the granite-concrete contact while vaterite precipitated in the pores of the concrete near the interface. This carbonation was explained by Szabó-Krausz et al. (2021) by reaction of Ca released by the dissolution of the cementitious material and  $\text{HCO}_3^-$  from the local granitic pore water. The carbonation process was found to reduce the porosity and permeability in the contact zone, avoiding or slowing down further interaction of the materials. Moreover, a frequent occurrence of titanite along or near the granite-concrete interface, but always on the side of the granite was observed, sometimes between the newly formed calcite precipitates and the granite. It was concluded by Szabó-Krausz et al. (2021) that titanite formed where i) the Ca concentration was not high enough to form carbonates, and ii) sufficient dissolved  $\text{SiO}_2$  was in

the solution, with the granite serving as a source of  $\text{TiO}_2$ . The observation of neighbouring calcite and titanite precipitation was seen as indicator for changing geochemical conditions within short distances at the reaction front (i.e., the granite-concrete interface).

### Analogues

A widely used example of natural analogues for concrete-rock interaction is the Maqarin area in Jordan, where different highly alkaline groundwaters occur, which are believed to be analogous to three different stages in the theoretical evolution of a cementitious repository for the disposal of low- to intermediate-level nuclear wastes. Although the rock affected by the alkaline water is a clay biomicrite, the data on the spatial and temporal changes to the host rock following reaction with the alkaline plume are transferable (with care) to fractured crystalline rocks (Alexander, 2012). The Maqarin analogue studies are described in more detail in chapter 4.2 addressing cement-clay interactions.

## 3.3 Application of conceptual and mathematical models

### 3.3.1 Concrete

Modelling of ageing and degradation of concrete and other cementitious materials are widely used in predicting performance of repository. In Figure 3-7 an example of this modelling is presented. Changes in mineralogy due to leaching was modelled using the geochemical modelling tool GEMS (Gibbs Energy Minimization Software for Geochemical Modelling). This example shows how the concrete material will be altered due to leaching/precipitation processes in the groundwater environment.

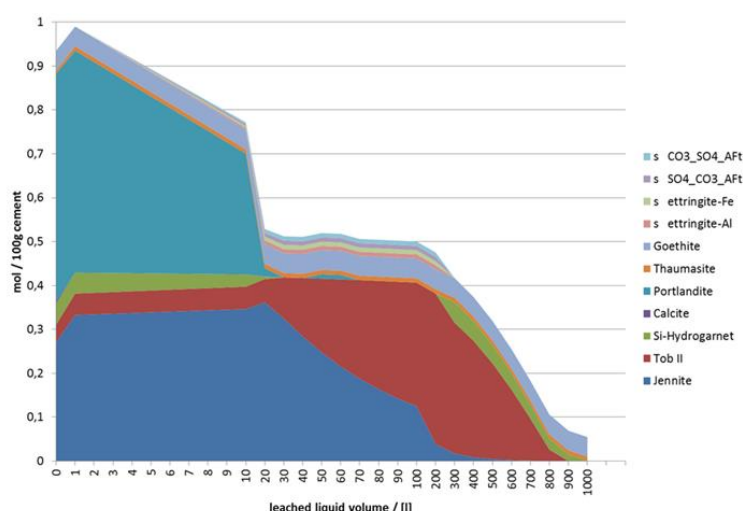


Figure 3-7 – Illustrative example for modelling of leaching of cementitious materials in the groundwater environment (Ferreira et al., 2014).

An example of modelling of a leaching front is presented in Figure 3-8 (Höglund, 2014). Leaching of portlandite is faster than the leaching of the less soluble C-S-H gel. When the leaching of portlandite has reached a certain depth, the corresponding gradient of the porewater concentrations near the surface of the concrete will fall below the solubility limit of the C-S-H gel, which will start to dissolve. The effect of this is that the leaching of portlandite will slow down to some extent as compared to the case where leaching of portlandite takes place as a pure phase.

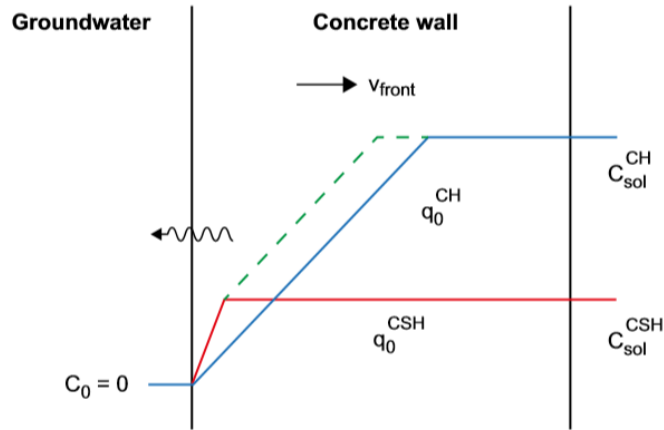


Figure 3-8 – Illustration of diffusion controlled simultaneous leaching of portlandite and CSH-gel in concrete. The blue line corresponds to a concentration gradient for the case of pure phase portlandite, green and red lines correspond to concentration gradients in the presence of both portlandite and C-S-H phases (Höglund, 2014).

A corrected estimate of the portlandite leaching can be made using the following expression:

$$h_{corr} = \sqrt{\frac{2 \cdot D_{e,ww} \cdot (c_{sol}^{CH} - c_{sol}^{CSH}) \cdot t}{q_0^{CH}}}$$

where:

- $h_{corr}$  = thickness of a weakly weathered zone of concrete corrected for the simultaneous leaching of portlandite and C-S-H-gel [m],
- $D_{e,ww}$  = effective diffusivity of weakly weathered zone [ $m^2 yr^{-1}$ ],
- $c_{sol}^{CH}$  = solubility of portlandite [ $kmol m^{-3}$ ],
- $c_{sol}^{CSH}$  = solubility of CSH-gel [ $kmol m^{-3}$ ],
- $q_0^{CH}$  = initial amount of free portlandite in concrete [ $kmol m^{-3}$ ].

Example calculations for the 1BMA repository are shown in Figure 3-9.

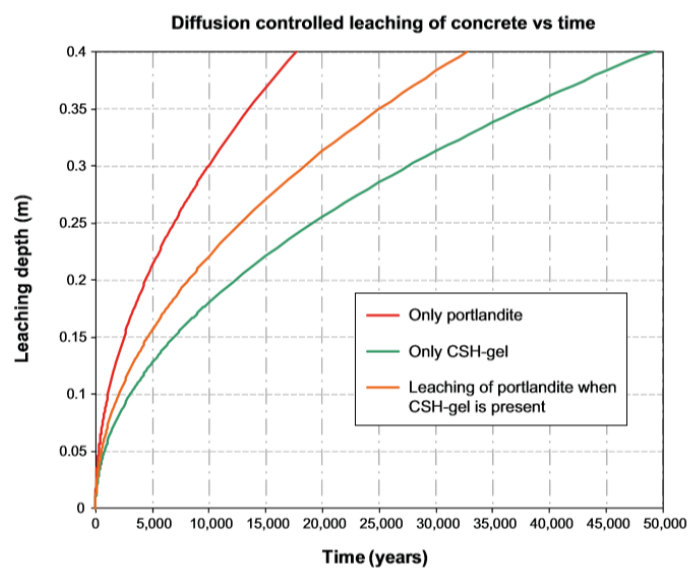


Figure 3-9 – Diffusion controlled leaching of concrete showing the calculated depth of depletion of portlandite or C-S-H-gel for different cases (Höglund, 2014).

### 3.3.2 Granite

As the reactions in granite are extremely slow, modelling is the way this phenomenon has been handled in literature. Modelling of these phenomena has started already in the 1980's (e.g., Haworth et al., 1987; Savage and Rochelle, 1993) and is still developing (e.g., Watson et al., 2017), using different modelling tools. Results are widely presented for example in the HPF-Experiment modelling report (Soler et al., 2006) and the LCS modelling report (Watson et al., 2017). The results were found to be heterogeneous, perhaps because of the highly complex nature of the experimental fracture. The present coupled calculation tools are adequate, although improvements could still be made (Alexander, 2012).

In the modelling, the importance of choosing the right and relevant model assumptions is shown in Figure 3-10. In this example, addressing the interaction of a hyper-alkaline (NaOH/KOH) leachate on the mineralogy and porosity of a generic quartz-feldspathic host rock for intermediate- and low-level nuclear waste, the simulated solution compositions for scenarios with and without inclusion of K-feldspar are compared (cf. Chen et al., 2015). The labels “(with)” means with K-feldspar, without “(with)” are only for quartz. It shows that more Si is released in the near-field in the combined quartz and K-feldspar scenario. However, the Si peak is lower in the far-field than that in the quartz-only scenario, due to the predicted precipitation of Si-bearing secondary phases such as nontronite. The influence of K-feldspar on pH is evident. The K-feldspar dissolution increases the pH and buffers it at a higher level relative to the quartz-only system (Chen et al., 2015).

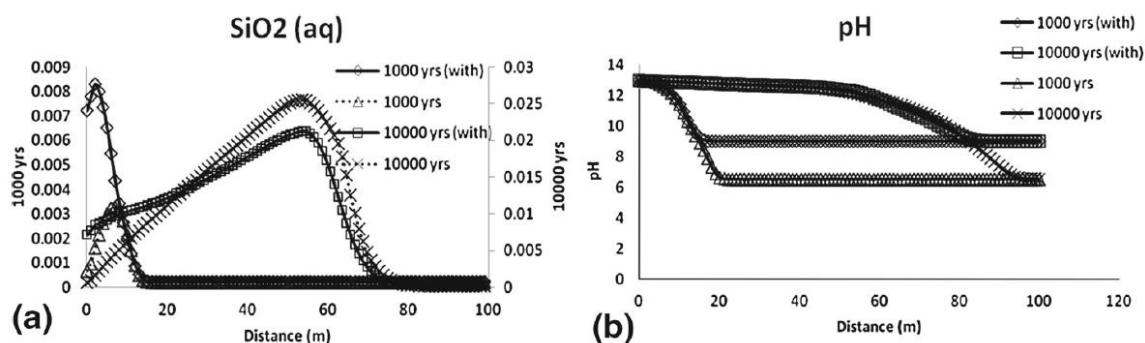


Figure 3-10 – Comparison of simulated scenarios for quartz only and quartz with K-feldspar: a SiO<sub>2</sub>; b pH (Chen et al., 2015).

Generally, these simulations show that:

- the model for the evolution of an alkaline plume in a host rock is largely consistent with experimental observations.
- alkaline pore water conditions generated by minerals analogous to those in cements can be long-lived (in excess of tens of thousands of years), depending on the site flow conditions and the nature of the cementitious material (e.g., dense, high performance cements or porous grouts, groundwater movement)
- reactions between alkaline waters and the host rock mostly have positive reaction volumes (some initial porosity increase is possible during the early KOH/NaOH phase) and thus fractures are sealed by the precipitation of secondary phases
- the effects of the site hydrology (and tectonic/erosional processes) upon fracture sealing need to be considered on a repository site-specific basis (Alexander and Neall, 2007).

## 3.4 Resume

An important step toward the development of concrete that performs well in aggressive underground environments is the understanding of the deterioration mechanisms of concrete by these aggressive media. Developments based on this knowledge will lead to an increase of the service life and performance of an LLW facility. The study of concrete that has been reacted under controlled laboratory conditions is the foundation to understand the sequence of mineralogical reactions that occur and relate the findings to exposure conditions and concrete mix design definition. In overall, it has been noted that

chemical alteration and ageing in underground repository conditions are very slow. Long-term experiments are therefore essential to provide data for modelling.

Granite alteration is also phenomena that should be taken in account. The alkaline plume caused by concrete will have an effect on granite but in different extent, depending on the geochemical and hydrological properties of repository. Also, the concrete properties vary in different concepts. Using low pH concrete for example will diminish the alkaline plume remarkably. Generally, the alteration processes effecting the granite host rock are slow.

### 3.5 References

- Alexander, R., 2012. The impact of a (hyper)alkaline plume on (fractured) crystalline rock. In: NEA, 2012. Cementitious materials in safety cases for geological repositories for radioactive waste: Role, evolution and interactions, NEA/RWM/R(2012)3/REV, 85-88.
- Alexander, W.R., Smellie, J.A.T., 1998. Maqarin natural analogue project. Nagra Project Report NPB98-08, Nagra, Wettingen, Switzerland.
- Alexander, W.R., Neall, F.B., 2007. Assessment of potential perturbations to Posiva's SF repository at Olkiluoto from the ONKALO facility. Posiva Working Report WR2007-35, Posiva, Olkiluoto, Finland.
- Alexander, M., Bertron, A., De Belie, N., 2013. Performance of cement based materials in aggressive aqueous environments. State of the Art Report RILEM TC 211, Springer.
- Bateman, K., Coombs, P., Noy, D.J., Pearce, J.M., Wetton, P., Haworth, A., Linklater, C., 1999. Experimental simulation of the alkaline disturbed zone around a cementitious radioactive waste repository: numerical modelling and column experiments. Geological Society of London, Special Publication 157, 183-194.
- Baker, A.J., Bateman, K., Hyslop, E.K., Ilett, D.J., Linklater, C.M., Milodowski, A.E., Noy, D.J., Rochelle, C.A., Tweed, C.J., 2002. Research on the alkaline disturbed zone resulting from cement-water-rock reactions around a cementitious repository. UK Nirex Limited Report N/054, UK Nirex Ltd., Harwell, Didcot, United Kingdom.
- Berner, U.R., 1992. Evolution of pore water chemistry during degradation of cement in a radioactive waste repository environment. Waste Management 12, 201-219.
- Cau Dit Coumes, C., Courtois, S., Nectoux, D., Leclercq, S., Bourbon, X., 2006. Formulating a low-alkalinity, high-resistance and low-heat concrete for radioactive waste repositories. Cement and Concrete Research 36, 2152-2163.
- Chen, X., Thornton, S.F., Small, J., 2015. Influence of hyper-alkaline pH leachate on mineral and porosity evolution in the chemically disturbed zone developed in the near-field host rock for a nuclear waste repository. Transport in Porous Media 107, 489-505.
- Ferreira, M., Koskinen, P., Vehmas, T., 2014. Durability of concrete barriers in underground nuclear waste repository conditions – Final Report of BetKYT 2014. VTT Research Report VTT-R-05746-14, VTT, Espoo, Finland.
- Haworth, A., Sharland, S.M., Tasker, P.W., Tweed, C.J., 1987. Evolution of the groundwater chemistry around a nuclear waste repository. Materials Research Society Symposium Proceedings 112, 425-434.
- Höglund, L.O., 2014. The impact of concrete degradation on the BMA barrier functions. SKB Report R-13-40, SKB, Stockholm, Sweden.
- Koskinen, K., 2014. Effects of cementitious leachates on the EBS. Posiva Report 2013-04, Posiva, Olkiluoto, Finland.
- Lagerblad, B., Trägårdh, J., 1994. Conceptual model for concrete long time degradation in a deep nuclear waste repository. SKB Technical Report TR 95-21, SKB, Stockholm, Sweden.

Lanyon, G.W., 2015. Modellers Summary of LCS Experiment 2 (F16) Tracer Testing. Nagra Aktennotiz AN 15-025-Rev.1. Nagra, Wettingen, Switzerland.

Mäder, U.K., Fierz, T., Frieg, B., Eikenberg, J., Rüthi, M., Albinsson, Y., Möri, A., Ekberg, S., Stille, P., 2006. Interaction of hyperalkaline fluid with fractured rock: Field and laboratory experiments of the HPF project (Grimsel Test Site, Switzerland). *Journal of Geochemical Exploration* 90, 68-94.

Milodowski, A.E., Nancarrow, P.H.A., Spiro, B., 1989. A mineralogical and stable isotope study of natural analogues of ordinary Portland cement (OPC) and CaO-SiO<sub>2</sub>-H<sub>2</sub>O (CSH) compounds. UK Nirex Safety Studies Report NSS/R240, UK Nirex Ltd., Harwell, Didcot, United Kingdom.

Milodowski, A.E., Pearce, J.M., Hyslop, E.K., Hughes, C.R., Inglethorpe, S.D.J., Strong, G.E., Wheal, N., McKenzie, A.B., Karnland, O., Khoury, H.N., 1998. Mineralogy and petrology. In: Linklater, C.M. (ed) A natural analogue study of cement-buffered, hyperalkaline groundwaters and their interaction with a repository host rock. Phase II. Nirex Science Studies Report S/98/003, UK Nirex Ltd., Harwell, Didcot, United Kingdom.

Moyce, E.B.A., Rochelle, C., Morris, K., Milodowski, A.E., Chen, X., Thornton, S., Small, J.S., Shaw, S., 2014. Rock alteration in alkaline cement waters over 15 years and its relevance to the geological disposal of nuclear waste. *Applied Geochemistry* 50, 91-105.

Pastina, B., Lehikoinen, J., Puigdomenech, I., 2012. Safety case approach for a KBS-3 type repository in crystalline rock. In: NEA, 2012. Cementitious materials in safety cases for geological repositories for radioactive waste: Role, evolution and interactions, NEA/RWM/R(2012)3/REV, 120-124.

Pfingsten, W., Paris, B., Soler, J., Mader, U., 2006. Tracer and reactive transport modelling of the interaction between high-pH fluid and fractured rock: Field and laboratory experiments. *Journal of Geochemical Exploration* 90, 95–113.

Pitty, A.F., Alexander, W.R. 2011. A natural analogue study of cement buffered, hyperalkaline groundwaters and their interaction with a repository host rock IV: an examination of the Khushaym Matruk (central Jordan) and Maqarin (northern Jordan) sites. Bedrock Geosciences Technical Report 11-02, Bedrock Geosciences, Auenstein, Switzerland.

POSIVA, 2012. Safety case for the disposal of spent nuclear fuel at Olkiluoto - Features, events and processes 2012. Posiva Report 2012-07, Posiva, Olkiluoto, Finland.

Savage, D., 1996. Zeolite occurrence, stability and behaviour. In: Smellie, J.A.T. (ed.) Maqarin Natural Analogue Study: Phase III. UK DOE Report DOE/HMIP/RR/95.020, Department of Energy, London, United Kingdom.

Savage, D., 2011. A review of analogues of alkaline alteration with regard to long-term barrier performance. *Mineralogical Magazine* 75, 2401-2418.

Savage, D., Rochelle, C., 1993. Modelling reactions between cement pore fluids and rock: Implications for porosity change. *Journal of Contaminant Hydrology* 13, 365-378.

Smellie, J.A.T. 1998. Maqarin natural analogue study: Phase III. SKB Technical report TR 98-04, SKB, Stockholm, Sweden.

Snelman, M., Vieno, T., 2005. Long-term safety aspects of the use of cement in a repository for spent nuclear fuel. Proceedings 2<sup>nd</sup> Workshop R&D on low pH cement for a geological repository, 15-16 June 2005, Madrid, Spain, 27-40.

Soler, J.M., Pfingsten, W., Paris, B., Mäder, U.K., Frieg, B., Neall, F., Källvenius, G., Yui, M., Yoshida, Y., Shi, P., Rochelle, C.H.A., 2006. HPF-Experiment: modelling report. Nagra Technical Report NTB-05-01, Nagra, Wettingen, Switzerland.

Stronach, S.A., Glasser, F.P., 1997. Modelling the impact of abundant geochemical components on phase stability and solubility of the CaO-SiO<sub>2</sub>-H<sub>2</sub>O system at 25°C: Na<sup>+</sup>, K<sup>+</sup>, SO<sub>4</sub><sup>2-</sup>, Cl<sup>-</sup> and CO<sub>3</sub><sup>2-</sup>. *Advances in Cement Research* 9, 167-181.

Szabó-Krausz, Z., Aradi, L.E., Király, C., Kónya, P., Török, P., Szabó, C., Falus, G., 2021. Signs of in-situ geochemical interactions at the granite–concrete interface of a radioactive waste disposal. *Applied Geochemistry* 126, 104881.

Watson, C., Savage, D., Wilson, J., 2017. Geochemical modelling of the LCS experiment. Quintessa Report QRS-1523D-2, Quintessa, Henley-on-Thames, United Kingdom.

## 4. Interface "cement/concrete – clay"

Guido Deissmann, Naila Ait Mouheb (FZJ)

In many disposal concepts for radioactive wastes, significant use is made of cementitious materials, for example as structural support material for access galleries and disposal drifts of cells (e.g., concrete/shotcrete), as well as containment material for low and intermediate level wastes (e.g., grouts/mortars). Thus these cementitious materials can be in contact with both, the host rock clay formation and bentonite barriers (cf. NEA, 2012; Sellin and Leupin, 2013). Due to the contrasting chemical and mineralogical properties of cementitious materials and clays, interactions will occur at the cement-clay interface as a result of the chemical gradients. For example, the pH of pore waters in either clay formations (e.g., Opalinus clay, Callovo Oxfordian clay, or Boom clay) and bentonite is typically in the range of pH 7 to 8.5. In contrast, the progressive degradation of cementitious materials after resaturation of the repository leads to a pH in the cement pore fluids ranging over time from 13.5 (for systems based on ordinary Portland cement, OPC) to 10, slowly approaching the pH of the surrounding ground water in the long-term (cf. Berner, 1992; Harris et al., 2002; Glasser, 2011; Beattie and Williams, 2012; Hoch et al., 2012; Drace and Ojovan, 2013). Even in so-called low-pH cementitious materials the initial pH of the young pore water can often be above pH 12 (e.g., Vehmas et al., 2016). The term low-pH cementitious material is used here for cementitious materials/concrete where significant amounts of OPC in the binder is replaced by siliceous supplementary cementing materials, in particular silica fume, ground granulated blast furnace slag, or fly ashes.

Within the context of geological disposal of nuclear waste, cement/clay interactions have been investigated for more than three decades by means of laboratory and *in situ* experiments, studies on natural and industrial analogues, and reactive transport modelling. Comprehensive reviews on various aspects of cement/clay interactions already have been published (e.g., Metcalfe and Walker, 2004; Michau, 2005; Gaucher and Blanc, 2006; Savage et al., 2007; Savage, 2009; Savage, 2011; Sidborn et al. 2014; Bildstein and Claret, 2015; Dauzères 2016; Claret et al., 2018; Savage and Cloet, 2018; Bildstein et al., 2019).

Short-term laboratory (e.g., Adler et al., 1999, 2001; Dauzères et al., 2010, 2014; Fernandez et al., 2016; Balmer et al. 2017) and longer-term *in situ* experiments (up to about 20 years) at different underground research laboratories like HADES, Mol, Belgium (Read et al., 2001), Mont Terri, Switzerland (e.g., Jenni et al., 2014; Dauzères et al. 2016; Lerouge et al., 2017; Mäder et al. 2017), Bure, Department Meuse/Haute Marne, France (e.g., Gaboreau et al., 2011, 2012; Dauzères et al., 2016), or at the Tournemire site in France (e.g., Tinseau et al., 2006; Techer et al., 2012a,b; Bartier et al., 2013; Lalan et al., 2016), as well as the FEBEX experiment in the Grimsel test site in Switzerland (e.g., Alonso et al., 2017; Fernandez et al., 2017; Turrero and Cloet, 2017) have demonstrated that at the cement/clay interface, alteration of both cement paste and clay material take place, leading to mineralogical changes that modify the microstructure of the altered region, which may influence transport relevant properties such as porosity and permeability, or the radionuclide retention behaviour of the materials.

### 4.1 Processes at the interface

Due to the contrasting chemical and mineralogical properties of cementitious materials and clay rocks or bentonite, reaction zones will develop, with diffusive transport of aqueous species across the material interface in response to chemical gradients. These gradients develop typically from the higher concentrations (activities) of species such as  $\text{OH}^-$ ,  $\text{K}^+$ ,  $\text{Na}^+$ , and  $\text{Ca}^{2+}$  in the cementitious materials, thus tending to diffuse towards the clay materials. In contrast, the concentrations of species such as  $\text{Mg}^{2+}$ ,  $\text{Al}^{3+}$ ,  $\text{SiO}_2(\text{aq})$  and  $\text{HCO}_3^-$ , are often higher in the pore water of the clay formation/bentonite, thus tending to diffuse into the cementitious materials. Based on the existing literature the following key have to be considered at cement/clay interfaces, as observed in laboratory and *in situ* experiments, and/or as inferred from natural analogues and modelling studies:

- Diffusion of hydroxyl anions from the cement into the clay will destabilize silicate/aluminosilicate minerals, leading to slow hydrolysis of montmorillonite and other aluminosilicate minerals

present (e.g., Cuevas et al., 2006; Yamaguchi et al., 2007), consuming  $\text{OH}^-$  ions and neutralising the high pH fluids, but leading to a decrease in swelling pressure of smectitic clays.

- Replacement of clay minerals by calcium silicate hydrates (C-S-H), sheet silicates, and or zeolites, with the secondary minerals forming in a zonal fashion (cf. Figure 4.1) (e.g., Gaucher and Blanc, 2006, Cuevas et al., 2006; Savage et al., 2007), potentially leading to an overall decrease in porosity (due to differences in molar volumes) and changes in the rheological properties of the clay (e.g., Jefferies et al. 1988).

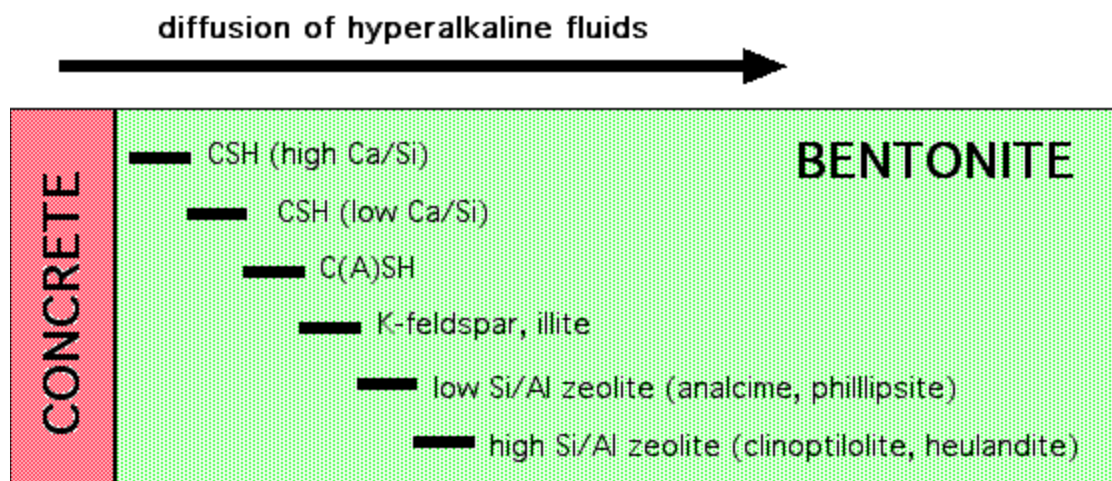


Figure 4-1 – Schematic diagram of the potential sequence of secondary mineral forming as consequence of the migration of hyperalkaline pore fluids through bentonite (Savage and Benbow, 2007; Bamforth et al., 2012). Na/K phases may be replaced by more Ca-rich ones as the composition of cementitious pore fluids evolves with time.

- Enhanced leaching of portlandite ( $\text{Ca}(\text{OH})_2$ ) and C-S-H, thus reducing its Ca/Si-ratio, in the cementitious material accompanied by rapid precipitation of Ca-carbonates, such as aragonite and calcite, directly at the interface, due to steep gradients in hydroxyl ion concentrations (higher on the cementitious material) and the partial pressure of carbon dioxide ( $\text{pCO}_2(\text{g})$ , higher in the clay rock formation) across the cement/clay-interface; these reactions lead to an increase in porosity in the cementitious material and a porosity decrease in the clay in the longer term. In low-pH cementitious materials, where portlandite is lacking, the decalcification of the C-(A)-S-H occurs directly and proceeds faster, leading to an earlier formation of amorphous silica as residue.
- Formation of calcium aluminium silicate hydrates (C-A-S-H) and (amorphous) magnesium silicate hydrates (M-S-H) at the interface, affecting porosity and transport properties at the interface (e.g., Dauzères et al., 2016), and replacement of portlandite, C-S-H gel and monosulphoaluminate by ettringite (e.g., Savage, 2014). Note that in low pH formulations, C-A-S-H can be present already as initial hydration phase.
- Redistribution of sulphate towards the unaltered cementitious matrix due to the decrease in pH close to the interface, destabilizing earlier formed Ca-Al-sulphates (ettringite, monosulphate) that re-precipitate in the higher pH regions (e.g., Mäder et al., 2017).
- Fast exchange of cations in interlayer sites in montmorillonite, due to diffusion of  $\text{K}^+$ ,  $\text{Na}^+$  and  $\text{Ca}^{2+}$  from the cementitious material into the clay will lead to, leading to a decrease of swelling pressure.
- Fast protonation-deprotonation reactions at clay edge sites, retarding the diffusive migration of hydroxyl ions due to reversible sorption processes.
- Slow hydrolysis of montmorillonite and other minerals present, either as additives (e.g. quartz sand), or as accessory minerals reactions consuming hydroxyl ions, thus chemically neutralizing the advancing cementitious porewater, leading to an increase in porosity and a decrease in clay swelling properties.

The studies performed have shown that there is a strong coupling between fluid and solute transport, dissolution of solids and precipitation of secondary phases, ion exchange and edge site sorption on clays, and the consequential changes in physical properties of the materials (i.e., porosity, permeability,

swelling pressure of clay) (cf. Savage and Cloet, 2018). Depending on the extent of porosity/permeability changes (e.g., pore clogging), changes in hydraulic conductivity, diffusivity, and gas permeability may occur. Moreover, the potential dissolution and replacement of clay minerals may alter the safety-relevant swelling properties and sorption capacity of the clay materials. The processes occurring at the cement/clay interface as well as their kinetics will depend to a large extent on the initial properties of the materials, such as the nature of the cementitious binder (OPC or low pH binder), the mineralogy and pore water composition of the clay material, and their initial transport properties (e.g., porosity, diffusivity, incl. water saturation) and thus on repository concept and site. Thus the extent and significance of these processes will need to be assessed on a site-specific basis (cf. NDA, 2016). Due to this complexity and diversity, it is difficult to establish a general sequence of secondary minerals forming in the cement domain due to the impact of the clay pore water.

## 4.2 Evidence from experiments and analogues

### *Experimental evidence*

Throughout the last three decades, a large number of experimental studies have been devoted to cement/clay interactions within the context of nuclear waste disposal (cf. Gaucher and Blanc, 2006; Bildstein and Claret, 2015; Dauzères, 2016; Bildstein et al., 2019). However, until the 2000s, work on cement/clay interfaces was mainly dedicated to the study of the potential impact of an alkaline plume on clay host rocks (e.g., Opalinus Clay, Callovo Oxfordian Clay, Boom Clay) or different types of bentonites/smectites (e.g., MX-80, FEBEX). For this purpose, mainly batch experiments using highly alkaline solutions were employed to mimic the effect of cementitious porewaters on clay material (cf. Gaucher and Blanc, 2006; Honty et al., 2010; Wang et al., 2010; Bildstein and Claret 2015; Dauzères, 2016). Laboratory experiments and *in situ* experiments addressing cement/clay interactions using cementitious materials in contact with clay materials have been conducted since the early 2000s (cf. Table 4.1) and have been discussed *inter alia* by Dauzères (2016), within the frame of the EC funded collaborative project CEBAMA (cf. Duro et al. 2020).

Read et al. (2001) performed a series of experiments on the development of various cementitious materials (i.a., OPC, OPC and fly ash, OPC and slag, NIREX reference vault backfill, and cemented wastes) in contact with a clay material (i.e. Boom Clay) in the HADES Underground Research Laboratory (Mol, Belgium) over periods of 12 to 18 months at temperatures of 25 °C and 85 °C. The OPC samples showed considerable deterioration after 12 months of interaction as well as the clay in contact. At 85 °C, well-defined reaction zones (100 to 250 µm width) were observed on both sides of the interface, revealing depletion of Al, Si, and Mg accompanied by Ca enrichment on the clay side, and Ca depletion and Al, S, Si and Mg enrichment in the altered cementitious material. Si-Mg and Al-Mg gels occurring in the first 10 µm of the cementitious material were identified as hydrotalcite and sepiolite.

Table 4-1 – Summary of laboratory and in situ experiments addressing cement/clay interactions using cementitious materials in contact with clay materials (modified after Dauzères, 2016).

Cementitious material	Clay	Type of experiment	Temperature	Duration	Observations cement side	Observations clay side	Reference
CEM I; CEM I + FA; CEM I + GGBS; NRVB; high alumina cement; cemented IER & research reactor waste (HCP)	Boom clay (Mol)	in situ	25 and 85 °C	12 to 18 m	strong alteration: decalcification, S, Al, Si and Mg-enrichments, precipitation of Mg-Si gel and Mg-Al gel close to interface	Ca-enrichment, Al, Si and Mg depletion	Read et al., 2001
CEM II (concrete)	Toarcian clay (Tournemire)	in situ.	variable	15 to 100 y	carbonation (calcite, vaterite)	Precipitation of gypsum, Na-zeolites and dolomite; dissolution of chlorite and kaolinite	Tinseau et al., 2006; Devol-Brown et al., 2008
CEM II (concrete)	Toarcian clay (Tournemire)	in situ	variable	15 y	carbonation (calcite/vaterite/aragonite)	Precipitation of gypsum, Na-zeolites and dolomite, calcite, vaterite, aragonite; dissolution of chlorite and kaolinite	Yamaguchi et al., 2009
CEM II (concrete)	Toarcian clay (Tournemire)	in situ	15 °C	15 y	alteration depth 10 to 15 mm; portlandite dissolution, C-S-H decalcification, calcite precipitation	alteration depth 18 to 20 mm; C-S-H precipitation; calcite dissolution; calcite reprecipitation in front of alkaline plume	Techer et al., 2012a,b
CEM II (concrete)	Toarcian clay (Tournemire)	in situ	15 °C	15 y	porosity increase over 1 to 1.5 cm	porosity clogging over 2 cm	Gaboreau et al., 2011
CEM II (HCP)	Toarcian clay (Tournemire)	in situ	15 °C	18 y	alteration depth few hundred µm; portlandite dissolution, decalcification of C-S-H; porosity increase	alteration depth 11 to 13 mm; C-S-H and calcite precipitation; illitization (?)	Bartier et al., 2013
CEM I (HCP)	Callovo Oxfordian clay	laboratory	25 °C	2, 6 and 12 m	< 1 mm alteration; low carbonation with diffuse calcite; portlandite dissolution, C-S-H decalcification; ettringite precipitation	illite/smectite mixed layer modification	Dauzères et al., 2010
Low pH cement (HCP)	Callovo-Oxfordian clay	laboratory	25 and 50 °C	2, 6 and 12 m	C-S-H decalcification; Mg-enrichment at the interface; possibly M-S-H precipitation	small Mg-enrichment close to interface	Dauzères, 2010
CEM I + FA	Callovo-Oxfordian clay	in situ	20 °C	5 y	gypsum precipitation	gypsum precipitation (due to pyrite oxidation)	Lerouge et al., 2014

Table 4-1 – continued

Cementitious material	Clay	Type of experiment	Temperature	Duration	Observations cement side	Observations clay side	Reference
CEM I, CEM I + filler (concrete)	Lower Lias clay	in situ	5 and 20 °C	1y / 9 y	high deterioration; formation of thaumasite	not characterized	Abubaker et al., 2014a,b
CEM I, ESDRED and LAC low-pH concrete	Opalinus clay (Mt. Terri)	in situ	20 °C	2.2 y	alteration depth few hundred µm; decalcification, carbonation, Mg-enrichment in particular close to interface (possibly due to M-S-H precipitation), ettringite precipitation	no alteration observed	Jenni et al., 2014
ESDRED and LAC low-pH concrete	Opalinus clay (Mt. Terri)	in situ	20 °C	2.5 and 5 y	alteration depth several mm; carbonation, strong decalcification of C-S-H, Mg-enrichment (probably due to M-S-H precipitation)	Mg-enrichment close to interface	Dauzères et al., 2016
CEM I (mortar)	FEBEX bentonite	laboratory	25, 60, and 120 °C	1, 6 and 12 m	alteration over several mm	alteration depth several mm; precipitation of C-S-H and brucite (25 and 60 °C); tobermorite and Mg-saponite formation (up to 10 mm depth) and analcime precipitation (120 °C)	Fernandez et al., 2006
CEM I (mortar)	FEBEX bentonite	laboratory	25, 60, and 120 °C	1, 6 and 12 m	carbonation	analcime precipitation	Cuevas et al., 2006

Research on the aging of OPC-based concrete with limestone additions in contact with the Toarcian argillite at Tournemire (Aveyron, France), an argillite with a composition close to the Callovo-Oxfordian clay was started in the 1990s, by sealing exploratory drillings with CEM II cement pastes and concrete. The interfaces between the materials were overcored after 15 years of interaction, revealing significant mineral transformations (Tinseau et al., 2006), such as precipitation of gypsum at the interface, local formation of a Na-zeolite, and precipitation of calcite and dolomite. Follow up studies on the cementitious material and its microstructure (Gaboreau et al., 2011; Techer et al., 2012a,b) revealed a thickness of the altered layer in the cementitious material of up to 10 - 15 mm after 15 years of interaction. Mineral transformations comprised mainly calcite formation (carbonation), portlandite dissolution, and partial decalcification of C-S-H, causing a porosity increase in the cementitious material. These results were confirmed by Bartier et al. (2013) on older interfaces (20 years), where the same porosity evolution due to similar mechanisms was observed, as well as on concrete placed in contact with the Opalinus clay at the Mont Terri URL, Switzerland (Jenni et al., 2014). Moreover, Yamaguchi et al. (2009) also characterized concrete/clay interfaces from Tournemire. In addition to the findings of Tinseau et al. (2006), it was found that the Ca-carbonates precipitated in three modifications, i.e., aragonite, calcite and vaterite. The authors stated that the precipitation of these minerals occurred at both sides of the interface along with the precipitation of C-S-H and ettringite. In contrast to the work of Tinseau et al. (2006), no zeolites were observed at the interface.

Gaboreau et al. (2011) investigated an *in situ* engineered analogue of an interface between an OPC type cement paste and the Toarcian clay rock at Tournemire that had undergone 15 years of interaction and presented a quantitative characterisation of the spatial distribution of the porosity in both, the cementitious material and the clay rock. The porosity measurements revealed clogging of the porosity in the clay rock whereas the porosity increased in the cementitious material. The zone of evolved porosity extended to up to one centimetre on both sides of the interface, but was found to be heterogeneously distributed, depending on the fissure network and the interface geometries. In a similar study, Gaboreau et al. (2012) investigated the *in situ* interaction of a cement paste and shotcrete with the Callovo Oxfordian clay in the Bure URL. After 4 to 5 years of interaction, chemical, mineralogical, and textural measurements provided evidence that the perturbations from the chemical contrast between the materials were limited to less than a cm scale on each side of the interfaces. Carbonation (as well as decalcification of C-S-H and dissolution of portlandite) was observed in the cementitious materials leading either to an opening of porosity (cement paste) or partial clogging (shotcrete). This contrasting behaviour was thought to be influenced by the heterogeneity in the hydrodynamic conditions and the buffering of the clay rock. No major evolution in the mineralogy of the clay rock was observed (i.e., no smectite illitization or zeolite formation), although the slight increase in CEC was interpreted as precipitation of C-S-H.

Fernandez et al. (2006) performed tests on the interface evolution between FEBEX bentonite and OPC-based mortar in laboratory experiments performed at 25 °C, 60 °C and 120 °C for up to 12 months. It was found that only the first few millimetres around the mortar/bentonite interface were chemically disturbed at 25 °C and 60 °C, leading to the precipitation of C-S-H and brucite at the clay side. At 120 °C, a more distinct degradation of the bentonite was observed with tobermorite precipitation at the interface, and formation of Mg-saponite and zeolites (e.g., analcime) up to 10 mm and 20 mm depth from the interface, respectively, in the bentonite. Cuevas et al. (2006) observed also analcime formation and carbonation due to interaction of FEBEX bentonite with OPC mortar.

Dauzères (2010) and Dauzères et al. (2010) conducted laboratory experiments with hardened cement paste (based on OPC and a low-pH cementitious binder (OPC + silica fumed + fly ash)) with Callovo Oxfordian clay at 25 and 50 °C, observing a similar material evolution in the OPC based material as in previous studies, such as low carbonation, decalcification leading to the formation of macropores, and precipitation of ettringite. However, in the low-pH cementitious material Si-Mg phases were identified inside the cementitious material in contact with the clay. Similar precipitates were observed in the same cementitious materials immersed in synthetic CO<sub>x</sub> pore solution (Dauzères et al., 2014), and was observed on low-pH cement/Opalinus clay interfaces from the Mont Terri Underground Research

Laboratory (Dauzères et al., 2016). In the framework of the Cement/Clay Interaction (CI) experiment at the Mont Terri URL interactions between low pH cements and Opalinus clay have intensely been studied (Mäder et al., 2017). Four main studies (Jenni et al., 2014; Dauzères et al., 2016; Lerouge et al. 2017, Mäder et al. 2017) provided a detailed analysis of mineralogical changes over periods of several years and under realistic boundary conditions. In this experiment, the interfaces of Opalinus Clay with three different types of cementitious materials (based on OPC and two low-pH binders, namely ESDRED (60% CEM I + 40% silica fume) and low alkali cement (LAC, 90% CEMIII/B +10% nanosilica) were investigated after 2.2, 2.5 and 4.9 years (Jenni et al., 2014; Dauzères et al., 2016; Mäder et al., 2017). Jenni et al. (2014) observed a complex zonation with a strong Mg enrichment adjacent to the interface of both low-pH cementitious materials studied and a decrease of the calcium content linked to a decalcification of the initial low-pH cements after 2.2 years. In addition, a decrease in pH and sulphate close to the interface in the cementitious material occurred, and diffusion of sulphate towards higher pH regions (away from the interface) was observed, leading to formation of additional ettringite there. Consistently, the carbonated zones showed a reduced porosity, however, the nature of the carbonate phases in low pH cementitious material remained unclear. Dauzères et al. (2016) confirmed the earlier work of Jenni et al. (2014) using the results obtained after 5 years of cement/clay interaction. In this case, the degraded region in both studied low-pH cementitious materials was between 2–4 mm, with a Mg enrichment and decalcification close to the interface. The mineralogical phase associated with the Mg enrichment was identified as a gel-like Mg–Si phase (M-S-H). Lerouge et al. (2017) described the results obtained after 5 years of interaction between LAC concrete and OPA, with the interactions limited to a roughly 1 mm thick highly porous white crust developed on the concrete side. Quantitative mineralogical mapping provided evidence of a Mg-rich phase associated with calcite, C-S-H and other cement phases. The Mg-rich phase was shown to be a tri-octahedral 2:1 phyllosilicate.

More recently, a number of studies on cement/clay interaction have been performed within the CEBAMA project, focussing in particular on low-pH cementitious materials (Duro et al., 2019). Bourbon et al. (2017) studied the evolution of two different low-pH concrete formulations (rich in fly ash and slag, respectively) in contact with Callovo Oxfordian clay in the Bure underground research laboratory. Samples taken indicated no significant evolution/transformation of neither concrete at the interface with the COx argillite, with the absence of cracks at a large scale. Lalan et al. (2016, 2019) studied the influence of temperature on the behaviour of high pH OPC based cement paste (CEM I) and different low-pH concrete formulations in contact with argillite from Tournemire. The low-pH cementitious material was initially thought to reduce the impact of the cement-based material on the clay rock. However, at 70 °C, the results showed a more pronounced degradation of the clay rock (dissolution of clay minerals) not observed in contact with the OPC based material. This was thought to be linked to the chemical transient during the cement paste hydration. In addition, the alteration of the cementitious material was more pronounced in the low-pH cementitious material (decalcification, M-S-H precipitation causing porosity opening) compared to the CEM I based material.

Gaboreau et al. (2019) and Phung et al. (2018) investigated the chemical evolution at the interfaces between cementitious materials and Boom Clay, focusing in particular on leaching and carbonation as important degradation processes. They investigated concrete materials from the underground research laboratory HADES (Mol, Belgium) had been in contact with Boom Clay for 14 years. The microtomography and autoradiography results on the porosity evolution at the interface revealed an increase in total porosity of the concrete interface due to Ca-leaching, which may indicate that clogging at the cementitious materials side might not occur. In contrast, the porosity in the clay side seemed to decrease, indicating some precipitations that may clog the clay pores in the long-term.

Studies within CEBAMA of the interface between OPC and bentonite from the FEBEX experiment, after 14 years of interaction, and from lab tests of 10 years of duration allowed the identification of the main processes occurring at the interfaces (cf. Torres et al., 2018). The processes observed were found to be compatible with those obtained from short-term alteration experiments (González-Santamaria et al., 2018), although their extent was less pronounced in the case of the short-term experiments. At the

bentonite interface with concrete, an accumulation of Ca and Mg was observed and penetration of Cl (up to 2-3 cm) and sulphate (up to 1-2 cm) was detected inside the concrete bulk.

#### *Natural analogues*

Although experimental studies (laboratory and *in situ*) on cement/clay interactions and interfaces can provide key evidence for reaction mechanisms, products and rates, they are limited in terms of timescales, compared to the time scales relevant to geological disposal, i.e., exceeding  $10^5$  years. Here, natural analogues may provide additional evidence, in particular on kinetically slow processes on longer time scales. In the context of nuclear waste disposal, many safety cases prepared over the last years have included natural, archaeological or industrial analogues in some way, e.g., to support conceptual model development, to test models, or with direct input of data.

One of the most intensely investigated analogues regarding cement/clay interaction is the Maqarin area in Jordan (Khoury et al., 1985; Alexander et al., 1992; Khoury et al., 1992; Smellie, 1998; Alexander and Smellie, 1998; Crossland, 2006; Savage, 2006; Milodowski et al., 2015). In this area, hyperalkaline groundwaters are the product of low-temperature leaching of an assemblage of natural cement minerals that were produced as a result of high-temperature/low-pressure pyro-metamorphism of marls (i.e., clay biomicrites) and limestones. Downstream of the cement zone, highly alkaline groundwater circulated through fractures within the biomicrite clay. The fracture surfaces show dissolution of different minerals (e.g., calcite, kaolinite, illite, albite, silica as well as organic matter), whereas within the fractures different opening/closing episodes may have taken place with complex mineralogical sequences, leading first to aragonite precipitation, followed by a solid solution of ettringite, thaumasite and gypsum. Moreover, precipitation of jennite and tobermorite in fractures as well as local formation of some zeolites (e.g., mordenite, laumontite, chabasite) was observed, the nature of the zeolites depending on the saturation state of the groundwater with respect to quartz. The perturbation front around the fractures were evaluated at about 40 mm for an interaction period of about 100,000 years. In the extended summary of the Maqarin analogue project of Smellie (1998) it is stated that the evidence from Maqarin shows that

- the sequences of minerals predicted by thermodynamic and coupled modelling are similar to those observed in hyperalkaline alteration zones,
- the rock matrix may be accessible to diffusion of aqueous species even during the phase of on-going wall-rock alteration, and
- the narrow aperture fractures will probably be self-healing.

Milodowski et al. (2015) concluded with respect to the evidence provided with respect to cement/clay interactions that:

- the detailed geomorphological reconstructions at Maqarin show that the pyrometamorphic rocks – the “natural cement zone” – are about 0.5 to 2 Ma old, and the hyperalkaline groundwater system has been operative for at least 80,000 to 100,000 years, i.e., addressing timescales directly relevant to the safety case timescales considered for a geological disposal facility;
- the hyperalkaline pore fluid conditions, generated by minerals analogous to those envisaged for cements, are long-lived at these sites (in excess of hundreds of thousands of years);
- the Maqarin study well-illustrates long-term cement/clay stability/degradation in the near-field, and the evolution and propagation of a high pH plume in both the nearfield and geosphere;
- the data from the Maqarin site have proved valuable for testing and validating the applicability of thermodynamic data to hyperalkaline conditions to predict the extent of high pH water/rock interaction and radionuclide transport,
- the reaction between hyperalkaline cement leachate and silicate rocks produces secondary phases with high molar volumes which suggest that the volume increase in secondary reaction products will tend to lead to sealing of flow paths, and
- the reactions and mineral precipitation sequences observed at Maqarin correspond closely to the observed and predicted behaviour of industrial cements, and the evolutionary sequence of mineralogical reactions associated with the propagation of a hyperalkaline plume.

Moreover, the stability of bentonites under influence of alkaline natural groundwaters with the same pH-range as low-pH cements have been investigated in both, the Philippine natural analogue study (e.g., Alexander et al., 2008; Reijonen and Alexander, 2015; Milodowski et al., 2015) and the Cyprus natural

analogue study (e.g., Alexander and Milodowski, 2011; Alexander et al., 2011, 2013; Milodowski et al., 2015, 2016). In both cases, the study areas consisted of ophiolites formed when ancient ocean crust has been thrust (obducted) onto the continental plates at convergent plate boundaries. Low-temperature reactions of near-neutral pH groundwater with the silicate minerals olivine and pyroxene present within the basic and ultrabasic rocks in the ophiolites produce highly alkaline groundwaters that are a common feature of many ophiolites worldwide (e.g., also in the Semail ophiolite in Oman; cf. Bath et al., 1987; Savage, 2005; Milodowski et al., 2015). Bentonites are often present within the sedimentary sequence deposited on top of the upper-most layer of igneous rock forming the oceanic crust, and are thus a common feature of many ophiolites. The results of these studies suggested that little reaction of the bentonite has occurred over millions of years.

Milodowski et al. (2015) concluded with respect to these analogue studies that

- the field conditions of this analogues are considered to realistically simulate those expected in a geological disposal facility,
- the results indicate minimal mineralogical alteration of bentonite by alkaline groundwater over periods  $10^5$  to  $10^6$  years with only very minor alteration and replacement of smectite by palygorskite along micro-fractures,
- the main effect of the interaction of bentonite and alkaline groundwater is a replacement of exchangeable Na in the bentonite by Ca, which can impact the swelling behaviour and plasticity of the bentonite, and
- that the studies suggests that it will be feasible to use bentonite clay barriers together with low-alkali cement and concrete in a deep geological repository (DGR), without deleterious effects on the bentonite barrier due to reaction with leachates derived from the cementitious materials.

### 4.3 Application of conceptual and mathematical models

Laboratory and *in situ* field experiments investigating cement/clay interactions have been performed for more than three decades, providing key evidence for reaction mechanisms, products and rates. However, by their very nature, they are limited in terms of timescales compared to those relevant for safety assessments for nuclear waste disposal, and the variability in experimental parameters (e.g., regarding different types of cementitious materials or concrete, types of clay rocks, and clay minerals, saturation, temperature, etc.) is limited. Due to these inherent limitations, in the last 15 years, substantial efforts have been made regarding predictive modelling of long-term interactions between cementitious materials and different clay materials, i.e., mainly clay rocks and bentonite (cf. reviews in Bildstein and Claret, 2015; Dautères, 2016; Claret et al., 2018; Savage and Cloet, 2018; Bildstein et al., 2019).

In these simulations, cement-clay interactions have been mainly modelled as coupled thermal-hydraulic-mechanical-chemical (THMC) processes in continuum scale reactive transport simulations, based on thermodynamic equilibria sometimes with the inclusion of kinetic data and diffusive transport, with various degrees of complexity. For example, in earlier calculations before about 2005, the cementitious materials were not represented as porous media, but rather as an alkaline plume imposed as a boundary condition on one side of the clay domain. Neretnieks (2014) proposed a simplified analytical model, which may be useful from a performance assessment point of view, but cannot reproduce the complex phenomena occurring at the cement interface. Very recently, pore scale modelling has also been applied to contribute to the process understanding of the interactions of these materials (Seigneur et al., 2017a, b; Patel et al., 2018).

The focus of the following sections is on (continuum-scale) reactive transport simulations of cement/clay interactions coupling transport and chemistry, referring to studies explicitly considering the interface and addressing both cementitious materials and clay rock as porous media. Table 4.2 provides an overview on a number of reactive transport modelling studies on cement/clay interactions, including studies addressing the simulation of laboratory and *in situ* experiments as well as long-term predictive studies. Generally, over the last decade, the simulations that have been performed used modelling strategies of growing complexity, taking into account more minerals and secondary phases and considering mineral dissolution and precipitation both at local equilibrium and kinetically controlled.

A large variety of reactive transport codes based on different concepts (e.g., regarding the chemical solver) has been used in the simulation studies on cement/clay interactions including RETRASO (Saaltink et al., 1998), HYTEC (van der Lee et al., 2003), QPAC (Quintessa, 2012), PhreeqC (Parkhurst and Appelo, 1999) or codes based thereon (e.g., Yamaguchi et al., 2008, 2013), TOUGHREACT (Xu et al., 2004; Burnol et al., 2006), ALLIANCES (PHREEQC/MT3D; Montarnal et al. 2007), CORE2D (Samper et al., 2003), CRUNCH (Bildstein and Claret, 2015), OpenGeoSys-GEM (Kolditz et al., 2012; Kosakowski and Watanabe, 2014), ORCHESTRA (Meeussen, 2003), FLOTRAN (Lichtner, 2007), MIN3P-THCm (Mayer et al., 2002) or iCP (Nardi et al., 2014). A detailed description of most of the codes can be found in Steefel et al. (2015). Recently, the accuracy, robustness, completeness, and numerical stability to describe multicomponent reactive transport across a cement/clay rock interface has been successfully benchmarked (cf. Marty et al., 2015; Bildstein and Claret, 2015; Bildstein et al., 2019). A variety of thermodynamic databases has been used, incl. EQ3/6 (Wolery 1983), CEMDATA2007 and successors (Lothenbach and Winnefeld, 2006; Matschei et al., 2007; Lothenbach et al., 2019), Nagra/PSI database (Hummel et al., 2002; Thoenen et al., 2014), ThermoChimie (Giffaut et al., 2014) or ThermoDEM (Blanc et al., 2012). In particular during the last years, the thermodynamic database for hydration phases in cementitious materials and clay minerals has been significantly improved (cf. Blanc et al., 2010a,b; 2015). The geometrical set ups (e.g. 1D/ 2D cartesian, 1D radial, 1D or 2D) and mesh size as well as transport parameters and the approaches to mineral dissolution/precipitation (i.e., local equilibrium and/or in kinetics) have recently been reviewed by (Claret et al. 2018).

Regarding the systems studied, most simulations concern the interactions between cementitious materials with natural clay rocks, whereas there are relatively fewer studies that have investigated the interaction with bentonites. In the majority of the cases, OPC-based high-pH cementitious materials were addressed (CEM I); only recently, interface processes between low pH cementitious materials have been addressed in reactive transport modelling studies at different time and length scales (Berner et al., 2013; Dauzères et al., 2016). Idiart et al. (2020) performed a benchmark study on the interaction of a low pH concrete (Cebama reference mix concrete) with a Callovo-Oxfordian clay rock (simulation time frame 100,000 years), comparing different codes, using a number of simulation cases with increasing complexity. Overall, the results a good agreement obtained with different codes was obtained, demonstrating the applicability of reactive transport modelling to support safety assessments. The impact of including the (slow) dissolution kinetics of the clay minerals was shown to be negligible in the studied system.

Most long-term simulation studies were performed for a temperature of 25 °C; only in a few cases the effects of temperatures above 25 °C were investigated. Here, greater rates of dissolution of montmorillonite and other minerals were noted; however, leading to relatively little differences compared to simulation results at 25 °C (cf. Savage and Cloet, 2018). While most simulations were conducted for fully water saturated conditions, simulations accounting for non-saturated or evolving conditions with respect to saturation state are rare. Generally, with very few exceptions (e.g., in some simulations with ORCHESTRA), anionic exclusion in clay and multi-components diffusion were not considered in the simulation studies.

With respect to the simulation of laboratory and *in situ* experiments, it can generally be concluded that reactive transport modelling shows a great capability for reproducing the experiments, e.g., regarding mineralogical transformation pathways and net porosity evolution (cf. Bildstein et al., 2019). Despite the differences in the practice of long-term simulation approaches addressing cement-clay interactions carried out in the last years, there are general similarities in terms of the predicted thickness of the altered zones in the clay and cement domain, the types of secondary solid products and changes in porosity. The simulations show a narrow zone (mainly in the order of cm to dm) of perturbed mineral and fluid chemistry located close to the interface, for timescales up to and beyond 100,000 years (cf. Savage and Cloet, 2018; Bildstein et al., 2019). Regarding the predicted mineral transformations there are recurring results, such as decalcification of cementitious material (portlandite dissolution, decrease of the Ca/Si ratio in C-S-H), precipitation of ettringite in the presence of sulphates, and/or carbonation and smectite dissolution, dedolomitisation, and formation of C-(A)-S-H solids, clay minerals (illite, saponite), zeolites and carbonates in the clay domain.

Critical parameters identified in the various studies comprise dissolution/precipitation kinetics and the description of evolving reactive surface areas that can play an important role in sequential minerals' appearance or disappearance, the localization of porosity reduction and increase, the kinetics and the laws controlling the porosity/permeability and porosity/diffusivity feedback, and the inclusion of certain secondary phases (e.g., zeolites) and their thermodynamic/kinetic parameters. For example, thermodynamic data for M-S-H and C-A-S-H phases only became available recently (cf. Roos et al., 2018; Lothenbach et al., 2019), and were thus not included in previous modelling studies.

Table 4-2 – Summary of simulation studies addressing i) laboratory and in situ experiments and ii) long-term predictions of cement/clay interactions.

Cementitious material	Clay	Simulation time	Code	Thermodynamic database	Temperature	Dimensions	Geometry	Conditions	Chemical reactions	Porosity update	Reference
CEM I	Boom Clay	1.5 y	RETRASO	EQ3/6 LLNL	25 °C / 85 °C	0.002 m	1D cartesian	saturated	local equilibrium and kinetics	yes	Read et al., 2001
CEM I (concrete)	Toarcian clay	15 y	HYTEC	EQ3/6 LLNL	15 °C	0.20 m	1D radial	saturated	local equilibrium and kinetics	yes	De Windt et al., 2008
CEM I	Toarcian clay	15 y	QPAC	LLNL	15 °C	0.5 m	1D radial	saturated	local equilibrium and kinetics	yes	Watson et al., 2013
CEM I	Toarcian clay	15 y	CrunchFlow	LLNL	15 °C	1.155 m	1D/2D radial	saturated	local equilibrium and kinetics	yes	Soler, 2013
CEM I	Toarcian clay	18 y	HYTEC	CHESSE CEMDATA07	25 °C	0.044 m	1D cartesian	saturated	local equilibrium and kinetics	yes	Bartier et al., 2013
CEM I	Toarcian clay	15 y	MC-CEMENT	various sources	15 °C	0.11 m	1D cartesian	saturated	local equilibrium and kinetics	yes	Yamaguchi et al., 2013
LAC / ESDRED low-pH concrete	Opalinus Clay	5 y	HYTEC	CHESSE CEMDATA07	25 °C	1 m	1D cartesian	saturated	local equilibrium and kinetics	yes	Dauzères et al., 2016
CEM I, low pH concrete	Opalinus Clay	5 y	FLOTRAN	EQ3/6 LLNL + CEMDATA07	25 °C	0.25 m	1D cartesian	saturated	local equilibrium and kinetics	yes	Jenni et al., 2017
CEM I (concrete)	FEBEX bentonite	1 y	CrunchFlow	extended LLNL	25 °C / 120 °C	0.029 m	1D cartesian	saturated	local equilibrium and kinetics	no	Fernandez et al., 2009
CEM I (concrete)	Toarcian clay	100,000 y	HYTEC	EQ3/6 LLNL	25 °C	20 m	1D cartesian	saturated	local equilibrium	yes	De Windt et al., 2004a
CEM I (concrete)	Toarcian clay	100,000 y	HYTEC	EQ3/6 LLNL	70 °C	35 m x 15 m	2D cylindrical	saturated	local equilibrium	not specified	De Windt et al., 2004b
CEM I	Callovo-Oxfordian clay	2,000 y	TOUGHREACT	EQ3/6	non isothermal	100 m	1D radial	unsaturated (evolving)	local equilibrium	no	Burnol et al., 2006
CEM I / CEM V (concrete)	Callovo-Oxfordian clay	1,000,000 y	HYTEC	EQ3/6 LLNL	25 °C	17.5 m	1D radial	saturated	local equilibrium	yes	Trotignon et al., 2006
CEM I / CEM V (concrete)	Callovo-Oxfordian clay	1,000,000 y	HYTEC	EQ3/6 LLNL	25 °C	17.5 m	1D radial	saturated	local equilibrium and kinetics	yes	Trotignon et al., 2007
CEM I	Callovo-Oxfordian clay	10 y	TOUGHREACT	Thermoddem	25 °C (initial)	40 m	1D radial	unsaturated / saturated	kinetic assumption	yes	Trotignon et al., 2011
CEM I (concrete)	Callovo-Oxfordian clay	1,000,000 y	TOUGHREACT	Thermochimie	25 °C	10 m	1D cartesian	saturated	local equilibrium and kinetics	yes	Marty et al., 2009
CEM I	Callovo-Oxfordian clay	100,000 y	PhreeqC	Thermochimie	25 °C	43 m / 45.4 m	1D cartesian and 1D radial	saturated	local equilibrium and kinetics	no/yes	Marty et al. 2014

Table 4-2 – continued

Cementitious material	Clay	Simulation time	Code	Thermodynamic database	Temperature	Dimensions	Geometry	Conditions	Chemical reactions	Porosity update	Reference
CEM I	Callovo-Oxfordian clay	10,000 y	Toughreact, PhreeqC, CRUNCH, HYTEC, ORCHESTRA, MIN3P-THCm	Thermoddem	25 °C	43 m	1D radial	saturated	local equilibrium and kinetics	no	Marty et al., 2015
CEBAMA low-pH concrete	Callovo-Oxfordian clay	100,000 y	iCP, CORE2D OpenGeoSys-GEM, MIN3P ORCHESTRA	Thermochemie/Thermoddem	25 °C	43 m	1D cartesian	saturated	local equilibrium and kinetics	yes *)	Idiart et al., 2020
ESDRED low-pH concrete	Opalinus Clay	10,000 and 30,000 y	OpenGeoSys-GEM	NAGRA-PSI + CEMDATA 07	25 °C	5.6 m	1D axial symmetric	saturated	local equilibrium and kinetics	yes	Berner et al., 2013
CEM I (concrete)	Opalinus Clay	2,000 – 4,000 y	OpenGeoSys-GEM	NAGRA-PSI	25 °C	46 m	1D linear	saturated	local equilibrium	yes	Kosakowski and Berner, 2013
CEM I	bentonite	1,000,000 y	CORE-2D	EQ3/6	time varying	25 m	1D axial symmetric	unsaturated (evolving)	local equilibrium	not defined	Yang et al., 2008
CEM I	bentonite	10,000 y	MC-BENT	various sources	25, 45, 50, and 60 °C	1.2 m	1D cartesian	saturated	local equilibrium and kinetics	not defined	Yamaguchi et al., 2008
CEM I	generic clay	80 y	OpenGeoSys-GEM	NAGRA-PSI + CEMDATA 07	25 °C	0.40 m	1D cartesian	saturated	local equilibrium	no	Kosakowski et al., 2009
CEM I (concrete)	clay rock/bentonite	100,000 y	ALLIANCES	not given	25 °C	60 m	2D cartesian	saturated	local equilibrium	not defined	Montarnal et al., 2007
CEM I	FEBEX bentonite	100,000 y	CrunchFlow	LLNL	80 °C	1.8 m	1D cartesian	saturated	kinetic assumption	no	Fernandez et al., 2009

\*) depending on calculation case

## 4.4 Resume

Large volumes of cementitious and clay materials will be used as backfill/barrier material or as structural support in a deep geological disposal facility for nuclear waste. In order to be able to license a final repository for radioactive waste, a profound understanding of how these barriers evolve with time is needed.

One important process that reduces the performances of the barriers over time is the leaching/degradation of the cementitious material, especially at the cement/clay interface in response to the chemical gradient between the various constituents of cement and clay pore waters. A substantial effort has been made in the characterization of the mineralogical changes over relatively long time periods. Additionally, reactive transport modelling appears to predict well the chemical evolution occurring during the alteration of the cementitious and clay materials.

To complete the description of the mineralogical and geochemical changes at the interface cement/clay and to obtain a better understanding of the impact that these processes can have on radionuclide (mainly anions) migration, further efforts would need to be part of a more realistic reactive transport modelling. These efforts consist on providing the following input parameters, in terms of mineralogy, with a quantification over time of the secondary phases (such as gypsum, calcite, Mg enriched area, etc.) formed during the alteration processes, and in terms of transport properties over time, with a quantification of reactive transport parameter values characteristic to the altered area at the cement/clay interface.

## 4.5 References

- Abubaker, F., Lynsdale, C., Cripps, J., 2014a. Laboratory study of the long-term durability of buried concrete exposed to Lower Lias Clay. *Construction and Building Materials* 64, 130-140.
- Abubaker, F., Lynsdale, C., Cripps, J. 2014b. Investigation of concrete–clay interaction with regards to the thaumasite form of sulfate attack. *Construction and Building Materials* 67A, 88-94.
- Adler, M., Mäder, U.K., Waber, H.N., 1999. High-pH alteration of argillaceous rocks: an experimental study. *Schweizerische Mineralogische und Petrographische Mitteilungen* 79, 445-454.
- Adler, M., 2001. Interaction of claystone and hyperalkaline solutions at 30°C: A combined experimental and modelling study. Ph.D. thesis, University of Bern, Bern, Switzerland.
- Alexander, W.R., Smellie, J.A.T., 1998. Maqarin natural analogue project. ANDRA, CEA, Nagra, Nirex and SKB synthesis report on Phases I, II and III. Nagra Technical Report NTB 98-08, Nagra, Wettingen, Switzerland.
- Alexander, W.R., Milodowski, A.E. (eds.), 2011. Cyprus Natural Analogue Project (CNAP) Phase II Final Report. Posiva Working Report WR2011-08, Posiva, Eurajoki, Finland.
- Alexander, W.R., Dayal, R., Eagleson, K., Eikenberg, J., Hamilton, E., Linklater, C.M., McKinley, I.G., Tweed, C.J., 1992. A natural analogue of high pH cement pore waters from the Maqarin area of northern Jordan. II: results of predictive geochemical calculations. *Journal of Geochemical Exploration* 46, 133-146.
- Alexander, W.R., Arcilla, C.A., McKinley, I.G., Kawamura, H., Takahashi, Y., Aoki, K., Miyoshi, S., 2008. A new natural analogue study of the interaction of low-alkali cement leachates and the bentonite buffer of a radioactive waste repository. *Materials Research Society Symposium Proceedings* 1107, 493.
- Alexander, W.R., Milodowski, A.E., Pitty, A.F. (eds.), 2011. Cyprus Natural Analogue Project (CNAP) Phase III Final Report. Posiva Working Report WR2011-77, Posiva, Eurajoki, Finland.
- Alexander, W.R., Milodowski, A.E., Pitty, A.F., Hardy, S.M.L., Kemp, S.J., Rushton, J.C., Siathas, A., Siathas, A., Mackenzie, A.B., Korkeakoski, P., Norris, S., Sellin, P., Rigas, M., 2013. Bentonite reactivity

in alkaline solutions: results of the Cyprus Natural Analogue Project (CNAP). *Clay Minerals* 48, 235-249.

Alonso, M.C., García Calvo, J.L., Cuevas, J., Turrero, M.J., Fernández, R., Torres, E., Ruiz, A.I., 2017. Interaction processes at the concrete-bentonite interface after 13 years of FEBEX-Plug operation. Part I: Concrete alteration. *Physics and Chemistry of the Earth, Parts A/B/C* 99, 38-48.

Balmer, S., Kaufhold, S., Dohrmann, R., 2017. Cement-bentonite-iron interactions on small scale tests for testing performance of bentonites as a barrier in high-level radioactive waste repository concepts. *Applied Clay Science* 135, 427-436.

Bamforth, P.B., Baston, G.M.N., Berry, J.A., Glasser, F.P., Heath, T.G., Jackson, C.P., Savage, D., Swanton, S.W., 2012. Cement materials for use as backfill, sealing and structural materials in geological disposal concepts. A review of current status. Serco Report SERCO/005125/001 Issue 3, Serco, Harwell, Didcot, United Kingdom.

Bartier, D., Techer, I., Dauzères, A., Boulvais, P., Blanc-Valleron, M.-B., Cabrera, J., 2013. In situ investigations and reactive transport modelling of cement paste/argillite interactions in a saturated context and outside an excavated disturbed zone. *Applied Geochemistry* 31, 94-108.

Bath, A.H., Christofi, N., Neal, C., Philp, J.C., Cave, M.R. McKinley, I.G., Berner, U. 1987. Trace element and microbiological studies of alkaline groundwaters in Oman: a natural analogue for cement porewaters. Nagra Technical Report NTB 87-16, Nagra, Wettingen, Switzerland.

Beattie, T.M., Williams, S.J., 2012. An overview of near-field evolution research in support of the UK geological disposal programme. *Mineralogical Magazine* 76, 2995-3001.

Bernard, E., Lothenbach, B., Rentsch, D., Pochard, I., Dauzères, A., 2017. Formation of magnesium silicate hydrates (M-S-H). *Physics and Chemistry of the Earth, Parts A/B/C* 99, 142-157.

Berner, U.R., 1992. Evolution of pore water chemistry during degradation of cement in a radioactive waste repository environment, *Waste Management* 12, 201-219.

Berner, U., Kulik, D.A., Kosakowski, G., 2013. Geochemical impact of a low-pH cement liner on the near field of a repository for spent fuel and high-level radioactive waste. *Physics and Chemistry of the Earth Parts ABC* 64, 46-56.

Bildstein, O., Claret, F., 2015. Stability of clay barriers under chemical perturbations. In: Tournassat, C., Steefel, C.I., Bourg, I.C., Bergaya, F. (eds.) *Natural and Engineered Clay Barriers, Developments in Clay Science* 6, 155-188.

Bildstein, O., Claret, F., Frugier, P., 2019. RTM for waste repositories. *Reviews in Mineralogy and Geochemistry* 85, 419-457, 2019.

Blanc, P., Bourbon, X., Lassin, A., Gaucher, E.C., 2010a. Chemical model for cement based materials: Temperature dependence of thermodynamic functions for nanocrystalline and crystalline C-S-H phases. *Cement and Concrete Research* 40, 851-866.

Blanc, P., Bourbon, X., Lassin, A., Gaucher, E.C., 2010b. Chemical model for cement based materials: thermodynamic data assessment for phases other than C-S-H. *Cement and Concrete Research* 40, 1360-1374.

Blanc, P., Lassin, A., Piantone, P., Azaroual, M., Jacquemet, N., Fabbri, A., Gaucher, E.C., 2012. ThermoDEM: A geochemical database focused on low temperature water/rock interactions and waste materials. *Applied Geochemistry* 27, 2107-2116,

Blanc, P., Vieillard, P., Gailhanou, H., Gaboreau, S., Marty, N., Claret, F., Madé, B., Giffaut, E. 2015. ThermoChimie database developments in the framework of cement/clay interactions. *Applied Geochemistry* 55, 95-107.

Bourbon, X., Yannick, L., Nicolas, G., 2017. Physical and chemical behaviour of low hydration heat/low pH concretes. In: Altmaier, M., Montoya, V., Duro, L., Valls, A. (eds.), Proceedings of the First Annual Workshop of the HORIZON 2020 CEBAMA Project. KIT Scientific reports 7734, 137-145.

Burnol, A., Blanc, P., Xu, T., Spycher, N., Gaucher, E.C., 2006. Uncertainty in the reactive transport model response to an alkaline perturbation in a clay formation. TOUGH Symposium 2006, Berkeley, California.

Claret, F., Marty, N., Tournassat, C., 2018. Modeling the long-term stability of multibarrier systems for nuclear waste disposal in geological clay formations. In: Xiao, Y., Whitaker, F., Xu, T., Steefel, C. (eds.) Reactive Transport Modeling: Applications in Subsurface Energy and Environmental Problems, Wiley, 395-436.

Cuevas, J., Vigil de la Villa, R., Ramirez, S., Sanchez, L., Fernández, R., Leguey, S., 2006. The alkaline reaction of FEBEX bentonite: a contribution to the study of the performance of bentonite/concrete engineered barrier systems. Journal of Iberian Geology 32, 151-174.

Crossland, I.C., 2006. Long-term properties of cement - Evidence from nature and archaeology. Crossland Report CCL/2006/01

Dauzères, A., 2010. Etude expérimentale et modélisation des mécanismes physicochimiques des interactions béton-argile dans le contexte du stockage géologique des déchets radioactifs. PhD thesis, University of Poitiers, Poitiers, France.

Dauzères, A., 2016. Geochemical and physical evolution of cementitious materials in an aggressive environment. In: Vehmas, T., Holt, E. (eds.) CEBAMA Deliverable D 1.03 - WP1 Experimental studies – State of the art literature review, 136-174 ([www.cebama.eu](http://www.cebama.eu)).

Dauzères, A., Le Bescop, P., Sardini, P., Cau Dit Coumes, C., 2010. Physico-chemical investigation of clayey/cement-based materials interaction in the context of geological waste disposal: Experimental approach and results. Cement and Concrete Research 40, 1327-1340.

Dauzères, A., Le Bescop, P., Cau-Dit-Coumes, C., Brunet, F., Bourbon, X., Timonen, J., Voutilainen, M., Chomat, L., and Sardini, P., 2014. On the physico-chemical evolution of low-pH and CEM I cement pastes interacting with Callovo-Oxfordian pore water under its in situ CO<sub>2</sub> partial pressure. Cement and Concrete Research 58, 76–88.

Dauzères, A., Achiedo, G., Nied, D., Bernard, E., Alahrache, S., Lothenbach, B., 2016. Magnesium perturbation in low-pH concretes placed in clayey environment—solid characterizations and modelling. Cement and Concrete Research 79, 137-150.

De Windt, L., Pellegrini, D., van der Lee, J., 2004a. Coupled modelling of cement/claystone interactions and radionuclide migration. Journal of Contaminant Hydrology 68, 165-182.

De Windt, L., Pellegrini, D., van der Lee, J., 2004b. Reactive transport modelling of a spent fuel repository in a stiff clay formation considering excavation damaged zones. Radiochimica Acta 92, 841-848.

De Windt, L., Marsal, F., Tinseau, E., Pellegrini, D., 2008. Reactive transport modeling of geochemical interactions at a concrete/argillite interface, Tournemire site (France). Physics and Chemistry of the Earth 33, 295-305.

Devol-Brown, I., Tinseau, E., Marsal, F., Pellegrini, D., Mifsud, A., Lemius, S., Stammose, D., Cabrera, J., 2008. Argillite/concrete and argillite/steel interactions: Experiences gained from the Tournemire Underground Research Laboratory. In: Lattefer, A.P. (ed.) Nuclear waste research: Siting, technology and treatment, Nova Science Publisher, 167-187.

Drace, Z., Ojovan, M.I., 2013. A summary of IAEA coordinated research project on cementitious materials for radioactive waste management, in: Bart, F., Cau-dit-Coumes, C., Frizon, F., Lorente, S. (eds) Cement-based materials for nuclear waste storage, Springer, 3-11.

- Duro, L., Altmaier, M., Holt, E., Mäder, U., Claret, F., Grambow, B., Idiar, A., Valls, A., Montoya, V., 2020. Contribution of the results of the CEBAMA project to decrease uncertainties in the Safety Case and Performance Assessment of radioactive waste repositories. *Applied Geochemistry* 112, 104479.
- Fernandez, R., Cuevas, J., Mäder, U.K., 2009. Modelling concrete interaction with a bentonite barrier, *European Journal of Mineralogy* 21, 177-191.
- Fernández, R., Ruiz A.I., Cuevas, J., 2016. Formation of C-A-S-H phases from the interaction between concrete or cement and bentonite. *Clay Minerals* 51, 223–235.
- Fernández, R., Torres E, Ruiz A.I, Cuevas J., Alonso M.C, García Calvo J.L., Rodríguez E., Turrero M.J., 2017. Interaction processes at the concrete-bentonite interface after 13 years of FEBEX-Plug operation. Part II: Bentonite contact. *Physics and Chemistry of the Earth, Parts A/B/C* 99, 49-63.
- Gaucher, E.C., Blanc, P., 2006. Cement/clay interactions - A review: Experiments, natural analogues, and modeling. *Waste Management*, 26, 776-788.
- Gaboreau, S., Pret, D., Tinseau, E., Claret, F., Pellegrini, D., Stammose, D., 2011. 15 years of in situ cement–argillite interaction from Tournemire URL: Characterisation of the multi-scale spatial heterogeneities of pore space evolution. *Applied Geochemistry* 26, 2159–2171.
- Gaboreau, S., Lerouge, C., Dewonck, S., Linard, Y., Bourbon, X., Fialips, C.I., Mazurier, A., Prêt, D., Borschneck, D., Montouillout, V., Gaucher, E.C., Claret, F. 2012. In-situ interaction of cement paste and shotcrete with claystones in a deep disposal context. *American Journal of Science*, 312, 314–356.
- Gaboreau, S., Phung, Q.T., Claret, F., Maes, N., 2019. Multi-Scale characterization of the spatial heterogeneities of microstructural and mineralogical evolution of 14 year in situ concrete-clay interfaces. In: KIT (ed.) *Proceedings of 5<sup>th</sup> International Workshop on Mechanisms and Modelling of Waste/Cement Interactions*, March, 25<sup>th</sup> – 27<sup>th</sup>, 2019 Karlsruhe, Germany.
- Giffaut, E., Grivé, M., Blanc, Ph., Vieillard, Ph., Colàs, E., Gailhanou, H., Gaboreau, S., Marty, N., Madé, B., Duro, L., 2014. Andra thermodynamic database for performance assessment: ThermoChimie. *Applied Geochemistry* 49, 225-236.
- Glasser, F.P., 2011. Application of inorganic cements to the conditioning and immobilisation of radioactive wastes. In: Ojovan, M.I. (ed.) *Handbook of advanced radioactive waste conditioning technologies*, Woodhead, 67-135.
- González-Santamaría, D.E., Angulo, M., Ruiz, A.I., Fernandez, R., Ortega, A., Cuevas, J., 2018. Low-pH cement mortar-bentonite perturbations in a small-scale pilot laboratory experiment. *Clay Minerals* 53, 237-254.
- Harris, A.W., Manning, M.C., Tearle, W.M., Tweed, C.J., 2002. Testing of models of the dissolution of cements - leaching of synthetic C-S-H gels. *Cement and Concrete Research* 32, 731-746.
- Hoch, A.R., Baston, G.M.N., Glasser, F.P., Hunter, F.M.I., Smith, V., 2012. Modelling evolution in the near field of a cementitious repository. *Mineralogical Magazine*. 76, 3055-3069.
- Honty, M., De Craen, M., Wang, L., Madejová, J., Czímerová, A., Pentrák, M., Stríček, I., Van Geet, M., 2010. The effect of high pH alkaline solutions on the mineral stability of the Boom Clay – Batch experiments at 60°C. *Applied Geochemistry* 25, 825-840.
- Hummel, W., Berner, U., Curti, E., Pearson, F.J., Thoenen, T., 2002. *Nagra/PSI Chemical Thermodynamic Data Base 01/01*. Universal Publishers.
- Idiart, A., Laviña, M., Kosakowski, G., Cochepin, B., Meeussen, J.C.L., Samper, J., Mon, A., Montoya, V., Munier, I., Poonosamy, J., Montenegro, L., Deissmann, G., Rohmen, S., Hax Damiani, L., Coene, E., Nieves, A., 2020. Reactive transport modelling of a low-pH concrete / clay interface. *Applied Geochemistry* 115, 104562.

- Jefferies, N.L., Tweed, C.J., Wisbey, S.J., 1988. The effects of changes in pH within a clay surrounding a cementitious repository. *Materials Research Society Symposium Proceedings* 112, 43-52.
- Jenni, A., Mäder, U., Lerouge, C., Gaboreau, S., Schwyn, B., 2014. In situ interaction between different concretes and Opalinus Clay. *Physics and Chemistry of the Earth, Parts A/B/C* 70, 71–83.
- Jenni, A., Gimmi, T., Alt-Epping, A., Mader, U., Cloet, V., 2017. Interaction of ordinary Portland cement and Opalinus Clay: Dual porosity modelling compared to experimental data. *Physics and Chemistry of the Earth, Parts A/B/C* 99, 22-37.
- Kaufhold, S., Dohrmann, R., Ufer, K., Kober, F., 2018. Interactions of bentonite with metal and concrete from the FEBEX experiment: mineralogical and geochemical investigations of selected sampling sites. *Clay Minerals* 53, 745-763.
- Khoury, H.N., Salameh, E., Abdul-Jaber, Q., 1985. Characteristics of an unusual highly alkaline water from the Maqarin area, northern Jordan. *Journal of Hydrology* 81, 79-91.
- Khoury, H.N., Salameh, E., Clark, I., Fritz, P., Bajjali, W., Milodowski A., Cave, M., Alexander, W.R., 1992. A natural analogue of high pH cement pore waters from the Maqarin area of northern Jordan: I. Introduction to the site. *Journal of Geochemical Exploration* 46, 117-132.
- Kolditz, O., Bauer, S., Bilke, L., Böttcher, N., Delfs, J., Fischer, T., Görke, U., Kalbacher, T., Kosakowski, G., McDermott, C., 2012. OpenGeoSys: an open-source initiative for numerical simulation of thermo-hydro-mechanical/chemical (THM/C) processes in porous media. *Environmental Earth Sciences* 67, 589-599.
- Kosakowski, G., Blum, P., Kulik, D.A., Pflingsten, W., Shao, H., Singh, A., 2009. Evolution of a generic clay/cement interface: first reactive transport calculations utilizing a Gibbs energy minimization based approach for geochemical calculations. *Journal of Environmental Science for Sustainable Society* 3, 41-49.
- Kosakowski, G., Berner, U., 2013. The evolution of clay rock/cement interfaces in a cementitious repository for low- and intermediate level radioactive waste. *Physics and Chemistry of the Earth Part A/B/C* 64, 65-86.
- Kosakowski, G., Watanabe, N., 2014. OpenGeoSys-GEM: A numerical tool for calculating geochemical and porosity changes in saturated and partially saturated media. *Physics and Chemistry of the Earth Part A/B/C* 70-71, 138-149.
- Lalan, P., Dauzères, A., De Windt, L., Bartier, D., Sammaljärvi, J., Barnichon, J.-D., Techer, I., Detilleux, V., 2016. Impact of a 70 °C temperature on an ordinary Portland cement paste/claystone interface: An in situ experiment. *Cement and Concrete Research* 83, 164-178.
- Lalan, P., Dauzères, A., De Windt, L., Sammaljärvi, J., Bartier, D., Techer, I., Detilleux, V., Siitari-Kauppi, M., 2019. Mineralogical and microstructural evolution of Portland cement paste/argillite interfaces at 70 °C – considerations for diffusion and porosity properties. *Cement and Concrete Research* 115, 414-425.
- Lerouge C., Gaboreau S., Grangeon S., Claret F., Warmont F., Jenni A, Cloet V, Mäder., 2017. In situ interactions between Opalinus Clay and Low Alkali Concrete. *Physics and Chemistry of the Earth, Parts A/B/C* 99, 3-21.
- Lichtner, P.C., 2007. *Flotran user's manual version 2.0: LA-CC 02-036*, Los Alamos National Laboratory, Los Alamos, NM, USA.
- Lothenbach, B., Winnefeld, F., 2006. Thermodynamic modelling of the hydration of Portland cement, *Cement and Concrete Research* 36, 209-226.
- Lothenbach, B., Kulik, D., Matschei, T., Balonis, M., Baquerizo, L., Dilnesa, B.Z., Miron, D.G., Myers, R. 2019. Cemdata18: A chemical thermodynamic database for hydrated Portland cements and alkali-activated materials. *Cement and Concrete Research* 115, 472-506.

- Mäder, U., Jenni, A., Lerouge, C., Gaboreau, S., Miyoshi, S., Kimura, Y., Cloet, V., Fukaya, M., Claret, F., Otake, T., Shibata, M., Lothenbach B., 2017. 5-year chemico-physical evolution of concrete–claystone interfaces, Mont Terri rock laboratory (Switzerland). *Swiss Journal of Geosciences*, DOI 10.1007/s00015-016-0240-5.
- Marty, N.C.M., Tournassat, C., Burnol, A., Giffaut, E., Gaucher, E.C., 2009. Influence of reaction kinetics and mesh refinement on the numerical modelling of concrete/clay interactions. *Journal of Hydrology* 364, 58-72.
- Marty, N.C.M., Munier, I., Gaucher, E., Tournassat, C., Gaboreau, S., Vong, C., Giffaut, E., Cochevin, B., Claret, F., 2014. Simulation of cement/clay interactions: feedback on the increasing complexity of modelling strategies. *Transport in Porous Media* 104, 385-405.
- Marty, N.C.M., Bildstein, O., Blanc, P., Claret, F., Cochevin, B., Gaucher, E.C., Jacques, D., Lartigues, J.-E., Liu, S., Mayer, K.U., Meussen, J.C.L., Munier, I., Pointeau, I., Su, D., Steefel, C.I., 2015. Benchmarks for multicomponent reactive transport across a cement/clay interface. *Computational Geosciences* 19, 635-653.
- Matschei, T., Lothenbach, B., Glasser, F., 2007. Thermodynamic properties of Portland cement hydrates in the system  $\text{CaO-Al}_2\text{O}_3\text{-SiO}_2\text{-CaSO}_4\text{-CaCO}_3\text{-H}_2\text{O}$ . *Cement and Concrete Research* 37, 1379-1410.
- Mayer, K.U., Frind, E.O., Blowes, D.W., 2002. Multicomponent reactive transport modeling in variably saturated porous media using a generalized formulation for kinetically controlled reactions. *Water Resources Research* 38, 13-11–13-21.
- Meeussen, J.C.L., 2003. ORCHESTRA: An object-oriented framework for implementing chemical equilibrium models. *Environmental Science and Technology* 37, 1175-1182.
- Metcalfe, R., Walker, C., 2004. Proceedings of the International Workshop on Bentonite-Cement Interaction in Repository Environments, Tokyo. Posiva Working Report WR2004-25, Posiva, Olkiluoto, Finland.
- Michau, N., 2005. ECOCLAY II: Effects of cement on clay barrier performance. Andra Report C.RP.ASCM.04.0009, Andra, Paris, France.
- Milodowski, A.E., Alexander, W.R., West, J.M., Shaw, R.P., McEvoy, F.M., Scheidegger, J.M., Field, L.P., 2015. A catalogue of analogues for radioactive waste management. British Geological Survey Commissioned Report CR/15/106, British Geological Survey, Keyworth, Nottingham, United Kingdom.
- Milodowski, A.E., Norris, S., Alexander, W.R., 2016. Minimal alteration of montmorillonite following long-term interaction with natural alkaline groundwater: Implications for geological disposal of radioactive waste. *Applied Geochemistry*, 66. 184-197.
- Montarnal, P., Mugler, C., Colin, J., Descostes, M., Dimier, A., Jacquot, E., 2007. Presentation and use of a reactive transport code in porous media. *Physics and Chemistry of the Earth* 32, 507-517.
- Nardi, A., Idiart, A., Trincherro, P., de Vries, L.M., Molinero, J., 2014. Interface COMSOL-PHREEQC (iCP), an efficient numerical framework for the solution of coupled multiphysics and geochemistry. *Computers & Geosciences* 69: 10-21.
- NDA, 2016. Geological disposal - Geosphere status report. NDA Report no. DSSC/453/01, Nuclear Decommissioning Authority, Harwell, Didcot, United Kingdom.
- NEA, 2012. Cementitious Materials in Safety Cases for Geological Repositories for Radioactive Waste: Role, Evolution and Interactions. NEA/RWM/R(2012)3/REV.
- Neretnieks, I., 2014. Development of a simple model for the simultaneous degradation of concrete and clay in contact. *Applied Geochemistry* 43, 101-113.

Parkhurst, D.L., Appelo, C. 1999. User's guide to PHREEQC (Version 2): A computer program for speciation, batch reaction, one-dimensional transport, and inverse geochemical calculations. USGS Water-Resources Investigations Report 99-4259, US Geological Survey, Denver, CO, USA.

Patel, R.A., Perko, J., Jacques, D., De Schutter, G., Ye, G., Van Breugel, K., 2018. A three-dimensional lattice Boltzmann method based reactive transport model to simulate changes in cement paste microstructure due to calcium leaching. *Construction and Building Materials* 166, 158-170.

Phung, Q.T., Gaboreau, S., Claret, F., Maes, N., 2018. Degradation of concrete in a clay environment. In: *Proceedings of the 4th International Conference on Service Life Design for Infrastructures (SLD4)*, 27-30 August 2018, Delft, The Netherlands.

Quintessa (2012) QPAC: Quintessa's general-purpose modelling software. Quintessa Report QRS-QPAC-11, Quintessa, Henley-on-Thames, United Kingdom.

Read, D., Glasser, F.P., Ayora, C., Guardiola, M.T., Sneyers, A., 2001. Mineralogical and microstructural changes accompanying the interaction of Boom Clay with ordinary Portland cement. *Advances in Cement Research* 13, 175-183.

Reijonen, H.M., Alexander, W.R. 2015. Bentonite analogue research related to geological disposal of radioactive waste – current status and future outlook. *Swiss Journal of Geosciences*, 108, 101-110.

Roosz, C., Vieillard, P., Blanc, P., Gaboreau, S., Gailhanoub, H., Braithwaite, D., Montouillout, V., Denoyel, R., Henocq, P., Madé, B., 2018. Thermodynamic properties of C-S-H, C-A-S-H and M-S-H phases: Results from direct measurements and predictive modelling. *Applied Geochemistry*, 92, 140-156.

Saaltink, M.W., Ayora, C., Carrera, J.A., 1998. A mathematical formulation for reactive transport that eliminates mineral concentrations. *Water Resources Research* 34, 1649-1656.

Samper, J., Yang, C., Montenegro, L., 2003. User's manual of CORE2D Version 4: A code for ground-water flow and reactive solute transport. Universidad de A Coruña, La Coruña, Spain.

Savage, D., 2006. Analogue evidence relevant to the alkaline disturbed zone - Report prepared for United Kingdom Nirex Limited. Quintessa Report QRS-1300A-1, Quintessa, Henley-on-Thames, United Kingdom.

Savage, D., 2009. A review of experimental evidence for the development and properties of cement bentonite interfaces with implications for gas transport. Nagra Report NAB 09-30, Nagra, Wetingen, Switzerland.

Savage, D., 2011. A review of analogues of alkaline alteration with regard to long-term barrier performance. *Mineralogical Magazine* 75, 2401-2418.

Savage, D., 2014. An assessment of the impact of the long term evolution of engineered structures on the safety-relevant functions of the bentonite buffer in a HLW repository. Nagra Technical Report TR 13-02, Nagra, Wetingen, Switzerland.

Savage, D., Benbow, S., 2007. Low pH cement. SKI Report 2007:32, Swedish Nuclear Power Inspectorate, Stockholm, Sweden.

Savage, D., Cloet, V. 2018. A review of cement-clay modelling. Nagra Report NAB 18-24, Nagra, Wetingen, Switzerland.

Savage, D., Noy, D., Mihara, M., 2002. Modelling the interaction of bentonite with hyperalkaline fluids. *Applied Geochemistry* 17, 207-223.

Savage, D., Walker, C., Arthur, R.C., Rochelle, C.A., Oda, C., and Takase, H., 2007. Alteration of bentonite by hyperalkaline fluids: a review of the role of secondary minerals. *Physics and Chemistry of the Earth* 32, 287-297.

Seigneur, N., L'Hôpital, E., Dauzères, A., Sammaljärvi, J., Voutilainen, M., Labeau, P.E., Dubus, A., Detilleux, V., 2017a. Transport properties evolution of cement model system under degradation - Incorporation of a pore-scale approach into reactive transport modelling. *Physics and Chemistry of the Earth, Parts A/B/C* 99, 95-109.

Seigneur, N., L'Hôpital, E., Dauzères, A., Sammaljärvi, J., Voutilainen, M., Labeau, P.E., Dubus, A., 2017b. Numerical representative elementary volume generation of a simplified cement paste and estimation of its diffusivity and comparison with dedicated experiments. *Journal of Porous Media* 20, 29-46.

Sellin, P., Leupin O. X., 2013. The use of clay as an engineered barrier in radioactive waste management - a review. *Clays and Clay Minerals* 61, 477–498.

Sidborn, M., Marsic, N., Crawford, J., Joyce, S., Hartley, L., Idiart, A., de Vries, L.M., Maia, F., Molinero, J., Svensson, U., Vidstrand, P., Alexander, R., 2014. Potential alkaline conditions for deposition holes of a repository in Forsmark as a consequence of OPC grouting. SKB Report R-12-17, SKB, Stockholm, Sweden.

Smellie, J., 1998. Maqarin natural analogue study: Phase III. SKB Technical Report TR-98-04. SKB, Stockholm, Sweden.

Soler, J.M., 2013. Reaction-transport modelling of concrete-clay interaction during 15 years at the Tournemire Underground Rock Laboratory. *European Journal of Mineralogy* 25: 639-654.

Steeffel, C.I., Appelo, C.A., Arora, B., Jacques, D., Kalbacher, T., Kolditz, O., Lagneau, V., Lichtner, P.C., Mayer, K.U., Meeussen, J.C., Molins, S., 2015. Reactive transport codes for subsurface environmental simulation. *Computational Geosciences* 19, 445-478.

Techer, I., Bartier, D., Boulvais, P., Tinseau, E., Suchorski, K., Cabrera, J., Dauzères, A., 2012a. Tracing interactions between natural argillites and hyper-alkaline fluids from engineered cement paste and concrete: Chemical and isotopic monitoring of a 15-years old deep-disposal analogue. *Applied Geochemistry* 27, 1384-1402.

Techer, I., Michel, P., Bartier, D., Tinseau, E., Devol-Brown, I., Boulvais, P., Suchorski, K., 2012b. Engineered analogues of cement/clay interactions in the Tournemire experimental platform (France): A couple mineralogical and geochemical approach to track tiny disturbances. In: NEA, 2012. Cementitious materials in safety cases for geological repositories for radioactive waste: Role, evolution and interactions, NEA/RWM/R(2012)3/REV, 182-185.

Thoenen, T., Hummel, W., Berner, U., Curti, E., 2014. The PSI/Nagra Chemical Thermodynamic Database 12/07. PSI Report 14-04, Paul Scherrer Institut, Villigen PSI, Switzerland.

Tinseau, E., Bartier, D., Hassouta, L., Devol-Brown, I., Stammose, D., 2006. Mineralogical characterization of the Tournemire argillite after in situ reaction with concretes. *Waste Management* 26, 789-800.

Torres, E., Turrero, M.J., Garralón, A., Cuevas, J., Fernandez, R., Ortega, A., Ruíz, A.I., 2018. Stable isotopes applied to the study of the concrete/bentonite interaction in the FEBEX in situ test. *Applied Geochemistry* 100, 432-443.

Trotignon, L., Peycelon, H., Bourbon, X., 2006. Comparison of performance of concrete barriers in a clayey geological medium. *Physics and Chemistry of the Earth* 31, 610-617.

Trotignon, L., Devallois, V., Peycelon, H., Tiffreau, C., Bourbon, X., 2007. Predicting the longterm durability of concrete engineered barriers in a geological repository for radioactive waste. *Physics and Chemistry of the Earth* 32, 259-274.

Trotignon, L., Thouvenot, P., Munier, I., Cochepein, B., Piault, E., Treille, E., Bourbon, X., Mimid, S., 2011. Numerical simulation of atmospheric carbonation of concrete components in a deep geological radwaste disposal during operating period. *Nuclear Technology* 174, 424-437.

Turrero, M.J., Cloet, V., 2017. FeBEX-DP concrete ageing, concrete/bentonite and concrete/rock interaction analysis. Nagra Report NAB 16-18, Nagra, Wettingen, Switzerland.

van der Lee, J., De Windt, L., Lagneau, V., Goblet, P., 2003. Module-oriented modeling of reactive transport with HYTEC. *Computational Geosciences* 29, 265-275.

Wang, L., Jacques, D., De Cannière, P., 2010. Effects of an alkaline plume on the Boom Clay as a potential host formation for geological disposal of radioactive waste: SCK-CEN-ER-28, SCK CEN, Mol, Belgium.

Watson, C., Savage, D., Wilson, J., Benbow, S., Walker, C., Norris, S., 2013. The Tournemire industrial analogue: reactive transport modelling of a cement-clay interface. *Clay Minerals* 48, 167-184.

Wersin, P., 2003. Geochemical modelling of bentonite porewater in high-level waste repositories. *Journal of Contaminant Hydrology* 61, 405-422.

Wolery, T.J., 1983. EQ3NR a computer program for geochemical aqueous speciation-solubility calculations: user's guide and documentation. Lawrence Livermore National Laboratory report UCRL-53414, Livermore, CA, USA.

Xu, T., Sonnenthal, E., Spycher, N., Pruess, K., 2004. TOUGHREACT user's guide: a simulation program for nonisothermal multiphase reactive geochemical transport in variable saturated geologic media. Lawrence Berkeley National Laboratory Report LBNL-55460, Berkeley, CA, USA.

Yamaguchi, T., Sakamoto, Y., Akai, M., Takazawa, M., Iida, Y., Tanaka, T., Nakayama, S., 2007. Experimental and modeling study on long-term alteration of compacted bentonite with alkaline groundwater. *Physics and Chemistry of the Earth* 32, 298-310.

Yamaguchi, T., Yamada, F., Negishi, K., Hoshino, S., Mukai, M., Tanaka, T., Nakayama, S., 2008. Development and verification of a reactive transport model for long-term alteration of bentonite-cement-seawater systems. *Physics and Chemistry of the Earth* 33, 285-294.

Yamaguchi, T., Mitsumoto, Y., Kadowaki, M., Hoshino, S., Maeda, T., Tanaka, T., Nakayama, S., Marsal, F., Pellegrini, D., 2009. Verification of a reactive transport model for long-term alteration of cement-clay systems based on laboratory experiments and in-situ observations. CEA - JAEA meeting 2009.

Yamaguchi, T., Kataoka, M., Sawaguchi, T., Mukai, M., Hoshino, S., Tanaka, T., Marsal, F., Pellegrini, D., 2013. Development of a reactive transport code MC-CEMENT ver. 2 and its verification using 15-year in situ concrete/clay interactions at the Tournemire URL. *Clay Minerals* 48: 185-197.

Yang, C., Samper, J., Montenegro, L., 2008. A coupled non-isothermal reactive transport model for long-term geochemical evolution of a HLW repository in clay. *Environmental Geology* 53, 1627-1638.

## 5. Interface "steel/iron – bentonite"

Maria J. Turrero, Elena Torres (CIEMAT), Jaime Cuevas (UAM), Javier Samper, Luis Montenegro (UDC)

Carbon steel canisters have been proposed for the storage and disposal of high level radioactive wastes (HLW) in deep geological repositories (DGR) in countries like Switzerland, France, Belgium, Germany, United Kingdom, Czech Republic, Spain, USA, China and Japan. The host rock and the design of the repository differ in each country but in many cases the canister will be in contact with compacted bentonite blocks or pellets, except in France or in concepts from Belgium and the Netherlands. The main perturbations at the steel/iron-bentonite interface are canister failure due to corrosion and the interaction of corrosion products with the bentonite, which could potentially result in the formation of new iron-rich minerals that alter some of its basic properties, such as hydraulic conductivity, diffusion coefficient and capacity to swell or retain radionuclides.

Canisters are estimated to provide isolation for at least 1,000 years, although results from experiments, analogues and models indicate that failure is unlikely in less than 10,000 years. It depends, among others, of its thickness and chemical reliability. A part of the broad objective of ACED is to investigate the chemical evolution of interacting materials in the repository in an effort to address some remaining uncertainties related to integrity and performance assessment of the engineered barrier system (EBS). This section has to do with what it is known so far on the evolution of the DGR environment (thermal, hydraulic and/or chemical gradients - redox, pH and dissolved species - from the initial post-closure stage until the system reaches equilibrium) and its impact on the chemical evolution of the steel/iron-bentonite interface. Investigations from laboratory and field experiments, evidences from natural analogues and modelling approaches are compiled considering the evolution of those conditions.

### 5.1 Processes at the interface

The changing environmental conditions during the life of the repository influence the corrosion process and products, the interaction of corrosion products with bentonite and finally, the integrity of both, the steel/iron and the bentonite. It is addressed in this and next sections considering aerobic/ $> 90\text{ }^{\circ}\text{C}$ <sup>3</sup> and anaerobic/ $< 90\text{ }^{\circ}\text{C}$  stages and taking into account the temperature and hydration transients from one to another, the influence of radiation and also the potential influence of microorganisms.

#### **Aerobic (and transient to anaerobic) conditions, temperature $> 90\text{ }^{\circ}\text{C}$ , $< 100\text{ years}$**

At the initial stages ( $\approx$ emplacement to 20(50) years) water vapor and dissolved oxygen act as the oxidizing agents. Low corrosion rates and general corrosion occur and no changes are expected in the bentonite properties.

- Oxidizing conditions will prevail before closure of the repository and in the post-closure stage. Oxygen trapped in the buffer and backfill materials will be consumed in several ways: corrosion of metallic elements, oxidation of pyrite (both in certain bentonites (e.g. FEBEX) and in host rock (e.g. Opalinus Clay and Callovo-Oxfordian formation) or microbial activity.
- Following the emplacement, the canister surface will be subjected to temperature  $> 90\text{ }^{\circ}\text{C}$  and thermally-induced drying at the canister surface/bentonite interface occurs (dry-out stage). Relative humidity will be low and under those conditions, low corrosion rates and general corrosion processes occur, which do not endanger the performance of the metallic canister.
- Aerobic corrosion under oxidizing/unsaturated conditions can produce multi-layered corrosion products, which in order of proximity to the metal surface can be magnetite/maghemite, hematite, goethite and lepidocrocite.
- At this phase, changes in the bentonite properties due to iron/clay interaction are not expected since there is no water to mobilize iron.

<sup>3</sup> Temperature at the initial stages depends on the concept. For example, the French repository is designed to operate at up to  $90\text{ }^{\circ}\text{C}$  and in Switzerland (Opalinus clay) is estimated that in the first 100 years temperature could reach  $150\text{ }^{\circ}\text{C}$ .

During the transient phase to anaerobic conditions ( $\approx 20(50)$  to 100 years), temperature and hydration gradients induce increase in the corrosion rate and localized corrosion. Mineralogy of the bentonite can be altered to non-swelling Fe-rich phyllosilicates.

- In this stage corrosion will occur mainly under unsaturated condition, but as system hydrates relative humidity will increase and a moisture film will form on the metal surface. The temperature at the canister/bentonite interface will be around 90 °C or higher, which have to be taken into account, as corrosion rate increase with that higher humidity and high temperature. The time leading from aerobic to anaerobic conditions will depend primarily on the (advective-)diffusive transport of oxygen, either in the gas or liquid phase, in the unsaturated compacted bentonite, and on the corrosion rate of iron and accessory minerals (e.g., pyrite) as well, as corrosion progressively consumes the oxygen of the system.
- The aqueous chemistry at the interface will depend on the interaction between the groundwater (fresh or saline) and the bentonite, which contains salts (e.g., NaCl and CaSO<sub>4</sub>). At this stage temperature is still high; the saturation of the system progresses and the bentonite at the interface remains unsaturated although relative humidity increases. Under those conditions, geochemical evolution of the bentonite barrier can result in the formation of saline fronts in the vicinity of the canister. The existence of hygroscopic salts can decrease the value of critical relative humidity (CRH) and significantly enhance corrosion process at relative humidity quite lower than 100%. Hygroscopic salts sorb moisture and form concentrated brines that promote the electrochemical corrosion of steel and the nucleation of pits on the metal surface leading to localized corrosion. The nucleation time for pits depends on factors such as the oxidizing character of the environment, the concentration of aggressive ions such as chlorides, pH and the alloy composition of the metal. Sulphates could also be relevant in the presence of microorganisms.
- As saturation advances, chemical composition of bentonite porewater will homogenize along the clay barrier due to diffusion. So, saline fronts generated will disappear. When the residual oxygen is consumed other mechanism could be responsible of localized corrosion, for example the reductive dissolution of Fe(III) corrosion products coupled to Fe dissolution of the inner layers (electrochemical corrosion). Once oxygen has been depleted and anaerobic conditions are reached, corrosion will turn general and uniform. Green Rust (GR), group of mixed Fe(II)/Fe(III) hydroxides will be the prevailing corrosion product in moderately reducing environments and circumneutral pH as those expected in this phase.
- As canister corrosion progresses and relative humidity increases alteration in the bentonite mineralogy can occur, in terms of precipitation of iron corrosion products in the surroundings of the interface, destabilization of montmorillonite and replacement by Fe-rich smectites or by non-swelling Fe-rich phyllosilicates and cementation due to precipitation of iron corrosion products or of SiO<sub>2</sub> resulting from montmorillonite transformation.

The radiation fields in the vicinity of the steel/bentonite interface may cause water to decompose into a range of redox-active species which can significantly influence corrosion kinetics. Then, an increasing of the corrosion rate of the steel can occur. Over a certain dose of  $\gamma$ -radiation ( $>10-20$  Gy h<sup>-1</sup>) the bentonite properties might be affected as well, mainly decreasing cation sorption capacity, what indeed affect the swelling potential of clay, and inducing changes in the redox reactivity of the material (through changes in the Fe(II)/Fe(III) ratio). During first stages of the repository life radiation could also have an impact on the decreasing of microbial activity at the steel-bentonite interface.

#### **Anaerobic conditions, temperature < 90 °C, >100 years**

Saturation of the clay, decreasing of temperature and reducing conditions will favour uniform corrosion. Anaerobic corrosion will lead to the generation of gas at this stage. Microbial-mediated corrosion could also occur.

- As time advances, average temperature in the steel surface will decrease to 50 or 60 °C, enhancing saturation and swelling of the bentonite at the contact. As relative humidity increases, canister surface will become uniformly wetted. In this phase, it is foreseen that residual oxygen has totally been depleted and reducing conditions are achieved. Then, anaerobic corrosion of the steel canister will occur and corrosion will become uniform.
- Anaerobic corrosion consumes water and involves the generation of gas (H<sub>2</sub>). Hydrogen produced could modify the mechanical properties of the metal and alter physical properties of

the bentonite (e.g., formation of microfractures or preferential pathways). However, the expected corrosion rates will be extremely low. Therefore, gas generation is expected to be low as well. Hydrogen pressure is unlikely to exceed the breakthrough pressure of compacted bentonite. In the case of exceeding it, bentonite is expected to be able to self-sealing under saturated conditions.

- Microbial activity may be important during this period by modulating redox conditions and transformation of iron phases; but temperature, low porosity and swelling pressure of saturated bentonite is expected to act as a protective film against microbial-influenced corrosion (MIC).
- Corrosion rate will be below  $10 \mu\text{m yr}^{-1}$  and corrosion products will be largely tied to site-specific conditions. Magnetite, siderite and iron sulphides will be mainly formed, depending on the clay and the chemistry of solution (e.g., carbonate, chloride and sulphide concentration), pH and redox potential.
- Sorption sites on the clay can be filled by ferrous ions, which may be a precursor of new Fe-Si phases. Also, reduction of structural Fe(III) can occur increasing the cation exchange capacity. Bentonite can be transformed into Fe-rich non-swelling silicates such as berthierine, cronstedtite or chlorite. It could jeopardize the long-term performance of the clay barrier by decreasing the swelling capacity, enhancing the hydraulic conductivity and increasing brittle failure.
- The formation of secondary minerals at the metal-bentonite interface can affect physical properties such as porosity and microstructure of the bentonite, which in turn would have an impact on reliability of the barrier.

## 5.2 Evidence from experiments and analogues

There are a number of papers about the corrosion of metals that provide results coming from laboratory experiments under a variety of conditions (e.g. Marsh et al., 1987, 1989; Gdowski and Bullen, 1988; Blackwood et al., 2002; Azcárate et al., 2004; Kursten et al., 2004a,b; King, 2008 (compilation of various experimental studies), King 2014; Necib et al., 2016, 2017a, b). Padovani et al. (2017) made an analysis of the expected corrosion behaviour of candidate container materials and future R&D work. Results of corrosion rates and products obtained from the study of archaeological objects can be found in Qin et al. (2004), Smart and Adams (2006), Neff et al. (2006, 2010), Yoshikawa et al. (2008) and Michelin et al. (2013), among others.

The interaction of corrosion products with bentonite has been reviewed in Marcos (2003), Landolt et al. (2009), Bradbury et al. (2014), Wilson et al. (2015) and Wilson (2017), among others. There are also various papers and reports from NF-PRO, PEBS, TBT, Mt. Terri and FEBEX\_DP projects presenting the results from both laboratory and *in situ* experiments designed to advance in the understanding of iron-bentonite (and clay rock) interaction (e.g. Guillaume et al., 2004; Charpentier et al., 2006; Wilson et al., 2006a, b; Carlson et al., 2007; Hunter et al., 2007; Smart et al., 2008; Milodowski et al., 2009; Fukushi et al., 2010; Osaky et al., 2010; 2013; Torres, 2011; Lanson et al., 2012; Schlegel et al., 2014; Torres et al., 2014; Cuevas et al., 2016; Wersin and Kober, 2017; Hadi et al., 2019). Some authors focused in the study of natural analogues from which obtaining information about influence of iron on the transformation of bentonite to iron-rich clays (e.g., Smart and Adams, 2006; Pelayo et al., 2011).

This section is based on many of those works and is planned dividing experiments, either laboratory or *in situ*, and analogues, either natural or anthropogenic (e.g., industrial and archaeological). As in previous section, the experiments and analogues sections have been divided into 2 subsections considering aerobic or anaerobic conditions. In addition, each section will deal with experiments devoted to corrosion rates and nature of corrosion products on one hand and transformation of bentonite/clay on the other. Moreover, although the state of the art points to the steel/iron-bentonite interaction as a goal, the evidence provided by the interaction of iron with other clays is also included since it makes available insights and valuable data to gain understanding on the nature and magnitude of the iron-clay interaction and is also useful for modelling purposes. As example, Jodin-Caumon et al (2010, 2012) analysed iron-bentonite and iron-claystone interaction by means of laboratory experiments mostly under the same experimental conditions and found that both evolved into similar iron-rich products, being chemical reactivity pathways similar, with iron corroding to magnetite, magnesium migration towards hottest parts and the formation of mixed-layer chlorite-smectite.

## 5.2.1 Laboratory experiments

### 5.2.1.1 Aerobic (and transient to anaerobic) conditions, $T > 90\text{ }^{\circ}\text{C}$

A number of experiments have been made assessing corrosion processes at the early and transient stages of the repository, when unsaturated conditions prevail, temperature is usually expected to be above or about  $100\text{ }^{\circ}\text{C}$  (with some exceptions as the French repository, which is designed to operate at up to  $90\text{ }^{\circ}\text{C}$ , which is likely to be reached about 20 years after emplacement), relative humidity is most of time below 80% (Phases 1 and 2 of Landolt et al., 2009; cf. Figure 5-1) and initial aerobic conditions prevail evolving to reducing conditions with time. At these stages, temperature, relative humidity, oxygen concentration, presence and redistribution of salts, microbes and radiation effects are the parameters conditioning the corrosion process.

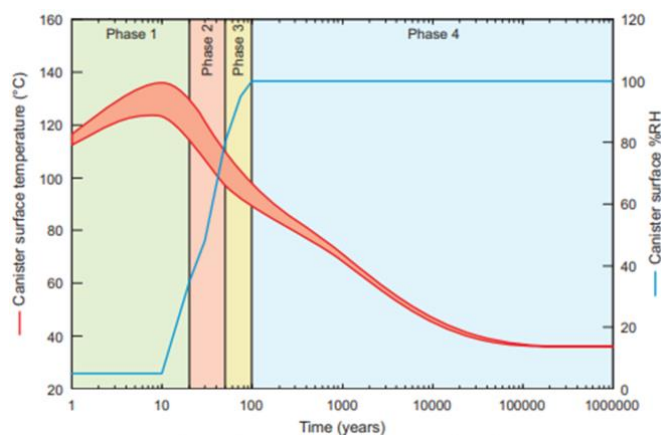


Figure 5-1 – Approximate evolution of temperature and relative humidity at the canister surface (from Landolt et al 2009).

### Corrosion rates and corrosion products

During early stage the canister surface will be subjected to aerobic conditions and high temperature (e.g., in Opalinus Clay, Johnson et al (2002) estimated that in the first 100 years temperatures could reach  $150\text{ }^{\circ}\text{C}$ ) induces drying at the canister surface/bentonite interface. Relative humidity will be lower than CRH or threshold value at which water vapour can condensate and form aqueous films on the metallic surface and corrosion is expected being very low. Dante and Kelly (1993) determined that an initial adsorption of 10 to 20 monolayers of water is the minimum amount of water necessary for electrochemical reactions and Lee and Staehle (1997) investigated how adsorption of water affects corrosion rates of different metals at different temperatures. These authors made experiments to determine mass changes of iron, among other metals, at 0% and 100% relative humidity (RH) and temperature range of  $7\text{ }^{\circ}\text{C}$  to  $90\text{ }^{\circ}\text{C}$ , under nitrogen and air environments. The results suggested that for iron, monolayer coverage of adsorbed water occurs at 10% RH at  $25\text{ }^{\circ}\text{C}$ , 10% RH at  $45\text{ }^{\circ}\text{C}$  and 6% RH at  $85\text{ }^{\circ}\text{C}$ . Isotherms indicated that iron surface reacts with adsorbed water and formed oxyhydroxides under humidified  $\text{N}_2$  and  $\text{O}_2$  environments. Multilayered physical adsorption and capillary condensation in pores were more significant at higher temperatures, although occur over all RH levels at all temperatures.

Ben Lagha et al. (2007) followed the corrosion of steel canister with time, as a function of RH, oxygen content and temperature. The authors observed the formation of multi-layered corrosion products consisting of oxide/hydroxides and a drastic mass increase at RH values above 70% was reported, though at the lower value of 50%, the amount of water adsorbed on the surface seems sufficient to induce electrochemical reactions. Raman spectrometric analyses indicated the formation of magnetite, maghemite and oxy-hydroxides species in the  $25$  to  $90\text{ }^{\circ}\text{C}$  temperature range, and for oxygen contents above 1 vol.%, whereas magnetite and hematite were only detected at  $90\text{ }^{\circ}\text{C}$ .

During transient stage, thermo-hydro-geochemical evolution of the bentonite barrier can result in the formation of saline fronts in the vicinity of the canister (e.g., Cuevas et al., 2002) and it is well documented that in this phase, when temperature is still high, the presence of salts can significantly enhance the corrosion process at humidity below the CRH (Kucera and Mattson, 1987; Torres et al., 2009). Schindelholz et al. (2014) examined the effect of relative humidity on corrosion when hygroscopic salts (e.g., NaCl) are present and then there is adsorbed water associated with the salt in contact with the steel. The authors observed that corrosion initiate by adsorbed water on NaCl crystals at 33% RH, which is explained by capillary condensation between contact points of the salts and metal surface.

Salts promote the electrochemical corrosion of steel and the nucleation of pits on the metal surface leading to localized corrosion surface (Druyts et al., 2001; Zhang et al., 2005; Bradbury et al., 2014). Song et al. (2017) analysed the effect of chloride on corrosion. The authors exposed polished coupons of iron and C-steel used for pipelines to soil samples with different amounts of NaCl to a temperature of 40 °C. The authors observed that low levels of chloride (0.0015 wt.%) tend to cause general corrosion and goethite and iron oxides as main corrosion products, while high levels of chloride likely induce localized corrosion and lepidocrocite and rust layers are dominant. Corrosion rate increases as chloride concentration is higher, but in all cases decreases with time.

Gdowski and Estill (1996) and Gdowski (1998) investigated corrosion of C-steel in the absence and presence of salts under humid air in the temperature range from 60 to 90 °C. Test durations were 7 to 14 days. The author concluded that in the absence of salts the short-term oxidation of carbon steel at 90% RH is very low. In presence of salts and temperatures of 80 °C C-steel is susceptible of corrosion at even 48% RH and the initial degradation accelerates as RH do. A decreasing of the corrosive effect with time is observed, which is attributed to the incorporation of the components of the salt into the corrosion products.

Torres et al. (2009) and Torres (2011) used small laboratory cells (25 mm height, 50 mm diameter) in which compacted bentonite (dry density of 1.65 g cm<sup>-3</sup>) in contact with iron powder (60 µm) was subjected to heating (100 °C) but no hydration in order to assure unsaturated conditions during the experiments. The cells were sequentially dismantled after 21 days and 2, 4 and 6 months of operation. The authors found that Fe powder was scarcely corroded and corrosion products were only found in the fraction just in contact with the bentonite surface. It seems that adsorbed water in the bentonite was evaporated, which caused the precipitation of salts (NaCl) on the metal surface. The salts enabled the formation of brines by sorbing environmental moisture initiating electrochemical corrosion. Corrosion occurred in all the experiments and main corrosion products found in the four tests included iron oxyhydroxides, either lepidocrocite and/or goethite. The latter seems thermodynamically favoured when RH is lower than 50% (Majzlan et al., 2003). Similar experiments by those authors, with bigger cells (100 mm height, 70 mm diameter) and longer times (up to 15 months), evidenced the formation of a thin layer of anhydrous oxides, hematite and poorly crystalized maghemite, both at the interface and in the iron powder. It was interpreted that desiccation could lead to transformation of goethite to hematite and maghemite. Additionally, a dry-corrosion mechanism according to which water vapor generated by high temperature acts as oxidizing agent is invoked to explain the formation of those corrosion products.

Torres et al (2011) show the results from a similar study to the above, using the same type of laboratory cells but replacing iron powder by carbon steel plates (2 mm height and 50 mm diameter). The cells were heated at 100 °C from the steel side and maintained without hydration for 17 and 22 months simulating the dry-out stage. The carbon steel plates exhibited several localized attacks on the surface. Pit depth was below 100 µm in all cases and pit density was very low; most part of the metal surface remained uncorroded. The authors point that salt and dust deposits could play a relevant role in the initialization of electrochemical corrosion by forming concentrated brines that were not homogeneously distributed. Formation of Cl-rich phases (akaganeite) was identified at the bottom of the pits in the steel plate. The sequence of formation of corrosion products begins with the precipitation of Fe(OH)<sub>3</sub> and lepidocrocite followed by goethite. The end-products of this transformation are anhydrous oxides (hematite, maghemite).

At this stage, Green Rust containing both Fe(II) and Fe(III) compounds may form as intermediate phases in the oxides transformations (e.g. to magnetite) (Cornell and Schwertmann, 1996; Torres et al., 2007).

Corrosion rates measured in the carbon steel plates were relatively low ( $5.5 \mu\text{m yr}^{-1}$  in the 17 months test and  $2.2 \mu\text{m yr}^{-1}$  in the 22 months test) if compared with data reported by other experimental works (e.g., Azcárate et al., 2004; Kursten et al., 2004a; Gaudin et al., 2013; Smart et al., 2017a). Slowing down corrosion rate is observed in the 22 months test, which according to the authors could mean that thickness of the corrosion products layer was sufficient to passivate the steel surface.

Peña et al. (2008) modelled the attenuation of the corrosion of carbon steel canisters due to the influence of diffusive transport through the corrosion product and compared it with data from Smart et al. (2006) that studied the corrosion rate of steel in bentonite under a wide range of conditions. Peña et al. (2008) conclude that there is a threshold thickness of magnetite ( $\sim 7 \mu\text{m}$ ) from which the speed of corrosion begins to decline fast and therefore corrosion rates will be very low.

Temperature is an essential parameter in order to understand the corrosion process, as corrosion rate will increase with temperature and also the formation of more-adherent protective surface corrosion products (e.g., Smart et al., 2002). In experiments made by Torres et al. (2007) at 25, 50 and 100 °C using iron powder in contact with bentonite, the corrosion products found consisted on  $\text{Fe}(\text{OH})_2$ , GR-Cl,  $\text{FeOOH}$  and  $\text{Fe}_3\text{O}_4$  in all cases. However, the magnetite layer was thicker at 100 °C than at lower temperatures. Transformation of  $\text{Fe}(\text{OH})_2/\text{GR-Cl}$  into magnetite via Schikorr reaction is favoured at temperatures above 50 °C.

#### *Effect of radiation*

Padovani et al. (2017) pointed out that radiation can influence the degradation of the mechanical properties of the canister (e.g., becoming brittle). One way it may happen is that radiation fields in the vicinity of the steel/bentonite interface may cause water to decompose into a range of redox-active species, both highly oxidizing (e.g.,  $\cdot\text{OH}$ ,  $\text{H}_2\text{O}_2$ ) and highly reducing (e.g.,  $\cdot\text{e}_{\text{aq}}^-$ ,  $\cdot\text{O}_2^-$ ), which can significantly influence corrosion kinetics (Joseph et al., 2008; Daub et al., 2010; Daub et al., 2011) in terms of both rate and nature of corrosion process. Existing studies have shown that  $\text{H}_2\text{O}_2$  reacts with some metal oxides via both electron-transfer and catalytic decomposition. The former reaction leads to corrosion while the latter consumes hydrogen peroxide leaving the oxide in its original oxidation state (Lousada et al., 2012). In this sense,  $\gamma$ -irradiation has a major impact on the nature of the corrosion process by increasing the rest potential in the system.

Kursten et al. (2004b) present a compilation of data on corrosion of metallic materials for HLW/SF containers that include some data on corrosion by  $\gamma$ -irradiation in different disposal environments. For example, in salt environments and temperature 150 °C, a  $\gamma$ -radiation field of  $10 \text{ Gy h}^{-1}$  in  $\text{MgCl}_2$ -rich brines has a higher impact on C-steel corrosion (increasing corrosion rate from  $47 \mu\text{m yr}^{-1}$  to  $72 \mu\text{m yr}^{-1}$ ) than in NaCl-rich brines (no influence). The authors also point out that in clay environment (e.g., Boom Clay) the presence of radiation field around  $400 \text{ Gy h}^{-1}$  affect particularly the weld material of the C-steel with a notable increase of corrosion rate and thickness reduction of around  $2000 \mu\text{m}$ .

Daub et al. (2011) run experiments at 150 °C and an equivalent  $\text{pH}_{25^\circ\text{C}}$  of 10.6 and observed that the surface oxide formed on carbon steel after  $\gamma$ -irradiation was non-porous and uniform, and susceptible to brittle fracture during cooling. The same authors observed that using neutral equivalent  $\text{pH}_{25^\circ\text{C}}$ , metal dissolution is significant and the surface oxide film is very porous. In both cases, the oxide film was composed of a mixture of  $\text{Fe}_3\text{O}_4$  and  $\gamma\text{-Fe}_2\text{O}_3$ .

Liu et al (2017) investigated the corrosion rate and corrosion products of low carbon steel canister with and without  $\gamma$ -irradiation. The authors buried two sets of four polished carbon steel pieces in Gaomiaozi bentonite (Na-Ca bentonite) containing 17% of Na-Cl- $\text{SO}_4$  type water exposed to air. Each set was loaded into a container. One container was irradiated by a Co-60 source at an absorption dose rate of  $2.98 \text{ kGy h}^{-1}$  for 42 days. The other container was kept at room temperature as a blank control. Later, both containers were thermally treated (90 °C) for 120 days. Results show that irradiation caused a 33%

increase of the average corrosion rate. The corrosion products of non-irradiated steel were magnetite, hematite and goethite and the irradiated ones had magnetite, siderite, maghemite and goethite.

Crusset et al. (2017) reported also some results on iron corrosion experiments carried out under  $\gamma$ -irradiation for 1 year. The results with dose rates of  $80 \text{ Gy h}^{-1}$  revealed an increase of the corrosion rate if a comparison is made with the same experiment without irradiation applied. However, no influence was observed when  $20 \text{ Gy h}^{-1}$  were applied.

#### *Effect of microbial activity*

Microbial induced corrosion (MIC) in oxic conditions can occur by microbial oxygen consumption at iron surface, triggering pitting at the surface (e.g., Starosvetsky et al., 2001). However, Shoesmith and King (1999) point the potential influence of radiation to retard MIC during the first stages of the repository. The authors refer to calculations by King and Stroes-Gascoyne (1995) and King (1996), which point that for the gamma dose rates expected at the surface of the waste package a “sterilized” environment potentially occurs in days-months. In addition, high temperatures expected at the metal surface prevent the survival of microorganisms (e.g. Azcárate et al., 2004). Pedersen (2017) points out to temperature, low porosity and swelling pressure as variables that can inhibit bacterial growth.

#### **Transformation of bentonite/clay**

Transformation of bentonite into other newly-formed clay phases by interaction with corrosion products (e.g., iron-rich phases) is contemplated in long-term predictions. However, during early stages of the repository no mineralogical changes in bentonite are expected due to iron/bentonite interaction. Experiments made by Torres et al. (2011) simulating the first stages of the repository (already described above), evidenced that bentonite analysed at the interface did not undergo any chemical or structural alteration. Most of the iron found at the steel/bentonite interface was segregated in the clay as FeOOH nanoparticles that migrated up to 6 mm into the bentonite. The authors discussed that Fe can move through compacted bentonite in two different ways: (1) as negatively charged complexes ( $\text{Fe}(\text{OH})_3^-$  or  $\text{Fe}(\text{OH})_4^-$ ), which are not retained by electrostatic interactions, contrary to what happens with ferrous ions; (2) FeOOH nanoparticles could move through low-density areas that could act as preferential pathways.

Nevertheless, as canister corrosion progresses and relative humidity increases alteration in the bentonite mineralogy can occur (e.g., sorption of Fe(II) derived from corrosion) when temperature is still high and transition to reducing conditions occur. Then, transformation to Fe-rich saponite-type clay or other non-swelling clays can occur (e.g., berthierine or chlorite). Most of laboratory experiments related to this transient stage focus on bentonite stability in contact with various metals, including magnetite, at temperatures as high as  $300 \text{ }^\circ\text{C}$  (e.g., Guillaume et al., 2003, 2004; Wilson et al., 2006a; Charpentier et al., 2006), which in fact are far from those expected at the repository. In the experiments iron-rich phyllosilicates form by the steel/clay interaction, which can alter the initial physico-chemical properties of the clay (e.g., layer charge, cation exchange, swelling, specific surface area, hydration properties).

Guillaume et al (2003; 2004) made batch experiments with a mixture of Fe and magnetite powders and MX80 bentonite with a mass ratio of 0.1 to investigate clay stability at  $300 \text{ }^\circ\text{C}$  in a low salinity NaCl-CaCl<sub>2</sub> solution under oxygen-free atmosphere. The aim of using the mixture was twofold: see whether bentonite may react with corrosion product and also try to buffer the redox of the transformation. The experiments lasted for 7, 30, 90 and 270 days. Magnetite partially transformed to maghemite, and newly formed quartz, feldspars and zeolites were detected. A sequence of clay transformation was established from montmorillonite to saponite and trioctahedral chlorite, which is quite limited to the iron source. The reactivity is lower than that using only iron.

Charpentier et al (2006) investigated the iron powder and magnetite/MX80 bentonite interaction by means of batch experiments at different temperatures ( $80$ ,  $150$  and  $300 \text{ }^\circ\text{C}$ ) and duration ( $90$ ,  $180$  and  $270$  days), and pH solution of  $12.35$  (i.e., the solution coming in contact with the interface went first through cement/concrete, e.g., a concrete plug of a disposal cell). The authors observed that at  $80$  and  $150 \text{ }^\circ\text{C}$  montmorillonite is enriched in iron and depleted in Si. At  $300 \text{ }^\circ\text{C}$ , Fe-vermiculite predominates,

and is associated with mordenite-type zeolite and saponite. The changes are quite limited to the zones closest to the iron source, but the authors warn that changes can affect to swelling, exchange and sorption capacity.

Wilson et al (2006a) conducted batch experiments to investigate the stability of Kunipia F bentonite in presence of native iron and magnetite under extreme conditions (e.g., high  $\text{Fe}^{2+}$  activities and high temperature – 80, 150 and 250 °C). The initial oxidation of native iron produced green-rust or magnetite. Depending on the experimental set, the major alteration products were an Fe(II)-saponite from loss of tetrahedral silica from some sheets and a 7Å berthierine-like phase.

Mosser-Ruck et al. (2010) compared the main mineralogical changes expected from iron-bentonite interaction under anoxic conditions based on some of the experiments described above, other data from the literature and results presented in their article. They carried out batch experiments to investigate the stability of MX-80 bentonite in contact with Fe metal and magnetite using a low salinity NaCl-CaCl<sub>2</sub> solution. The authors used different liquid to clay ratio, Ar atmosphere and 80, 150 and 300 °C for experiments with duration of 90 and 365 days. They summarized the following mineralogical sequences as a function of temperature, pH, Fe/clay (Fe/C) and liquid/clay (L/C) ratios:

- (1) up to 150 °C, under neutral pH, and L/C > 5: dioctahedral smectite (di-sm) → 7Å Fe-rich phase (berthierine, odinite\_cronstedtite) for large Fe/C ratios (>0.5), or di-sm → Fe-rich di-sm + Fe-rich trioctahedral smectite (tri-sm) for small Fe/C ratios (0.1);
- (2) up to 150 °C, under alkaline pH (10-12), and L/C > 5: di-sm → Fe di-sm (Npalygorskite) for a small Fe/C ratio (0.1);
- (3) at 300 °C, Fe/C = 0.1, and L/C > 5: di-sm → Fe-rich saponite → trioctahedral chlorite + feldspar + zeolite (near-neutral pH); di-sm → Fe-rich vermiculite + mordenite (pH 10-12).

In addition to destabilization of montmorillonite and replacement by Fe-rich phases Mosser-Ruck et al. (2010) and Bradbury et al. (2014) identified processes as cementation due to precipitation of iron corrosion products or of SiO<sub>2</sub> resulting from montmorillonite transformation.

Jodin-Caumon et al (2010) investigated the effect of the temperature gradient (90(100)-300 °C) on the iron-MX-80 bentonite interaction from tube-in-tube experiments (powder-powder and plate-powder mixture at different mass ratios), with duration from 30 to 300 days and using different solutions (H<sub>2</sub>O or low salinity NaCl-CaCl<sub>2</sub>). Temperature enhanced iron corrosion. At higher temperatures (300 °C) more reduced conditions were achieved. Migration of Mg towards the hottest areas occurred. The authors observed that at temperature ≤100 °C bentonite evolved to a trioctahedral smectite enriched in Fe and Mg and in the hottest area Fe-chlorite was the final product. A loss of Si was observed, which was balanced by the precipitation of different siliceous products (including quartz) as a function of temperature.

Jodin-Caumon et al (2012) investigated the effect of temperature gradient (80-150 °C and 150-300 °C) on the iron-claystone (illite and illite-smectite from Callovo-Oxfordian formation in France) interaction from tube-in-tube (powder-powder and plate-powder mixture at different mass ratios) and batch experiments (powder-powder and fluid-powder mixture with mass ratio 1 and 10, respectively) with duration of 90 and 180 days and using different solutions (H<sub>2</sub>O or low salinity NaCl-CaCl<sub>2</sub>). Iron corrosion was enhanced by the thermal gradient and made the system basic and reductive. Magnesium enrichment occurred in the hottest part (thermal-induced migration). At the end of the experiments the authors observed mixed-layer phases between the initial illite-smectite and a Fe-rich clay mineral. The main end products were poor crystalline Fe-serpentine at 150 °C, and Fe or Fe,Mg-chlorite at 300 °C.

Table 5-1 summarizes the experiments described above and the main transformations that occurred in the clay.

Table 5-1 – Summary of clay transformation from laboratory experiments considering high temperature and transient from aerobic to anaerobic conditions.

Materials	Time	Temp	Clay transformation	Reference
iron metal and magnetite powder/ bentonite MX-80 – batch exp	270 days	300 °C	saponite and chlorite (limited to the metal interface)	Guillaume et al. 2003
iron metal and magnetite powder/ bentonite MX-80 – batch exp	270 days	300 °C	saponite and chlorite	Guillaume et al. 2004
native iron, magnetite/ Kunipia F bentonite - batch exp	93-114 days	80, 150, 250 °C	saponite and berthierite	Wilson et al. 2006a
iron metal and magnetite / bentonite MX-80 – batch exp	270 days	300 °C	zeolite and saponite	Charpentier et al. 2006
iron metal and magnetite / bentonite MX-80 – batch exp	90 and 365 days	80, 150 °C → 300 °C →	≈neutral pH → berthierine, odinite_cronstedtite (Fe/Clay >0.5) ≈neutral pH → chlorite + feldspar + zeolite (Fe/Clay 0.1)	Mosser-Ruck et al. 2010
iron powder/compacted FEBEX bentonite – column exp - unsaturated	180, 450 days	100 °C	No (iron segregated in the clay as FeOOH nanoparticles)	Torres 2011
iron metal and magnetite / bentonite MX-80 – batch exp	300 days	80-150 °C → 150-300 °C →	Fe-enriched tri-octahedral smectite Fe-chlorite	Jodin-Caumon et al., 2010
iron metal and magnetite / illite-ill-smec (COx) – batch exp	90, 180 days	80-150 °C → 150-300 °C →	poor crystalline Fe-serpentine Fe-chlorite	Jodin-Caumon et al., 2012

*Effects of radiation*

Bentonite will be exposed to  $\gamma$ -radiation even when the canister is intact (Jonsson, 2012). The total  $\gamma$ -dose will be in the order of 40–200 kGy, although may be below that depending on the design and of the thickness of the canister (plus casing in some cases). For this reason, it is important to elucidate the effect of ionizing radiation on the barrier properties of bentonite, and also the combined effect with the  $\gamma$ -radiation–driven increase in iron corrosion rate.

Among the observed effects of radiation in clay, the most relevant are (Allard and Calas 2009; Allard et al., 2012; Holmboe et al., 2012; Lainé et al., 2017): local and limited alteration of specific surface area and exchange capacity for high doses, enhanced colloidal stability of bentonite suspensions, decreased cation sorption capacity and changes in the redox reactivity of the material. The latter is attributed to reversible changes in the Fe(II)/Fe(III) ratio. In any case, mineralogical alteration studies of bentonite under this phenomenon and the combined action with higher corrosion rates are scarce and reaction products are poorly known. However, the overall results point toward the need to have a very high dose to significantly damage the structure of clay (amorphization dose). Otherwise, the defect (electronic defects) disappears with time.

5.2.1.2 Anaerobic conditions, T < 90 °C

The experiments summarized in this section represent corrosion and clay transformation over long periods, in a transient state to equilibrium conditions, and usually are performed at temperatures about or lower than 90 °C, considering the absence of oxygen and relative humidity above 80% (Phases 3 and 4 of Landolt et al., 2009; cf. Figure 5-1). At these stages bentonite is completely (or almost) saturated and redistribution of salts has occurred. The chemical species at the interface influence the corrosion progression and the type of corrosion products and its interaction with the bentonite.

### Corrosion rates and corrosion products

At this stage chemical environment at the iron/bentonite interface is anoxic and pH is close to neutral, by combination between an increase due to iron corrosion and iron-silicate neoformation. Under those conditions corrosion of iron should be a slow process (limited availability of  $H^+$  and kinetically slow down formation of  $H_2$ ) following proton reduction to  $H_2$  as cathodic reaction ( $Fe^0 + 2H^+ \rightarrow Fe^{2+} + H_2$ ). Additionally, depending on the chemistry of solution at the interface (e.g., concentration of carbonate, chloride and sulphide), steel corrosion products can include magnetite, iron carbonates (such as siderite) (e.g., Torres et al., 2007) and iron sulphides (e.g., Necib et al., 2019).

Madina et al. (2002) and Azcárate et al. (2004) made a series of experiments dealing with the corrosion of C-steel in contact with bentonite (FEBEX). Steel probes were embedded in saturated compacted bentonite and then placed in autoclaves and tested to 25, 50, 75 and 100 °C for a variable time between 1 and 18 months. The authors observed non-uniform generalized corrosion, with a stabilised corrosion rate  $10 \mu m yr^{-1}$  and a maximum depth of attack of 100  $\mu m$ . They explain the lack of uniformity to the random distribution of the electrolyte surrounding the steel probe. This creates areas with different potential of corrosion on the metal surface and a less uniform attack than in a homogeneous media such as liquid solution. A summary of the results obtained is presented in Table 5-2. The main corrosion product is siderite at any tested temperature, which the authors explain by the presence of carbonate in the bentonite. The authors discussed that siderite acts as an adherent component that passive and protects the steel at the conditions of the tests. The decreasing of the corrosion rate supports it. According to the authors bentonite didn't undergo alteration in any of the experiments due to very low iron availability in the experiment. Low specific area of iron, combined with low corrosion rate and formation of siderite, make difficult the formation of Fe-rich silicates.

Smart et al. (2017a) made five laboratory experiments to measure the corrosion rate of C-steel wires (0.4 mm diameter, 5 mm length) mixed with MX-80 bentonite under anoxic conditions and then compacted. Two of the experiments were made with pre-corroded wires. The experiments run in anaerobic conditions (glove box) at 60 °C. Cells were hydrated with isotopically labelled Opalinus Clay porewater. The authors measured initial corrosion rates  $\approx 30 \mu m yr^{-1}$  that decreased to  $< 1 \mu m yr^{-1}$  after 2.8 years and to  $\approx 0.5 \mu m yr^{-1}$  after around 6.5 years of duration of the experiment. The authors give an average corrosion rate  $\approx 3.5 \mu m yr^{-1}$ , including the pre-corrosion stage. The average oxide layer thickness is estimated to be  $\approx 6$  to 12  $\mu m$ , depending on the sample. Some localized corrosion occurred and pits  $\approx 10 \mu m$  depth and  $\approx 20$ -40  $\mu m$  wide were measured. Corrosion products included akaganeite, lepidocrocite, hematite (due to pre-corrosion stage) and sub-stoichiometric magnetite, the latter being the predominant one.

Wersin et al. (2003), Smart et al (2004), and Torres et al (2006), among others, reported the formation of magnetite at different redox conditions and a range of temperatures (from 50 to 100 °C). Most of laboratory experimental studies of the corrosion of iron in clay show that corrosion product layers are generally thin ( $< 1 \mu m$ ) with magnetite, siderite or 'green rust' occurring depending upon temperature and redox.

Table 5-2 – Influence of exposure time (months) on the average uniform corrosion rate ( $V_{corr}$ ), maximum depth of pitting attack ( $D_{max}$ ), average pit depths ( $D_{aver}$ ) and pitting factor calculated for the fine-grained carbon steel TStE355 exposed to saturated FEBEX bentonite at different temperatures (25, 50, 75 and 100 °C) (based on Madina et al., 2002; Azcárate et al., 2004).

Corrosion media	Temp °C	Exposure time months	General corrosion $V_{corr}$ ( $\mu\text{m yr}^{-1}$ )	Local corrosion		
				$D_{max}$ ( $\mu\text{m}$ )	$d_{av}$ ( $\mu\text{m}$ )	Pitting factor
Fine-grained C-steel in contact with saturated FEBEX bentonite/ granitic water	25	1	11.0	---	---	---
		6	4.0	---	---	---
		9	3.4	---	---	---
	50	1	32.0	---	---	---
		3	11.0	15.0	2.8	5.4
		6	11.0	20.0	5.5	3.6
		9	10.0	43.0	7.5	5.7
	75	18	6.7	56.0	10.5	5.9
		1	45.0	---	---	---
		3	17.0	30.0	4.3	7
		6	20.0	44.0	10.0	4.4
	100	9	13.0	53.0	9.8	5.4
		18	10.0	98.0	15.0	6.5
		1	57.0	30.0	4.8	6.3
		3	34.0	40.0	8.5	4.7
		6	24.0	58.0	12.0	4.8
	100	9	14.0	60.0	10.5	5.7
		18	6.3	50.0	6.3	7.9

$V_{corr}$ : average uniform corrosion rate

$D_{max}$ : maximum pit depth

$D_{av}$ : average pit depth

Kursten et al. (2004a,b) summarized the average corrosion rates determined by different institutions (COBECOMA project) by contacting Fe with different clays under reducing conditions, temperatures close to 80 °C and various water chemistries. The results were summarized as a table presented below (Table 5-3).

Table 5-3 – Average corrosion rates determined by the UK AEA, JNC, SCK-CEN, NAGRA and CEA in different clays and with various water chemistries (Kursten et al., 2004a).

Reducing conditions (80 or 85°C)				
Environment	Water type	Organization	Time (years)	Rate ( $\mu\text{m/y}$ )
Compacted clay	Granitic	NAGRA	0.5	15
		UKAEA	1	10
		CEA	1	8
	Clay porewater	SCK-CEN	8.5	4
	Distilled	JNC	1	5
	Seawater	JCN	4	3.5
Immersion	Cl+HCO <sub>3</sub> <sup>-</sup>	JCN	4	2.5
		JNC	0.7	7
	Granitic	NAGRA	0.7	7
		JNC	1	15
		JNC	0.25	2.5

### Gas generation

Anaerobic corrosion consumes water and involves the generation of gas. However, corrosion rates expected in the long-term will be extremely low and gas generation will be also low. However, at this moment there are no evidences of the development of pressure-induced gas pathways that in any way could compromise the sealing capacity of the bentonite barrier. Hydrogen generated during anaerobic corrosion could be physically or chemically sorbed in the corrosion products layer and could also diffuse into the steel microstructure, which could enhance the embrittlement of the canister.

*Effect of microbial activity*

Previously mentioned experiments show results considering a slow process of abiotic corrosion. However, microorganisms can initiate localized corrosion or accelerate already initiated corrosion in environments with very low or without oxygen, pH >6 (Ismail et al., 2014) and temperature that allows survival of microbial communities (e.g., Azcárate et al., 2004), which is called anaerobic microbial influenced corrosion. The microbial group present in most of anoxic environments is the sulphate-reducing bacteria (SRB) (Beech and Sunner, 2007) and most studies highly concerned by bacterial corrosion (e.g., oil pipes) focus on them. SRB can act as direct (Electrical-MIC, direct bacterial consumption of iron-derived electrons) or indirect (Chemical-MIC, through H<sub>2</sub>S from microbial sulphate reduction) catalyst of anaerobic iron corrosion. While CMIC seems not to accelerate iron corrosion, EMIC can corrode iron at very high rates and form large amounts of inorganic corrosion products (e.g., Venzlaff et al., 2013; Enning and Garrelfs, 2014). Enning and Garrelfs (2014) point to another damage mechanism induced by SRB, which is slowing down the formation of H<sub>2</sub> at the metal surface. Then hydrogen atoms could diffuse into the metal matrix and combine there to form H<sub>2</sub> inclusions that convert the metal in a brittle metal susceptible of cracking (sulphide stress cracking – SSC).

In the case of repositories, SRB are present in most of hosting rocks or buffers. A great effort has been made to analyse bacteria populations in Opalinus Clay (Switzerland) (e.g., Bagnoud et al., 2016; Leupin et al., 2017) and its impact on corrosion (e.g., Smart et al., 2017b), as well as in bentonite (e.g. Fru and Athar, 2008; Stone et al., 2016; Bengston and Pedersen, 2017; Engel et al., 2019; Matschiavelli et al., 2019). Although microbial activity may be important during this period saturated bentonite is expected to act as a protective film against microbially-mediated corrosion (Stroes-Gascoyne et al., 2007).

Experiments from Azcárate et al (2004) seem to indicate that temperature can condition the effect of microbes. From the experiments described above, the authors indicate that at 50 °C, and to a lesser extent, at 25 °C S-rich corrosion products were found in the steel probes, which points to influence of bacteria in the corrosion phenomena, mainly SRB caught in bentonite. These corrosion products are not observed at 75 °C and 100 °C, mainly due to the optimal growth temperature of the SRB between 10 and 50 °C.

Kuang et al (2007) analysed the effects of SRB on the corrosion behaviour of C-steel in laboratory experiments, in which metal was introduced in synthetic de-aerated seawater inoculated with SRB. During the experiment the authors monitored pH, redox potential, concentration of dissolved oxygen, changes in corrosion rate and SRB growing process. The authors concluded that corrosion rate of carbon steel accelerates during exponential growth of SRB but is not linked to the number of active SRB and is related to the accumulation of its metabolism products.

Masurat et al. (2010) analysed the presence of SRB in bentonite MX-80 in laboratory experiments under controlled anoxic conditions. The authors made tests of temperature tolerance (75, 90, 100 and 120 °C) of indigenous bentonite SRB and observed a loss of viability of SRB after 20 hours of bentonite treatment at 100 °C and 120 °C. It seems that the strong water affinity of bentonite desiccates cells, which become dormant desiccated cells (DDC). However, DDC has long survival and then maybe that when water is added to the cell, metabolism and viability can be restored.

Rajala et al (2015) made experiments exposing C-steel coupons to anoxic Olkiluoto-type groundwater, at 6 °C (*in situ* temperature) and at room temperature (RT), for 90 and 240 days. The experiments were replicated without C-steel. The authors observed that microorganisms formed biofilms on the surface of the C-steel causing pitting corrosion and clustered inside the corrosion pits. The microbial community in the experiment with C-steel was more abundant (x100) than in the environment without C-steel because the presence of hydrogen used as energy source. The bacteria found included iron reducing bacteria (IRB) and SRB. Of the latter, the most abundant in the experiment with C-steel were direct catalysts (E-MIC) of C-steel corrosion by using Fe(0) as electron donor for sulphate reduction. The corrosion deposits at short times included Fe, S, O and C, but S in deposits formed at RT was higher (x14) than in deposits at 6 °C.

Related to IRB Esnault et al. (2011) studied the impact of IRB on the stability of corrosion protective layer formed under anaerobic corrosion of metallic containers. The authors concluded that IRB promote the reactivation of corrosion processes in corrosive environments by altering the protective layer.

### Transformation of bentonite/clay

Sorption sites on the clay can be filled by ferrous ions (Charlet and Tournassat, 2005; Géhin et al., 2007), which can compete with radionuclides. To counteract that effect, high-surface-area of Fe(II)/Fe(III) corrosion products could provide adsorption sites for radionuclides (e.g., Granizo and Missana, 2006). Also, reduction of structural Fe(III) can occur and bentonite can be transformed into Fe-rich non-swelling silicates such as berthierine, cronstedtite or chlorite (Montes et al., 2005a; Lantenois et al., 2005; Bildstein et al., 2006; Wilson et al., 2006a; Lanson et al., 2012). Bradbury et al. (2014) calculated that with an average corrosion rate of  $1 \mu\text{m yr}^{-1}$  and 10,000 years of SF-canister corrosion, about 8% of montmorillonite could be converted to berthierine and 3% to chamosite. It could jeopardize the long-term performance of the clay barrier (Savage et al., 2010). In Leupin and Johnson (2013) an estimation of the qualitative influence of complete replacement of montmorillonite by Fe-rich clay minerals on the safety-relevant properties of bentonite can be found.

Ishidera et al. (2008) placed C-steel in contact with compacted bentonite Kunipia F and Kunigel V1 under anaerobic conditions for ten years at 80 °C. The authors observed that CEC of montmorillonite adjacent to the carbon steel decreased significantly but the clay was scarcely altered. Amorphous  $\text{Fe}(\text{OH})_2$  was formed and small amounts of lepidocrocite and green rust containing  $\text{Cl}^-$  were found in Kunipia F but not in Kunigel V1.

Carlson et al (2008) made anaerobic corrosion experiments on C-steel wires and coupons (and cast iron coupons)/compacted MX-80 bentonite interaction at temperature of 30 and 50 °C. The samples were immersed into NaCl and  $\text{NaCO}_3$  solutions at pH 10.4 and run between 356 and 911 days. Results indicate that alteration was higher in experiments with wires than with coupons due to much higher surface area of wires. Bentonite of coupon tests remained essentially unchanged, while bentonite of wire tests was strongly aggregated and got a colour characteristic of reducing environments. Iron from corrosion entered the bentonite matrix in zones close to the wires by some mass transport process, so that the total iron content of the bentonite matrix had an additional 6.6-8.7% of iron. However, the authors didn't find iron-rich clay minerals or corrosion products within the bentonite matrix and explain that temperatures higher than 50 °C are needed for the transformation to iron-rich minerals.

Jeannin et al (2010) investigated the role of 200–500  $\mu\text{m}$  thick deposits of different minerals in the corrosion processes of C-steel in NaCl solutions. The results indicated that the deposits favoured a general corrosion process, although the behaviour of steel covered by montmorillonite deposit was different. The authors discussed that montmorillonite induced pitting corrosion, which led to a local production of  $\text{H}^+$  due to magnetite formation. In their experiments this acidification provoked a local and partial dissolution of montmorillonite.  $\text{Fe}^{2+}$  could then diffuse through the clay deposit, leading to the formation of green rust or Fe(III) oxyhydroxides (lepidocrocite or goethite).

Lantenois et al. (2005) studied the interaction between metal iron and a variety of di- and tri- octahedral smectites, both natural and synthetic. 0.6 g of the clay powder were mixed with 0.6 g of metal Fe powder and 30 mL of deionized water to maximize the contact surface Fe-clay and favour reducing conditions. The mix was heated at 80 °C and experiments at different exposition times (maximum 120 days) were made. The authors concluded that dioctahedral smectites are destabilized under such conditions, leading to the precipitation of magnetite and of 1:1 Fe-rich phyllosilicates (odinite, cronstedtite). The amount of structural Fe, the presence of tetrahedral substitutions and the nature of interlayer cations are parameters that influence the smectite destabilization. Trioctahedral smectites are essentially unaffected under similar experimental conditions.

Perronet et al. (2007) concluded that smectite stability in the presence of iron depends on the energetic heterogeneity of smectite edge faces. Under reducing conditions, a high reactivity of the edge surface of montmorillonite platelets can be expected, which increases the energetic heterogeneity of edge faces

and the probability for Fe(0) to find unstable sites on the smectite edges to transfer electrons and initiate smectite destabilization associated to a formation of Fe(II)-rich minerals such as magnetite, siderite and clay minerals of serpentine group or chlorite.

Perronnet et al. (2008) investigated the evolution of the bentonite FoCa7 properties in contact with metallic iron through batch experiments with a wide range of iron/clay mass ratios that lasted 45 days at 80 °C. The main conclusion was that bentonite was altered into SiAlFe gels that evolve to different Fe-rich di-trioctahedral phyllosilicates depending on the available quantity of Fe(0). The formation of those Fe-rich phyllosilicates occurs at I/C ratio between 1/7.5 and 1/5, although at I/C > 1/3.75 iron oxides are strongly consumed and participate in the incorporation of Fe<sup>2+</sup> and Fe<sup>3+</sup> in gels or new phyllosilicates octahedra.

Martin et al. (2008) and Schlegel et al. (2008) studied the chemical and mineralogical transformations of a saturated iron-clay (Callovo-Oxfordian Formation, Paris) interface reacted at 90 °C and 50 bars during 8 months. The results show a corrosion layer of magnetite and a clay transformation layer to Fe-phyllsilicate enriched in Na with traces of goethite. The clay transformation layer is composed by Fe-rich carbonate (siderite). The corrosion thickness was 19 ± 9 µm. The presence of magnetite and siderite indicates that reducing conditions were achieved at the Fe–clay interface. The authors calculated that more than half of oxidized iron could be transported away from the interface and could be incorporated in the siderite layer or precipitate with silica. Figure 5-2 shows the transfers at the interface as illustrated by these authors.

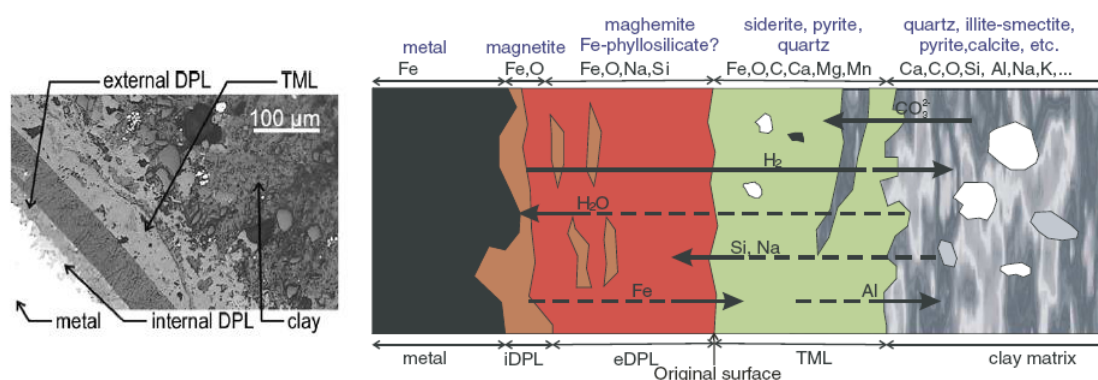


Figure 5-2 – Elemental transfers at the Fe–clay corroded interface reacted at 90 °C and 50 bars during 8 months (iDPL: internal dense product layer; eDPL: external dense product layer; TML: transformed medium layer (from Schlegel et al., 2008).

Milodowski et al. (2009) investigated the reaction between carbon steel wires and bentonite MX-80 at 50 °C under reducing conditions in three experiments lasted 99 (pH 11), 193 and 198 days (pH 8.4). A 1M NaCl solution was infiltrated in the experiments. For the three experiments akagenite, Fe(O,OH,Cl) was found, as well as magnetite. Iron moved into the bentonite forming halos around the wires, although no discrete bentonite iron oxide particles were found in the bentonite matrix. The authors observed a slightly increased  $d_{002}/d_{003}$  value in the bentonite in contact with the wires that suggest an increase in the total number of electrons in the octahedral layers. The authors indicate that it could be precursor of further alteration of bentonite.

Kumpulainen et al (2010) present the results of: (1) Cast iron cylinder-compacted MX-80 bentonite interaction experiments under anoxic conditions at 25 °C for 8 years. The authors observe an iron diffusion front of around 7-8 mm from the interface into the bentonite. Gas analysis indicate the presence of H<sub>2</sub> (corrosion product) and CO<sub>2</sub> (calcite dissolution). There are no changes in the MX-80 mineralogy and calcite, aragonite and hematite were detected close to the interface. The authors discuss tiny and not conclusive changes in XRD peaks that could indicate a slight increase of illite fraction and decrease of swelling capacity. Also, cementation of the bentonite to some extent in the vicinity of the iron cylinder was detected. The average corrosion rate estimated from iron profiles is about 1.7 µm yr<sup>-1</sup>; (2) Batch iron powder-purified Kunipia F bentonite interaction experiments under anoxic conditions at room

temperature for 10 years. The extreme conditions of this experiment led to bentonite transformed into a non-swelling 7Å clay phase, berthierine-type. In both type of experiments the chemistry of hydrating solutions was controlled. Authors conclude that pH had great impact on the results; while in the set of experiment (1) pH remained almost stable at  $\approx 8$ , the pH in the set (2) was about 12.7.

Osacký et al. (2013) studied the stability of dioctahedral smectites (SAz-1) in the presence of iron to simulate the possible transformation of clays. For this, the authors run batch experiments at 75 °C in air. The Fe-clay interaction leads to the formation of magnetite and 7Å phyllosilicates. However, the authors indicated that under aerobic conditions magnetite formation and smectite destabilization are inhibited if compared with the same type of experiments made under nitrogen atmosphere (Osacký et al., 2010).

Bourdelle et al (2014) made anaerobic, 90 °C, batch tests to investigate different size iron powder/COx interaction focusing on the effect of specific surface area of metal on the reaction paths. During the experiments pH maintains around 7 controlled by the iron-clay interaction. The authors observe a rapid dissolution of powdered iron and the crystallization of smectite-Fe-rich silicates formed from the dissolution of the clay, mostly the illite fraction, which represents a first step in the transformation to odinite–greenalite. The Fe/clay and L/clay ratio mostly impact the reaction rate and the development of new phases either smectitic serpentine or pure serpentine.

Pignatelli et al (2014) analysed the iron/clay (Callovo-Oxfordian clay from Bure) in anaerobic conditions in a 90 °C to 40 °C step-by-step experiment. The paper reports the reaction path leading to mineralogical changes of the claystone mineralogy (clays, calcite, quartz, pyrite and other accessories minerals), with a particular attention to the formation of iron-rich T–O phyllosilicates (cronstedtite and greenalite). The authors hypothesize on the formation of greenalite in two ways, related to dissolution of kaolinite or neoformed depending on local variations of the Si/Fe ratio and pH, mainly depending of quartz dissolution and magnetite and siderite precipitation. These processes could imply clogging and reduction of porosity. The authors point out that only a slight reduction in the cation exchange capacity and the degree of swelling of the barrier will occur.

Le Pape et al (2015) made batch experiments to understand the interaction Fe(0)/clay (Callovo-Oxfordian clay from Bure). The experiments had duration of 60 days and were made under anoxic conditions, at 90 °C. It was found that magnetite was the main corrosion product at the Fe(0) surface and serpentine was the end product of clay alteration. Close to the iron surface a compacted Fe-Si phyllosilicate ring was found and further a heterogeneous deposit of aggregates containing variable amounts of Al replacing Fe.

Rivard et al (2015) made batch experiments to understand the interaction Fe(0)/clay (Callovo-Oxfordian clay from Bure). The clay was used in different forms: bulk clay, clayey fraction and mixtures of the clay fraction with quartz, calcite or pyrite. The experiments had duration of 30, 90 and 270 days and were made under anoxic conditions, at 90 °C. Metallic iron oxidized very fast leading to acidification and decreasing of Eh that favoured dissolution of clay phases. The final product was Fe-serpentine. One of the most interesting issues of the investigation was to highlight not only common trends, also differences in the reaction pathways, particularly the importance of quartz in the development of the precursor of the serpentine, a FeSiAl gel that only forms in the presence of this mineral.

Experiments by Smart et al (2017b) (C-steel wires mixed with compacted bentonite, described in previous section) did not show new mineral alteration products of the bentonite, but an increase in the iron concentration in the bentonite matrix immediately close to the wires surface. A gradual decrease of iron was observed up to 300  $\mu\text{m}$  away from the wires surface. Element mapping showed that microfractures and discontinuities provided preferential pathways for the iron released from the steel. Authors discuss that those microfractures developed during the course of the experiment. In some cases an increase of calcium was observed just along the wire-bentonite interface and the replacement of Na/K interlayer cations with Fe released during corrosion was observed in the montmorillonite.

Table 5-4 – Summary of corrosion products and clay transformation from laboratory experiments made under anaerobic conditions and temperature ≤ 100 °C.

Materials	Time	Temp	Corrosion products	Clay transformation/ Alteration of properties	Reference
iron powder/ bentonite MX-80 and Montigel	100 days	80 °C	magnetite	No/No	Mueller-Voumoos et al. 1991
iron/ bentonite MX-80	180 days	80 °C	magnetite	No/No	Madsen, 1998
C-steel probes/FEBEX bentonite	30, 540 days	25, 50, 75, 100 °C	siderite	No/No	Madina el al. 2002; Azcárate et al. 2004
steel/bentonite Kunipia F and Kunigel V1	3650 days	80 °C	amorphous Fe(OH) <sub>2</sub> , lepidocrocite, green-rust (Cl)	No/Yes (CEC)	Ishidera et al., 2008
iron powder/powder synthetic di- and tri-octahedral smectites	45-120 days	80°C	magnetite	dioctahedral → odinite and cronstedtite trioctahedral → unaffected	Lantenois et al., 2005
steel coupons-wires/bentonite MX-80	900 days	30-50 °C	magnetite, goethite, hematite	No/Yes (CEC, hydraulic cond.)	Carlson et al., 2007, 2008
iron/bentonite FoCa	45 days	80 °C	magnetite, siderite	odinite and greenalite/Yes (CEC)	Perronet et al., 2007, 2008
saturated iron-Calovo-Oxfordian clay	240 days	90 °C	magnetite, maghemite, siderite	Fe-rich dioctahedral phyllosilicates	Schlegel et al., 2008
C-steel wires/bentonite MX-80/NaCl solution	93, 193, 198 days	50 °C	akaganeite, Fe(O,OH,Cl), magnetite	No	Milodowski et al., 2009
C-steel/montmorillonite			Fe(III) oxyhydroxides, green-rust, magnetite	partial dissolution (by local H <sup>+</sup> production due to magnetite formation)	Jeannin et al., 2010
cast iron/compacted MX-80 bentonite	2920 days	room temp		No	Kumpulainen et al. 2010
iron powder/Kunipia F bentonite (powder) - batch experiment	3650 days	room temp		berthierite-type	Kumpulainen et al. 2010
iron foil/ Calovo-Oxfordian Clay	180-540 days	90 °C	magnetite, siderite	berthierite, nontronite, minnesotaite	de Combarieu et al., 2011
iron/montmorillonite and beidellite	45 days	80 °C	magnetite	berthierite, odinite, cronstedtite	Lanson et al. 2012
iron powder/ montmorillonitebeidellite and ferruginous smectite	35 days	75 °C	magnetite	berthierite	Osacky et al., 2013
iron powder/Calovo-Oxfordian clay - batch exps	180 days	90 °C to 40 °C step-by-step	magnetite	cronstedtite, greenalite	Pignatelli et al., 2014
iron powder (different sizes)/Calovo-Oxfordian clay - batch experiments	90 days	90 °C	magnetite, green rust	odinite, greenalite, Fe-serpentine	Bourdelle et al. 2014, 2017
iron/Calovo-Oxfordian Clay – batch exps	60 days	90 °C	magnetite	7Å Fe-rich serpentine	Le Pape et al. 2015
iron/Calovo-Oxfordian Clay – batch exps	30, 120, 270 days	90 °C	magnetite	serpentine particles	Rivard et al., 2015
C-steel wires/MX-80 bentonite	970, 2370 days	60 °C	magnetite	No	Smart et al. 2017

### 5.2.2 Mock-up and field scale experiments

Large-scale field tests have been made or are in progress in crystalline and sedimentary rocks, which include use of highly compacted bentonite around the steel containers: Mol (HADES) in Belgium, Olkiluoto (ONKALO) in Finland, Bure (Meuse-Haute Marne) and Tournemire in France, Pinawa in Canada, Honorobe and Mizunami in Japan, URT in Korea, Äspö in Sweden, Grimsel Test Site (GTS) and Mt Terri in Switzerland. This section summarizes results from experiments in some of those URLs.

#### Corrosion rates and corrosion products

##### Experiments at Mol

SCK-CEN (Debruyn et al., 1990; Cornelis and Van Iseghem, 1993; Kursten et al., 1997, 1999) tested the corrosion of carbon steel specimens under three different environmental conditions: direct contact with saturated bentonite, humid clay atmosphere and saturated bentonite with concrete porewater. The results are presented in Table 5-5.

*Table 5-5 – Calculated average uniform corrosion rates ( $V_{corr}$ ) and maximum pit depths ( $D_{max}$ ) of the carbon steel samples obtained from in situ corrosion experiments (from Debruyn et al., 1990; Cornelis and Van Iseghem, 1993; Kursten et al., 1997, 1999).*

Corrosion media	Temperature °C	Exposure time months	$V_{corr}$ $\mu\text{m}/\text{year}$	$D_{max}$ $\mu\text{m}$
Direct contact with Boom Clay	170	4.7	8.59	n.d.
	90	1.7	7.68	240
		7.0	4.65	90 (material) 130 (welding)
	16	4.7	1.81	100-120 (material)
3.0		8.57 (ar) 5.47 (p)	260 (ar) 45 (p)	
Contact with humid clay atmosphere	90	2.0	9.03 (ar) 3.24 (p)	180 (ar) 30 (p)
	16	2.5	5.13 (ar) 0.40 (p)	195 (ar) 75 (p)
Contact with saturated bentonite with concrete porewater	90	2.0	0.73 (ar)	60 (ar)
	16	2.5	9.48 (ar) 1.31 (p)	235 (ar) 50 (p)

$V_{corr}$ : average uniform corrosion rate  
 $D_{max}$ : maximum pit depth  
 ar: samples tested "as received" (no surface treatment)  
 p: sample tested in the polished condition

##### Experiments at GTS

FEBEX (Full-scale Engineered Barrier Experiment in Crystalline Host Rock) was a research and demonstration project that was initiated by ENRESA (Spain) with the objective of demonstrating the feasibility of constructing the engineered barrier system in a horizontal configuration according to the Spanish concept for DGR and understanding coupled thermo-hydro-mechanical and geochemical processes. The experimental set-up consisted in a horizontal drift with a diameter of 2.28 m was excavated in the Grimsel granodiorite, which contained two electrical heaters (a C-steel cylinder, wall thickness 100 mm) as the reference canister, introduced in the gallery by using a liner (steel perforated guide tube, 15 mm thick). Bentonite blocks were used to fill the gaps between the heaters and the rock (Fuentes-Cantillana and García-Siñeriz, 1998). One heater was dismantled after 5 years of operation and the other after 18 years of operation.

Madina and Azkárate (2004) investigated the corrosion of metal components after the first dismantling. The authors reported the presence of goethite ( $\alpha$ -FeOOH) and  $\text{Fe}(\text{OH})_3$  as main corrosion products in the surface of the steel canister in contact with bentonite. The heater underwent a very slight generalized corrosion, due to the absence of humidity around it, which prevented or slowed down the advance of generalized and/or localized corrosion. The liner presented a stronger generalized corrosion than the heater; the authors refer that its contact with the bentonite and the presence of a higher degree of humidity can account for the corrosion processes undergone by this component. The C-steel coupons showed very slight generalized corrosion with corrosion rates  $0.10 \mu\text{m yr}^{-1}$ , probably because they were embedded in unsaturated bentonite with very low water content. Finally, the sensors were the components that underwent the greatest corrosion damage due to the presence of sulphides generated by SRB.

Madina (2016) and Wersin and Kober (2017) reported the following aspects on the different iron elements in the FEBEX experiment dismantled after 18 years of operation: (1) The heater underwent very slight uniform generalised corrosion over its whole surface, with oxide layers less than  $20 \mu\text{m}$  thick in all the cases examined. No localised corrosion phenomena were observed. The main reasons are an almost complete absence of humidity around the heater (heating at  $100 \text{ }^\circ\text{C}$ ) and the fact that the heater was not in direct contact with the bentonite, which avoided or slowed down the progression of generalised corrosion, as well as the start and progression of localised corrosion phenomena. The two lid-cylinder welded joints at the top and back side of the heater showed a good condition. The predominant identified corrosion products were Fe(III) oxides (mainly goethite, but also hematite, lepidocrocite, maghemite) associated to akaganeite ( $\text{Fe}^{3+}(\text{O}, \text{OH}, \text{Cl})$ ). Chloride was detected in almost all the corrosion products analysed on the surface of the heater. (2) The liner showed non-uniform generalised corrosion (greater than heater) that did not advance uniformly, with maximum values of penetration of the corrosion of approximately  $130 \mu\text{m}$  on the external surface and  $200 \mu\text{m}$  on the internal surface. The liner was in direct contact with the bentonite. The humidity conditions were higher, which would justify the higher extension of generalized corrosion. (3) The corrosion damage observed on the carbon steel components used for anchoring the sensors to the rock and to the liner is a generalized extensive corrosion, with an important generation of reddish corrosion products that correspond mainly to hematite but also siderite highlighting that conditions were partially anaerobic. A significant chloride peak is detected in all the EDS analyses carried out on the corrosion products. No significant differences in the corrosion extension were observed between components close to the rock and those close to the liner.

#### Experiments at Tournemire

Gaudin et al. (2013) and Dauzères et al. (2013) made *in situ* experiments in the Tournemire URL. Toarcian argillite/carbon steel discs interaction was analysed after 2, 6 and 10 years of interaction. The corrosion initiated by trapped oxygen in the claystone porosity, which reacted with iron to form goethite/lepidocrocite minerals. Even after six years of reaction, there is no observed evidence of the anoxic corrosion of steel. The authors observed corrosion rates of  $\approx 3 \mu\text{m yr}^{-1}$  for carbon steels and  $\approx 0.1 \mu\text{m yr}^{-1}$  for stainless steels. Alteration thickness of  $50\text{-}300 \mu\text{m}$  was measured. Iron from corrosion diffuses up to  $5 \text{ mm}$  into the argillite. Calcium phases are dissolved due to acidification of the claystone porewater attributed to the presence of sulphate reducing bacteria, a key parameter in the geochemical evolution of the system. The steel corrosion caused a porosity opening in the corrosion products, but the iron released precipitates at the interface partially clogging the clay porosity.

#### Experiments at Bure

Schegel et al. (2014) investigated the chemical and mineralogical transformations formed on two iron probes (a massive iron rod and a model overpack) in saturated Callovo-Oxfordian formation (Paris basin, France) interacting at  $90 \text{ }^\circ\text{C}$  for two years. The corrosion rate of the massive rod was monitored *in situ* and decreased from  $90 \mu\text{m yr}^{-1}$  during the first month to less than  $1 \mu\text{m yr}^{-1}$  after two years of reaction. The average corrosion rate was  $13 \pm 1 \mu\text{m yr}^{-1}$  for the massive rod and  $15 \pm 1 \mu\text{m yr}^{-1}$  for the overpack. Non-homogeneous corrosion occurred and both probes have similar corrosion interfaces.

Necib et al (2016, 2017a) show the results of experiments on corrosion of C-steel in contact with clay in the Meuse/Haute-Marne URL in Bure (France). C-steel coupons were introduced in a packed-off section of a vertical borehole drilled under anoxic conditions to prevent oxidation of the rock. The section was heated to 85 °C and coupons were left to react from 77 to 1800 days, one set of samples in gas phase and the other in liquid phase. Corrosion in samples submitted to the gas phase was very limited (mean value 2  $\mu\text{m yr}^{-1}$ ), with non-uniform general corrosion prevalence and magnetite, siderite and Fe sulphides as main corrosion products. Corrosion in samples submitted to liquid phase was one order of magnitude greater than in the gas phase. Redox measurements indicated that reducing conditions were attained after around 300 days and pH passed through an acidic stage (minimum 4.5 at 200 days) that promoted corrosion rates up to 250  $\mu\text{m yr}^{-1}$  and formation of a Fe-hydroxychloride compound, which seems to favour active corrosion, as well as mackinawite, which authors attribute to the metabolisms of SRB, and siderite. The coupons exposed to near-neutral pH conditions had non-uniform general corrosion, average corrosion rates of 10  $\mu\text{m yr}^{-1}$  and crondstedtite, greenalite and/or magnetite as main corrosion products, which act as protective layers of the metal surface.

#### Experiments at Mt Terri

Necib et al. (2017b, 2019) made two types of corrosion experiments in the Mont Terri URL in St. Ursanne (Switzerland) to measure corrosion of C-steel: (1) C-steel in contact with Opalinus Clay. The experiment was made in a borehole drilled in Opalinus clay purged with nitrogen and lasted for 7 years. Experiments were maintained at ambient temperature for two years, and then increased to 85 °C up to dismantling. Corrosion rates evolved from initial values 15  $\mu\text{m yr}^{-1}$  to final values around 1  $\mu\text{m yr}^{-1}$  (pH near neutral and redox potential below -300 mV during the experiment). Non uniform general corrosion occurred. The inner layers of corrosion products include mixed magnetite and Cl containing iron compounds, then a layer of chukanovite and Fe silicate, and siderite surrounded by akaganeite. Intermediate layer (trace of original surface) contains siderite and extended domains of goethite, lepidocrocite, Fe sulphide and a thin layer enriched in Fe silicate, the outer layer was siderite; (2) C-steel in contact with MX-80 bentonite. C-steel coupons were embedded into blocks of bentonite compacted at different densities or into a powder-pellets mixture of bentonite with a dry density of 1.45  $\text{g cm}^{-3}$ . A total of twelve modules were introduced in a borehole drilled in Opalinus Clay under anoxic conditions and then pre-saturated in anoxic synthetic Opalinus Clay porewater. The authors present the results of three of those modules dismantled after 20 months of operation. Averaged corrosion rates between 1.5 and 2.25  $\mu\text{m yr}^{-1}$  were measured. The corrosion product found in all cases mainly consisted of a non-stoichiometric magnetite or mixed phase spinel. From those experiments the authors highlight the reproducibility of mechanisms at the corrosion interface.

Smart et al. (2017b) present the results of an experiment lasted 20 months consisting in C-steel pieces embedded in compacted bentonite (blocks and pellets) with different densities and prepared under anoxic conditions. The experiment was installed in a 15 m deep vertical borehole drilled in Opalinus Clay at Mt. Terri URL (Switzerland). To maintain anoxic conditions the borehole was flushed with argon and sealed with a hydraulic packer. During exposure temperature was ~14 °C. Results highlighted the influence of density on corrosion, as highest bentonite density implies less extent of corrosion. Further, the corrosion is lower when bentonite blocks are used instead of pellets, even when dry density of the block is lower than that of the pellet. Magnetite was identified as main corrosion product. Results are similar to those from laboratory experiments made by the authors at higher temperatures.

### *Effect of microbial activity*

#### Experiments at Bure

Experiments by Necib et al. (2017a) at Bure described above included the analysis of microbial activity. The authors detected SRB and thiosulphate reducing bacteria (ThRB) during the whole experiment, although could not establish a relationship between corrosion rate and bacteria content. However, they found that C-steel coupons lasted longer time had higher content of bacteria and attribute the presence of mackinawite to the metabolism of SRB.

#### Experiments at Äspo

Fru and Athar (2008) investigated the presence of microorganisms in a bentonite recovered from tests carried out at Äspo URL in Sweden. The main conclusion of the study by the authors is that high density of the compacted bentonite and elevated temperatures inhibits the presence of SRB in the bentonite, although they are present in the groundwater.

#### Experiments at GTS

The microbiological corrosion of steel sensors at GTS (Madina and Azcárate, 2004) produced black iron sulphides, and chrome enrichment was also detected in the bentonite surrounding the sensors, thus the presence of green amorphous hydrated chrome oxides ( $\text{Cr}_2\text{O}_3 \cdot \text{H}_2\text{O}$ ) was not discarded. Likewise, chlorine and nickel-rich yellow corrosion products were also generated. Consequently, the corrosion of the sensors indicates that the damage was done by bacteria activity, as well as by the effect of chlorides in the environment. Transgranular cracking and localized pitting were the corrosion phenomena identified in the sensors. The experiment “Materials Corrosion Test” at Grimsel has been used to analyse microbial communities in MX-80 bentonite compacted at two densities ( $1.25$  and  $1.50 \text{ g cm}^{-3}$ ) containing metal coupons (Engel et al., 2019). The material was emplaced in boreholes at 9m depth and first samples of bentonite and surrounding groundwater were taken after 13 months of operation and analysed. Engel et al (2019) found little microbial growth inside the bentonite and found SRB in borehole solution. Further analysis with time is required to confirm microbial viability in the bentonite.

#### Experiments at Mt. Terri

The experiments by Necib et al. (2017b, 2019) described above investigated the effect of microbial activity on C-steel corrosion in clay rock and bentonite at the conditions of a DGR. C-steel-Opalinus Clay experiment revealed SRB and ThRB at the metal surface in low concentrations. The authors indicate that the low corrosion rate measured in the experiment point to small impact of SRB on the expected lifetime of the C-steel canister in a confined diffusive regime. C-steel-bentonite experiment showed that at lowest dry density highest number of anaerobic heterotrophs is found, which points out that microbes have limited viability in highly compacted bentonite. Smart et al. (2017b) investigated the anaerobic corrosion of carbon steel in compacted bentonite (blocks and pellets) exposed to natural Opalinus Clay porewater containing native microbial populations for 20 months. The authors analysed the effect of bentonite density on microbial activity and MIC, as well as the weld corrosion. Metal coupons were inserted into the bentonite and introduced in boreholes (anoxic porewater). The experiments showed an increase of the Fe content in the bentonite up to  $100 \mu\text{m}$  from the steel surface. Corrosion rates ranged from  $1.21$  to  $3.38 \mu\text{m yr}^{-1}$ . However, corrosion rates were lower in the bentonite blocks than in bentonite pellets and in bentonite blocks with higher density. The main alteration product was magnetite, although a mixed phase spinel and some hematite was also found (the latter attributed to pre-test surface preparation). A set of bacteria including aerobic, anaerobic and sulphate reducing was identified in bentonite and in porewater. SRB were active mainly on the interior of the bentonite, which is interpreted as originated in the bentonite itself rather than the porewater. The SRB numbers are higher than those obtained in FEBEX bentonite also tested at Mt. Terri URL by Stroes-Gascoyne et al (2013). The first  $20 \mu\text{m}$  of bentonite from the steel pieces were finer-grained and more dispersed and presented a high number of anaerobic and aerobic heterotrophs bacteria. The authors also concluded that there is a threshold density for microbial activity in MX-80 that may be between  $1.25$  and  $1.45 \text{ g cm}^{-3}$ .

## Transformation of bentonite/clay

A number of mock-ups and *in situ* tests have been carried out in underground rock laboratories in order to explore the performance of the Engineered Barrier System and specifically the interaction between the steel canister and bentonite barrier. These include the FEBEX experiment at the Grimsel Test Site, with two steel canisters at 100 °C in contact with bentonite, which were dismantled after 5 and 18 years of operation (Huertas et al., 2006; García-Siñeriz et al., 2016; Wersin and Kober, 2017; Hadi et al., 2019), the ABM and TBT experiments at Äspö (Svensson and Hansen, 2013; Wersin et al., 2015; Smart et al., 2017a) or the *in situ* tests in Tournemire (Gaudin et al., 2009), Bure (Crusset et al., 2017) and Mont Terri (Johnson and King, 2008; Smart et al., 2017b; Necib et al., 2017b, 2019). Duration of these tests has ranged from 18 months to 18 years. As discussed in these reports, the major part of the bentonite backfill remained intact, and only small alterations of the mineralogical, chemical and mechanical properties were detected in these experiments. Despite the duration of the test or the nature of the clay material (claystone or bentonite), in all cases, a Fe-rich front resulting from the iron diffusion from the corroded steel was detected.

### Experiments at Tournemire

Stainless steel samples were buried in Tournemire argillite (Gaudin et al., 2009, 2013; Dauzères et al., 2013) where reaction occurred under oxidizing conditions. There was a dissolution process of argillite particles which was mainly associated to the formation of Fe(III)-rich phases (goethite, lepidocrocite and some traces of magnetite) near the steel surface and to a decrease of the pH more likely responsible for argillite destabilization. The general processes consisted in the dissolution of calcite, phyllosilicate (I/S) and pyrite and crystallization of some traces of gypsum and melanterite. Similar results were observed in Mont Terri and Grimsel. Magnetite was identified in the contact with steel, whereas goethite was identified product in the red and orange zones observed in the bentonite blocks.

### Experiments at Bure

The experiments by Schegel et al. (2014) described above show the presence of a discontinuous layer of magnetite in contact with iron, and a layer of Fe-rich phyllosilicates and Ca-enriched siderite (ankerite) in the transformed Callovo-Oxfordian clay (Figure 5-3). The results were comparable to those laboratory experiments from Schlegel et al. (2008) (Figure 5-2).

### Experiments at Äspö

Svensson and Hansen (2013), Wersin et al. (2015) and Smart et al (2017) characterized bentonite samples coming from experiments ABM (130 °C, 1 year) and TBT (larger dimensions than ABM, 130 °C, 7 years) in Äspö. ABM samples in contact with the metal surface showed the formation of a 10 mm thick layer of different bentonite coloration in the bentonite directly contacting the simulated canister composed of siderite, magnetite, goethite and lepidocrocite. It was attributed to iron diffusion and iron-bentonite interaction. Samples showed an increase of the Fe(II)/Fe(III) ratio either due to the reduction of structural Fe(III) or sorption of Fe(II) on edge sites. The same was observed by Hadi et al (2019) after dismantling the FEBEX experiment in Grimsel Test Site. In general, neoformation of clay minerals or clay transformation was not detected, but bentonite in contact with steel was Fe-enriched and its textural properties were modified (Smart et al., 2017). Wersin et al. (2015) observed Mg<sup>2+</sup> enrichment in the contact interface and signs of dissolution of SiO<sub>2</sub>. Nevertheless, in the ABM test, Svensson and Hansen (2013) and Kaufhold et al. (2017) observed the formation of smectite-type trioctahedral clay minerals. Svensson and Hansen (2013) pointed as possible origin cristobalite and available Mg<sup>2+</sup>, instead of from the alteration of montmorillonite. The TBT samples had less alteration, which is explained by longer periods to attain saturation and larger quantities of oxygen.

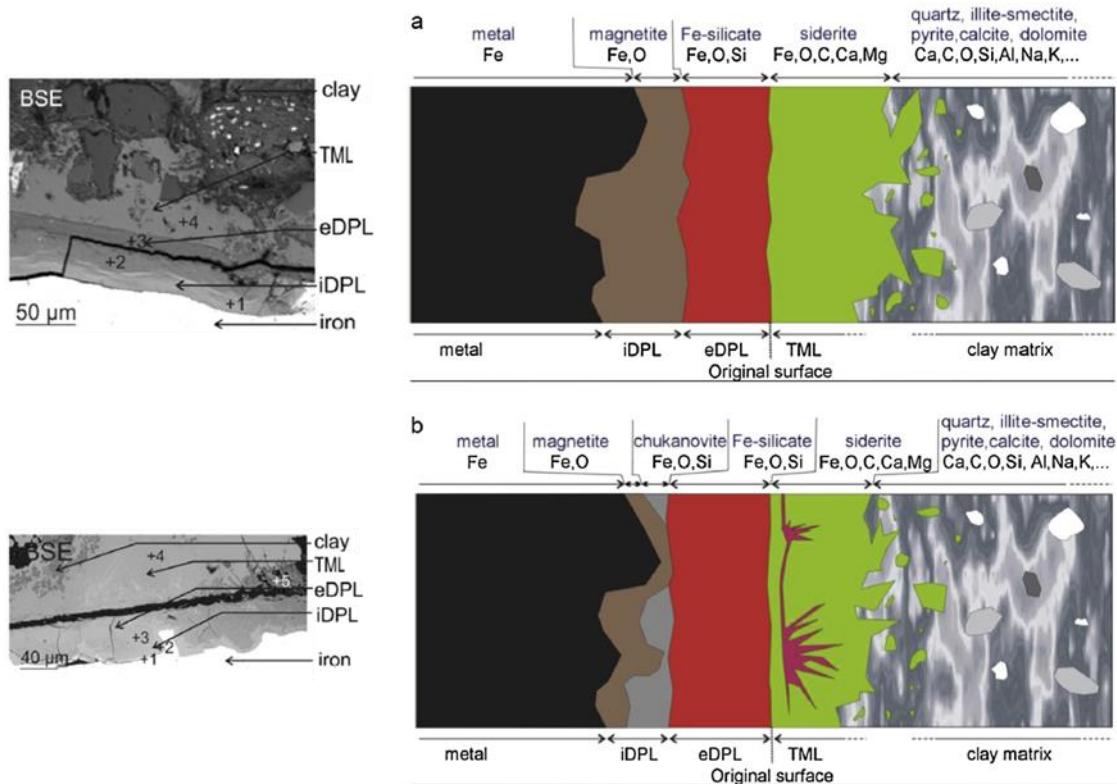


Figure 5-3 – (a) Elemental transfers at the massive iron rod–clay (Callovo-oxfordian) interface reacted at 90 °C during 2 years. (b) *Idem* at the model overpack–clay (Callovo-oxfordian) interface. (iDPL: internal dense product layer; eDPL: external dense product layer; TML: transformed medium layer (from Schlegel et al., 2014).

### Experiments at GTS

Wersin and Kober (2017) and Hadi et al. (2019) reported transformations of bentonite by the steel-bentonite interaction in the FEBEX *in situ* test after 18 years of operation. Alterations of the clay at the steel contact were minor. Increase of Mg towards the heater was noted mainly due to the effect of temperature. The dissolution of some SiO<sub>2</sub> and formation of minor Mg-rich smectite (saponite) close to the heater could be detected partly related to the increase in Mg. The main fraction of enriched Fe in the clay consisted of Fe(III) oxides (mainly goethite), manifested by a reddish halo contacting the corrosion layer. The clay adjacent to this Fe(III)-enriched zone was still slightly enriched in Fe, displaying a higher Fe(II)/Fe(III) ratio. This zone, recognisable by the blueish-greenish colour, may extend to thicknesses of up to 200 mm. Excess Fe<sup>2+</sup> was found to have diffused further into the clay. The results indicate the occurrence of newly formed octahedral Fe<sup>2+</sup> either as Fe<sup>2+</sup> sorbed on the clay or as structural Fe<sup>2+</sup> inside the clay. No other indications of clay transformation or newly formed clay phases were found. The authors indicate that probably diffusion of Fe was initiated when oxidizing conditions were still prevailing inside the bentonite block, resulting in the accumulation of Fe<sup>3+</sup> close to the interface, and continued when reducing conditions were reached, allowing deeper diffusion of Fe<sup>2+</sup> into the clay.

### 5.2.3 Natural/Archaeological/Industrial analogues

It is not possible to simulate the very long-term process that might affect the safety performance of a repository in laboratory or *in situ* studies. For this reason, natural (>10,000 years), archaeological (150 to 10,000 years) and industrial (<150 years) analogue studies are used. For example, archaeological analogues can serve to analyse the stability of metals located in subsurface environments similar to those in a DGR. However, geological analogues will provide information on the stability of metals in different types of rocks or the stability of mineral phases as magnetite in different geological environments. Then, analogues can be used to develop the basic studies required to obtain a sound

understanding of the corrosion mechanism and the clay transformation in the different stages of the repository life. In fact, validation of mechanistically based models has been supported in mechanistic information from analogues, which are realistic in terms of lifetime calculations; e.g., generalized corrosion (King, 1995; Yoshikawa et al., 2008; Saheb et al., 2013) and MIC (Féron et al., 2008). This section compiles some existing literature on analogues dealing with corrosion and clay transformation.

### Corrosion rate and corrosion products

**Industrial analogues** - There are a number of situations in modern industrial applications where anoxic water is present in contact with iron (e.g., Smart and Adams, 2006): (1) Hot water systems where copper pipes and steel radiators are exposed to near neutral waters; (2) Corrosion of seabed and buried pipelines. Corrosion of the pipes often occurs due to an electrochemical mechanism, which both changes the pH environment and releases iron ions into the clay. This can cause chemical alteration to clay minerals and corrosion products (Cole and Marney, 2012; Wang et al., 2017). Post-mortem analyses of buried pipelines show corrosion rates in the range 1-10  $\mu\text{m yr}^{-1}$  (Orazem, 2014); (3) A “semi-natural” analogue was investigated by Kamei et al. (1999) in a bentonite mine in Japan where an arch-shaped iron-support of a gallery was in contact with wet Na-bentonite for about 2000 days. The colour of the bentonite near the support had change from pale to green. Bulk analyses of the altered bentonite showed a remarkable increase in iron (6.3 to 14.4 wt.%  $\text{Fe}_2\text{O}_3$  versus 2.3 wt.% in the unaltered bentonite). Since the amount of the exchangeable cations  $\text{Na}^+$ ,  $\text{K}^+$ ,  $\text{Ca}^{2+}$  and  $\text{Mg}^{2+}$  was significantly reduced in the altered bentonite (22-30 meq per 100 g versus about 55 meq per 100g for the unaltered bentonite), and the CEC remained essentially unchanged, Kamei et al. (1999) assumed that  $\text{Fe}^{2+}$  released from iron corrosion was exchanged with the interlayer cations. XRD suggested that no  $\text{Fe}^{2+}$  had entered the octahedral layers.

#### *Effect of microbial activity*

Li et al. (2017) investigated the effect of MIC on oil production equipment as a function of the temperature (37, 55 and 65 °C) in anoxic environment. The authors provide data on the increasing changes of microbial communities as a function of the temperature; SRB are observed at 35 °C while at the higher temperatures thiosulphate reducers (ThRB) are dominant. Corrosion rates are higher in sterilized than in non-sterilised environment.

Usher et al (2014) made a review on MIC of external walls of buried carbon steel pipes. According to the authors, corrosion rates and corrosion products can be predicted if soil moisture, pH, concentration of ions, organic carbon and oxygen are known. However, the authors highlight the investigations that indicate that some microbes catalyse the oxidation of Fe(0) and consume the electrons (E-MIC), which enhance corrosion significantly. The authors indicate that this mechanism is little known and further investigation should be made in that direction.

**Archaeological analogues** - Although it is recognized that it is impossible to find archaeological analogues exposed to exactly the same conditions as in a geological repository, particularly in terms of temperature, radiation flux and microbial activity, archaeological analogues have provided data on corrosion rates and corrosion products of metals which have survived for centuries or millennia under specific environmental conditions that can be assumed similar to the environmental conditions of some stages of the DGR.

For the characterization of the anaerobic corrosion of iron, two types of archaeological analogues have been studied: (1) objects lost at sea which have been encased in marine sediments (e.g., iron artefacts from shipwrecks), which led to the development of anoxic conditions around the objects; (2) artefacts in land burial sites where residual oxygen has been depleted.

Johnson and Francis (1980) studied different metals from archaeological sites to provide insights to optimum storage environments. The authors concluded that dry or low relative humidity environments are optimum for metal preservation and the data obtained from metals submitted to those conditions are suitable to extrapolate to preservation of nuclear waste containers. Most of examples given provide corrosion rates 0.1 to 10  $\mu\text{m yr}^{-1}$ , even when the burial environment is different. The observed corrosion

rates depend on the medium and, particularly, on the oxygen content and the redox potential (Dillmann et al., 2014) but in general the corrosion rates obtained on archaeological objects can be compared with data from laboratory experiments of shorter duration under representative conditions.

Neff et al. (2004) studied the corrosion of archaeological iron artefacts from 800 years ago and identified as main corrosion products goethite, magnetite, sometimes siderite and  $\text{Fe}_2(\text{OH})_3\text{Cl}$ . Corrosion rates were estimated in  $1\mu\text{m}/\text{year}$  and diffusion of iron into the soil was observed. However, to date, archaeological analogues have not provided relevant information about the iron-bentonite interaction, as the focus has been on the corrosion rates and products but influence of iron corrosion products on the adjoining soil has not been regarded.

Crossland (2005) made a compilation of corrosion rates of iron and steel exposed to soils and natural waters distinguishing aerobic from anaerobic environments. The author observed a decrease of corrosion rate with time. Recent results on the characterizations of archaeological artifacts seem to confirm the long-term passive state of C-steel materials in clay soils (Saheb et al., 2013).

Bellot-Gurlet et al. (2009) analyzed by Raman spectroscopy the corrosion forms observed in buried artefacts for anoxic and aerated soils of five different French archaeological sites. These authors found two main corrosion forms according to anoxic or aerated conditions. The main phases found in anoxic conditions were siderite and magnetite. Siderite was also found by Matthiesen et al. (2003) and Saheb et al. (2008). Samples from aerated soil comprise goethite and mixed magnetite/maghemite.

New aspects such as porosity of the corrosion products layers and its effect on the kinetics of the corrosion process have been considered. Michelin et al. (2013) found that, in anoxic environments, a specific layer less than  $1\mu\text{m}$  thick controlled the kinetics of corrosion by limiting the access of the electrolyte to the metal substrated. With regard to the transport of species the porosity of layers several centuries old can be measured and added to the corrosion models (Neff et al., 2010; Dillmann et al., 2014).

Leon et al. (2014) analysed archaeological nails corroded in an anoxic carbonate environment. The authors found an interfacial layer of a mixture of magnetite and maghemite (Fe(II), Fe(III)) between the metal (Fe(0)) and the outer carbonate corrosion siderite (Fe(II)) layer (Figure 5-4). The interest of this study is the coincidence with other studies on the sequence of corrosion products and also the deuterium labelling that suggested that the iron oxide interfacial layer is less porous than the outer carbonated corrosion layer, which may influence the corrosion kinetic.

Most of results obtained from archaeological remains highlight the fact that corrosion rates predicted for the steel container under disposal conditions are very conservative and that laboratory experiments under similar environmental conditions provide a sequence of corrosion products which is obstinately the same (e.g., Rangel et al., 1986; Schegel et al., 2008).

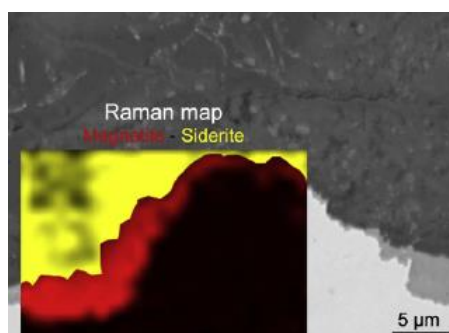


Figure 5-4 – Raman distribution map at the metal-corrosion interface of nails cross-sections (figure from Leon et al., 2014).

### Transformation of bentonite/clay

**Natural analogues** - The use of natural analogues could provide an insight about the thermodynamic stability of thermal Fe-clay systems in nature, although in the case of iron-bentonite interactions, useful natural analogues are very limited (Marcos, 2003; Wersin et al., 2007). However, deposits of bentonite in Greece and Spain that have been affected by iron-rich solutions under hydrothermal regimes can be useful to understand the potential transformation of bentonite to Fe-rich minerals. Furthermore, general observations from natural systems and the NF-PRO project (Kickmaier et al., 2005) suggest the uptake of iron could reduce swelling pressures of bentonites.

Buatier et al. (1993) investigated the chemical changes at the phase transition of Fe-rich clays (smectite to glauconite) formed by precipitation from low-temperature hydrothermal fluids in the Galapagos Spreading Centre. According to the authors the iron is entirely in octahedral positions in the Fe-smectite, while Fe in glauconite is in tetrahedral and octahedral sites. The authors found small particles of iron oxides in glauconite that interpreted as formed by smectite alteration. The authors propose a sequence of transformation from dissolution of Fe-rich smectite to precipitation of glauconite and iron oxides.

Christidis and Scott (1997) studied bentonites from the Aegean Islands of Milos and Kimolos (Greece). The process of formation of smectite and the factors causing the incorporation of Fe in the smectite structure were not well known. The uptake of iron could depend on its availability, redox conditions and partitioning of Fe and Mg in the octahedral sites. The authors discuss that Fe<sup>3+</sup> oxides might have formed from oxidation of pyrite or by recrystallization of iron hydroxide-rich gels, which are precursors of smectite.

The BARRA-project dealing with studies of bentonite/smectites from Almería (Spain) is the only project that has approached the influence of iron on bentonite considering the thermal effect (Pérez del Villar et al. 2003, 2005). It was observed that the smectites close to a volcanic dome are Fe-rich (Fe content as Fe<sub>2</sub>O<sub>3</sub> varies from 4.33 to 13.77 wt.%) and formed at a temperature range from 75 °C to 95 °C. At the same place bentonites far from the dome are dioctahedral Al-smectites with Fe content (Fe<sub>2</sub>O<sub>3</sub>) from 4.36 to 7.44 wt.%. Pelayo et al. (2011) studied the Morrón de Mateo deposit (Almería, Spain) as a natural analogue of the thermal and geochemical effects on a bentonite barrier in the DGR. The presence of corrensite in the epiclastic rocks suggests that in the Morrón de Mateo area a hydrothermal alteration process occurred after bentonite formation, which transformed Fe–Mg-rich smectites into corrensite. This transformation was probably favoured by the intrusion of the Morrón de Mateo volcanic dome, which produced a temperature increase in the geological media and a supply of Fe–Mg-rich solutions. Inoue and Utada (1991) and Beaufort et al. (1997) concluded from their experiments that corrensite is formed as an intermediate mineral phase in the transformation of Fe–Mg-smectite to chlorite at high temperature (100 and 200 °C).

Fukushi et al. (2010) investigated greenish veins in brecciated bentonite in the Kawasaki bentonite deposit in Japan that suggested the interaction of Fe-rich hydrothermal solutions with bentonite. Chemical analyses of this Fe-rich veins revealed that the clay minerals in the vein fillings are most likely Fe-K-rich and dioctahedral. Additional alteration minerals in the veins are pyrite and opal. The authors concluded that the vein minerals had formed at temperatures about 100 °C and that the pH and Eh conditions of the reacted solution were neutral to alkaline pH and reducing. Clay minerals from the altered bentonite adjacent to the veins were identified to be most likely dioctahedral Al-smectites containing Fe.

Complementarily to the study of bentonite deposits in contact with Fe-rich fluids, transformations of Fe-rich clay minerals observed in marine sediments (e.g., Bailey, 1988; Hornibrook and Longstaffe, 1996) have also been used for the characterization of the Fe-related processes occurring in the bentonite/steel container interface. Odinite is the typical mineral phase formed in these environments and is the precursor of berthierine in reducing environments. The compilation by Marcos (2003) includes investigations by Mata et al. (2002), which reported the occurrence of berthierine as an intermediate phase in the smectite-to-chlorite transformation, especially in the evolution of marine sediments; and the results found by López Munguira and Nieto (2000) and Schmidt et al. (1999), which also found

interlayered berthierine, chlorite and saponite in evolved marine sediments of volcanic origin. These studies suggest that berthierine becomes more stable relative to chlorite with increasing the proportion of Fe in a 20%.

Based on observations of natural systems and also laboratory experiments (e.g., Mosser-Ruck et al., 2016), Savage et al. (2010) have argued that chlorite is likely the most stable alteration mineral of iron-bentonite interaction also at low temperatures, but that its formation is kinetically inhibited and proceeds in an Ostwald step rule sequence with magnetite, odinite, crondstedtite and berthierine as transient precursor minerals.

#### *Effect of radiation*

The main effect of radiolysis in the DGR system is the alteration of geochemical conditions in the canister-bentonite interface. Radiolysis has been identified in uranium ores with high radiation as Oklo and Cigar Lake, and others as Cluff Lake and Rabbit Lake (Canada), Shinkolobwe and Menzenschwand (Germany), which represent different geological environments and chemical conditions. The study of these systems contributes to a better understanding of the radiolysis process, mainly to determine the fraction of the total radiation impacting the surrounding water producing reductor and oxidant agents that can affect canister corrosion.

#### *Effect of microbial activity*

The study of microbial populations and its role in different geological environments has been made in natural analogues related to uranium ores (Palmottu, Poços de Caldas, El Berrocal) and in hyperalkaline media (Oman, Maqarin) but the investigations were mainly focused to identify the type of microorganisms in the conditions of radiation, temperature and chemical environment of the sites and the energy sources for the microorganisms. However, none of these investigations accounted for corrosion processes or mineral transformation.

### 5.3 Application of conceptual and mathematical models

The understanding of the interactions at the interface steel/iron-bentonite is continuously growing on the basis of laboratory experiments, field experiments in underground research laboratories and modelling studies. Extensive experimental studies and numerical models of the steel/iron-bentonite interactions under typical HLW-EBS conditions and the effects of corrosion products on the bentonite have been performed in the last two decades (Montes et al., 2005; Bildstein et al., 2006; Wilson et al., 2006b; Wersin et al., 2008; Samper et al., 2008; Savage et al., 2010; Marty et al., 2010; Lu et al., 2011; Bildstein et al., 2012; Ngo et al., 2014; Wersin and Birgersson, 2014; Ngo et al., 2015; Wilson et al., 2015; Bildstein et al., 2016; Cuevas et al., 2016; Samper et al., 2016; Balmer et al., 2017; Mon et al., 2017; Fernández et al., 2019; Kaufhold et al., 2019).

Savage (2012) reported that most of modelling studies of the iron-bentonite interactions have treated this issue as a THC problem, with most models predicting that magnetite is the principal steel corrosion product, along with significant alteration of the clay minerals of the bentonite to a mixture of non-swelling silicates, such as chlorite, berthierine or cronstedtite and zeolites. In these models, mineral dissolution/precipitation reactions were initially treated as equilibrium reactions (Montes et al., 2005; Bildstein et al., 2006). Subsequent studies have used kinetic approaches (Samper et al., 2008; Wersin et al., 2008; Savage et al., 2010; Lu et al., 2011; Samper et al., 2016; Mon et al., 2017). As discussed by Lichtner and Carey (2006), the uncertainties associated with kinetic data do not justify that the rates adopted for reaction transport calculations should be infinite (equilibrium assumption) rather than finite values (kinetic assumption). Some numerical models predict that magnetite will be the main corrosion product (Bildstein et al., 2006; Hunter et al., 2007; Samper et al., 2008; Lu et al., 2011, Bildstein et al., 2012; Samper et al., 2016; Mon et al., 2017) while others predict also the formation of Fe-bearing aluminosilicates (Wersin et al., 2008; Savage et al., 2010; Marty et al., 2010; Ngo et al., 2014; Wilson et al., 2015).

Bildstein and Claret (2015) presented a modelling review of the impact on steel/iron-natural/engineered clay interfaces under different HLW-EBS conditions as a result of the dissolution of primary minerals and precipitation of secondary minerals, as well as modifications of mineral properties (especially related to the exchange capacity, the interlayer cation content, and the swelling ability of clay minerals) and transport properties through modifications in porosity, permeability and tortuosity.

Claret et al. (2018) presented a review focused on recent improvements and perspectives for reactive transport modelling in the framework of studies on predicting the evolution of radioactive waste disposal in clay formations. The barrier properties and the different interfaces as the iron/steel-clay interface evolve in time in response to the physical and chemical interactions between the various constituents of the barriers and the surrounding environment. They also show a detailed description of the main modelling approaches, assumptions and simplifications used in the most recent reactive transport model focused on the iron/steel-clay interface at the scale of the disposal cell.

Bildstein et al. (2019) presented a comprehensive review of the reactive transport modelling studied at the iron-clay interface at the lab scale and at the scale of the disposal cell for waste repositories. They conclude that: (1) The most abundant corrosion product predicted by the models in the long-term is magnetite, sometimes with Fe-carbonates (siderite) and Fe-silicates (greenalite), sometimes incorporating Al (berthierine, cronstedtite); (2) Primary minerals in clay are often destabilized in favour of Fe-phylosilicates or zeolites if they are allowed to precipitate; (3) Numerical studies often differ on the precise nature of the main secondary minerals; (4) The transformation of clay minerals into Fe-chlorite, and the timing, very much depend on whether it is included as a secondary mineral (in which case it is the most stable phase and precipitates from the beginning of the simulation) or it results from a ripening process; (5) One of the most sensitive parameter is the corrosion rate; (6) The extent of the perturbation is always predicted to be limited to a few centimetres, up to 20 centimetres into the clay barrier; and (7) Porosity clogging is considered in some simulations under different assumptions. Bildstein et al. (2019) also pointed out that a complete inhibition of the corrosion process has never been observed in experiments, even if a dense corrosion product layer is often identified, and the ubiquity of magnetite in simulation results as the dominant corrosion product in the long-term is questioned by many experimental results and archaeological analogues.

Bildstein et al. (2006) modelled the interactions of a carbon steel canister with the MX-80 bentonite and a clay formation with a 1D purely diffusive model under full saturation conditions. The model accounts for a 7 cm thick stainless steel canister, an 80 cm thick MX-80 bentonite-based EBS, and a 10 m long geological barrier of clay host rock. The reaction-transport code CRUNCH was used to investigate the iron-clay interactions at 50 °C over 10.000 years. A constant corrosion rate of  $4.3 \mu\text{m yr}^{-1}$  was considered. They considered the following corrosion products: iron oxides and hydroxides, iron carbonates, and iron-rich smectite and Fe-phylosilicates. Their simulations showed that most of iron released during corrosion processes was partly immobilized by the precipitation of iron oxides (mainly magnetite) and small amounts of siderite. In the bentonite or the argillite in contact with the container, the primary clay minerals are destabilized and iron-rich serpentine-like minerals precipitate as observed in the experiments (cronstedtite and berthierine). These minerals show low cation exchange and swelling capacities (Montes et al., 2005).

Wersin et al. (2008) studied the impact of iron components released from the canister corrosion on the bentonite buffer (MX-80) for the KBS-3H concept at the Olkiluoto site in Finland. They performed 1D diffusion reactive transport model simulations with CrunchFlow. They accounted for iron corrosion, cation exchange, protonation/deprotonation, Fe(II) surface complexation and thermodynamic and kinetic mineral dissolution/precipitation. They concluded that the extent of the bentonite zone transformed to non-swelling material is likely to remain spatially limited (a few centimetres) for very long times.

Samper et al. (2008) presented a 1-D and 2-D axisymmetric water flow and multicomponent reactive solute transport models to simulate canister corrosion, the interactions of corrosion products with bentonite and the long-term hydrochemical evolution of porewater composition in the near field of a repository in fractured granite. Numerical simulations were performed at a constant temperature of 25 °C for 0.3 Ma. Coupled hydrogeochemical calculations of interactions of corrosion products with bentonite have been performed with CORE2D V4. They found that: (1) Magnetite is the main corrosion product; (2) Fe diffusion from canister into bentonite leads to magnetite precipitation in the buffer; (3) Siderite precipitation is small due to the limited carbonate availability; (4) Corrosion causes an increase of pH in the bentonite; (5) Proton surface complexation is the main pH buffering mechanism. Other mechanisms such as  $\text{Fe}^{2+}$  exchange and calcite and iron minerals dissolution/precipitation are much less effective; and (6) Magnetite precipitation causes a reduction of porosity in bentonite. The largest changes in porosity occur at canister–bentonite interface. Corrosion products have a larger volume than carbon-steel, but not large enough to clog bentonite pores. Lu et al. (2011) presented an updated version of the model of Samper et al. (2008), which considers 3 types of sorption sites in the bentonite, kinetically-controlled canister corrosion and magnetite precipitation, and the competition of dissolved  $\text{Ni}^{2+}$  for sorbing sites. Simulations were carried out with CORE2D V4 at a constant temperature of 25 °C for a time horizon of 0.3 Ma. Model results show that: (1) Accounting for kinetically-controlled canister corrosion leads to a significant reduction in the corrosion rate; (2) The uncertainties in the surface complexation model play a minor role in the time evolution of the computed pH in the bentonite and the granite. The computed concentrations of dissolved and sorbed Fe, on the other hand, are very sensitive to changes in the surface complexation model; (3) The apparent  $K_a$  of Fe is 10 times larger for the triple-site sorption model; (4) The concentration of dissolved Fe computed with kinetic magnetite precipitation is smaller than that obtained at local equilibrium; and (5) The competition of  $\text{Ni}^{2+}$  for sorption sites affects significantly the chemical evolution of the bentonite porewater. The pH in the bentonite porewater decreases compared to the value computed without Ni transport because the sorption of  $\text{Ni}^{2+}$  releases protons. The sorption of  $\text{Ni}^{2+}$  leads to a smaller concentration of sorbed Fe and a larger concentration of dissolved Fe in the bentonite water for  $t < 10^5$  years.

Savage et al. (2010) reported a model of iron-bentonite interactions based on natural analogues. They claimed that the sequence of the alteration of the clay by Fe-rich fluids may proceed via an Ostwald step sequence. They modelled iron corrosion and the alteration of the MX-80 bentonite by incorporating processes of nucleation, growth, precursor cannibalisation, and Ostwald ripening (Steeffel and Van Cappellen, 1990) to address the issues of the slow growth of bentonite alteration products by modifying the computer code QPAC. They modelled iron corrosion (corrosion rate of  $\sim 2 \mu\text{m yr}^{-1}$ ) and the alteration of MX-80 bentonite in a typical EBS environment. Their model neglected protonation-deprotonation reactions at clay edge sites and cation exchange reactions. They considered two model cases; one with fixed reactive surface areas for secondary minerals; and one with time-dependent variation of the surface areas of secondary minerals. According to Savage et al. (2010), simulations with fixed mineral surface areas showed that berthierine dominates the solid product assemblage, with siderite replacing it at simulation times greater than 10,000 years. The simulations with time-dependent mineral surface areas show the following sequence: magnetite-cronstedtite-berthierine-chlorite. The evolution of the secondary minerals is somewhat different to that predicted by the fixed surface area model. Near to the corroding canister, at first magnetite is the dominant Fe-bearing mineral; this is followed by cronstedtite, which dominates between  $\sim 0.04$  years and 500 years. Berthierine is again present throughout, but in reduced quantities compared with the fixed surface area model; after 500 years cronstedtite dissolves away and berthierine is the dominant Fe-bearing mineral. Eventually, after about 5,000 years, chlorite grows in, using the berthierine surface growth sites rather than nucleating directly. Further into the clay, there is much less Fe-based mineral precipitation than in the fixed surface area case, with only small amounts of berthierine present.

Marty et al. (2010) modelled the long-term alteration of the engineered bentonite barrier in an underground radioactive waste repository. Their study focused on the feedback effects of geochemical reactions on the transport parameters of compacted MX-80 bentonite. The system was modelled in reducing conditions by using the KIRMAT code. The model considers a 1 m thick buffer of MX-80

bentonite which is in contact on one side with a geological fluid (Callovo-Oxfordian groundwater at 25 °C) diffusing into the engineered barrier. Their calculations assumed a constant temperature of 100 °C to estimate the maximum thermal effect on the mineralogy of the engineered barrier. The model was run for  $10^5$  years. By considering the temperature and the long-term evolution of the system, the mineralogical transformations were considered as being more important than the surface complexation and cation exchange reactions. As a consequence, these reactions were neglected in the model. After 100,000 years of simulated mass transport-reaction, the model predicted mineralogical modifications of the EBS in contact with the geological interacting fluid and with  $\text{Fe}^{2+}$  ions provided by the corrosion of the steel overpacks. According to the degree of smectite transformations the mineralogical modifications of the MX-80 bentonite until 100,000 years showed three distinct zones: (1) The first zone results from the mass transport of the groundwater through MX-80 bentonite. The resulting alteration front corresponds to a strong illitization of the montmorillonite together with the precipitation of quartz, saponite and vermiculite; (2) In the middle of the EBS, the volume of montmorillonite remains constant. The saponitization and the illitization processes can be distinguished in lower proportions as minor phase; and (3) The third alteration front is constituted by significant precipitations of Fe(II)Al-chlorite, Fe(II)-saponite and magnetite in contact with the steel overpack. The precipitation of these phases decreases significantly the porosity of the EBS. Marty et al. (2010) concluded that only the outer parts of the simulated system are significantly affected. The dissolution of the montmorillonite contained in the MX-80 bentonite is mainly observed in the zone influenced by the groundwater mass transport and partly in a zone adjacent to the container.

Ngo et al. (2014) presented a coupled transport-reaction model for the long-term interactions of iron, bentonite and Callovo-Oxfordian (COx) claystone which extended the work of Marty et al. (2010) by investigating the influence of the reactive surface area of the primary minerals on the bentonite and the COx claystone and the diffusion coefficient on the evolution of the iron-bentonite system.

Wilson et al. (2015) presented three fully-coupled reactive transport models of a steel-bentonite interface to provide new insights into the nature of steel-bentonite interactions, especially the potential for the alteration of the montmorillonite component of bentonite to iron-rich clay minerals. The conceptual model comprises a 1D cross section through a cylindrical bentonite/sand buffer (70 cm thick) that surrounds a steel overpack and inner waste package with a combined diameter of 82 cm. The temperature was set at a constant value of 70 °C. In the simulations, which were undertaken using the multi-purpose modelling code QPAC, the following processes were included: steel corrosion, mineral dissolution, mineral precipitation, cation exchange, diffusion and porosity evolution (Archie's Law). The three models simulated were: (1) steel corrosion reaction applied on a boundary directly in contact with bentonite at a fixed rate; (2) steel corrosion reaction applied on a boundary directly in contact with bentonite at a diffusion-limited rate; and (3) a corrosion cell representation with a fixed steel corrosion rate. In models 1 and 3 steel corrosion was assumed to occur at a fixed rate of  $1 \mu\text{m}/\text{y}$  while in Model 2, the corrosion reaction was assumed to be diffusion limited. The extent and nature of the alteration predicted by the models was found to be sensitive to model conceptualisation. The corrosion cell assumption leads to steel corrosion products including magnetite and siderite and the alteration of primary minerals to berthierine. In contrast, the boundary corrosion assumption with a fixed steel corrosion rate leads to quicker alteration to iron-rich clay minerals. If the diffusion-limited corrosion rate assumption is made, the steel corrosion rate varies over time as the bentonite porewater composition evolves, and the spatial extent of alteration is much more limited (mm scale).

Samper et al. (2016) presented a non-isothermal reactive transport model for the long-term (1 Ma) interactions of the corrosion products and compacted bentonite in a HLW repository in granite. Simulations were carried out with the multicomponent reactive transport code CORE2D V4. Canister corrosion causes an increase in the pH and the concentration of dissolved  $\text{Fe}^{2+}$  of the bentonite porewater. Iron precipitates as magnetite and siderite and sorbs via cation exchange and surface complexation on weak sites. The largest pH in the bentonite is almost 9.5 at  $2 \cdot 10^5$  years. Several fronts are observed in the concentration of dissolved  $\text{Fe}^{2+}$ , pH and Eh which are related to sorption and mineral dissolution/precipitation fronts. Magnetite is the main corrosion product and its precipitation reduces

significantly the porosity of the bentonite barrier near the canister and could even clog the pores. The thickness of the bentonite zone affected by the decrease of porosity increases with time and is equal to 7 cm at  $t = 1$  Ma. A detailed sensitivity analysis has been performed to changes in model parameters and conceptual model assumptions.

Mon et al. (2017) presented a non-isothermal multicomponent reactive transport model of the long-term (1Ma) interactions of the compacted bentonite with the corrosion products of a carbon-steel canister and the concrete liner of the engineered barrier of a HLW repository in clay. Simulations were carried out with CORE2D V4. Model results show that: (1) Magnetite is the main corrosion product and its precipitation reduces significantly the porosity of the bentonite near the canister; (2) The degradation of the concrete liner leads to the precipitation of secondary minerals and the reduction of the porosity of the bentonite and the clay formation at their interfaces with the concrete liner. The reduction of the porosity becomes especially relevant at  $t=10^4$  years; (3) The zones affected by pore clogging at the canister-bentonite and concrete-clay interfaces at 1 Ma are approximately equal to 1 and 3.3 cm thick, respectively; (4) The hyper-alkaline front ( $\text{pH} > 8.5$ ) spreads 2.5 cm into the clay formation after 1 Ma. Sensitivity runs were performed to analyse the uncertainties in cation exchange selectivities and evaluate the relevance of surface complexation reactions, kinetic smectite dissolution, and Mg-saponite precipitation.

Table 5-6 provides a comparison of the main assumptions and results obtained in the previously explained modelling exercises at the disposal scale.

Another approach to iron corrosion modelling was presented by Bataillon et al. (2010). They developed the Diffusion Poisson Coupled Model (DPCM) as a tool to investigate the corrosion processes at the surface of the carbon steel canisters. This model was proposed to describe the oxidation of iron in anaerobic neutral or slightly alkaline conditions. These chemical conditions correspond to those expected in the French HLW disposal concept. The model assumes that the solution is in contact with a dense disordered spinel-like oxide layer which covers the iron. Two interfaces bound the oxide layer: (1) The inner interface which corresponds to the metal/oxide layer; and (2) The outer interface which corresponds to the oxide layer/solution interface. The metal (an electronic conductor) could be charged either by accumulation or depletion of electrons. The solution (ionic conductor) could be charged either by accumulation of cations or anions. The oxide layer is a mixed electronic and ionic conductor. The outer and the inner interfaces could move with time. The model considers the electrostatic and kinetic effects and accounts for moving boundaries. The electrostatic module gives the potential profile in the solution-oxide layer–metal system. The kinetics module gives the concentration profiles; one per each charge carrier. The moving boundaries module gives the locations of the two interfaces which bound the oxide layer. These three modules are coupled because each module involves the solution of the others. Bataillon et al. (2010) tested the DPCM in a simplified situation where the locations of the outer and the inner interfaces are fixed and after that with moving boundaries.

A numerical method for a partial differential equations system for the simulation of corrosion model with moving oxide layer using the DPCM model was proposed in Bataillon et al. (2012). The numerical scheme was implemented in the simulation code CALIPSO. The model allows assessing the evolution of the carbon steel corrosion rate (reduction by oxide layer formation), the chemical species release and the characteristic time of these processes. These data could be used to estimate the lifetime of the carbon steel overpack and the pressure rise resulting from hydrogen release. The convergence of the scheme was studied by Chainais-Hillairet et al. (2015) for the two-species model on a fixed domain. Chainais-Hillairet and Gallouët (2016) presented an updated version of the model of Bataillon et al. (2012) by studying the pseudo-stationary state for a corrosion model. The approach implemented in the CALIPSO code has the potential to be coupled with multicomponent reactive-transport models to study the interactions at the interface steel/iron-bentonite under typical HLW-EBS conditions and the effects of corrosion products on the bentonite. The DPCM model is also discussed in section 6.3.

Table 5-6 – Comparison of the recent reactive transport models at the disposal scale (modified from Bildstein et al., 2019).

Reference	Type of interface	T (°C)	Simulation time (years)	Corrosion rate	Assumptions	Main corrosion product	Main secondary minerals	Maximal perturbation extent	Relevant results
Bildstein et al. (2006)	Fe-MX80 bentonite	50	10	Constant (4.3 µm/yr)	1D diffusive model Porosity feedback	Magnetite	Cronstedtite Berthierine	5 cm	Porosity clogging after 5.000 years
Wersin et al. (2008)	Fe-MX80 bentonite	100	500	Constant (1 µm/yr)	1D model (Test case D0) Porosity update Clay reactions are considered Use of cation exchange and surface complexation	Magnetite	Cronstedtite Berthierine	Few cm	The interaction of Fe with bentonite remains spatially limited for very long times mainly because of Fe clay re-precipitation and diffusional limitation
Samper et al. (2008)	Fe-FEBEX bentonite	25	300	Constant (0.2 µm/yr)	1D and 2D model No reactivity for clay minerals Use of cation exchange and surface complexation	Magnetite	Siderite Goethite	7 cm	Bentonite porosity decreases due to magnetite precipitation (no clogging) Proton surface complexation is highly effective in buffering pH in bentonite
Savage et al. (2010)	Fe-MX80 bentonite	-	1.000.000	Constant (~2 µm/yr)	Time-dependent variation of reactive surface areas for the Fe-bearing minerals The sequence of the alteration of the clay by Fe-rich fluids may proceed via an Ostwald step sequence	Sequence of precipitation: magnetite-cronstedtite-berthierine-chlorite	Cronstedtite Berthierine	-	The secondary minerals evolution is different to that predicted by the fixed surface area model
Marty et al. (2010)	Fe-MX80 bentonite	100	100	Non-constant (decreases from 5 to 0.2 µm/yr)	Porosity update Clay reactions are considered	Magnetite	Fe-chlorite Fe-saponite	15 cm	Porosity clogging after 100.000 years
Lu et al. (2011)	Fe-FEBEX bentonite	25	300	Constant (0.1 µm/yr) and non-constant (max. of 0.7 µm/yr)	1D model (Test case D0) Porosity update Clay reactions are considered Use of cation exchange and surface complexation Kinetically-controlled canister corrosion and magnetite precipitation	Magnetite		-	Accounting for kinetically-controlled canister corrosion leads to a significant reduction in the corrosion rate The concentration of dissolved Fe computed with kinetic magnetite precipitation is smaller than that obtained at equilibrium

Reference	Type of interface	T (°C)	Simulation time (years)	Corrosion rate	Assumptions	Main corrosion product	Main secondary minerals	Maximal perturbation extent	Relevant results
Ngo e al. (2014)	Fe-MX80 bentonite	100	10	Non-constant (decreases from 5 to 0.2 µm/yr)	Similar to Marty et al. (2010) Porosity update Clay reactions are considered With and without accounting for the influence of the reactive surface areas of the primary minerals	Magnetite	Greenalite Fe-saponite Fe-chlorite Berthierine	10 cm	The large surface area of the primary clay minerals provides a significant decrease in porosity in the zone in contact with the steel overpack, which in turn limited the diffusion of the aqueous corrosion products toward the bentonite barrier. This induced an important porosity reduction and intense mineralogical transformation in the bentonite zone close to the bentonite/steel overpack interface.
Wilson et al. (2015)	Fe-bentonite	70	100	Constant (1 µm/yr) and non-constant (diffusion limited)	Model 1: fixed steel corrosion rate Model 2: diffusion-limited corrosion rate Model 3: corrosion cell approach	M1 and M2: - M3: Magnetite Siderite	M1: Berthierine Fe-saponite Greenalite M2 and M3: Berthierine	2 cm	The extent and nature of the alteration predicted by the models is sensitive to model conceptualisation
Samper et al. (2016)	Fe-FEBEX bentonite	Non-isothermal	1.000.000	Constant (2 µm/yr) and non-constant corrosion rate (T and chemical conditions dependence)	1D model Use of cation exchange and 3 types of sorption sites in the bentonite Kinetically-controlled canister corrosion and magnetite precipitation Smectite dissolution is considered	Magnetite	Analcime Cronstedtite	7 cm	Magnetite precipitation reduces significantly the porosity of the bentonite near the canister (7 cm thickness of the zone of reduced porosity at 1 Ma) The thickness ranges from less than 5 cm for a corrosion rate of 5 µm/yr to nearly 12 cm for a rate of 0.5 mm/year. The thickness increases significantly when the corrosion rate dependence on the chemical conditions is considered and decreases 3 cm when smectite dissolution and analcime precipitation are taken into account
Mon et al. (2017)	Fe-Febex bentonite	Non-isothermal	1.000.000	Constant corrosion rate (2 µm/yr)	1D model Use of cation exchange and 3 types of sorption sites in the bentonite. Smectite dissolution is considered	Magnetite	Gypsum Sepiolite	1 cm	Pore clogging at the canister-bentonite interface Narrow alteration zones Limited smectite dissolution after 1 Ma

## 5.4 Resume

The evolution of the DGR environment (thermal, hydraulic and/or chemical gradients - redox, pH and dissolved species - from the initial post-closure stage until the system reaches equilibrium) will impact on the chemical evolution of the steel/iron-bentonite interface. Laboratory and *in situ* experiments, as well as investigations on analogues, evidence that many of the processes and mechanisms occurring at the steel canister/bentonite interface are reproducible under similar conditions and are well understood under a broad range of temperature and physico-chemical conditions. Results show that corrosion rates and products are well established and can be predicted by reactive transport models if a number of variables such as humidity, pH, concentrations of dissolved salts, organic carbon and oxygen concentration are known in each stage of the repository. However, to do that is necessary to establish clearly the evolution of the system from the dry-out stage up to system get equilibrium conditions, which is a difficult issue since is highly dependent not only on *in situ* conditions at each stage, but also on variables still not well known, such as the role of gamma-radiation in the corrosion rate during first stages of the repository and also the role of microbes along the lifetime of the repository.

Experiments made on bulk solutions indicate that corrosion rate decreases with time due to the formation of a protective layer of magnetite (or siderite depending on the chemistry of the site). This protective layer forms at early stages and reaches a steady-state of the order of 0.1 to 1  $\mu\text{m}$  in few months. However, as a consequence of the temperature and hydration gradients geochemical conditions change over time and the related geochemical processes, such as dissolution of accessory minerals, formation of saline fronts and dilution and transport of potentially aggressive ions such as chloride and sulphate towards the steel-bentonite interface occur, and are crucial for the mechanism of corrosion. Laboratory experiments seem to demonstrate that formation of oxyhydroxides and anhydrous oxides will take place at the dry-out and early transient stages, when RH is low. Evidences on the occurrence of pitting corrosion during the post-closure stage can create uncertainty about the performance of the metallic containers. However, the characterization of the steel plates in contact with unsaturated compacted bentonite in experiments simulating the post-closure stage and *in situ* experiments (e.g. FEBEX) highlighted that most of the metallic surface kept its initial metallic luster. The lack of hydration and the high temperature at the interface will preserve the metal surface from corrosion and the thin layer of anhydrous oxides will have a protective role against further corrosion during saturated conditions. However, the timing of ingress of oxygen until complete reducing conditions are achieved has to be well defined.

The results of the laboratory and *in situ* experiments, as well as from archaeological or natural analogues highlight the ability of the clay to absorb or react with Fe(II) when anaerobic corrosion occurs. Swelling capacity of the smectite may decrease as a consequence of the formation of Fe-rich non-swelling clays (e.g., berthierine, crondstedtite and chlorite). Also, sorption sites on the clay can be filled by ferrous ions that can compete with radionuclides. To counteract that effect, high-surface-area of Fe(II)/Fe(III) corrosion products could provide adsorption sites for radionuclides. Those results are quite conservative at least when considering first stages of the repository, since they are obtained always within a range of temperature higher than expected when reducing conditions are achieved (quite below 100  $^{\circ}\text{C}$ ) and considering highly reactive iron powder and iron to clay or liquid to clay ratios much higher than expected. This is due to the difficulties in having Fe-clay reactivity at lower temperatures or material ratios. An upscaling exercise is necessary to extrapolate experimental results to long-term conditions expected in the repository to improve the conceptual model on the spatial and temporal evolution of the interface and transformations affecting the porous media and degrading materials, which is one of the main objectives of ACED. What is expected after ACED is “to integrate knowledge on the geochemical processes in and between the materials in a disposal cell for ILW and HLW waste in order to understand and assess the long-term evolution of such complex system”. One way to do that is advancing in the upscaling of processes and also trying to obtain more precise data on: diffusion of species (e.g., sulphates), Fe/clay interaction at nano/microscale (including aspects as clogging), deepening in aspects as  $\text{SiO}_2$  dissolution/precipitation and its role in clay transformation, analysis of changes in porosity, swelling and hydraulic properties of the clay.

The project does not include aspects as radiation and microbe involvement. However, it should be necessary to complete the database on corrosion and clay transformation considering that MIC and radiation can significantly enhance the corrosion process and accelerate the transformation process of clay.

## 5.5 References

- Allard, T., Calas, G., 2009. Radiation effects on clay mineral properties. *Applied Clay Science* 43, 143-149.
- Allard, T., Balan, E., Calas, G., Fourdrin, C., Morichon, E., Sorieul, S., 2012. Radiation-induced defects in clay minerals: A review. *Nuclear Instruments and Methods in Physics Research B* 277, 112-120.
- Azkárate, I., Insausti, M., Madina, V., 2004. Estudio de los productos de CORROSIÓN de la cápsula y su interacción con la barrera arcillosa de BENTonita CORROBEN. ENRESA, Madrid, Spain.
- Bagnoud, A., Chourey, K., Hettich, R.L., de Bruijn, I., Andersson, A.F., Leupin, O.X., Schwyn, B., Bernier-Latmani, R., 2016. Reconstructing a hydrogen-driven microbial metabolic network in Opalinus Clay rock. *Nature Communications* 7, 12770.
- Bailey, S.W., 1988. Odinite, a new dioctahedral-trioctahedral Fe<sup>3+</sup>-rich 1:1 clay mineral. *Clay Minerals* 23, 237-247.
- Balmer, S., Kaufhold, S., Dohrmann, R., 2017. Cement-bentonite-iron interactions on small scale tests for testing performance of bentonites as a barrier in high-level radioactive waste repository concepts. *Applied Clay Science* 135, 427-436.
- Bataillon, C., Bouchon, F., Chainais-Hillairet, C., Desgranges, C., Hoarau, E., Martin, F., Tupin, M., Talandier, J., 2010. Corrosion modelling of iron based alloy in nuclear waste repository. *Electrochimica Acta* 55, 4451-4467.
- Bataillon, C., Bouchon, F., Chainais-Hillairet, C., Fuhrmann, J., Hoarau, E., Touzani, R., 2012. Numerical methods for the simulation of a corrosion model with moving oxide layer. *Journal of Computational Physics* 231, 6213-6231.
- Beaufort, D., Baronnet, A., Lanson, B., Meunier, A., 1997. Corrensite: a single phase or a interstratified phyllosilicate in the saponite-to-chlorite conversion series? A case study of Sancerre-Couy deep drill hole (France). *American Mineralogist* 82, 109-124.
- Beech, I.B., Sunner, I.A., 2007. Sulphate-reducing bacteria and their role in corrosion of ferrous materials. In: Barton, L.L., Hamilton, W.A. (eds.) *Sulphate-reducing bacteria: environmental and engineered systems*. Cambridge University Press, 459-482.
- Bellot-Gurlet, L., Neff, D., Réguer, S., Monnier, J., Saheb, M., Dillmann, P., 2009. Raman studies of corrosion layers formed on archaeological irons in various media. *Journal of Nano Research* 8, 147-156.
- Ben Lagha, S., Crusset, D., Mabilie, I., Tran, M., Bernard, M.C., Sutter, E., 2007. Corrosion of iron: A study for radioactive waste canisters. *Journal of Nuclear Materials* 362, 485-492.
- Bengtsson, A., Pedersen, K., 2017. Microbial sulphide-producing activity in water saturated Wyoming MX-80, Asha and Calcigel bentonites at wet densities from 1500 to 2000 kg m<sup>-3</sup>. *Applied Clay Science* 137, 203-212.
- Bildstein, O., Trotignon, L., Perronet, M., Jullien, M., 2006. Modelling iron-clay interactions in deep geological disposal conditions. *Physics and Chemistry of the Earth* 31, 618-625.
- Bildstein, O., Lartigue, J., Pointeau, I., Cochevin, B., Munier, I., Michau, N., 2012. Chemical evolution in the near field of HLW cells: interactions between glass, steel and clay-stone in deep geological conditions. 5<sup>th</sup> ANDRA International Meeting, 22–25 Oct 2012, Montpellier, France.

- Bildstein, O., Claret, F. 2015. Stability of clay barriers under chemical perturbations. In: Tournassat, C., Steefel, C.I., Bourg, I.C., Bergaya, F. (eds.) *Natural and Engineered Clay Barriers, Developments in Clay Science* 6, 155-188.
- Bildstein, O., Lartigue, J.-E., Schlegel, M.L., Bataillon, C., Cochapin, B., Munier, I., Michau N., 2016. Gaining insight into corrosion processes from numerical simulations of an integrated iron-claystone experiment. *Geological Society of London Special Publication* 443, 253-267.
- Bildstein, O., Claret, F., Frugier, P., 2019. RTM for waste repositories. *Reviews in Mineralogy and Geochemistry* 85: 419-457.
- Blackwood, D.J., Gould, L.J., Naish, C.C., Porter, F.M., Rance, A.P., Sharland, S.M., Smart, N.R., Thomas, M.I., Yates, T., 2002. The localised corrosion of carbon steel and stainless steel in simulated repository environments. Report AEAT/ERRA-0318, AEA Technology, Harwell, United Kingdom.
- Bourdelle, F., Truche, L., Pignatelli, I., Mosser-Ruck, R., Lorgeoux, C., Roszypal, C., Michau, N., 2014. Iron–clay interactions under hydrothermal conditions: Impact of specific surface area of metallic iron on reaction pathway. *Chemical Geology* 381, 194-205.
- Bourdelle, F., Mosser-Ruck, R., Truche, L., Lorgeoux, C., Pignatelli, I., Michau, N., 2017. A new view on iron-claystone interactions under hydrothermal conditions (90 °C) by monitoring in situ pH evolution and H<sub>2</sub> generation. *Chemical Geology* 466, 600-607.
- Bradbury, M.H., Berner, U., Curti, E., Hummel, W., Kosakowski, G., Thoenen, T., 2014. The long term geochemical evolution of the nearfield of the HLW repository. Nagra Technical Report NTB 12-01, Nagra, Wettingen, Switzerland.
- Buatier, M.D., Ouyang, K., Sánchez, J.P., 1993. Iron in hydrothermal clays from the Galapagos spreading centre mounds: Consequences for the clay transition mechanism. *Clay Minerals* 28, 641-655.
- Carlson, L., Karnland, O., Oversby, V.M., Rance, A., Smart, N., Snellman, M., Vähänen, M., Werme, L.O., 2007. Experimental studies of the interactions between anaerobically corroding iron and bentonite. *Physics and Chemistry of the Earth* 32, 334-345.
- Carlson, L., Karnland, O., Olsson, S., Rance, A., Smart, N., 2008. Experimental studies on the interactions between anaerobically corroding iron and bentonite. SKB Report R-08-28, SKB, Stockholm, Sweden.
- Chainais-Hillairet, C., Colin, P.-L., Lacroix-Violet, I., 2015. Convergence of a finite volume scheme for a corrosion model. *International Journal on Finite Volumes* 12, 1-27.
- Chainais-Hillairet, C., Gallouët, T.O., 2016. Study of a pseudo-stationary state for a corrosion model: existence and numerical approximation. *Nonlinear Analysis: Real World Applications* 31, 38-56.
- Charlet, L., Tournassat, C., 2005. Fe(II)-Na(I)-Ca(II) cation exchange on montmorillonite in chloride medium: evidence for preferential clay adsorption of chloride - metal ion pairs in seawater. *Aquatic Geochemistry* 11, 115-137.
- Charpentier, D., Devineau, K., Mosser-Ruck, R., Cathelineau, M., Villiéras, F., 2006. Bentonite–iron interactions under alkaline condition: an experimental approach. *Applied Clay Science* 32, 1-13.
- Christidis, G.E., Scott, P.W., 1997. The origin and control of colour of white bentonites from the Aegean islands of Milos and Kimolos, Greece. *Mineralium Deposita* 32, 271-279.
- Claret, F., Marty, N., Tournassat, C., 2018. Modeling the long-term stability of multibarrier systems for nuclear waste disposal in geological clay formations. In: Xiao, Y., Whitaker, F., Xu, T., Steefel, C. (eds.) *Reactive transport modeling: Applications in subsurface energy and environmental problems*, Wiley, 395-436.
- Cole, I.S., Marney, D., 2012. The science of pipe corrosion: A review of the literature on the corrosion of ferrous metals in soils. *Corrosion Science* 56, 5-16.

Cornelis, B., Van Iseghem, P., 1993. In situ tests on waste package materials in clay concept and performance. Testing of Radioactive Waste Forms and Engineered Barriers. Conference European Commission, Corsendonk, Belgium.

Cornell, R.M., Schwertmann, U., 1996. The Iron Oxides. VCH, New York.

Crossland, I., 2005. Long term corrosion of iron and copper. ICEM'05: 10th International Conference on Environmental Remediation and Radioactive Waste Management, September 4-8, 2005, Glasgow, United Kingdom.

Crusset, D., Deydier, V., Necib, S., Gras, J.M., Combrade, P., Féron, D., Burger, E., 2017. Corrosion of carbon steel components in the French high-level waste programme: evolution of disposal concept and selection of materials. Corrosion Engineering, Science and Technology 52, 17-24.

Cuevas, J., Villar, M.V., Martín, P.L., Cobeña, J., Leguey, S., 2002. Thermo-hydraulic gradients on bentonite: Distribution of soluble salts, microstructure and modification of the hydraulic and mechanical behavior. Applied Clay Science 22, 25-38.

Cuevas, J., Ruíz, A.I., Fernández, R., Torres, E., Escribano, A., Regadío, M., Turrero, M.J., 2016. Lime mortar-compacted bentonite-magnetite interfaces: An experimental study focused on the understanding of the EBS long-term performance for high-level nuclear waste isolation DGR concept. Applied Clay Science 124-125, 79-93.

Daub, K., Zhang, X., Noël, J.J., Wren, J.C., 2010. Effects of gamma-radiation versus H<sub>2</sub>O<sub>2</sub> on carbon steel corrosion. Electrochimica Acta 55, 2767-2776.

Daub, K., Zhang, X., Noël, J.J., Wren, J.C., 2011. Gamma-radiation-induced corrosion of carbon steel in neutral and mildly basic water at 150°C. Corrosion Science 53, 11-16.

Dauzères, A., Maillet, A., Gaudin, A., El Albani, A., Vieillard, P., 2013. Ten years of Toarcian argillite – carbon steel in situ interaction. Procedia Earth and Planetary Science 7, 195-198.

Debruyne, W., Dresselaers, J., Vermeiren, P., Kelchtermans, J., Tas, H., 1990. Corrosion of container and infrastructure materials under clay repository conditions. SCK-CEN, Mol, Belgium.

Dillmann, P., Neff, D., Féron, D., 2014. Archaeological analogues and corrosion prediction: from past to future. A review. Corrosion Engineering, Science and Technology 49. 567-576.

Druyts, F., Kursten, B., Van Iseghem, P., 2001. Corrosion evaluation of metallic materials for long-lived HLW/Spent Fuel disposal containers. Final report to EDF for the period 1996-1998. SCK.CEN report R-3533, SCK CEN, Mol, Belgium.

Engel, K., Ford, S.E., Coyotzi, S., McKelvie, J., Diomidis, N., Slater, C., Neufeld, J.D., 2019. Stability of microbial community profiles associated with compacted bentonite from the Grimsel underground research Laboratory. American Society for Microbiology, mSphere 4, e00601-19.

Enning, D., Garrelfs J., 2014. Corrosion of iron by sulfate-reducing bacteria: New views of an old problem. Applied and Environmental Microbiology 80, 1226-1236.

Esnault, L., Jullien, M., Mustin, C., Bildstein, O., Libert, M., 2011. Metallic corrosion processes reactivation sustained by iron-reducing bacteria: Implication on long-term stability of protective layers. Physics and Chemistry of the Earth, Parts A/B/C 36, 1624-1629.

Fernandez, A.M., Kaufhold, S., Sanchez-Ledesma, D.M., Rey, J.J., Melon, A., Robredo, L.M., Fernandez, S., Labajo, M.A., Clavero, M.A., 2019. Evolution of the THC conditions in the FEBEX in situ test after 18 years of experiment: smectite crystallochemical modifications after interactions of the bentonite with a C-steel heater at 100 °C. Applied Geochemistry 98, 152-171.

Féron, D., Crusset, D., Gras, J.M., 2008. Corrosion issues in nuclear waste disposal. Journal of Nuclear Materials 379, 16-23.

- Fru, E.C., Athar, R., 2008. In situ bacterial colonization of compacted bentonite under deep geological high-level radioactive waste repository conditions. *Applied Microbiology and Biotechnology* 79, 499-510.
- Fuentes-Cantillana, J.L., García-Siñeriz, J.L., 1998. FEBEX full-scale engineered barriers experiment in crystalline host rock. Final design and installation of the "in situ" test at Grimsel. ENRESA Technical Report 12/98, ENRESA, Madrid, Spain.
- Fukushi, K., Sugiura, T., Morishita, T., Takahashi, Y., Hasebe, N., Ito, H., 2010. Iron-bentonite reactions in the Kawasaki bentonite deposit, Zao area, Japan. *Applied Geochemistry* 25, 1120-1132.
- García-Siñeriz, J.L., Abós, H., Martínez, V., De la Rosa, C., Mäder, U., Kober, F., 2016. FEBEX DP: Dismantling of heater 2 at the FEBEX "in situ" test. Description of operations. Nagra Report NAB 16-11, Nagra, Wettingen, Switzerland.
- Gaudin, A., Gaboreau, S., Tinseau, E., Bartier, D., Petit, S., Grauby, O., Foct, F., Beaufort, D., 2009. Mineralogical reactions in the Tournemire argillite after in-situ interaction with steels. *Applied Clay Science* 43, 196-207.
- Gaudin, A., Bartier, D., Truche, L., Tinseau, E., Foct, F., Dyja, V., Maillet, A., Beaufort D., 2013. First corrosion stages in Tournemire claystone/steel interaction: In situ experiment and modelling approach. *Applied Clay Science* 83–84, 457-468.
- Gdowski, G.E., Bullen, D.B., 1988. Survey of degradation modes of candidate materials for high-level radioactive waste disposal containers. Oxidation and corrosion. LLNL Report UCID-21362, Vol. 2., Lawrence Livermore National Laboratory, Livermore, CA, USA.
- Gdowski, G.E., Estill, J.C., 1996. The effect of water vapor on the steel at 65°C. *Materials Research Society Symposium Proceedings* 412, 533-535.
- Gdowski, G.E., 1998. Humid air corrosion of YMP waste package candidate material. LLNL Report UCRL-JC-130202, Lawrence Livermore National Laboratory, Livermore, CA, USA.
- Géhin, A., Grenèche, J.-M., Tournassat, C., Brendlé, J., Rancourt, D.G., Charlet, L., 2007. Reversible surface sorption induced electron transfer oxidation of Fe(II) at reactive sites on a synthetic clay mineral. *Geochimica Cosmochimica Acta* 71, 863-876.
- Guillaume, D., Neaman, A., Cathelineau, M., Mosser-Ruck, R., Peiffert, C., Abdelmoula, M., Dubessy, J., Villiéras, F., Baronnet, A., Michau, N., 2003. Experimental synthesis of chlorite from smectite at 300 °C in the presence of metallic Fe. *Clay Minerals* 38, 281-302.
- Guillaume, D., Neaman, A., Cathelineau, M., Mosser-Ruck, R., Peiffert, C., Abdelmoula, M., Dubessy, J., Villiéras, F., Michau, N., 2004. Experimental study of the transformation of smectite at 80 and 300 °C in the presence of Fe oxides. *Clay Minerals* 39, 17-34.
- Granizo, N., Missana, T., 2006. Mechanisms of cesium sorption onto magnetite. *Radiochimica Acta* 94, 671-677.
- Hadi, J., Wersin, P., Serneels, V., Grenèche, J.M., 2019. Eighteen years of steel–bentonite interaction in the FEBEX in situ test at the Grimsel Test Site in Switzerland. *Clays and Clay Minerals* 67, 111-131.
- Holmboe, M., Jonsson, M., Wold, S., 2012. Influence of  $\gamma$ -radiation on the reactivity of montmorillonite towards H<sub>2</sub>O<sub>2</sub>. *Radiation Physics and Chemistry* 81, 190-194.
- Hornibrook, E.R.C., Longstaffe, F.J., 1996. Berthierine from the lower Cretaceous Clearwater Formation, Alberta, Canada. *Clays and Clay Minerals* 44, 1-21.
- Huertas, F., Fariñas, P., Farias, J., García-Siñeriz, J.L., Villar, M.V., Fernández, A.M., Martín, P.L., Elorza, F.J., Gens, A., Sánchez, M., Lloret, A., Samper, J., Martínez, M.A., 2006. Full-scale Engineered Barriers Experiment. Updated Final Report 1994–2004. Enresa Technical Report 05/2006, Enresa, Spain.

Hunter, F.M.I., Bate, F., Heath, T.G., Hoch, A.R., 2007. Geochemical investigation of iron transport into bentonite as steel corrodes. SKB Technical Report TR-07-09, SKB, Stockholm, Sweden.

Inoue, A., Utada, M., 1991. Smectite-to-chlorite transformation in thermally metamorphosed volcanoclastic rocks in the Kamikita area, northern Honshu, Japan. *American Mineralogist* 76, 628-640.

Ishidera, T., Ueno, K., Kurosawa, S., Suyama, T., 2008. Investigation of montmorillonite alteration and form of iron corrosion products in compacted bentonite in contact with carbon steel for ten years. *Physics and Chemistry of the Earth, Parts A/B/C* 33, 269-275.

Ismail, M., Noor, N.M., Yahaya, N., Abdullah, A., Rasol, R., Rashid, A.S., 2014. The effect of pH and temperature on corrosion of steel subject to sulphate-reducing bacteria. *Journal of Environmental Science and Technology* 7, 209-217.

Jeannin, M., Calonnec, D., Sabot, R., Refait, Ph., 2010. Role of a clay sediment deposit on the corrosion of carbon steel in 0.5 mol/L NaCl solutions. *Corrosion Science* 52, 2026-2034.

Jodin-Caumon, M.C., Mosser-Ruck, R., Rousset, D., Randi, A., Cathelineau, M., Michau, N., 2010. Effect of a thermal gradient on iron-clay interactions. *Clays and Clay Minerals* 58, 667-681.

Jodin-Caumon, M.C., Mosser-Ruck, R., Randi, A., Pierron, O., Cathelineau, M., Michau, N., 2012. Mineralogical evolution of a claystone after reaction with iron under thermal gradient. *Clays and Clay Minerals* 60, 443-455.

Johnson, A.B., Francis, B., 1980. Durability of metals from archaeological objects, metal meteorites, and native metals. Report PNL-3198/UC-70, Pacific Northwest Laboratory, Richland, WA, USA.

Johnson, L.H., Niemeyer, M., Klubertanz, G., Siegel, P., Gribi, P., 2002. Calculations of the temperature evolution of a repository for spent fuel, vitrified high-level waste and intermediate-level waste in Opalinus Clay, Nagra Technical Report NTB 01-04, Nagra, Wettingen, Switzerland.

Johnson, L., King, F. 2008. The effect of the evolution of environmental conditions on the corrosion evolutionary path in a repository for spent fuel and high-level waste in Opalinus Clay. *Journal of Nuclear Materials* 379, 9-15.

Jonsson, M., 2012. Radiation effects on materials used in geological repositories for spent nuclear fuel. *ISRN Materials Science* 2012, 639520.

Joseph, J.M., Choi, B.S., Yakabuskie, P., Wren, J.C., 2008. A combined experimental and model analysis on the effect of pH and O<sub>2</sub>(aq) on gamma-radiolytically produced H<sub>2</sub> and H<sub>2</sub>O. *Radiation Physics and Chemistry* 77, 1009-1020.

Kamei, G., Oda, C., Mitsui, S., Shibata, M., Shinozaki, T., 1999. Fe(II)–Na ion exchange at interlayers of smectite: adsorption–desorption experiments and a natural analogue. *Engineering Geology* 54, 15-20.

Kaufhold, S., Dohrmann, R., Götze, N., Svensson, D., 2017. Characterization of the second parcel of the alternative buffer material (ABM) experiment. I. Mineralogical reactions. *Clays and Clay Minerals*, 65, 27-41.

Kaufhold, S., Dohrmann, R., Ufer, K., Kober, F., 2019. Interactions of bentonite with metal and concrete from the FEBEX experiment: mineralogical and geochemical investigations of selected sampling sites. *Clay Minerals* 53, 745-763.

King, F., Stroes-Gascoyne, S., 1995. Microbially influenced corrosion of nuclear fuel waste disposal containers. *Proceedings International Conference on Microbially Influenced Corrosion*, Miami, FL, USA, 35/1-35/14.

King, F., 2008. Corrosion of carbon steel under anaerobic conditions in a repository for SF and HLW in Opalinus Clay. Nagra Technical Report NTB 08-12, Nagra, Wettingen, Switzerland.

King, F., 2009. Microbiologically influenced corrosion of nuclear waste containers. *Corrosion* 65, 233-251.

King, F., 2014. Durability of high level waste and spent fuel disposal containers – an overview of the combined effect of chemical and mechanical degradation mechanisms. Quintessa Report QRS-1589A-R1\_AppB2, Quintessa, Henley-on-Thames, United Kingdom.

Kuang, F., Wang, J., Yan, L., Zhang, D., 2007. Effects of sulfate-reducing bacteria on the corrosion behavior of carbon steel. *Electrochimica Acta* 52, 6084-6088.

Kucera, V., Mattson, E., 1987. Atmospheric corrosion. In: Mansfeld, F. (ed.) *Corrosion mechanisms*, Marcel Dekker, 211-284.

Kumpulainen, S., Kiviranta, L., Carlsson, T., Muurinen, A., Svensson, D., Sasamoto, H., Yui, M., Wersin, P., 2010. Long-term alteration of bentonite in the presence of metallic iron. SKB Report R-10-52, SKB, Stockholm, Sweden (also published as POSIVA report WR2010-71).

Kursten, B., Cornelis, B., Labat, S., Van Iseghem, P., 1997. Completion of the corrosion programme in Boom Clay - in situ experiments. SCK-CEN, Mol, Belgium.

Kursten, B., Van Iseghem, P., 1999. In situ corrosion studies on candidate container materials for the underground disposal of high-level nuclear radioactive waste in Boom Clay. EUROCORR'98, San Antonio, Texas, USA.

Kursten, B., Smailos, E., Azkarate, I., Werme, L., Smart, N.R., Santarini G., 2004a. COBECOMA, State-of-the-art document on the COrrOsion BEhaviour of COntainer MAterials. European Commission, Contract N° FIKW-CT-20014-20138 Final Report.

Kursten, B., Smailos, E., Azkarate, I., Werme, L., Smart, N.R., Marx, G., Cuñado, M.A., Santarini, G., 2004b. Corrosion evaluation of metallic materials for long-lived HLW/Spent Fuel disposal containers: Review of 15-20 years of research. Euradwaste04, 6<sup>th</sup> EC Conference on the Management and Disposal of Radioactive Waste, 29 March – 1 April 2004, Luxembourg.

Lainé, M., Balan, E., Allard, T., Paineau, E., Jeunesse, P., Mostafavi, M., Robert, J.L., Le Caër, S., 2017. Reaction mechanisms in swelling clays under ionizing radiation: influence of the water amount and of the nature of the clay mineral. *RSC Advances* 7, 526-534.

Landolt, D., Davenport, A., Payer, J., Shoesmith, D., 2009. A review of materials and corrosion issues regarding canisters for disposal of spent fuel and high-level waste in Opalinus Clay. Nagra Technical Report NTB 09-02, Nagra, Wettingen, Switzerland.

Lanson, B., Lantenois, S., van Aken, P.P., Bauer, A., Plançon, A., 2012. Experimental investigation of smectite interaction with metal iron at 80 °C: structural characterization of newly formed Fe-rich phyllosilicates. *American Mineralogist* 97, 864-871.

Lantenois, S., Lanson, B., Muller, F., Bauer, A., Jullien, M., Plançon, A., 2005. Experimental study of smectite interaction with metal Fe at low temperature: 1. Smectite destabilization. *Clays and Clay Minerals* 53, 597-612.

Lee, S., Staehle, R.W., 1997. Adsorption of water on copper, nickel and iron. *Corrosion* 53, 33-42.

Le Pape, P., Rivard, C., Pelletier, M., Bihannic, I., Gley, R., Mathieu, S., Salsi, L., Migot, S., Barres, O., Villiéras, F., Michau, N., 2015. Action of a clay suspension on an Fe(0) surface under anoxic conditions: Characterization of neoformed minerals at the Fe(0)/solution and Fe(0)/atmosphere interfaces. *Applied Geochemistry* 61, 62-71.

Leon, Y., Saheb, M., Drouet, E., Neff, D., Foy, E., Leroy, E., Dynes, J.J., Dillmann, P., 2014. Interfacial layer on archaeological mild steel corroded in carbonated anoxic environments studied with coupled micro and nano probes. *Corrosion Science* 88, 23-35.

Leupin, O., Johnson, L.H., 2013. Buffer requirements for a SF/HLW repository in Opalinus Clay. Nagra Report NAB 13-46, Nagra, Wettingen, Switzerland.

Leupin, O.X., Bernier-Latmani, R., Bagnoud, A., Moors, H., Leys, N., Wouters, K., Stroes-Gascoyne, S., 2017. Fifteen years of microbiological investigation in Opalinus Clay at the Mont Terri rock laboratory (Switzerland). *Swiss Journal of Geosciences* 110, 343-354.

Li, X., Yang, T., Mbadanga, S.M., Liu, J.F., Yang, S.Z., Gu, J.D., Mu, B.Z., 2017. Responses of microbial community composition to temperature gradient and carbon steel corrosion in production water of petroleum reservoirs. *Frontiers in Microbiology* 8, 2379.

Lichtner, P.C., Carey, J.W., 2006. Incorporating solid solutions in reactive transport equations using a kinetic discrete-composition approach. *Geochimica Cosmochimica Acta* 70, 1356-1378.

Liu, C., Wang, J., Zhang, Z., Han, E.H., 2017. Studies on corrosion behaviour of low carbon steel canister with and without  $\gamma$ -irradiation in China's HLW disposal repository. *Corrosion Engineering, Science and Technology* 52, 136-140.

López Munguira, A., Nieto, F., 2000. Transmission electron microscopy study of very low-grade metamorphic rocks in Cambrian sandstones and shales. *Clays and Clay Minerals* 48, 213-223.

Lousada, C.M., Johansson, A.J., Brinck, T., Jonsson, M., 2012. Mechanism of H<sub>2</sub>O<sub>2</sub> decomposition on transition metal oxide surfaces. *The Journal of Physical Chemistry C* 116, 9533-9543.

Lu, C., Samper, J., Fritz, B., Clement, A., Montenegro, L., 2011. Interactions of corrosion products and bentonite: An extended multicomponent reactive transport model. *Physics and Chemistry of the Earth* 36, 1661-1668.

Madina, V., 2016. Corrosion Study of FEBEX-DP components. Nagra Technical Report NTB 16-54, Nagra, Wettingen, Switzerland.

Madina, V., Azkárate, I., 2004. FEBEX project post-mortem analysis: Corrosion study. ENRESA Technical Report 08/2004, ENRESA, Madrid, Spain.

Madsen, F.T., 1998. Clay mineralogical investigations related to nuclear waste disposal. *Clay Minerals* 33, 102-109.

Majzlan, J., Grevel, K.-D., Navrotsky, A., 2003. Thermodynamics of Fe oxides: Part II. Enthalpies of formation and relative stability of goethite ( $\alpha$ -FeOOH), lepidocrocite ( $\gamma$ -FeOOH) and maghemite ( $\gamma$ -Fe<sub>2</sub>O<sub>3</sub>). *American Mineralogist* 88, 855-859.

Marcos, N., 2003. Bentonite-iron interactions in natural occurrences and in laboratory - the effects of the interactions on the properties of bentonite: a literature survey. Posiva Working Report WR2003-55, Posiva Oy, Oikiluoto, Finland.

Marsh, G.P., Harker, A.H., Taylor, K.J., 1989. Corrosion of carbon steel nuclear waste containers in marine sediment. *Corrosion* 45, 579-589.

Marsh, G.P., Taylor, K.J., Sharland, S.M., Tasker, P.W., 1987. An approach for evaluation the general and localised corrosion of carbon-steel containers for nuclear waste disposal. *Materials Research Society Symposium Proceedings* 84, 227.

Martin, F.A., Bataillon, C., Schlegel, M.L., 2008. Corrosion of iron and low alloyed steel within a water saturated brick of clay under anaerobic deep geological disposal conditions: An integrated experiment. *Journal of Nuclear Materials* 379, 80-90.

Marty, N.C.M, Fritz, B., Clément, A., Michau, N., 2010. Modelling the long term alteration of the engineered bentonite barrier in an underground radioactive waste repository. *Applied Clay Science* 47, 82-90.

Masurat, P., Eriksson, S., Pedersen, K. 2010. Evidence of indigenous sulphate-reducing bacteria in commercial Wyoming bentonite MX-80. *Applied Clay Science* 47, 51-57.

Mata, M.P., Casas, A.M., Canals, A., Gil, A., Pocovi, A., 2002. Thermal history during Mesozoic extension and Tertiary uplift in the Cameros Basin, northern Spain. *Basin Research* 13, 91-111.

Matschiavelli, N., Kluge, S., Podlech, C., Standhaft, D., Grathoff, G., Ikeda-Ohno, A., Warr, L.N., Chukharkina, A., Arnold, T., Cherkouk, A., 2019. The year-long development of microorganisms in uncompacted Bavarian bentonite slurries at 30 and 60 °C. *Environmental Science and Technology* 53, 10514-10524.

Matthiesen, H., Hilbert, L.R., Gregory, D.J., 2003. Siderite as a corrosion product on archaeological iron from a waterlogged environment. *Studies in Conservation* 48, 183-194.

Michelin, A., Drouet, E., Foy, E., Dynes, J.J., Neff, D., Dillmann, P., 2013. Investigation at the nanometre scale on the corrosion mechanisms of archaeological ferrous artefacts by STXM. *Journal of Analytical Atomic Spectrometry* 28, 59-66.

Milodowski, A.E., Cave, M.R., Kemp, S.J., Taylor, H., Green, K., Williams, C.L., Shaw, R.A., Gowing, C.J.B., Eatherington, N.D., 2009. Mineralogical investigations of the interaction between iron corrosion products and bentonite from the NF-PRO experiments. SKB Technical Report TR-09-03, SKB, Stockholm, Sweden.

Mon, A., Samper, J., Montenegro, L., Naves, A., Fernández, J., 2017. Reactive transport model of compacted bentonite, concrete and corrosion products in a HLW repository in clay. *Journal of Contaminant Hydrology* 197, 1-16.

Montes, G.H., Fritz, B., Clement, J.A., Michau, N., 2005a. Modeling of transport and reaction in an engineered barrier for radioactive waste confinement. *Applied Clay Science* 29, 155-171.

Montes, G.H., Marty, N., Fritz, B., Clement, A., Michau, N., 2005b. Modelling of long-term diffusion-reaction in a bentonite barrier for radioactive waste confinement. *Applied Clay Science* 30, 181-198.

Mosser-Ruck, R., Cathelineau, M., Guillaume, D., Charpentier, D., Rousset, D., Barres, O., Michau, N., 2010. Effects of temperature, pH, and iron/clay and liquid/clay ratios on experimental conversion of dioctahedral smectite to berthierine, chlorite, vermiculite, or saponite. *Clays and Clay Minerals* 58, 280-291.

Mosser-Ruck, R., Pignatelli, I., Bourdelle, F., Abdelmoula, M., Barres, O., Guillaume, D., Charpentier, D., Rousset, D., Cathelineau, M., Michau, N., 2016. Contribution of long-term hydrothermal experiments for understanding the smectite-to-chlorite conversion in geological environments. *Contributions to Mineralogy and Petrology* 171, 97.

Necib, S., Linard, Y., Crusset, D., Michau, N., Daumas, S., Burger, E., Romaine, A., Schlegel, M.L., 2016. Corrosion at the carbon steel–clay borehole water and gas interfaces at 85 °C under anoxic and transient acidic conditions. *Corrosion Science* 111, 242-258.

Necib, S., Linard, Y., Crusset, D., Schlegel, M., Daumas, S., Michau, N., 2017a. Corrosion processes of C-steel in long-term repository conditions. *Corrosion Engineering, Science and Technology* 52, 127-130.

Necib, S., Diomidis, N., Keech, P., Nakayama, M., 2017b. Corrosion of carbon steel in clay environments relevant to radioactive waste geological disposals, Mont Terri rock laboratory (Switzerland). *Swiss Journal of Geosciences* 110, 329-342.

Necib, S., Schlegel, M.L., Bataillon, C., Daumas, S., Diomidis, N., Keech, P., Crusset, D., 2019. Long-term corrosion behaviour of carbon steel and stainless steel in Opalinus clay: influence of stepwise temperature increase. *Corrosion Engineering, Science and Technology* 54, 516-528.

Neff, D., Reguer, S., Bellot-Gurlet, L., Dillmann, Ph., Bertholon, R., 2004. Structural characterisation of corrosion products on archaeological iron. An integrated analytical approach to establish corrosion forms. *Journal of Raman Spectroscopy* 35, 739-745.

Neff, D., Dillmann, P., Descostes, M., Beranger, G., 2006. Corrosion of iron archaeological artefacts in soil: Estimation of the average corrosion rates involving analytical techniques and thermodynamic calculations. *Corrosion Science* 48, 2947-2970.

Neff, D., Saheb, M., Perrin, S., Descostes, M., L'Hostis, V., Crusset, D., Millard, A., Dillmann, Ph., 2010. A review of the archaeological analogue approaches to predict the long-term corrosion behaviour of carbon steel overpack and reinforced concrete structures in the French disposal systems. *Journal of Nuclear Materials* 402, 196-205.

Ngo, V.V., Delalande, M., Clément, A., Michau, N., Fritz, B., 2014. Coupled transport reaction modelling of the long-term interaction between iron, bentonite and Callovo-Oxfordian claystone in radioactive waste confinement systems. *Applied Clay Science* 101, 430-443.

Ngo, V.V., Clément, A., Michau, N., Fritz, B., 2015. Kinetic modeling of interactions between iron, clay and water: Comparison with data from batch experiments. *Applied Geochemistry* 53, 13-26.

Orazem, M.E. (ed.), 2014. *Underground pipeline corrosion. Detection, analysis and prevention.* Woodhead Publishing Series in Metals and Surface Engineering 63, Elsevier.

Osacký, M., Šucha, V., Czímerova, A., Madejová, J., 2010. Reaction of smectites with iron in a nitrogen atmosphere at 75 °C. *Applied Clay Science* 50, 237-244.

Osacký, M., Šucha, V., Czímerova, A., Madejová, J., 2013. Reaction of smectites with iron in aerobic conditions at 75 °C. *Applied Clay Science* 72, 26-36.

Padovani, C., King, F., Lilja, C., Féron, D., Necib, S., Crusset, D., Deydier, V., Diomidis, N., Gaggiano, R., Ahn, T., Keech, P.G., Macdonald, D.D., Asano, H., Smart, N., Hall, D.S., Hänninen, H., Engelberg, D., Noël, J.J., Shoesmith, D.W., 2017. The corrosion behaviour of candidate container materials for the disposal of high-level waste and spent fuel – a summary of the state of the art and opportunities for synergies in future R&D. *Corrosion Engineering, Science and Technology*, 52, 227-231.

Pedersen, K., 2017. Bacterial activity in compacted bentonites. Deliverable 2.4 MIND Project. 27 pp.

Pelayo, M., García-Romero, E., Labajo, M.A., Pérez del Villar, L. 2011. Occurrence of Fe–Mg-rich smectites and corrensite in the Morrón de Mateo bentonite deposit (Cabo de Gata region, Spain): A natural analogue of the bentonite barrier in a radwaste repository. *Applied Geochemistry* 26, 1153-1168.

Peña, J., Torres, E., Turrero, M.J., Escribano, A., Martín, P.L., 2008. Kinetic modelling of the attenuation of carbon steel canister corrosion due to diffusive transport through corrosion product layers. *Corrosion Science* 50, 2197-2204.

Pérez del Villar, L., Delgado, A., Reyes, E., Pelayo, M., Fernández-Soler, J.M., Cózar, J.S., Tsige, M., Raya, J., 2003. Thermochemically-induced transformations in Al-smectites from Morrón de Mateo: an analogue process of the clayey-barrier behaviour (Cabo de Gata, Almería). BARRA II Project Thermal Effect. CIEMAT interim report CIEMAT/DIAE/54450/3/03, CIEMAT, Madrid, Spain.

Pérez del Villar, L., Delgado, A., Reyes, E., Pelayo, M., Fernández-Soler, J.M., Cózar, J.S., Tsige, M., Quejido, A.J., 2005. Thermochemically induced transformations in Al-smectites: a Spanish natural analogue of the bentonite barrier behaviour in a radwaste disposal. *Applied Geochemistry* 20, 2252-2282.

Perronet, M., Villières, F., Jullien, M., Razafitianamaharavo, A., Raynal, J., Bonnin, D., 2007. Towards a link between the energetic heterogeneities of the edge faces of smectites and their stability in the context of metallic corrosion. *Geochimica Cosmochimica Acta* 71, 1463-1479.

Perronet, M., Jullien, M., Villières, F., Rayna, J., Bonnin, D., Bruno, G., 2008. Evidence of a critical content in Fe(0) on FoCa7 bentonite reactivity at 80 °C. *Applied Clay Science* 38, 187-202.

Pignatelli, I., Bourdelle, F., Bartier, D., Mosser-Ruck, R., Truche, L., Mugnaioli, E., Michau, N., 2014. Iron–clay interactions: Detailed study of the mineralogical transformation of claystone with emphasis on

the formation of iron-rich T–O phyllosilicates in a step-by-step cooling experiment from 90 °C to 40 °C. *Chemical Geology* 387, 1-11.

Qin, Z., Demko, B., Noël, J., Shoesmith, D., King, F., Worthingham, R., Keith, K., 2004. Localized dissolution of millscale-covered pipeline steel surfaces. *Corrosion* 60, 906-914.

Rajala, P., Carpén, L., Vepsäläinen, M., Raulio, M., Sohlberg, E., Bomberg, M., 2015. Microbially induced corrosion of carbon steel in deep groundwater environment. *Frontiers in Microbiology* 6, 647.

Rangel, C.M., Fonseca, I.T., Leitão, R.A., 1986. Some aspects of the electrochemical behaviour of mild steel in carbonate/bicarbonate solutions. *Electrochimica Acta* 31, 1659-1662.

Rivard, C., Pelletier, M., Michau, N., Razafitianamaharavo, A., Abdelmoula, M., Ghanbaja, J., Villiéras, F., 2015. Reactivity of Callovo-Oxfordian Claystone and its clay fraction with metallic iron: role of non-clay minerals in the interaction mechanism. *Clays and Clay Minerals* 63, 290-310.

Saheb, M., Neff, D., Dillmann, Ph., Matthiesen, H., Foy, E., 2008. Long-term corrosion behaviour of low-carbon steel in anoxic environment: Characterisation of archaeological artefacts. *Journal of Nuclear Materials* 379, 118-123.

Saheb, M., Neff, D., Dillmann, P., Descostes, M., Matthiesen, H., 2013. Long-term anoxic corrosion of iron. In: Dillmann, P., Watkinson, D., Angelini, E., Adriaens, A. (eds.) *Corrosion and conservation of cultural heritage metallic artefacts*, Woodhead Publishing, 260-284.

Samper, J., Lu, C., Montenegro, L., 2008. Coupled hydrogeochemical calculations of the interactions of corrosion products and bentonite. *Physics and Chemistry of the Earth* 33, 306-316.

Samper, J., Naves, A., Montenegro, L., Mon., A., 2016. Reactive transport modelling of the long-term interactions of corrosion products and compacted bentonite in a HLW repository in granite: Uncertainties and relevance for performance assessment. *Applied Geochemistry* 67, 42-51.

Savage, D., Watson, C., Benbow, S., Wilson, J., 2010. Modelling iron-bentonite interactions. *Applied Clay Science* 47, 91-98.

Savage, D., 2012. Prospects for coupled modelling. Report STUK-TR 13, STUK, Helsinki, Finland.

Schindelholz, E., Risteen, B.E., Kelly, R.G., 2014. Effect of relative humidity on corrosion of steel under sea salt aerosol proxies. I. NaCl. *Journal of the Electrochemical Society* 161, C450-C459

Schlegel, M.L., Bataillon, C., Benhamida, K., Blanc, C., Menut, D., Lacour, J.L., 2008. Metal corrosion and argillite transformation at the water-saturated, high-temperature iron–clay interface: A microscopic-scale study. *Applied Geochemistry* 23, 2619-2633.

Schlegel, M.L., Bataillon, C., Brucker, F., Blanc, C., Prêt, D., Foy, E., Chorro, M., 2014. Corrosion of metal iron in contact with anoxic clay at 90 °C: Characterization of the corrosion products after two years of interaction. *Applied Geochemistry* 51, 1-14.

Shoesmith, D.W., 2008. The role of dissolved hydrogen on the corrosion/dissolution of spent nuclear fuel. Technical Report NWMO TR-2008-19, NWMO, Toronto, Ontario, Canada.

Shoesmith, D.W., King, F., 1999. The effects of gamma radiation on the corrosion of candidate materials for the fabrication of nuclear waste packages. Report AECL-11999, AECL, Pinawa, Manitoba, Canada.

Smart, N.R., Blackwood, D.J., Werme, L., 2002. Anaerobic corrosion of carbon steel and cast iron in artificial groundwaters: Part 1—Electrochemical aspects. *Corrosion* 58, 547-559.

Smart, N.R., Rance, A.P., Werme, L.O., 2004. Anaerobic corrosion of steel in bentonite. *Materials Research Society Symposium Proceedings* 807, 441-449.

Smart, N.R., Adams, R., 2006. Natural analogues for expansion due to the anaerobic corrosion of ferrous materials. SKB Technical Report TR-06-44, SKB, Stockholm, Sweden.

Smart, N., Rance, A.P., Carlson, L., Werme, L.O., 2006. Further studies of the anaerobic corrosion of steel in bentonite. *Materials Research Society Symposium Proceedings* 932, 32.1.

Smart, N.R., Carlson, L., Heath, T.G., Hoch, A.R., Hunter, F.M., Karnland, O., Kemp, S.J., Milodowski, A.E., Pritchard, A.M., Rance, A.P., Reddy, B., Werme L.O., 2008. Interactions between iron corrosion products and bentonite. *NF-PRO Final Report. Serco/TAS/MCRL/19801/C001 Issue 2.*

Smart, N., Reddy, B., Rance, A.P., Nixon, D.J., Diomidis, N., 2017a. The anaerobic corrosion of carbon steel in saturated compacted bentonite in the Swiss repository concept. *Corrosion Engineering, Science and Technology* 52(S1), 113-126.

Smart, N., Reddy, B., Rance, A.P., Nixon, D.J., Fruttschi, M., Bernier-Latmani, R., Diomidis, N., 2017b. The anaerobic corrosion of carbon steel in compacted bentonite exposed to natural Opalinus Clay porewater containing native microbial populations. *Corrosion Engineering, Science and Technology* 52(S1), 101-112.

Schmidt, D., Livi, K.J.T., Frey, M., 1999. Reaction progress in chloritic mineral: An electron microbeam study of the Taveyanne greywacke, Switzerland. *Journal of Metamorphic Geology* 17, 229-241.

Song, Y., Jiang, G., Chen, Y., Zhao, P., Tian, Y., 2017. Effects of chloride ions on corrosion of ductile iron and carbon steel in soil environments. *Scientific Reports* 7, 6865.

Starosvetsky, D., Armon, R., Yahalom, J., Starosvetsky, J., 2001. Pitting corrosion of carbon steel caused by iron bacteria. *International Biodeterioration & Biodegradation* 47, 79-87.

Steeffel, C.I., Van Cappellen, P., 1990. A new kinetic approach to modeling water-rock interaction: the role of nucleation, precursors, and Ostwald ripening. *Geochimica Cosmochimica Acta* 54, 2657-2677.

Stone, W., Kroukamp, O., Moes, A., McKelvie, J., Korber, D.R., Wolfaardt, G.M., 2016. Measuring microbial metabolism in atypical environments: Bentonite in used nuclear fuel storage. *Journal of Microbiological Methods* 120, 79-90.

Stroes-Gascoyne, S., Hamon, C.J., Dixon, D.A., Kohle, C., Maak, P., 2007. The effects of dry density and porewater salinity on the physical and microbiological characteristics of highly compacted bentonite. *Materials Research Society Symposium Proceedings* 985, 0985-NN13-02.

Stroes-Gascoyne, S., Hamon, C.J., Maak, P., Russell, S., 2010. The effects of the physical properties of highly compacted smectitic clay (bentonite) on the culturability of indigenous microorganisms. *Applied Clay Science* 47, 155-162.

Svensson, P.D., Hansen, S., 2013. Redox chemistry in two iron-bentonite field experiments at Äspö hard rock laboratory, Sweden: an XRD and FE K-edge XANES study. *Clays and Clay Minerals* 61, 566-579.

Torres, E., Turrero, M.J., Peña, J., Martín, P.L., Escribano, A., Alonso, U., Villar, M.V., 2007. Interaction iron-compacted bentonite: corrosion products and changes in the properties of the bentonite. *Final Report NF-PRO\_Deliverable D2.3.2 of Component 2.*

Torres, E., Escribano, A., Baldonado, J.L., Turrero, M.J., Martín, P.L., Peña, J., Villar, M.V., 2009. Evolution of the geochemical conditions in the bentonite barrier and its influence on the corrosion of the carbon steel canister. *Materials Research Society Symposium Proceedings* 1124, 301-306.

Torres, E., 2011. Geochemical processes at the C-steel / bentonite interface in a deep geological repository: experimental approach and modeling. *Ph.D. thesis, Universidad Complutense de Madrid.*

Torres, E., Turrero, M.J., Escribano, A., Martín, P.L., 2014. Formation of iron oxide and oxyhydroxides under different environmental conditions. *Iron/bentonite interaction. PEBS Project, Deliverable D2.3-6-2.*

Usher, K.M., Kaksonen, A.H., Cole, I., Marney, D., 2014. Critical review: Microbially influenced corrosion of buried carbon steel pipes. *International Biodeterioration & Biodegradation* 93, 84-106.

- Venzlaff, H., Enning, D., Srinivasan, J., Mayrhofer, K.J.J., Hassel, A.W., Widdel, F., Stratmann, M. 2013. Accelerated cathodic reaction in microbial corrosion of iron due to direct electron uptake by sulfate-reducing bacteria. *Corrosion Science*, 66: 88-96.
- Wang, W.G., Robert, D.J., Zhou, A., Li, C.Q., 2017. Effect of corrosion influencing factors of cast iron pipes in clay soil. In: Zhang, H. (ed.) *Mechanics of structures and materials: Advancements and challenges*. Taylor & Francis, 357-362.
- Wersin, P., Johnson, L.H., Schwyn, B., Berner, U., Curti, E., 2003. Redox conditions in the near field of a repository for SF/HLW and ILW in Opalinus Clay. Nagra Technical Report NTB 02-13, Nagra, Wettingen, Switzerland.
- Wersin, P., Johnson, L.H., McKinley, I.G., 2007. Performance of the bentonite barrier beyond 100 °C: a critical review. *Physics and Chemistry of the Earth* 32, 780-788.
- Wersin, P., Birgersson, M., Olsson, S., Karnland, O., Snellman, M., 2008. Impact of corrosion-derived iron on the bentonite buffer within the KBS-3H disposal concept: The Olkiluoto site as case study. SKB Report R-08-34. SKB, Stockholm, Sweden.
- Wersin, P., Birgersson, M., 2014. Reactive transport modelling of iron-bentonite interaction within the KBS-3H disposal concept: the Olkiluoto site as a case study. *Geological Society of London, Special Publication* 400, 237-250.
- Wersin, P., Jenni, A., Mäder, U., 2015. Interaction of corroding iron with bentonite in the ABM1 experiment at ÄSPÖ, Sweden: A microscopic approach. *Clays and Clay Minerals* 63, 51-68.
- Wersin, P., Kober, F., 2017. FEBEX-DP: Metal corrosion and iron-bentonite interaction studies. Nagra Report NAB 16-16, Nagra, Wettingen, Switzerland.
- Wilson, J., Cressey, G., Cressey, B., Cuadros, J., Ragnarsdottir, K.V., Savage, D., Shibata, M., 2006a. The effect of iron on montmorillonite stability. (II) Experimental investigation. *Geochimica Cosmochimica Acta* 70, 323-336.
- Wilson, J., Savage, D., Cuadros, J., Shibata, M., Ragnarsdottir, K.V., 2006b. The effect of iron on montmorillonite stability. (I) Background and thermodynamic considerations. *Geochimica Cosmochimica Acta* 70, 306-322.
- Wilson, J., Benbow, S., Sasamoto, H., Savage, D., Watson, C., 2015. Thermodynamic and fully-coupled reactive transport models of a steel–bentonite interface. *Applied Geochemistry* 61, 10-28.
- Wilson, J.C., 2017. FEBEX-DP: Geochemical modelling of iron-bentonite interactions. Quintessa Report QRS-1713A-R3, Quintessa, Henley-on-Thames, United Kingdom.
- Yoshikawa, H., Gunji, E., Tokuda, M., 2008. Long term stability of iron for more than 1500 years indicated by archaeological samples from the Yamato 6th tumulus. *Journal of Nuclear Materials* 379, 112-117.
- Zhang, J., Wang, J., Wang, Y., 2005. Micro-droplets formation during the deliquescence of salt particles in atmosphere. *Corrosion* 61, 1167-1172.



## 6. Interface "steel/iron – cement/concrete"

Bruno Kursten, Eef Weetjens, Diederik Jaques (SCK CEN)

An interface between steel and cement-based materials is present in many disposal concepts for geological disposal of radioactive waste in Europe (Neeft et al., 2020). The interface between steel and cement-based materials may occur at different locations and with different functions/roles.

In some disposal systems, reinforced concrete is used with carbon steel, for example for the container of ILW waste packages. In this case, carbon steel / concrete interface is typically located at a few centimetres from the boundary of the concrete component.

In HLW disposal concepts, carbon steel is used as overpack of the vitrified waste package. In some countries, a cement-based buffer is placed around the overpack to ensure high pH conditions for a long period of time (e.g., supercontainer concept in Belgium and The Netherlands). Here, the concrete cover is typically several decimetres thick. Calculations in, e.g., the Belgian programme (supercontainer in clay host rock, see Neeft et al., 2020) indicated that it will take several ten thousands of years before the geochemical conditions of the cement-based material at the carbon steel / buffer interface will change due to contact with (mainly) the pore water chemistry of the host rock.

In ILW, waste packages may contain also stainless steel or waste canisters are made of stainless steel (e.g., CSD-C<sup>4</sup> canisters). The latter is often immobilized inside a concrete or steel container with a cement-based material such as mortar.

In this overview, we limit the scope to carbon steel / cement interfaces as these interfaces are more relevant for the long-term performance and safety of the disposal cells. There exists a significant amount of literature of processes at the steel-concrete interface under oxic conditions, which is relevant for many civil structures. However, most of the discussion is limited to anoxic conditions, as the oxic period, even if it lasts several hundreds of years, will most probably occur under conditions of a high pH (cement-based buffers) with low passive corrosion rates.

### 6.1 Processes at the interface

#### 6.1.1 Description

For this interface, mainly corrosion processes and coupled processes are relevant. In geological disposal conditions, the main corrosion process would be passive corrosion of steel/iron in anoxic, alkaline conditions. Depending on the steel type and the evolution of the environment under study, corrosion processes can be influenced by a number of factors (temperature, saturation and radiation gradients, presence of corrosion-aggressive species (Cl, sulphate, thiosulphate), and presence of microbes). Corrosion products may take a volume that is larger than the bare material, leading in turn to stress and (local) alteration of the pore structure at the interface.

In a deep geological repository in saturated conditions, oxygen is assumed to be depleted relatively quickly (see Figure 6-1), so that anoxic conditions will be established soon after repository backfilling and closure. Oxic conditions then mainly prevail during the operational phase and when the disposal cell is not completely saturated. However, many different processes in a ILW or HLW disposal compete for oxygen (corrosion, oxidation of minerals, microbial respiration). In addition, the steel interface is embedded in mortar or concrete materials (reinforced concrete in HLW and ILW disposal cells, overpack in HLW disposal cells, waste containers and waste in ILW disposal cells) which pose diffusion-limited oxygen availability at the interface and induce a protective layer at the steel-concrete interface. Several studies show that a passive layer and passive corrosion layers are reached relative fast for different environmental conditions (L'Hostis et al., 2001; Chomat et al., 2017).

---

<sup>4</sup> CSD-C: 'Conteneur Standard de Déchets Compactés', the standard canister for compacted waste that is the product of reprocessing at the ORANO facilities at La Hague, France.

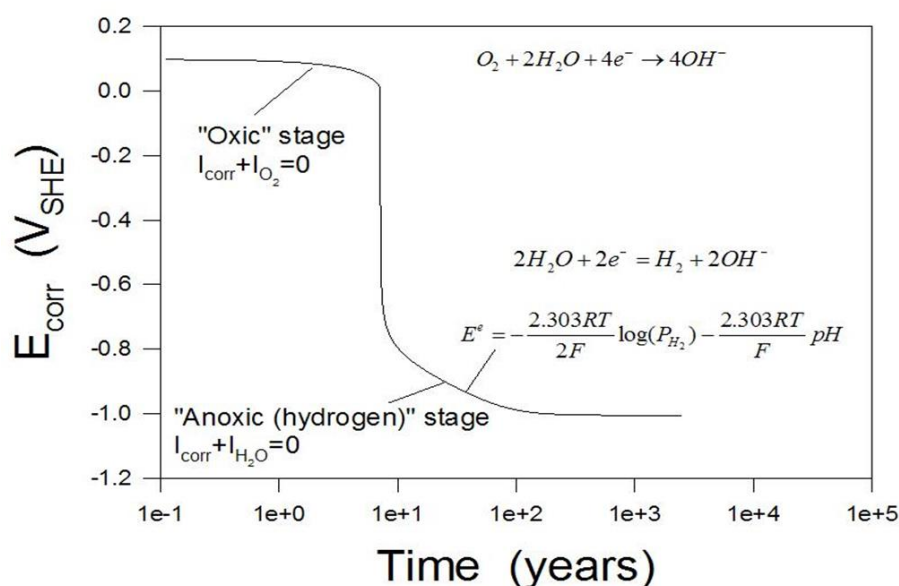


Figure 6-1 – Evolution of corrosion potential as predicted by the Mixed Potential Model (MPM) (Engelhardt et al., 2014).

For a HLW disposal cell, a transition phase is sometimes thought to exist due to the presence of radiolysis products<sup>5</sup>, which would temporarily sustain relatively constant, mildly oxidising conditions (Kursten et al., 2011). However, experiments by (Smart et al., 2019) seem to indicate that corrosion potentials become more negative (small decrease by 30-50 mV) under gamma irradiation (25 Gy h<sup>-1</sup>) at 80 °C. Similar, but less marked changes were observed at 25 °C. This is in contrast to what is typically reported in the literature on both mild steel and stainless steel in near-neutral pH conditions, in which an increase in Eh is thought to be associated with the effect of oxidising radicals. However, such results (whether theoretical or experimental) are only obtained for much higher dose rates than what would be relevant for geological disposal of HLW after an on-surface cooling period.

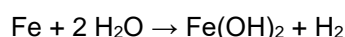
Corrosion processes may be subdivided into a uniform passive corrosion mechanism and localised corrosion mechanisms (e.g., pitting corrosion, crevice corrosion and stress corrosion cracking). In a concrete-based geological disposal concept, the followed strategy is usually to demonstrate that localised corrosion phenomena cannot occur in highly alkaline disposal conditions. Therefore, the focus of the experimental studies with respect to this interface is on rate measurements of uniform passive corrosion through different methods and techniques.

Oxic corrosion of iron is described by following global reaction:

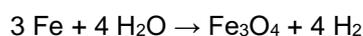


which the geochemical conditions in the direct surroundings. Corrosion products under oxic conditions are for example goethite, ferrihydrite and lepidocrocite (L'Hostis et al., 2011).

Anaerobic corrosion of iron is associated with the generation of hydrogen through the following global reaction:



or, if the Schikorr reaction occurs, by the reaction:



<sup>5</sup> Radiolysis of water produces hydrogen, oxygen, hydrogen peroxide and reactive radicals.

The rate of hydrogen generation can be monitored with experimental methods, and this principle is often used in experimental programmes to estimate the corrosion rate assuming either iron(II) hydroxide (1 mol hydrogen per mol iron) or magnetite (1.33 mol hydrogen per mol iron) as main corrosion product. At the end of a corrosion experiment, post-mortem analysis can be done by imaging and spectroscopy techniques, a.o. to confirm the nature of the corrosion products. Under anoxic conditions, corrosion products as magnetite and hematite are formed (L'Hostis et al., 2011).

## 6.1.2 Factors influencing the corrosion rate in a cementitious environment

### 6.1.2.1 Temperature

#### *Potential impact of temperature on corrosion*

Temperature can play an important role in the corrosion of steel in concrete in many different ways because all the processes and parameters involved in corrosion can be influenced by changes in temperature, such as

- kinetic parameters of the corrosion reaction (e.g., Tafel slopes, exchange current densities);
- rate of diffusion of O<sub>2</sub> and aggressive ions into the concrete;
- dissolved oxygen solubility;
- pore solution chemistry of concrete (e.g., viscosity, ionic flow through concrete).

The corrosion of steel reinforcement is an electrochemical reaction and, as for any chemical reaction, its rate is greatly affected by temperature. Generally, the corrosion rate increases significantly as temperature increases. The increased corrosion rate results from increased activation energy for chemical and electrochemical reactions, as illustrated by the Arrhenius equation:

$$k = A \cdot e^{\left(\frac{-\Delta E}{RT}\right)} \quad (6-1)$$

where  $k$  is the rate constant,  $A$  is a pre-exponential factor (constant),  $\Delta E$  is the activation energy,  $R$  is the universal gas constant ( $\approx 8.314 \text{ J mol}^{-1} \text{ K}^{-1}$ ), and  $T$  is the absolute temperature.

Equations (6-2) and (6-3) clearly show that, from a theoretical point of view, the Tafel slopes increase with increasing temperature (Shoesmith, 1996; Pour-Ghaz, 2007):

$$\beta_a = \frac{2.303R}{\alpha z F} \cdot T \quad (6-2)$$

$$\beta_c = \frac{-2.303R}{(1-\alpha)zF} \cdot T \quad (6-3)$$

where  $\beta_a$  and  $\beta_c$  are the Tafel slopes of the anodic and cathodic reactions, respectively,  $R$  is the universal gas constant,  $T$  is the absolute temperature,  $z$  is the number of electrons involved in the metal dissolution reaction,  $\alpha$  is the symmetry factor (transfer coefficient) and  $F$  is the Faraday constant ( $\approx 96,480 \text{ C mol}^{-1}$ ).

A relationship exists between the exchange current density,  $i_0$  (in  $\text{A m}^{-2}$ ), and temperature as described by Equation (6-4) (Bard and Faulkner, 2001):

$$i_0 = F A k^0 C_O^* e^{-\frac{\alpha F}{RT}(E_{eq} - E^{0'})} \quad (6-4)$$

where  $F$  is the Faraday constant,  $A$  is the electrode area,  $k_0$  is the standard rate constant,  $C_{O^*}$  is the bulk concentration of species  $O$  in  $O + ne^- \leftrightarrow R$ ,  $\alpha$  is the symmetry factor,  $R$  is the universal gas constant,  $T$  is the absolute temperature,  $E_{eq}$  is the equilibrium potential of the electrode and  $E^{0'}$  is the formal potential of the electrode (i.e., the potential where the forward and reverse rate constants have the same value). From Equation (6-4), it is evident that the exchange current density is directly proportional to the standard rate constant,  $k_0$ , which is known to vary with temperature.

The diffusion coefficient,  $D$ , is known to increase with temperature. With an increase in  $D$ , the limiting diffusion current density,  $i_L$ , also increases, as illustrated in Equation (6-5), and thus so will the corrosion rate (because more oxygen becomes available for the cathodic reduction process).

$$i_L = \frac{nFDC}{\delta} \tag{6-5}$$

where  $n$  is the number of electrons transferred,  $F$  is the Farady constant,  $C$  is the concentration of the diffusing species in the bulk electrolyte and  $\delta$  is the thickness of the diffusion layer (McCafferty, 2010).

On the other hand, the solubility of oxygen in water is known to decrease with increasing temperature, which results in a significant decrease of the concentration of dissolved oxygen as reactant for the process of steel corrosion, thereby lowering down the corrosion rate (Davis, 2000; Živica, 2002). This effect stems directly from Equation (6-5), in which it is seen that  $i_L$  is directly proportional to  $C$ , the concentration of dissolved  $O_2$ .

Other physicochemical properties affected by temperature are the viscosity and the conductivity of the concrete pore solution. The viscosity will decrease with increasing temperature, which will aid oxygen diffusion. Ionic mobility will also increase with temperature, increasing the overall conductivity of the electrolyte.

Several studies (Hussain and Rasheeduzaffar, 1993; Hussain et al., 1996; Maslehuddin, 1994; Maslehuddin et al., 1996) found that temperature can significantly influence the chloride binding capacity of cements. The  $Cl^-/OH^-$  ratio significantly increased as temperature was increased from 20 to 70 °C. This steep increase was caused by an increase in the free chloride concentration, which is attributed to the decomposition of Friedel’s salt (formed by the reaction of  $C_3A$  hydrates with chlorides) at elevated temperature, and a simultaneous reduction in the hydroxyl ion concentration. This effect was more pronounced in the temperature range above 55 °C.

Temperature can also affect the onset of different modes of localized corrosion. An increase in chloride concentration in the pore solution of chloride contaminated concrete can play an important role on the stability of the passive film because the breakdown potential tends to decrease with increasing temperature. On the other hand, at low enough oxygen concentration, the driving force will become zero and localized corrosion cannot occur (provided other oxidants are not present) (Blackwood et al., 2002).

*Relevant conclusions from literature*

Naish, Smart and co-workers also found that the initial corrosion rates increased with increasing temperature according to the Arrhenius relationship (see Eq. 6-1) (Smart et al., 2004).

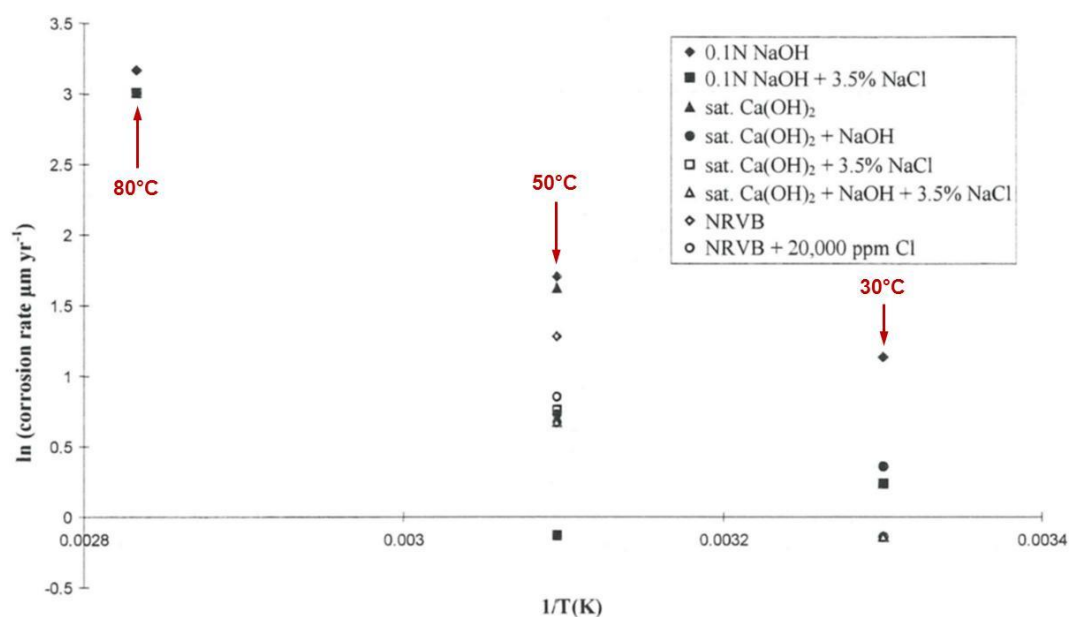


Figure 6-2 – Effect of temperature on the anaerobic corrosion rate of carbon steel in various alkaline solutions. The anaerobic corrosion rate is plotted as a function of reciprocal temperature (highest temperature: left side of the graph; lowest temperature: right side of the graph) (adapted from Smart et al., 2004).

This temperature dependency effect was supported by Japanese studies (Fujisawa et al., 1997; Fujisawa et al., 1999). Hydrogen generation increased with temperature according to the following observations (see Figure 6-3a):

- at 15 °C, hydrogen gas generation was not detected during a period of ~100 days, after which it increased at an almost constant rate with time (with a corresponding corrosion rate of 4 nm yr<sup>-1</sup>);
- at 30 °C, hydrogen gas was not generated during an initial period of ~10 days, after which corrosion proceeded at an almost constant rate of 20 nm yr<sup>-1</sup> for ~160 days before the rate started decreasing;
- at 45 °C, hydrogen gas generation started immediately with a high corrosion rate of 200 nm yr<sup>-1</sup> during an initial period of ~50 days, and then diminished.

They calculated an apparent activation energy of the order of ~100 kJ mol<sup>-1</sup> for the overall corrosion process of carbon steel exposed to highly alkaline anoxic solutions (pH = 12.6; 12.8) in the temperature range 15–45 °C (Figure 6-3b). This value was found to be compatible with that reported by Posey and Palko (1979) in deaerated 4 M NaCl solutions at temperatures from 25 to 200 °C, that is approximately 33 kJ mol<sup>-1</sup> in the neutral pH range (pH between 5 and 7) and approximately 18 kJ mol<sup>-1</sup> in moderately acidic solutions (pH between 2 and 3) (Posey et al., 1978; Posey and Palko, 1979).

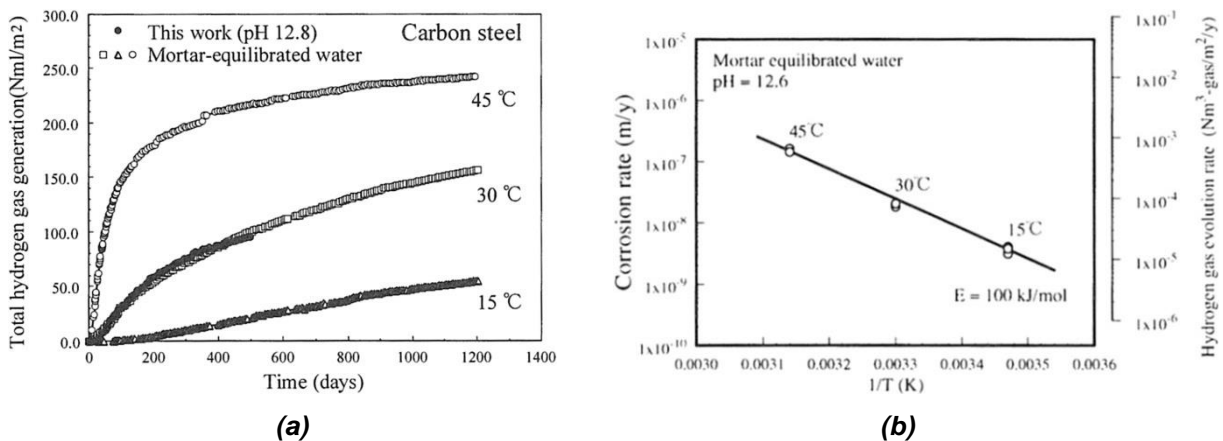


Figure 6-3 – Effect of temperature on the anaerobic corrosion rate and hydrogen gas evolution rate of carbon steel in saturated Ca(OH)<sub>2</sub> solutions (pH = 12.8) and in mortar-equilibrated water (pH = 12.6). (a) plot of hydrogen gas generation versus exposure time (Fujisawa et al., 1999), (b) plot of the corrosion rate versus reciprocal of temperature (1/T) (Fujisawa et al., 1997).

Figure 6-4 summarizes the uniform corrosion rate data reported in the literature for carbon steel in anoxic alkaline environments for different temperatures. Only long-term corrosion rate values (i.e., data coming from experiments lasting longer than 365 days) are considered. This figure clearly shows that at the later stages of the corrosion process (i.e., when steady state conditions prevail), temperature no longer has an effect on the uniform corrosion rate.

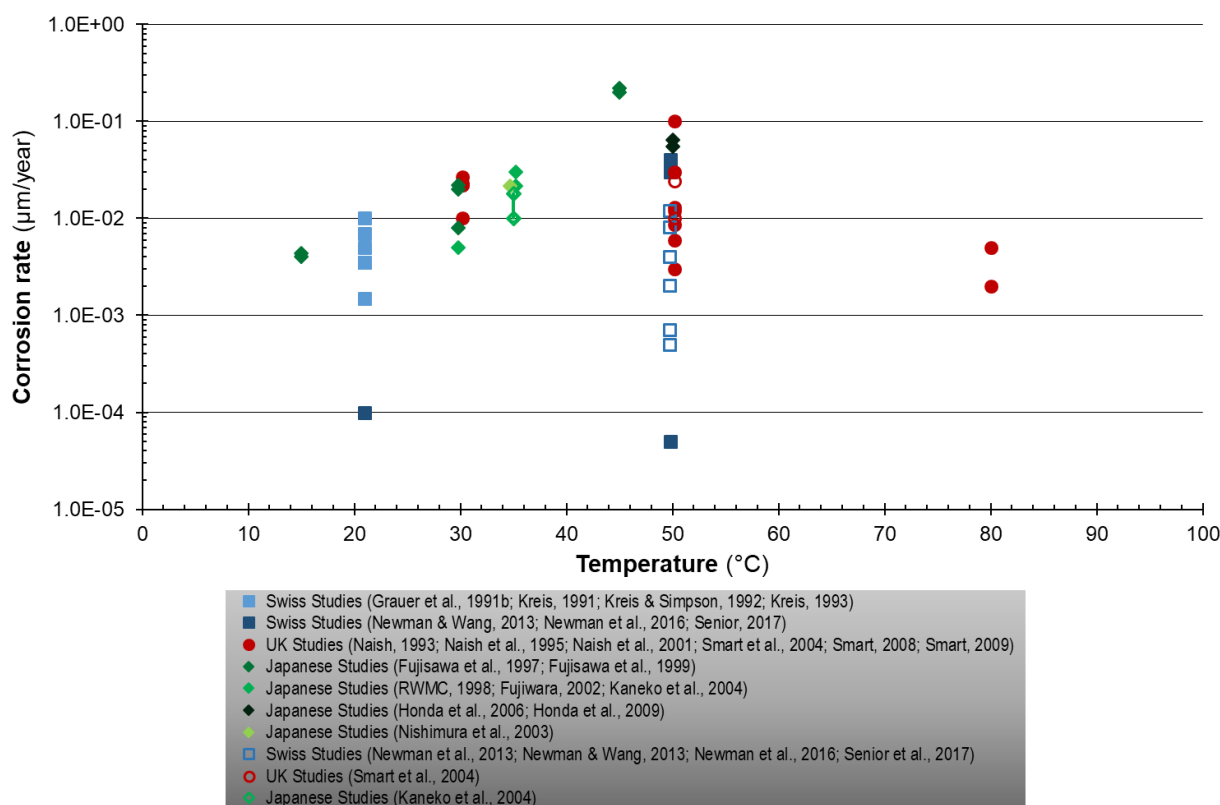


Figure 6-4 – Effect of temperature on the long-term ( $t > 365$  days) uniform corrosion rate of carbon steel exposed to alkaline and anoxic environments. Closed symbols represent tests conducted in solutions; open symbols represent tests conducted in cement.

#### 6.1.2.2 Water saturation degree

Corrosion of steel in concrete strongly depends on the moisture condition of the concrete. This is due to the fact that moisture affects both the resistivity of the concrete and the diffusion rate of oxygen. In dry concrete, which is characterized by a high resistivity, oxygen diffusion can take place unhindered. The corrosion rate then is said to be under ohmic control (i.e., the corrosion rate depends on the resistivity of the concrete). The resistivity in water saturated concrete is low but, on the other hand, the diffusion rate of oxygen is slow compared to the diffusion rate in dry concrete. This means that the corrosion rate is slow and that the corrosion is under diffusion control (Bertolini et al., 2004; Ahlström, 2014).

Tuutti (1982) first described the evolution of the corrosion rate of steel reinforcements as a function of relative humidity of the concrete (see Figure 6-5a). He reported that the corrosion rate reaches a maximum for a moisture content equivalent to the equilibrium with a relative atmospheric humidity of about 95%. Moving away from these values of humidity in either direction, the corrosion rate decreases (Bertolini et al., 2004). The findings of Tuutti were corroborated by Chitty et al. (2008) who attempted to deterministically model the long-term corrosion behaviour of rebars embedded in concrete considering the kinetics of (i) oxygen diffusion through the concrete and (ii) oxygen consumption at the metal/oxide layer interface. Figure 6-5b shows the evolution of the corrosion rate with the water saturation degree of a carbonated CEM I Portland cement paste for two different cover depths (4 cm and 1 m). They also found that the saturation degree for which the maximum corrosion rate is obtained depends on the cover depth: 0.96 and 0.69 for a 4 cm and 1 m cover, respectively. Additionally, they observed that lower corrosion rates were reached for higher cover depths (Chitty et al., 2008).

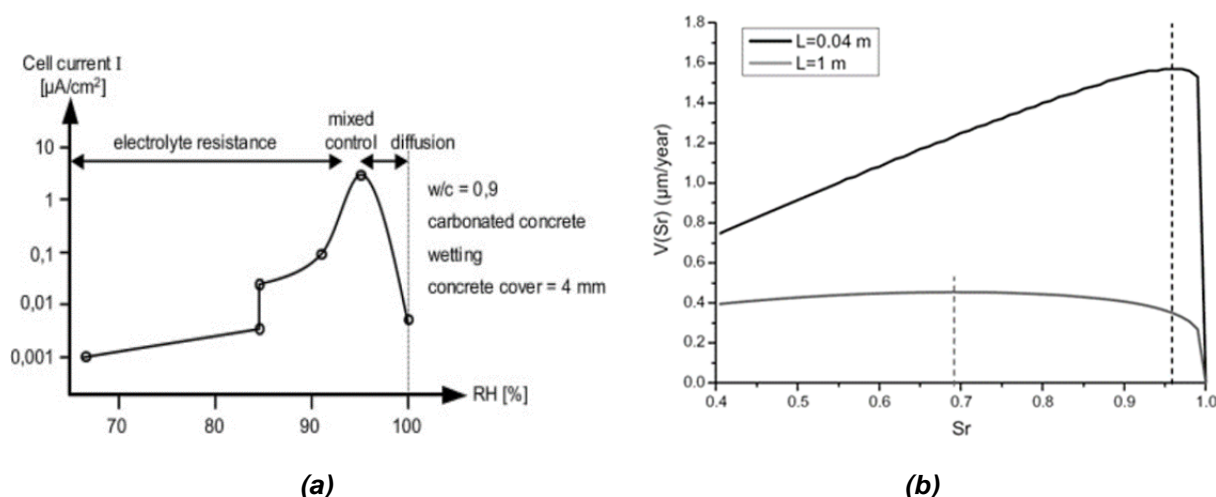


Figure 6-5 – Evolution of the corrosion rate as a function of (a) the relative humidity (Vu, 2011; adapted from Tuutti, 1982), (b) the saturation degree of a carbonated CEM I Portland cement paste for different cover depths (Chitty et al., 2008).

On the other hand, ionic mobility will increase with increasing saturation degree, thereby facilitating transport of aggressive species (e.g. chlorides) towards the overpack surface.

Michel et al. (2013) showed that when steel in concrete is in a passive state, the corrosion rate is not affected by the moisture conditions of the concrete

#### 6.1.2.3 pH

The protective oxide film is believed to remain stable as long as the pH stays higher than a threshold value ( $\sim 9 < \text{pH} < \sim 11.5$ ). If, for any reason, the pH should drop to below this threshold value, depassivation of the steel surface can take place and protection is lost.

A fall in pH can also have an effect on the susceptibility to localized corrosion. It has been suggested that a threshold concentration of chloride ions exists that must be exceeded before depassivation can take place, and that this threshold concentration is a function of the pH, i.e., the  $\text{OH}^-$  ion concentration as illustrated in Figure 6-6. Although this assumption has been generally accepted, there is little agreement concerning the quantitative function relating the two. The two diagonal lines in Figure 6 represent two different quantitative functions, formulated by two different research groups, describing the relationship between the pH and the threshold chloride concentration (Bentur et al., 1997):

- Hausman suggested that the threshold  $\text{Cl}^-$  ion concentration is about 0.6 times the  $\text{OH}^-$  ion concentration (based on measurements in  $\text{Ca}(\text{OH})_2$  solutions with a pH below 12.5);
- Diamond found that at higher pH levels (including measurements in  $\text{NaOH}$ ,  $\text{pH} > 12.5$ ), a limiting  $\text{Cl}^-/\text{OH}^-$  ratio of  $\sim 0.3$  (rather than 0.6 used by Hausman) might be more appropriate.

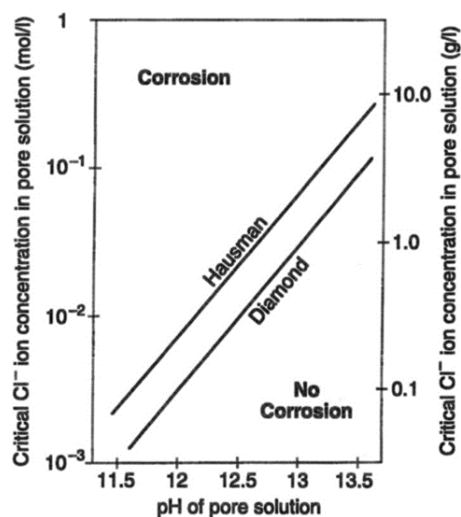


Figure 6-6 – Relationship between chloride threshold concentration and the pH of the concrete pore solution (Bentur et al., 1997).

#### 6.1.2.4 Aggressive species

##### Effect of chloride in aerobic alkaline environments

A huge amount of information is available in the literature on the effect of chloride on the corrosion rate of carbon steel in concrete under oxic conditions. This information largely originates from the non-nuclear waste management literature, because for industrial applications (longevity of bridge decks, garage platforms, ...), the effect of de-icing salts on the corrosion behaviour of the steel reinforcements is of a major concern. In these studies, specimens are often subjected to repetitive wet-dry cycles in simulated concrete pore solutions with the addition of incrementally increasing concentrations of chloride. From the literature, a general trend of increasing corrosion rate with increasing chloride concentration could be observed. For the purpose of illustration, we incorporate a couple of examples.

Goñi and Andrade (1990) reported corrosion rate data (expressed as a corrosion current density) of carbon steel rebars in synthetic concrete pore solutions (saturated  $\text{Ca}(\text{OH})_2$  solution) of different pH (ranging from 11.64 to 13.22) and various chloride concentrations at 21 °C. The pH was changed by adding 0, 0.2 or 0.5 N KOH to the  $\text{Ca}(\text{OH})_2$  solution. Chloride ions were added either as NaCl or  $\text{CaCl}_2$ . Polarization resistance measurements were performed to calculate the instantaneous corrosion rate (a B-value of 26 mV was used). The influence of chloride additions on the corrosion rate of carbon steel in a saturated  $\text{Ca}(\text{OH})_2 + 0.2$  N KOH solution is illustrated in Figure 6-7a for NaCl and in Figure 6-7b for  $\text{CaCl}_2$ . The boundary  $i_{\text{CORR}}$  range ( $\sim 0.1$ - $0.2 \mu\text{A cm}^{-2}$ ) between active and passive corrosion for carbon steel in concrete is also indicated on the graphs.

In the chloride-free solution, the steel rebars remained passivated during the entire experiment (with a measured corrosion current density of  $0.05 \mu\text{A cm}^{-2}$ , corresponding to a corrosion rate of  $\sim 0.6 \mu\text{m yr}^{-1}$ , after about 80 days). In the NaCl solutions, the addition of 0.1 N  $\text{Cl}^-$  increased the corrosion rate slightly but still remained in the passive region ( $\sim 1.0 \mu\text{m yr}^{-1}$ ). The addition of 0.5-1.0 N  $\text{Cl}^-$  showed corrosion rate values in the active domain ( $13.5$ - $18 \mu\text{m yr}^{-1}$ ), but without significant differences among them. The corrosion rate values in the  $\text{CaCl}_2$  solutions were of the same order of magnitude for 0.5 N and 0.75 N  $\text{Cl}^-$ , compared to their corresponding NaCl solutions. However, the addition of 0.1 N and 1.0 N  $\text{Cl}^-$  seemed to be much more aggressive in the  $\text{CaCl}_2$  solutions. A fivefold (for 0.1 N  $\text{Cl}^-$ ) to tenfold (for 1.0 N  $\text{Cl}^-$ ) increase of the corrosion rate was observed.

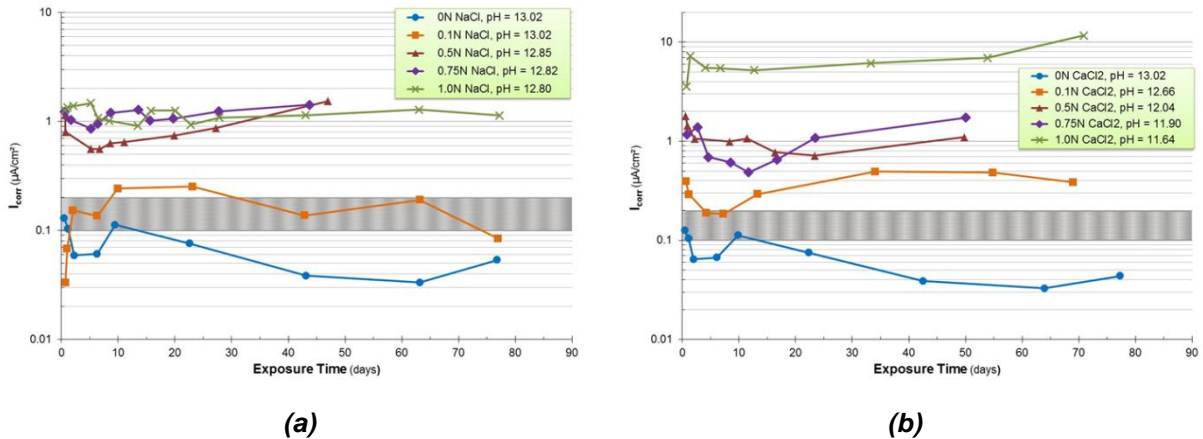


Figure 6-7 – Evolution of the corrosion rate of carbon steel in saturated  $\text{Ca}(\text{OH})_2 + 0.2 \text{ N KOH}$  solution at 21 °C as a function of chloride addition (adapted from Goñi and Andrade (1990)). (a) Chlorides added as NaCl salt, (b) chlorides added as  $\text{CaCl}_2$  salt.

The Texas Department of Transportation (TxDOT) funded a research project to compare the corrosion resistance of various types of polymer-coated rebars (PVC- and nylon-coated rebars) and metal-clad rebars (stainless steel-clad and galvanized rebars) to conventional carbon steel rebars. Polarization resistance measurements, from which the corrosion rate was estimated, were conducted in a saturated  $\text{Ca}(\text{OH})_2$  solution ( $1.85 \text{ g L}^{-1} \text{ Ca}(\text{OH})_2$ ) for a period of 6 days. During the first 2 days, the specimens were immersed in a chloride-free saturated  $\text{Ca}(\text{OH})_2$  solution. After 2 days, increasing amounts of NaCl were added to the test solution: for the third and fourth day,  $0.67 \text{ g L}^{-1} \text{ NaCl}$  ( $0.01146 \text{ mol L}^{-1}$ ) was added; for the fifth and sixth day, the NaCl concentration was increased to  $\sim 3.5\%$  ( $0.51334 \text{ mol L}^{-1}$ ). Bent rebar specimens were used (Deshpande, et al, 2000). Figure 6-8 shows the variation of the corrosion rate in time for carbon steel immersed in a saturated calcium hydroxide solution. The corrosion rate decreased initially during the 2 day exposure period to the chloride-free  $\text{Ca}(\text{OH})_2$  solution. This initial drop was attributed to the formation of the passive film. On addition of increasing amounts of NaCl, the corrosion rate progressively increased to a value of  $\sim 80 \mu\text{m yr}^{-1}$  after 6 days.

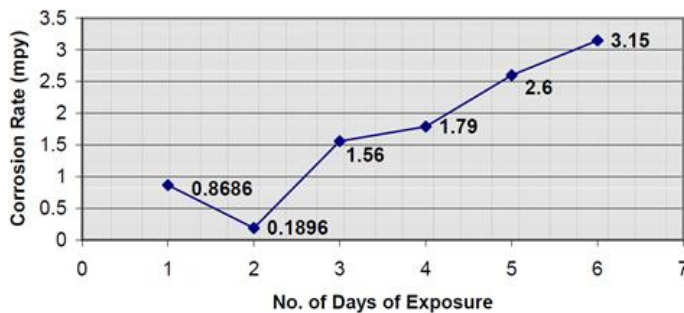


Figure 6-8 – Corrosion rate versus exposure time for carbon steel immersed in a  $1.85 \text{ g L}^{-1} \text{ Ca}(\text{OH})_2$  solution with increasing NaCl concentrations (days 1-2: chloride-free sat.  $\text{Ca}(\text{OH})_2$ ; days 3-4: sat.  $\text{Ca}(\text{OH})_2 + 0.67 \text{ g L}^{-1} \text{ NaCl}$ ; days 5-6: sat.  $\text{Ca}(\text{OH})_2 + 35 \text{ g L}^{-1} \text{ NaCl}$ ) (Deshpande et al., 2000). Conversion factor:  $1 \text{ mpy} \sim 25.4 \mu\text{m yr}^{-1}$ .

Although the literature clearly shows an increasing trend of the corrosion rate with increasing additions of chloride, it is very difficult to assign an absolute value (in terms of corrosion rates in  $\mu\text{m yr}^{-1}$ ) to the effect of chloride concentration, because from the data reported in the literature it is impossible to discriminate between the effect of increasing exposure time and the effect of increasing chloride concentration (in these tests, chloride concentration is gradually increased in time). This is illustrated in Figure 6-9. This figure shows the current density results from potentiostatic polarization experiments carried out at +200 mV (vs. SCE) in a saturated  $\text{Ca}(\text{OH})_2$  solution (pH 12.6) (Hurley and Scully, 2002). After a 24-hour stabilization period (without chloride), chlorides (NaCl) were added incrementally to the test solution in 24-hour cycles. In chloride-free  $\text{Ca}(\text{OH})_2$  solutions, the current density decreased from

$5 \cdot 10^{-7} \text{ A cm}^2$  ( $\sim 6 \mu\text{m yr}^{-1}$ ) to  $1.3 \cdot 10^{-7} \text{ A cm}^2$  ( $\sim 1.5 \mu\text{m yr}^{-1}$ ) over a 1-day period. When chlorides were added to the test solution, the current density increased with time to a value of  $2 \cdot 10^{-4} \text{ A cm}^2$  ( $\sim 2.40 \cdot 10^3 \mu\text{m yr}^{-1}$ ) for 0.0034 M NaCl addition (i.e. for a  $[\text{Cl}^-]/[\text{OH}^-]$  ratio of 0.14). According to the authors, the increase of the corrosion rate is to be interpreted as an effect of time rather than an effect of chloride additions because the increase (of  $i_{\text{CORR}}$ ) showed no abrupt changes at the times of chloride additions but occurred at an approximately constant rate.

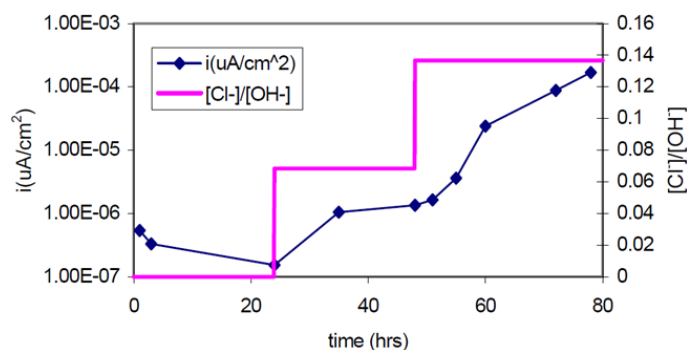


Figure 6-9 – Plot of current density (determined potentiostatically) as a function of chloride content versus time for A615 grade carbon steel in saturated  $\text{Ca}(\text{OH})_2$  solution at 25 °C (Hurley and Scully, 2002).

Zhang et al. (2009) studied the chloride threshold concentration at which the corrosion of various types of steel (carbon steel, stainless steel, Cr steel) changed from a passive state to an active state when exposed to a saturated  $\text{Ca}(\text{OH})_2$  solution ( $\text{pH} = 12.6$ ). The corrosion potential and the corrosion rate were monitored in time while adding sodium chloride (NaCl) to the test solution step by step (0%, 0.61%, 1.2%, 1.8%, 2.4%, 3.0%). The linear polarization resistance technique was used to determine the electrochemical resistance ( $R_p$ ) and the corrosion rate (expressed as the corrosion current density). The samples were immersed in a saturated  $\text{Ca}(\text{OH})_2$  solution for 2 days before testing to allow a passive film to be formed at the surface. This study concluded that the chloride threshold concentration of carbon steel in saturated  $\text{Ca}(\text{OH})_2$  is about 1.0 wt% (i.e.  $\sim 6,000 \text{ mg L}^{-1} \text{ Cl}^-$ ) (average from 4 replicate experiments), as illustrated in Figure 6-10. This figure shows the evolution of the corrosion potential and the corrosion current density of carbon steel in a saturated  $\text{Ca}(\text{OH})_2$  solution in time (bottom X axis) and with chloride concentration (top X axis).  $i_{\text{CORR}}$  decreased sharply from about  $0.05 \mu\text{A cm}^{-2}$  ( $\sim 0.6 \mu\text{m yr}^{-1}$ ) (passive state) to  $0.01 \mu\text{A cm}^{-2}$  ( $\sim 0.1 \mu\text{m yr}^{-1}$ ) after three days, indicating a continued formation and growth of the passive film on the surface in an environment of  $\text{pH}=12.6$ . When 0.61 wt% of chlorides were added to the solution,  $i_{\text{CORR}}$  showed a relatively large increase from  $0.01 \mu\text{A cm}^{-2}$  ( $\sim 0.1 \mu\text{m yr}^{-1}$ ) to  $0.1 \mu\text{A cm}^{-2}$  ( $\sim 1.2 \mu\text{m yr}^{-1}$ ) (both were still passive though) before it started to decrease again to a value of  $0.035 \mu\text{A cm}^{-2}$  ( $\sim 0.4 \mu\text{m yr}^{-1}$ ) after six days. This clearly showed the interference of chlorides on the passive film formation followed by the recovery of the passive film at this small concentration of chlorides. When the  $\text{Cl}^-$  concentration was increased to 1.2 wt% (i.e.  $\sim 7,300 \text{ mg L}^{-1}$ ),  $i_{\text{CORR}}$  significantly increased by two orders of magnitude from  $0.035 \mu\text{A cm}^{-2}$  ( $\sim 0.4 \mu\text{m yr}^{-1}$ ) (passive state) to  $3.35 \mu\text{A cm}^{-2}$  ( $\sim 40 \mu\text{m yr}^{-1}$ ) (active state). For chloride concentrations higher than 1.2 wt%,  $i_{\text{CORR}}$  remained fairly constant in time.

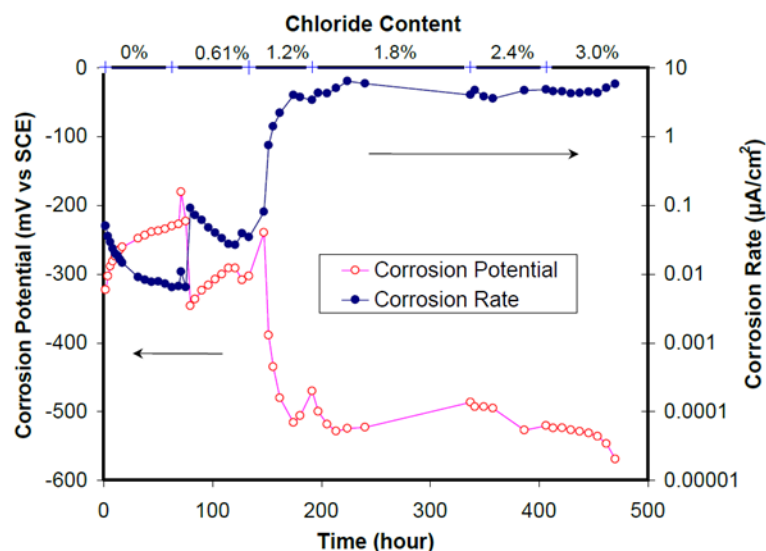


Figure 6-10 – Evolution of the corrosion potential and corrosion rate (expressed as a corrosion current density) of carbon steel in saturated  $\text{Ca(OH)}_2$  solution as a function of chloride addition (Zhang, et al, 2009).

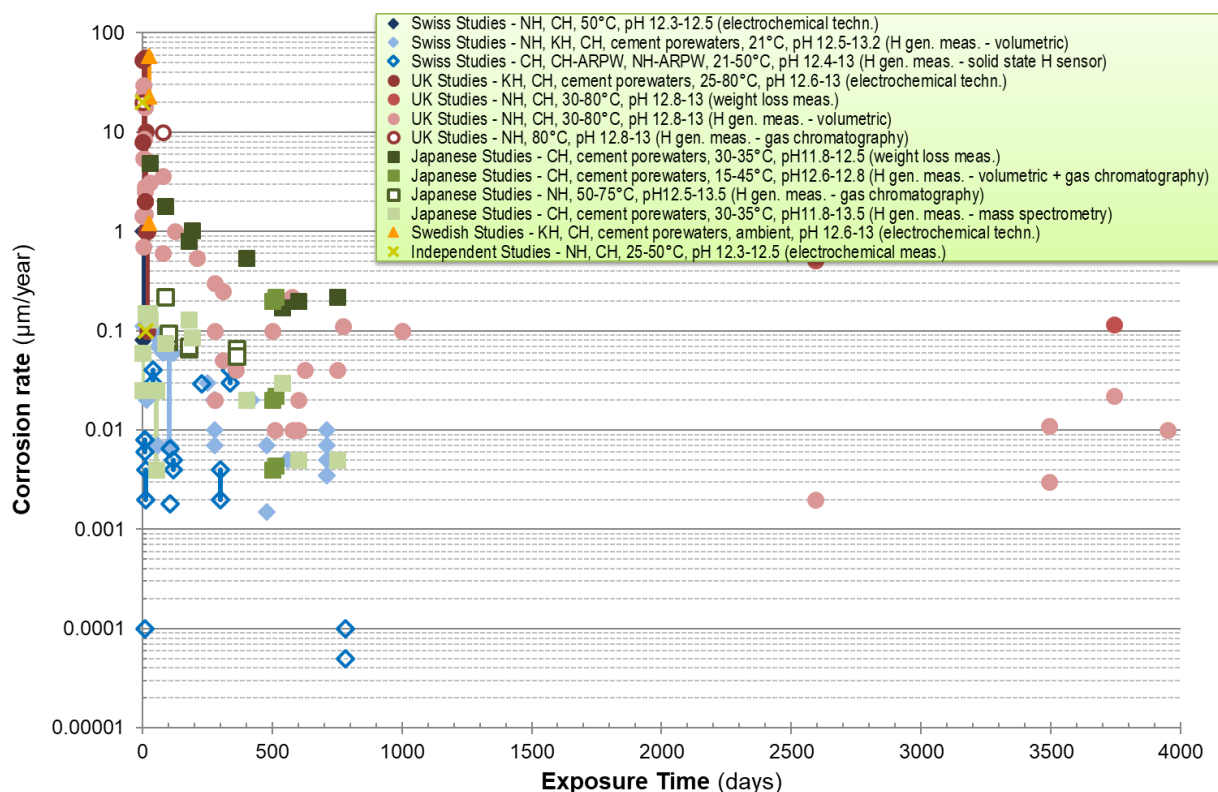
#### Effect of chloride in anaerobic alkaline environments

Most of the data in alkaline solutions under anoxic conditions originated from studies performed under the auspices of various national nuclear waste management authorities (LLW and ILW programmes). Figure 6-11 summarizes the corrosion rate data reported in the nuclear waste management and non-nuclear industrial literature for mild steel in anoxic and alkaline chloride-free solutions. The data in Figure 6-11 clearly exhibit a decreasing tendency of the uniform corrosion rate with increasing time of exposure towards a constant and very low value. Long-term corrosion rates ( $> 365$  days) in the range of  $0.1 \mu\text{m yr}^{-1}$  or lower have been reported for temperatures up to  $80 \text{ }^\circ\text{C}$  in chloride-free solutions with a pH between 11.8 and 13.5.

A number of experiments have been conducted with the addition of chloride:

- in the UK studies, chloride was added up to  $20,000 \text{ mg L}^{-1}$  (Naish, 1993; Naish et al., 1995; Naish et al., 2001; Smart et al., 2004; Smart, 2008; Smart, 2009);
- Fujisawa and co-workers (Fujisawa et al., 1999) measured the corrosion rate (volumetric hydrogen generation measurements) of carbon steel exposed to  $\text{Ca(OH)}_2/\text{CaCO}_3$  solutions of pH 10.5 or 12.8 with the addition of  $19,525 \text{ mg L}^{-1}$  chloride;
- Mihara and co-workers (Mihara et al., 2002) performed weight loss and hydrogen generation experiments in NaOH solutions containing  $19,000 \text{ mg L}^{-1}$  chloride at  $50 \text{ }^\circ\text{C}$ ;
- Nishimura and co-workers (Nishimura et al., 2003) measured the hydrogen generation rate from carbon steel in saturated  $\text{Ca(OH)}_2$  solution containing  $3,000 \text{ mg L}^{-1}$  chloride using mass spectrometry at  $35 \text{ }^\circ\text{C}$ ;
- Fujiwara and Kaneko et al. (Fujiwara, 2002; Kaneko et al., 2004) investigated the effect of chloride concentration (up to  $20,000 \text{ mg L}^{-1}$ ) on the hydrogen generation rate (mass spectrometry) of carbon steel in saturated  $\text{Ca(OH)}_2$  solution. They also studied the effect of pH in saturated  $\text{Ca(OH)}_2$  solution containing  $5,000 \text{ mg L}^{-1}$  chloride;
- Kaesche and Grubitsch (Kaesche, 1965; Grubitsch et al., 1970; Grubitsch et al., 1979) studied the active-passive corrosion behaviour of mild steel by recording potentiodynamic polarization scans in saturated  $\text{Ca(OH)}_2$  solutions containing various chloride concentrations in the range from 50 to  $12,770 \text{ mg L}^{-1}$ .

The corrosion rate data reported in the nuclear waste management and non-nuclear industrial literature for mild steel in anoxic and alkaline solutions containing chloride concentrations are summarized in Figure 6-12.

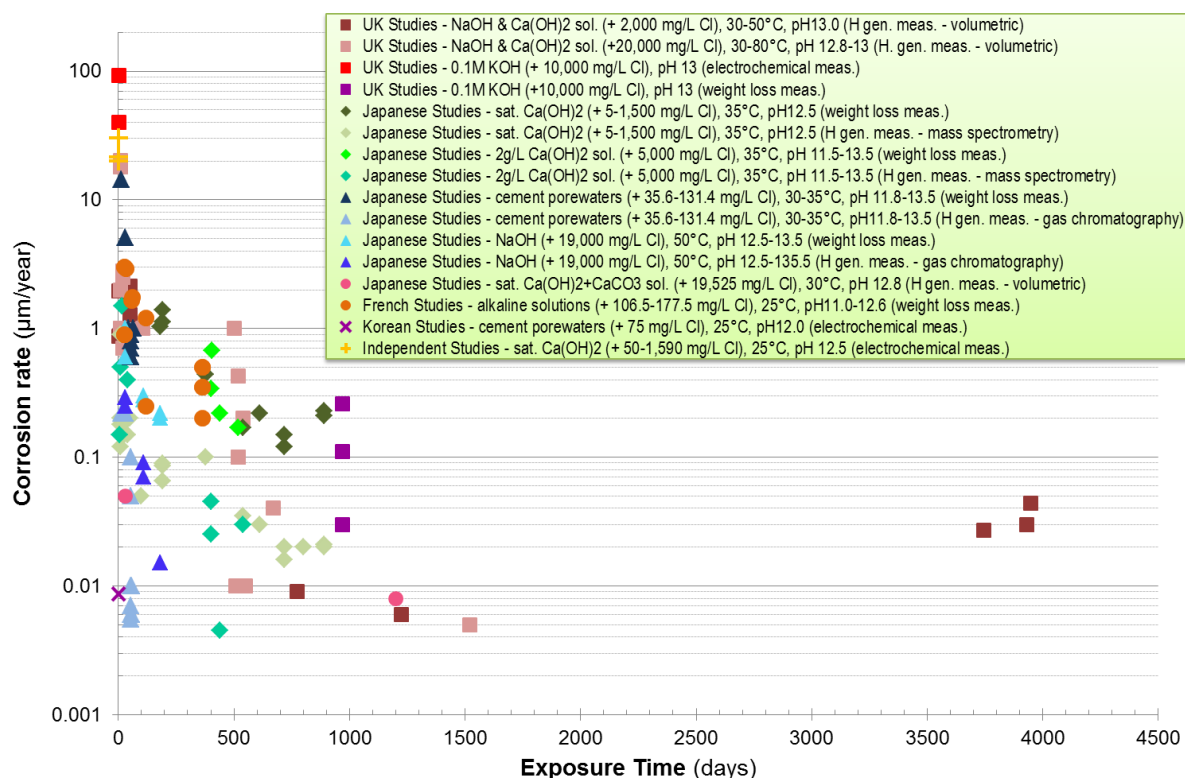


NH: NaOH ; CH: saturated Ca(OH)<sub>2</sub> ; KH: KOH ; CH-ARPW: Ca(OH)<sub>2</sub> saturated artificial rock pore water; NH-ARPW: 0.1 M NaOH saturated artificial rock pore water.

The graph is compiled from data reported in the following references:

- ◆ (Grauer, 1988);
- ◆ (Grauer *et al.*, 1991a; Grauer *et al.*, 1991b; Kreis, 1991; Kreis and Simpson, 1992; Kreis, 1993);
- ◇ (Newman & Wang, 2013; Newman *et al.*, 2013; Newman *et al.*, 2016; Senior, 2017; Senior *et al.*, 2017)
- (Naish, 1993; Smart *et al.*, 2004; Smart, 2008; Smart, 2009);
- (Smart *et al.*, 2004; Smart, 2008; Smart, 2009);
- (Naish, 1993; Naish *et al.*, 1995; Naish *et al.*, 2001; Smart *et al.*, 2004; Smart, 2008; Smart, 2009);
- (Naish *et al.*, 2001);
- (RWMC, 1998; Fujiwara, 2002; Kaneko *et al.*, 2004);
- (Fujisawa *et al.*, 1997);
- (Honda *et al.*, 2006; Honda *et al.*, 2009);
- (RWMC, 1998; Fujiwara, 2002; Kaneko *et al.*, 2004);
- ▲ (Hansson, 1984; Hansson, 1985; Hansson, 1985a; Hansson, 1987);
- × (Heusler *et al.*, 1958; Kaesche, 1965; Grubitsch *et al.*, 1970; Grubitsch *et al.*, 1979);

Figure 6-11 – Compilation of uniform corrosion rates (reported in the non-nuclear industrial and nuclear waste management literature) of carbon steel in anoxic and alkaline chloride-free solutions (pH ~ 12–13.5).



The following electrochemical techniques were used in the various national waste management R&D programmes:

- Korean studies (×): TP<sup>6</sup>;
- independent studies (+): PCD<sup>7</sup> (potentiodynamic);
- UK studies (■): PCD<sup>a</sup> (potentiodynamic);

The graph is compiled from data reported in the following references:

- (Smart *et al.*, 2004; Smart, 2008; Smart, 2009);
- (Naish, 1993; Naish *et al.*, 1995; Naish *et al.*, 2001; Smart *et al.*, 2004; Smart, 2008; Smart, 2009);
- ; ■ (Smart *et al.*, 2004; Smart, 2008; Smart, 2009);
- ◆; ◆; ◆; ◆ (Fujiwara, 2002; Kaneko *et al.*, 2004);
- ▲; ▲ (Matsuda *et al.*, 1995; RWMC, 1998; Fujiwara *et al.*, 2001);
- ▲; ▲ (Mihara *et al.*, 2002);
- (Fujisawa *et al.*, 1999)
- (L'Hostis *et al.*, 2011);
- × (Jung *et al.*, 2011);
- + (Kaesche, 1965; Grubitsch *et al.*, 1970; Grubitsch *et al.*, 1979);

Figure 6-12 – Compilation of uniform corrosion rates (reported in the non-nuclear industrial and nuclear waste management literature) of carbon steel in anoxic and alkaline solutions (pH ~ 12-13.5) containing various chloride concentrations up to 20,000 mg L<sup>-1</sup>.

The data in Figure 6-12 show that the measured corrosion rate decreased with increasing exposure time, even in the presence of chlorides. From comparison of the data Figure 6-11 (without chloride) with the data shown in Figure 6-12 (with chloride), it can be concluded that the presence of chloride (up to 20,000 mg L<sup>-1</sup>) has no discernible effect on the long-term corrosion rate of carbon steel in anaerobic high pH media.

<sup>6</sup> Tafel slope extrapolation method.

<sup>7</sup> Passive Current Density measurements: the passive current densities were derived graphically from the polarization curves (recorded either potentiostatically or potentiodynamically).

### Conclusions

The study of Zhang et al. (2009) is of a major importance because it shows that with the addition of ~6,000 mg L<sup>-1</sup> Cl<sup>-</sup> (~1 wt% NaCl) to highly alkaline environments, the corrosion regime of carbon steel changes from passive to active corrosion (under oxic conditions). This is most likely coupled with the destruction of the protective oxide film.

It is important to mention that high chloride concentrations, combined with the potential risk of the passive film being destroyed locally, may result in a significant increased susceptibility to localized corrosion phenomena (such as pitting corrosion, crevice corrosion and SCC).

The effect of these high chloride concentrations on the stability of the protective oxide film should be studied experimentally. Experiments should be performed to evaluate the effect of chloride on (1) the corrosion rate of carbon steel under oxic conditions and on (2) the occurrence of localized corrosion phenomena.

#### 6.1.3 Consequence of corrosion on concrete properties

The stability of the passivation layer depends on the geochemical conditions of the surrounding environment (*in casu* cement). Cement ageing processes (especially leaching and carbonation upon interaction with other disposal cell components) can influence the corrosion processes, for example, a pH decreases as a consequence of carbonation. Another process is ingress of aggressive species such as chloride as discussed previously. The depassivation of the steel (dissolution of the protective cover) initiates active corrosion of the steel bars which will be faster under aerobic than under anaerobic conditions.

When steel reinforcements corrode (embedded in a concrete structure), a layer of corrosion products is formed on the surface of the steel. The volume of these corrosion products can be much larger than that of the bare metal (i.e. known as the Pilling-Bedworth ratio (McCafferty, 2010; Broomfield, 2007; Caré et al., 2008)). The corrosion products will first fill the available pores near the interface. The available pore space depends on the chemical state of the concrete and the process that initiated the faster corrosion. With the ingress of aggressive species, initiation of active corrosion may occur without significantly change the microstructural properties of the concrete and thus the available pore space is close to the initial porosity of the concrete. However, when active corrosion occurs as a consequence of a pH decrease due to chemical degradation of concrete, the available pore space might be smaller or larger depending of carbonation (resulting typically in a porosity decrease) or calcium leaching (resulting typically in a porosity decrease) is the dominant degradation process (see e.g. Glasser et al., 2008, for a description of these processes).

After filling of the pore space, the corrosion products will gradually increase the mechanical stress in the concrete. Fracture formation is initiated when the mechanical stress exceeds the tensile strength (Höglund, 2014) but the time for the first appearance of the fractures depends on different factors such as thickness of concrete cover, quality and strength of the concrete, corrosion rate (Andrade et al., 2011). Also the porosity in the layer with corrosion products will have an impact on the concrete (Höglund, 2014). Höglund (2014) gives different models to assess the time of fracturing and the fracture width. Note that creep of concrete can accommodate partly the effects caused by the corrosion products retarding to a given extent the initiation of fracture formation.

Fractures initiated by the corrosion products may influence the geochemical evolution of concrete near the concrete / steel interface, especially when they are fully penetrating (i.e., from the concrete/steel interface to the boundary of the concrete (e.g., interface with host rock)). From these fractures, alteration fronts may develop within the concrete matrix and thus possibly create larger regions in the concrete with a pH decrease. Degradation fronts in fracture-matrix concrete systems can be described with approximated analytical models (e.g. Höglund, 2014), or with coupled reactive transport models (e.g., Perko et al., 2010; Perko et al., 2015).

There exist other processes that potentially initiate fracture formation such as drying shrinkage, heating, cooling, internal swelling reactions, etc. Again, when these fractures are partially or fully penetrating the concrete from the concrete boundary towards the steel-concrete interface, both ingress of aggressive species (e.g. Cl) or advancement of concrete alteration fronts may increase resulting thus in faster depassivation of the steel with initiation of active corrosion as a consequence.

As is mentioned in the next paragraph, there are indications that a Fe-enriched layer will form in the mortar/concrete close to the interface. Fe will interact with the cement minerals and may form Fe-containing cement minerals. Thermodynamic modelling with state-of-the-art thermodynamic databases may indicate which Fe-containing cement minerals could potentially being formed (calculated saturation index close to or larger than zero). For example, the database CEMDATA18 (Lothenbach et al., 2018) contains thermodynamic information on Fe-containing cement hydrates.

## 6.2 Evidence from experiments and analogues

### 6.2.1 Experiments

In this section, the discussion is limited to experiments of corrosion of carbon steel under anaerobic alkaline conditions. The study of Smart et al. (2019) provides a recent study relevant for HLW disposal cell. The other examples show evidence of Ca and Fe transport processes near the steel - cement interface. Corrosion rates under relevant environmental conditions were already discussed in section 6.1.2.

A recent report (Smart et al. 2019) by Wood Nuclear Limited documents the extensive programme of experimental work that was carried out in support of the development of the Niras-Ondraf 'Supercontainer' concept. The programme involved a matrix of gas cell experiments in which hydrogen production is monitored during corrosion of steel in a simplified simulant of the porewater, denoted YCW (Young Concrete Water), with a composition of 0.14 M Na<sup>+</sup>, 0.37 M K<sup>+</sup>, 2 mM SO<sub>4</sub><sup>2-</sup> and a calculated initial pH value of 13.7. The effects of several environmental parameters were investigated such as temperature (25 °C and 80 °C), dose rate (0 and 25 Gy h<sup>-1</sup>), chloride concentration (0 and 100 mg L<sup>-1</sup>) and the presence of sulphide (0 and 500 mg L<sup>-1</sup>) and thiosulphate (0 and 100 mg L<sup>-1</sup>). Also, a few experiments were carried out in solid buffer material, either on its own or surrounded by YCW to ensure it remained saturated. The results of the gas cell experiments carried out in the absence of sulphide and thiosulphate indicate that long-term corrosion rates display a limited sensitivity towards all the varied environmental parameters (temperature, chloride and presence of radiation) within the envelope tested. In all cases, long-term rates below the detection limit of the technique (which was around 0.1 µm yr<sup>-1</sup>) were typically found after a few years of monitoring. Initial corrosion rates and the timescales over which the corrosion rates decrease to low levels (due to steel passivation), however, display some sensitivity towards temperature and, to a lesser extent, the presence of radiation. Reliable electrochemical measurements could mainly be obtained at the beginning of the tests, resulting in Eh values in the order of -800 to -500 mV, corresponding to anoxic conditions. These potentials correlate well with the stability of magnetite based on the Pourbaix diagram of iron in the conditions of interest.

Smart et al. (2019) also provides a series of SEM images and EDX spectra obtained from the surface of carbon steel wires from selected gas cells. Overall, the SEM analysis indicated that a highly crystalline corrosion product was formed at 80 °C (see example in Figure 6-13), but that such material was much less crystalline at 25 °C. EDX analysis of the crystalline deposits shows predominantly Fe and O (iron corrosion products) but also indicate in some cases presence of other species.

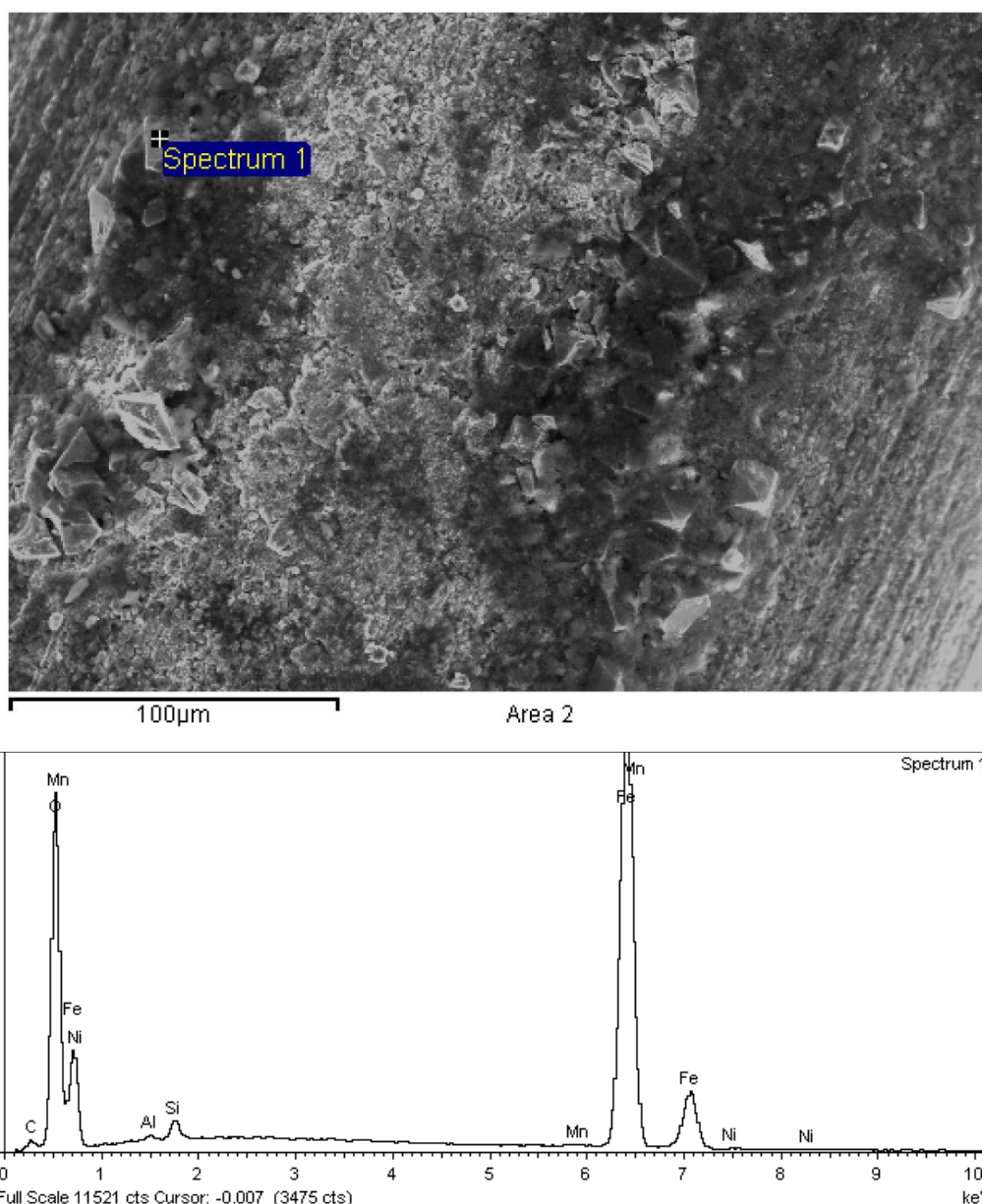


Figure 6-13 – Top: SEM image from the surface of carbon steel wire specimen after 13,600h in YCW at 80 °C. Bottom: EDX spectrum from “crystalline” material formed on the wire surface at the indicated location. (Figure 105 from Smart et al. (2019).

Raman analysis on corrosion products formed both at 25 °C and 80 °C was consistent with magnetite. Test cases in chloride containing solution did not suggest a clear role of chloride in the corrosion process, as post-mortem EDX analysis did not show significant quantities of chloride in the corrosion product.

In addition to using glass gas cells, a small number of gas generation experiments were also carried out using sealed metal autoclaves, to demonstrate that high sensitivity can be achieved with this technique (see Smart et al., 2019, for further details). Very low long-term corrosion rates ( $<0.03 \mu\text{m yr}^{-1}$ ) were recorded using this setup. The inclusion of gas analysis in these experiments confirmed that the gas produced during steel corrosion is predominantly hydrogen, but that trace amounts of methane or other low molecular weight organic gases are also produced. Through comparison with similar observations in the literature (e.g. Deng et al., 1997), it is suggested that the mechanism of formation of the organic species could be analogous to the Fischer-Tropsch process, in which hydrocarbons are produced from a mixture of CO and H<sub>2</sub>, in the presence of an iron catalyst.

The study of L'Hostis et al. (2011) indicated corrosion rates for metallic samples embedded in mortar (CEM I, different relative humidities, solution simulation clay rock underground conditions) typical for passive conditions. They observed iron and calcium transport processes at the interface: Ca is present in the initial corrosion product layer and Fe is present in the mortar surrounding the metallic parts. Similarly, Chomat et al. (2014, 2017) identified an iron-enriched layer between the corrosion product layer or the steel layer and the unaltered part of the cement for CEM-I and CEM-V. From these short-term experiments (up to 3 years), it seems that both the corrosion products, the thickness of the corrosion product layer, and the thickness of the iron-enriched layer (~some tens of  $\mu\text{m}$ ) do not evolve significantly over time (except for CEM-I in a de-aerated environment in which magnetite appears over time).

### 6.2.2 Analogues

Considering the extreme timescales associated with applications of nuclear waste disposal, evidence from corrosion experimental programmes and semi-empirical modelling is no longer sufficient to make confident predictions of the component's service life. Therefore, a mechanistic understanding is necessary, ideally supported by archaeological evidence used to confirm the long-term kinetics and the validity of the mechanisms identified by short-term experiments. Although the material characteristics and the environment in which ancient ferrous objects are found are often different from the highly engineered systems in a nuclear waste disposal context, valuable information in terms of corrosion mechanisms and rates can be derived.

A review paper by Dillman et al. (2014) provides a number of available analogues and discusses the influence of environment (varying from oxidising conditions to buried anoxic and sea water environments) on one hand and the influence of material (archaeological ferrous objects are heterogeneous by nature and may contain variable quantities of carbon and non-metallic inclusions) on the other hand. Although some examples of corroded ferrous objects in anoxic conditions are provided, no analogue of iron/steel in highly alkaline (cementitious) conditions is mentioned.

In the framework of a research programme set up by ANDRA on the corrosion of buried archaeological items, Saheb has published a thesis (Saheb, 2009) and a number of articles (e.g. (Saheb et al., 2010, 2014) on corrosion mechanisms of ferrous artefacts in anoxic conditions, aiming at identifying corrosion mechanisms and their link to the environmental conditions, notably the electrolyte chemical composition. The study focuses on the archaeological site of Glinet (Normandy, France) where the main phases constitutive of the corrosion layer on the studied objects are siderite ( $\text{FeCO}_3$ ), an iron carbonate containing hydroxide groups (probably chukanovite  $\text{Fe}_2(\text{OH})_2\text{CO}_3$ ) and magnetite ( $\text{Fe}_3\text{O}_4$ ). Thermodynamic modelling was applied to correlate the corrosion products to the environmental data, obtained from on-site measurement campaigns of pore water chemistry (Saheb et al. (2010). Although the study is relevant as an example of developing a mechanistic understanding of long-term corrosion processes in a carbonate rich environment, it does not provide a direct analogue for corrosion of iron in cement or concrete.

## 6.3 Application of conceptual and mathematical models

In Smart et al. (2019), the authors state that the consensus view of the structure of the passive film on carbon steel in alkaline conditions is that there is a very thin inner barrier layer covered by a much thicker precipitated outer layer. This passive film structure has been modelled by Macdonald and co-workers using the Point Defect model (PDM) (MacDonald, 2008, 2011), although other models have also been applied. The PDM provides a comprehensive basis for describing the formation and destruction of passive films. The reaction scheme adopted for PDM is illustrated in Figure 6-14. The PDM postulates that the bilayer passive film is composed of a highly defective barrier layer that grows into the metal and an outer layer that forms via the hydrolysis of cations transmitted through the barrier layer and the subsequent precipitation of a hydroxide, oxyhydroxide, or oxide, depending upon the formation conditions. The passive behaviour of the film can mainly be attributed to the presence of the barrier layer. The PDM further postulates that the point defects present in a barrier layer are, in general, cation

vacancies ( $V_M^{\chi'}$ ), oxygen vacancies ( $V_O^{\cdot\cdot}$ ) and cation interstitials ( $M_i^{\chi+}$ ). Cation vacancies are electron acceptors, thereby doping the barrier layer p-type, whereas oxygen vacancies and metal interstitials are electron donors, resulting in n-type doping. Thus, on both pure metals and alloys, the barrier layer is essentially a highly doped, defect semi-conductor. According to the PDM, the defect structure of the barrier layer (bl) can be understood in terms of the set of defect generation and annihilation reactions occurring at the metal/bl interface and at the bl/outer layer (solution) interface. Looking at the scheme in Figure 6-14 in more detail, it is clear that the generation of oxygen vacancies via reaction (3) at the metal/bl interface and their annihilation via reaction (6) at the bl/solution interface is responsible for the growth of the bl, which occurs directly into the metal, without participation by species in the solution with the exception of water, which is the source of oxygen for oxide film formation. Reaction (7) describes the dissolution of the existing film at the bl/solution interface. From this, it is evident that the passive state exists by virtue of a judicious relationship between the rate of bl formation via reaction (3) and bl destruction via reaction (7).

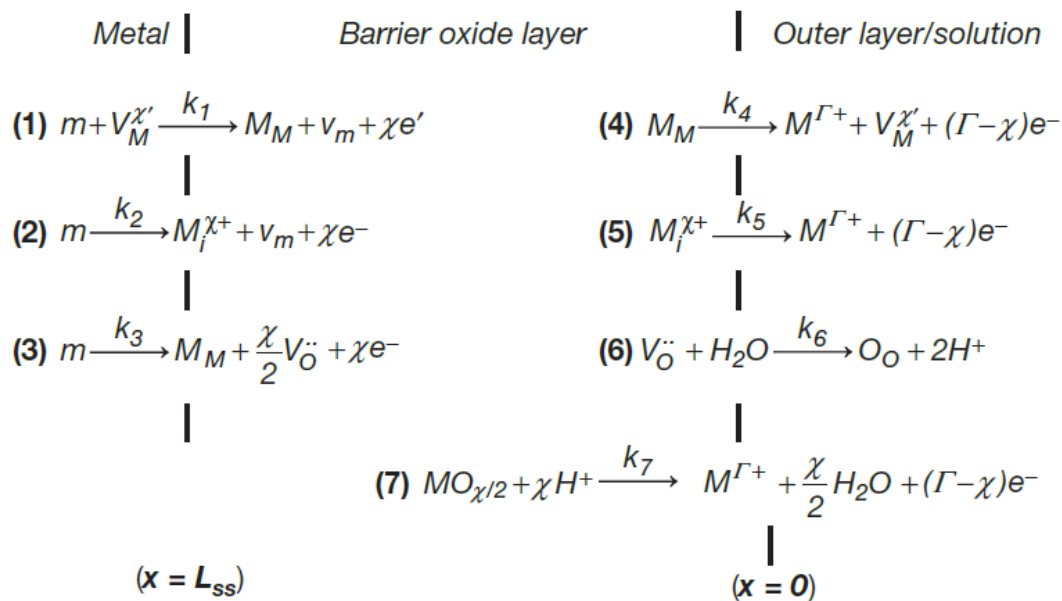


Figure 6-14 – Film growth model for carbon steel in alkaline conditions according to the Point Defect Model (PDM) (McDonald, 2011).

$m$  = metal atom,  $V_M^{\chi'}$  = cation vacancy on the metal sublattice of the barrier layer (bl),  $M_i^{\chi+}$  = interstitial cation,  $M_M$  = metal cation on the metal sublattice of the bl,  $V_O^{\cdot\cdot}$  = oxygen vacancy on the oxygen sublattice of the bl,  $O_O$  = oxygen anion on the oxygen sublattice of the bl,  $M^{\Gamma+}$  = metal cation in solution.

Bataillon et al. (2010, 2012) developed another tool to describe the evolution of a dense oxide layer, taking into account moving interfaces. This numerical model is called the Diffusion Poisson Coupled Model (DPCM). The linear convection-diffusion mass transport equations are given by the two Fick Laws. They are coupled with the Poisson equation for calculating the electrical potential profile in the oxide layer. The reaction scheme adopted in the DPCM is shown in Figure 6-15. The DPCM assumes solid state transport of charge carriers through the dense oxide layer. These charge carriers could be iron cations, electrons or oxygen vacancies. The whole system consists of a solution in contact with an oxide layer that covers a metal. The oxide layer is bound by two interfaces. One is the inner interface, which corresponds to the metal/oxide interface. The other is the outer interface, which corresponds to the oxide/solution interface. The metal is an electronic conductor. It could be charged either by accumulation or depletion of electrons. The solution is an ionic conductor that could be charged either by accumulation of cations or anions. The oxide layer is a mixed electronic and ionic conductor (see

Figure 6-15 (a)). The DPCM postulates that neither combination nor creation of charge carriers occurs inside the oxide layer. The charge carriers are created at one interface (inner or outer) and are consumed at the other (outer or inner). Inside the oxide layer, each charge carrier flux is assumed independent of the others because the physical mechanism for transport is generally typical of the kind of charge carrier (electronic transport in a conduction band, transport of ions by a vacancy mechanism, etc.). The DPCM also assumes that the outer and inner interfaces could move with time. The origin of the space axis is the location of the outer interface  $X_0(0)$  at the initial time ( $t = 0$ ). The initial thickness  $L_0$  of the oxide layer defines the initial location of the inner interface  $X_1(0) = L_0$  (see Figure 6-15 (a)). The shift of the outer interface is monitored by the “Oxide Host Lattice dissolution” step, whereas the shift of the inner interface is monitored by the “Oxide Host Lattice growth” step (see Figure 6-15(b)). The latter step corresponds to the oxidation of iron into its oxide. As the molar volumes of the metal and the oxide are quite different, this solid state oxidation leads to an expansion of the oxide layer through the Pilling-Bedworth ratio. The numerical code solving the equations of the DPCM is called CALIPSO. This code calculates the potential and the concentration profiles in the system.

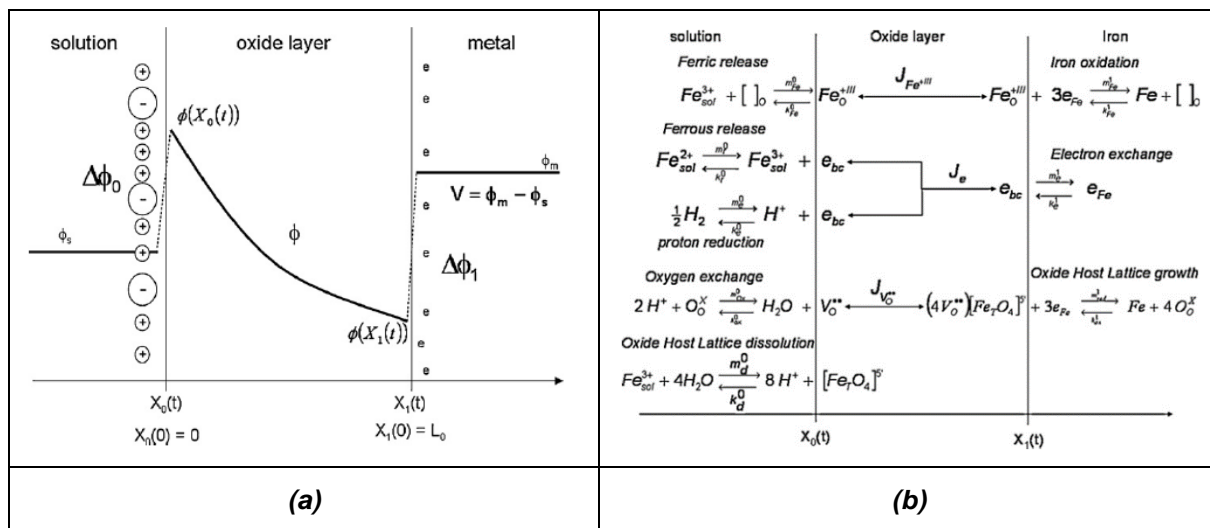


Figure 6-15 – Film growth model for carbon steel in alkaline conditions according to the Diffusion Poisson Coupled Model (DPCM) (Bataillon et al., 2010).

(a) Potential profile in the solution/oxide layer/metal system.

(b) Reaction path.

Another approach consists of thermodynamic modelling of the solution chemistry, e.g., calculating saturation indexes of ferrous and ferric minerals. The available information in the literature either focuses on corrosion in alkaline conditions (with a substantial knowledge base on reinforcement corrosion in concrete structures) or in anoxic conditions (e.g. such as in Saheb et al., 2010). However, no examples have been found for thermodynamic modelling of iron/steel in both anoxic and alkaline conditions.

In the middle of modelling cement-steel interactions under oxic and anoxic conditions is the electrochemical model for corrosion. Linking such models to models that describe diffusion of chemical species through the cement material to the corrosion layers and take into account geochemical alterations (so-called reactive transport models) could result in significant advances in modelling the concrete/steel interface (Bildstein et al., 2019)<sup>8</sup>.

<sup>8</sup> Bildstein et al. (2019) gave an overview of kinetic and thermodynamic modelling of the steel-clay interface.

## 6.4 Resume

Albeit there exist a lot of information of steel-concrete interactions under oxic conditions, this stage is short relative to the full time-scale of the life time of a DGR and the low corrosion rates in a high-pH environment (passive corrosion). In a concrete-based geological disposal concept, one focus on the demonstration that localised corrosion phenomena cannot occur in highly alkaline disposal conditions and focus on uniform passive corrosion under aerobic conditions. Temperature has a significant effect on the corrosion rate as it influences many processes and parameters affecting corrosion. The water saturation degree potentially has an effect as well, but not when the steel is in a passive state in concrete. The surrounding pH is an important factor for uniform corrosion as the protective oxide film is believed to remain stable as long as the pH stays higher than a threshold value ( $\sim 9 < \text{pH} < \sim 11.5$ ); low pH values may lead to depassivation of the steel surface and lost of protection. In addition, Cl concentrations leading to detrimental consequences (localized corrosion) is also a function of the pH. Under oxic condition, high Cl concentrations has a significant effect. The collected data shown that that the presence of chloride (up to 20,000 mg L<sup>-1</sup>) has no discernible effect on the long-term corrosion rate of carbon steel in anaerobic high pH media.

Corrosion products, that have a higher molar volume than that of the bare metal, may reduce porosity, leading to clogging and gradually increase the mechanical stress in the concrete leading ultimately potentially to fracture formation. The duration of this process depends on many factors, the cause of depassivation being one of them (pH drop due to carbonation or leaching, or the invasion of aggressive species). Furthermore, there are indications that a Fe-enriched layer will form in the mortar/concrete close to the interface. Fe will interact with the cement minerals and may form Fe-containing cement minerals. The cementitious material may also alter the composition of the corrosion product layer with an enrichment with Ca closer to the interface of the corrosion product layer and the cement/concrete.

Almost now reactive transport models integrating steel and concrete in the context of a DGR are available up to now, i.e. under anoxic-alkaline conditions. However, similar tools as for the other interfaces, particular the steel-clay interface could be used.

## 6.5 References

- Andrade, C., Tavares, F., Toro, L., Fullea, J., 2011. Observation on the morphology of oxide formation due to reinforcement corrosion. In: Andrade, C., Mancini, G. (eds.) Modelling of corroding concrete structures. Proceedings of the Joint fib-RILEM Workshop, Madrid, Spain, 22–23 November 2010, Springer, 179-194.
- Bard, A.J., Faulkner, L.R., 2001. Electrochemical methods: Fundamentals and applications. 2<sup>nd</sup> edition, John Wiley & Sons, 87-107.
- Bataillon, C., Bouchon, F., Chainais-Hillairet, C., Desgranges, C., Hoarau, E., Martin, R., Perrin, S., Tupin, M., and Talandier, J., 2010. Corrosion modelling of iron based alloy in nuclear waste repository. *Electrochimica Acta* 55, 4451-4467.
- Bataillon, C., Bouchon, F., Chainais-Hillairet, C., Fuhrmann, J., Hoarau E., Touzani, R., 2012. Numerical methods for the simulation of a corrosion model with moving oxide boundaries. *Journal of Computational Physics* 231, 6213-6231.
- Bentur, A., Diamond, S., Berke, N.S., 1997. Steel corrosion in concrete: fundamentals and civil engineering practice. E & FN Spon.
- Bertolini, L., Elsener, B., Pedferri, P., Polder, R., 2004. Corrosion of steel in concrete: prevention, diagnosis, repair. Wiley-VCH Verlag.
- Bildstein, O., Claret, F., Frugier, P., 2019. RTM for waste repositories. *Reviews in Mineralogy and Geochemistry* 85, 419-457.

Blackwood, D.J., Gould, L.J., Naish, C.C., Porter, F.M., Rance, A.P., Sharland, S.M., Smart, N.R., Thomas, M.I. Yates, T., 2002. The localized corrosion of carbon steel and stainless steel in simulated repository environments. Report AEAT/ERRA-0318, AEA Technology, Harwell, Didcot, United Kingdom.

Broomfield, J.P., 2007. Corrosion of steel in concrete: Understanding, investigation and repair (2<sup>nd</sup> edition). Taylor & Francis.

Caré, S., Nguyen, Q.T., L'Hostis, V., Berthaud, Y., 2008. Mechanical properties of the rust layer induced by impressed current method in reinforced mortar. *Cement and Concrete Research* 38, 1079-1091.

Chitty, W.J., Dillmann, P., L'Hostis, V., Millard, A., 2008. Long-term corrosion of rebars embedded in aerial and hydraulic binders – Parametric study and first step of modelling. *Corrosion Science* 50, 3047-3055.

Chomat, L., L'Hostis, V., Amblard, E., Bellot-Gurlet, L., 2014. Long term study of passive corrosion of steel rebars in Portland mortar in context of nuclear waste disposal. *Corrosion Engineering, Science and Technology* 49, 467-472.

Chomat, L., Amblard, E., Varlet, J., Blanc, C., Bourbon, X., 2017. Passive corrosion of steel reinforcement in blended cement-based material in the context of nuclear waste disposal. *Corrosion Engineering, Science and Technology* 52, 148-154.

Davis, J.R. (ed.) 2000. Corrosion: Understanding the basics. ASM International, Materials Park, Ohio, USA.

Deng, B., Campbell, T.J., Burris, D.R., 1997. Hydrocarbon formation in metallic iron/water systems. *Environmental Science and Technology* 31; 185-1190.

Deshpande, P.G., Seddelmeyer, J.D., Wheat, H.G., Fowler, D.W., Jirsa, J.O., 2000. Corrosion performance of polymer-coated, metal-clad and other rebars as reinforcement in concrete. Report FHWA/TX-03/4904-2, Texas Department of Transportation (TxDOT), Austin, TX, USA.

Dillmann, P., Neff, D., Féron, D., 2014. Archaeological analogues and corrosion prediction: from past to future. A review. *Corrosion Engineering, Science and Technology* 49, 567-576.

Engelhardt, G.R., Kursten, B., Macdonald, D.D., 2014. Corrosion of carbon steel in physically-constrained locations in HLNW isolation. *ECS Transactions* 58, 35-53.

Fujisawa, R., Cho, T., Sugahara, K., Takizawa, Y., Horikawa, Y., Shiomi, T., Hironaga, M., 1997. The corrosion behaviour of iron and aluminium under waste disposal conditions. *Materials Research Society Symposium Proceedings* 465, 675-682.

Fujisawa, R., Kurashige, T., Inagaki, Y., Senoo, M., 1999. Gas generation behaviour of transuranic waste under disposal conditions. *Materials Research Society Symposium Proceedings* 556, 1199-1206.

Fujiwara, A., Yasutomi, I., Fukudome, K., Tateishi, T., Fujiwara, K., 2001. Influence of oxygen concentration and alkalinity on the hydrogen gas generation by corrosion of carbon steel. *Materials Research Society Symposium Proceedings* 663, 497-505.

Fujiwara, A., 2002. Gas generation by steel corrosion under reductive conditions – Continuous measurement test Presented at the GASNET Workshop, 12-14 November, 2002, Cologne, Germany.

Glasser, F.P., Marchand, J., Samson, E., 2008. Durability of concrete - Degradation phenomena involving detrimental chemical reactions. *Cement and Concrete Research* 38, 226-246.

Goñi, S., Andrade, C., 1990. Synthetic concrete pore solution chemistry and rebar corrosion rate in the presence of chlorides. *Cement and Concrete Research* 20, 525-539.

Grauer, R., 1988. The corrosion behaviour of carbon steel in Portland cement. Nagra Technical Report NTB 88-02E, Nagra, Wetztingen, Switzerland.

Grauer, R., Knecht, B., Kreis, P., Simpson, J.P., 1991. Hydrogen evolution from corrosion of iron and steel in intermediate level waste repositories. Materials Research Society Symposium Proceedings 212, 295-302.

Grauer, R., Knecht, B., Kreis, P., Simpson, J.P., 1991. The long term corrosion rate of passive iron in anaerobic alkaline solutions. Werkstoffe und Korrosion 42, 637-642.

Grubitsch, H., Miklautz, H., Hilbert, F., 1970. Potentiodynamische und potentiostatische Messungen an gespannten Drahtelektroden in gesättigten  $\text{Ca}(\text{OH})_2$ -Lösungen mit verschiedenen Zusätzen. Werkstoffe und Korrosion, 21:485-495.

Grubitsch, H., Binder, L., Hilbert, F., 1979. The influence of various concentrations of chloride ions on the active-passive corrosion susceptibility of steel in saturated calcium hydroxide solution. Werkstoffe und Korrosion 30, 241-245.

Hansson, C.M., 1984. The corrosion rate of mild steel in deaerated synthetic cement pore solution. SKB Technical Report TR 1984-11-14, SKB, Stockholm, Sweden.

Hansson, C.M., 1985. The corrosion of steel and zirconium in anaerobic concrete. Materials Research Society Symposium Proceedings 50,475-482.

Hansson, C.M., 1985. Hydrogen evolution in anaerobic concrete resulting from corrosion of steel reinforcement. Report SKB Teknisk PM Nr. 30, SKB, Stockholm, Sweden.

Hansson, C.M., 1987. The corrosion of steel in anaerobic concrete and the associated evolution of hydrogen. Report SFR-87-02, SKB, Stockholm, Sweden.

Heusler, K.E., Weil, K.G., Bonhoeffer, K.F., 1958. Die Bedeutung des Flade-Potentials für die Passivität des Eisens in alkalischen Lösungen. Zeitschrift für Physikalische Chemie, Neue Folge 15, 149-161.

Höglund L.O., 2014. The impact of concrete degradation on the BMA barrier functions. SKB Report R-13-40, SKB, Stockholm, Sweden.

Honda, A., Kato, T., Tateishi, T., Imakita, T., Masuda, K., Kato, O., Nishimura, T., 2006. Chemical transition of nitrate ions accompanied by corrosion of carbon steel under alkaline conditions. Corrosion Engineering 55, 635-649.

Honda, A., Masuda, K., Imakita, T., Kato, O., Nishimura, T., 2009. Modelling of chemical transition of nitrate accompanied by corrosion of carbon steel under alkaline conditions. Corrosion Engineering 58, 219-234.

Hurley, M.F., Scully, J.R., 2002. Chloride threshold levels in clad 316L and solid 316LN stainless steel rebar. CORROSION2002, Paper no. 02224, 7-11 April, 2002, Denver, CO, USA.

Hussain, S.E., Rasheeduzzafar, 1993. Effect of temperature on pore solution composition in plain cements. Cement and Concrete Research 23, 1357-1368.

Hussain, S.E., Al-Gahtani, A.S., Rasheeduzzafar, 1996. Chloride threshold for corrosion of reinforcement in concrete. ACI Materials Journal 94, 534-538.

Jung, H., Kwon, K. J., Lee, E., Kim, D. G., Kim, G.Y., 2011. Effect of dissolved oxygen on corrosion properties of reinforcing steel. Corrosion Engineering, Science and Technology 46, 195-198.

Kaesche, H., 1965. Untersuchungen über die Korrosion unlegierter Stähle in Kalziumhydroxydlösung und in feuchtem Beton. Archiv für Eisenhüttenwesen 36, 911-922.

Kaneko, M., Miura, N., Fujiwara, A., Yamamoto, M., 2004. Evaluation of gas generation rate by metal corrosion in the reducing environment. Report RWMC TRE 03003, Radioactive Waste Management Funding and Research Center (RWMC), Japan.

Kreis, P., 1991. Hydrogen evolution from corrosion of iron and steel in low/intermediate level waste repositories. Nagra Technical Report NTB 91-21, Nagra, Wetingen, Switzerland.

Kreis, P., Simpson, J.P., 1992. Hydrogen gas generation from the corrosion of iron in cementitious environments. In: Corrosion problems related to nuclear waste disposal, European Federation of Corrosion Publication number 7, Institute of Materials, London, UK, 57-72.

Kreis, P., 1993. Wasserstoffentwicklung durch Korrosion von Eisen und Stahl in anaeroben, alkalischen Medien im Hinblick auf ein SMA-Endlager. Nagra Technical Report NTB 93-27, Nagra, Wettingen, Switzerland.

Kursten, B., Druyts, F., Macdonald, D., Smart, N., Gens, R., Wang, L., Weetjens, E., Govaerts, J., 2011. Review of corrosion studies of metallic barrier in geological disposal conditions with respect to Belgian Supercontainer concept. Corrosion Engineering, Science and Technology, 46, 91-97.

L'Hostis, V., Amblard, E., Blanc, C., Miserque, F., Paris, C., Bellot-Gurlet, L., 2011. Passive corrosion of steel in concrete in context of nuclear waste disposal. In: Lyon, S., Kursten, B. and Druyts, F. (eds.) Proceedings of the Fourth International Workshop on Long-Term Prediction of Corrosion Damage in Nuclear Waste Systems, June 28 – July 2, 2010, Bruges, Belgium, Corrosion Engineering, Science and Technology 46, 177-181.

Lothenbach, B., Kulik, D.A., Matschei, T., Balonis, M., Baquerizo, L., Dilnesa, B., Miron, G.D., Myers, R.J., 2019. Cemdata18: A chemical thermodynamic database for hydrated Portland cements and alkali-activated materials. Cement and Concrete Research 115, 472-506.

Maslehuddin, M., 1994. The influence of Arabian Gulf environment on mechanisms of reinforcement corrosion. Ph.D. Thesis, The University of Aston in Birmingham, United Kingdom.

Maslehuddin, M., Page, C.L., Rasheeduzzafar, Al Mana, A.I., 1996. Effect of temperature on pore solution chemistry and reinforcement corrosion in contaminated concrete. In: Page, C.L., Bamforth, P.B., Figg, J.W. (eds.) Corrosion of reinforcement in concrete construction, RSC Special Publications 183, 67-75.

Matsuda, F., Wada, R., Fujiwara, K., Fujiwara, A., 1995. An evaluation of hydrogen evolution from corrosion of carbon steel in low/intermediate level waste repositories. Materials Research Society Symposium Proceedings 353, 719-726.

McCafferty, E., 2010. Introduction to Corrosion Science. Springer.

Macdonald, D.D., 2008. On the tenuous nature of passivity and its role in the isolation of HLNW. Journal of Nuclear Materials 379, 24-32.

Macdonald, D.D., 2011. The history of the point defect model for the passive state, A brief review of film growth aspects. Electrochimica Acta 56, 1761-1772.

Michel, A., Nygaard, P.V., Geiker, M.R., 2013. Experimental investigation on the short term impact of temperature and moisture on reinforcement corrosion. Corrosion Science 72, 26-34.

Mihara, M., Nishimura, T., Wada, R., Honda, A., 2002. Estimation on gas generation and corrosion rates of carbon steel, stainless steel and zircaloy in alkaline solutions under low oxygen condition. JNC Technical Review 15, 91-101 (in Japanese).

Naish, C.C., 1993. Corrosion aspects of the proposed Sellafield waste repository. UK Corrosion '93.

Naish, C.C., Blackwood, D.J., Taylor, K.J., Thomas, M.I., 1995. The anaerobic corrosion of stainless steels in simulated repository backfill environments. Report NSS/R307, AEA Technology, Harwell, Didcot, United Kingdom.

Naish, C.C., Blackwood, D.J., Thomas, M.I., Rance, A.P., 2001. The anaerobic corrosion of carbon steel and stainless steel. Report AEAT/R/ENV/0224, AEA Technology, Harwell, Didcot, United Kingdom.

Neeft, E., Weetjens, E., Vokal, A., Leivo, M., Cochapin, B., Martin, C., Munier, I., Deissmann, G., Montoya, V., Poskas, P., Grigaliuniene, D., Narkuniene, A., Garcia, E., Samper, J., Montenegro, L. and

Mon, A., 2020. Treatment of chemical evolution in National Programmes, D 2.4 of the HORIZON 2020 project EURAD. EC Grant agreement no: 847593

Newman, R.C., Wang, S., 2013. Understanding and quantifying the corrosion of carbon steel in grouts relevant to the Swiss L/ILW repository – Status reports 2011 and 2012. Nagra Technical Report NTB 13-08, Nagra, Wettingen, Switzerland.

Newman, R.C., Wang, S., Johnson, L., Diomidis, N., Carbon steel corrosion and hydrogen generation in cementitious grouts. In: Shaw, R.P. (ed.) Gas generation and migration, International FORGE Symposium and Workshop Proceedings, 5-7 February 2013, Luxembourg, FORGE report D0.09, Nuclear Energy Agency (NEA), France, 70-73.

Newman, R.C., Wang, S., Senior, N., 2016. Understanding and quantifying the corrosion of carbon steel in grouts relevant to the Swiss L/ILW repository. Nagra Report NAB 15-17 Rev.1, Nagra, Wettingen, Switzerland.

Nishimura, T., Wada, R., Fujiwara, K., 2003. Evaluation of gas generation rates caused by metal corrosion under the geological repository conditions. R&D Kobe Steel Engineering Reports 53, 78-83 (in Japanese).

Perko, J., Jacques, D., Seetharam, S.C., Mallants, D., 2010. Long-term evolution of the near surface disposal facility at Dessel. ONDRAF/NIRAS, NIROND-TR 2010-04 E.

Perko, J., Mayer, K.U., Kosakowski, G., De Windt, L., Govaerts, J., Jacques, D., Su, D., Meeussen, J.C.L., 2015. Decalcification of cracked cement structures. Computational Geosciences 19, 673-693.

Posey, F.A., Palko, A.A., Bacarella, A.L., 1978. Corrosivity of geothermal brines – Progress report for period ending September 1977 (Final report). Report ORNL/TM-6308, Oak Ridge National Laboratory (ORNL), Oak Ridge, TN, USA.

Posey, F.A., Palko, A.A., 1979. Corrosivity of carbon steel in concentrated chloride solution. Corrosion 35, 38-43.

Pour Ghaz, M., 2007. A novel approach for practical modelling of steel corrosion in concrete. Ph.D. Thesis, Carleton University, Ottawa, Ontario, Canada.

RWMC, 1998. Verification test on advanced radioactive waste disposal systems, volume 1 and 2. 1998 report, Radioactive Waste Management Funding and Research Center (RWMC), Japan.

Saheb, M., 2009. Les analogues archéologiques ferreux pour la compréhension des mécanismes de corrosion multiséculaire en milieu anoxique. Matériaux. Université Paris-Est, Paris, France.

Saheb, M., Descostes, M., Neff, D., Matthiesen, H., Michelin, A., Dillmann, P., 2010. Iron corrosion in an anoxic soil: comparison between thermodynamic modelling and ferrous archaeological artefacts characterised along with the local in situ geochemical conditions. Applied Geochemistry 25, 1937-1948.

Saheb, M., Gallien, J.-P., Descostes, M., Raimbault, L., Perez, A., Neff, D., Marsal, F., Pellegrini, D., Dillmann, P., 2014. Influence of an aerated/anoxic transient phase on the long-term corrosion of iron. Corrosion Science 86, 71-80.

Shoesmith, D.W., 1996. Kinetics of aqueous corrosion. In: Davis, J.R., Destefani, J.D., Frissell, H.J., Crankovic, G.M. and Jenkins, D.M. (eds.) ASM Handbook, Volume 13: Corrosion, American Society for Metals (ASM) International, 29-36.

Senior, N., 2017. Anoxic corrosion of steel in a Swiss L/ILW repository environment. Nagra Report NAB 17-19, Nagra, Wettingen, Switzerland.

Senior, N., Newman, R., Wang, S., Diomidis, N., 2017. Understanding and quantifying the anoxic corrosion of carbon steel in a Swiss L/ILW repository environment. 6th International Workshop on Long-term Prediction of Corrosion Damage in Nuclear Waste Systems, 9 - 12 May, 2016, Toronto, Canada, Corrosion Engineering, Science and Technology 52(S1), 78-83.

Smart, N.R., Blackwood, D.J., Marsh, G.P., Naish, C.C., O'Brien, T.M., Rance, A.P., Thomas, M.I., 2004. The anaerobic corrosion of carbon and stainless steels in simulated cementitious repository environments: a summary review of Nirex research. Report AEAT/ERRA-0313, AEA Technology, Harwell, Didcot, United Kingdom.

Smart, N.R., 2008. The corrosion behaviour of carbon steel radioactive waste packages: A summary review of Swedish and U.K. research. CORROSION/2008, paper no. P3013, 16 20 March, 2008, New Orleans, LA, USA.

Smart, N.R., 2009. The corrosion behaviour of carbon steel radioactive waste packages: A summary review of Swedish and U.K. research. Corrosion 65, 195-212.

Smart, N.R., Rance, A.P., Fennell, P.A.H., Reddy, B., Padovani, C., 2019. Experimental studies of radiation induced corrosion in support of the Belgian Supercontainer concept. Wood Reference 207022/01, Issue 1.

Tuutti, K., 1982. Corrosion of steel in concrete. Report no. 4 82, Swedish Cement and Concrete Research Institute, Stockholm, Sweden.

Vu, N.T., 2011. Contribution à l'étude de la corrosion par carbonation du béton armé: Approche expérimentale et probabiliste. Ph.D. Thesis, Université de Toulouse, Toulouse, France.

Zhang, J.Y., Qian, S.Y., Baldock, B., 2009. Laboratory study of corrosion performance of different reinforcing steels for use in concrete structures. Report IRC RR 284, National Research Council Canada (NRCC), Ottawa, Ontario, Canada.

Živica, V., 2002. Significance and influence of the ambient temperature as a rate factor of steel reinforcement corrosion. Bulletin Material Science 25, 375-379.

*References summarizing experimental data on corrosion rates*

Kursten, B. 2019. Uniform corrosion evaluation of C-steel in cementitious environments relevant to the supercontainer design – Summary of corrosion rates from available literature and O/N funded RD&D programmes, report SCK·CEN-ER-094, SCK·CEN, Mol, Belgium.

Smart, N.R., Hoch, A.R. 2006. A survey of steel and Zircaloy corrosion data for use in the SMOGG gas generation model, report SA/ENV-0841, issue 1, Serco Assurance, Harwell, Didcot, United Kingdom.

Swanton, S.W., Baston, G.M.N., Smart, N.R. 2015. Rates of steel corrosion and carbon-14 release from irradiated steels – state-of-the-art review (D2.1), report CAST-2015-D2.1, AMEC, Harwell, Didcot, United Kingdom.



## 7. Interface "steel/iron – granite"

Mervi Somervuori, Leena Carpen (VTT)

### 7.1 Processes at the interface

In repository conditions, the interface steel-granite does not really exist, because steel and granite are not in direct contact with each other in any of the repository designs. There is always concrete or bentonite between the steel container and the bedrock to prevent flowing of water and therefore contact between steel and granite is via granitic water. For example, in Finland at the Olkiluoto site, a part of the low and medium level waste is packed into steel containers that are buried into concrete layered bedrock silos located 60-100 m under the sea level. The steel containers are usually made of carbon steel but the waste contains both carbon steel and stainless steels.

The granitic bedrock forms a natural barrier that limits and delays the migration of the radionuclides to the environment. However, also other barriers like concrete or bentonite are needed because the bedrock contains crevices filled with water and without any filling material the repository containers are directly exposed to the groundwater which may be very corrosive to the steel. Concrete liner generates an alkaline environment, which is assumed to diminish the corrosion rate of metallic waste and containers (see chapter 6). Nevertheless, over time the pH of the water starts to decrease, for example due to the carbonization of concrete, which may affect the corrosion rate of the steel containers. In addition to that, also microbial processes can decrease the local pH as soon as four years after storage started (Small et al., 2008).

In anoxic conditions, corrosion rate of carbon steel is very low unless the groundwater is highly acidic or microbial activity is high. High acidity or microbial activity enable corrosion initiation by altering local conditions to direction where corrosion can initiate (Rajala, 2017). Microbes and their metabolism can affect the corrosion of steel and therefore it is important to consider also microbially-induced corrosion (MIC) when evaluating long-term safety of disposal of radioactive waste in deep bedrock.

This chapter considers only the interaction of steel with bedrock groundwater in a geological repository because granite is not affected by presence or corrosion of steel. However, geological investigations have to be done before a repository of high-level waste is constructed because the high temperature can cause cracking in bedrock and therefore enhance migration of the nuclides after the steel canister is leaking.

### 7.2 Evidence from experiments and analogues

The interaction of steel with real groundwater has been studied at VTT in several projects financed by Finnish Research Programme on Nuclear Waste Management (KYT). Studies have also been made in cooperation with Finnish Nuclear Power Companies.

Corrosion of carbon steel and two type of stainless steels in real groundwater and biocide treated groundwater has been studied in the project "Risks of microbiologically influenced corrosion in the Finnish nuclear waste repository" (KYT-REMIC 2011-2014). The study contained experiments both in laboratory and at the repository site. Part of the studies were performed in the alkaline environment produced by concrete and part was performed in environment simulating the possible nutrients flow released from degradation of organic waste or from methane rich groundwater flow.

The studies on the same subject continued in the project "Microbially induced corrosion of low and intermediate level radioactive waste" (KYT-CORLINE 2015-2018), where real groundwater with different microbial enrichments or sterile ground water was used. An *in situ* corrosion monitoring system was developed to monitor real-time corrosion rates of steels in the drill holes of the repository. Field trials were performed in the Olkiluoto VLJ cave drill holes during a two-year experiment. The measuring equipment was installed in the spring of 2016 and included a corrosion measurement unit (electrochemical and weight loss samples) and an OsmoSampler water sampler collecting 5-14 ml of water sample per month (Carpén et al., 2018). Also a large-scale *in situ* gas generation experiment

(GGE) started in 1997 is still going on to simulate the gas generation from LLW under geological repository conditions (Small et al., 2008, 2017).

The effect of activation of the steel on the corrosion rate and the corrosion risk of pressure vessel steels and other steels as well as decommissioning metal waste in different repository conditions in Finland will be evaluated in the project “Corrosion of low and intermediate level steel waste under *in situ* repository condition” (KYT-TERKOR 2019-2022). Long-term electrochemical and gravimetric measurements will be made for different steels in both biotic and abiotic environments. Short-term tests will be used to evaluate corrosion properties of different groundwater on the point of view of the steels on investigation.

In groundwater, corrosion of steel is affected by pH, temperature, oxygen content (redox), composition of water, radiation and microbes. The importance of each factor and some research results are considered in this chapter

### *pH*

The pH conditions in bedrock groundwater are heterogeneous. In natural state, the pH is close to neutral (about 8). Presence of concrete is found to rise the pH of the water and decrease corrosion rate of carbon steel at first but in time the pH will decrease because of carbonation of concrete. Another effect of aging of concrete is that chlorides can penetrate inside to concrete and thus come in contact with metallic waste or metallic containers. However, to consider repository time of hundreds of thousands of years, the effect of concrete is only temporary. VTT has performed corrosion experiments in groundwater with and without concrete. The presence of concrete diminishes corrosion rate of carbon steel. However, in the presence of concrete the localized corrosion is possible (Carpén et al., 2012a, 2013a, 2014a, 2015a).

### *Temperature*

Temperature is an important factor in corrosion of steel because a higher temperature usually means accelerated corrosion reactions. In the bedrock, the temperature depends on the depth from the surface and therefore the temperature has to be investigated locally. The temperature at the repository level in Finnish bedrock is from 6 to 10 °C and therefore most of VTT’s experiments in groundwater have been performed at temperature 10 to 12 °C.

The effect of temperature on corrosion of carbon steel in natural granitic groundwater has been studied at VTT at temperatures +6 °C and +22 °C. The results showed that the temperature has an effect on corrosion layers of carbon steel, the species composition and the number of microbes even in short-term experiments. The effect of temperature on corrosion rate was not clear in the experiment since a part of the samples did not stay in anoxic state (Carpén et al., 2012a, 2013a, 2014a, 2015a). Disposal of HLW in the bedrock rises the temperature of the bedrock for several decades and has to be taken into account when planning repositories.

Ahn and Soo (1995) studied the corrosion of steel in concentrated synthetic groundwater at 80 to 150 °C. In the aerated conditions under gamma-radiation, the uniform corrosion rates measured for four months were from 10 to 40  $\mu\text{m yr}^{-1}$ . Smart et al. (2001) found a large increase in the initial corrosion rates by increasing temperature when they studied corrosion of carbon steel in anaerobic artificial Swedish granite groundwater at temperatures of 30 °C, 50 °C and 85 °C. The initial corrosion rates were at the level of 10 to 30  $\mu\text{m yr}^{-1}$  but after the oxide film had formed, the corrosion rates were  $< 0.1 \mu\text{m yr}^{-1}$ . The initial corrosion rates increasing with increasing temperature indicates the corrosion process to be controlled by activation i.e. anodic reactions. However, when an oxide film forms on the surface, diffusion of various species through the film becomes more determinative and the process becomes less sensitive to temperature.

### *Oxygen content (redox)*

The redox environment is very important in corrosion because many corrosion reactions need oxygen. In oxygen containing water environments the corrosion rates of iron and carbon steel are typically from

0.05 to 0.15 mm yr<sup>-1</sup> (Tunturi, 1988). In oxygen free (anoxic) water, the corrosion of carbon steel is very low unless the water is acidic or there is microbiological activity on the surfaces.

The groundwater in Finnish bedrock is anoxic at the repository level and therefore most of the studies made at VTT are performed in anoxic environments. In the anoxic abiotic environment (bioside treated or sterilized) the average corrosion rate of carbon steel was between 1.1 µm yr<sup>-1</sup> and 0.4 µm yr<sup>-1</sup>, which was higher than the recorded values for corrosion rates of the stainless steels. The stainless steels did not suffer any weight loss during the test. According to electrochemical measurements, both steel types were prone to localized corrosion, especially in the sulphate reducing bacteria (SRB) containing environment (Carpén et al., 2016, 2017, 2018).

The results of *in situ* corrosion monitoring of stainless steels types EN 1.4301 and EN 1.4404 in bedrock groundwater for two years showed that the conditions in the drill holes are reducing and the calculated corrosion rates are low for most of the exposure time. However, the steel type EN 1.4404 had slightly higher corrosion rates than the steel type EN 1.4301 and some signs of pitting were seen after the exposure, which indicates a possible role of microbial activity in corrosion (Carpén et al., 2018). In anaerobic conditions, formation of magnetite film on carbon steel retards the rate of corrosion in artificial groundwater (Smart et al., 2001).

#### Composition of the groundwater

Groundwater has been in bedrock for thousands of years, and it contains salts and other components dissolved from the bedrock. From corrosion point of view, the amounts of chlorides and sulphates are of most interest because they are known to cause corrosion of steel. The chloride content of groundwater can be even at the level of the salinity of brackish water. The results of groundwater analyses from the repository places show that the composition of the groundwater can vary locally at the same area and as well as over the time. As an example, the variation of water analyses results of some drill holes at Olkiluoto repository site are presented in Table 7-1.

Table 7-1 – Analyses of water from drill holes in the TVO repository area (Carpén et al., 2012b).

Drill hole	pH	Cl mg/l	SO <sub>4</sub> mg/l	HCO <sub>3</sub> mg/l	Ca mg/l	Conductivity mS/cm
A	8.0 - 8.1	439 - 570	116 - 140	277 - 319	50 - 119	2.1 - 2.6
B	7.9 - 8.0	1110 - 1470	191 - 230	218 - 276	145 - 348	4.2 - 5.3
C	7.9 - 8.0	533 - 636	127 - 140	278 - 308	64 - 140	2.4 - 2.8

In previous projects, groundwater from Olkiluoto repository area has been used but in the ongoing project KYT-TERKOR the long-term corrosion experiments will be performed in groundwater from the Loviisa repository area. Some short-term electrochemical measurements have been performed to evaluate corrosion properties of groundwater from different repository sites.

#### Radiation

The effect of radiation on corrosion of steel is not clear and there are wide variations in results. Ahn and Soo (1995) found that in synthetic water the effects of gamma irradiation on uniform corrosion of low-carbon steel were not discernible in four months. Some pitting was found but the pitting factor was small. However, under irradiation conditions hydrogen generation was found to be greater than in conditions without irradiation and large amounts of hydrogen were absorbed in the steel during corrosion under irradiation. Although the general corrosion rates of 10 to 40 µm yr<sup>-1</sup> appear to be low enough to maintain the integrity of the carbon steel containers for an extended period, there is a possibility of early failure of the canister due to environmental-assisted cracking.

Liu et al. (2017) studied carbon steel as a canister material for high-level waste. The samples were exposed to bentonite containing 17 % groundwater and were aged. In their tests, gamma radiation

accelerated the corrosion of carbon steel by 33 %. At VTT is an ongoing project KYT-TERKOR, where the effect of radiation, i.e. activation of the steel, on corrosion of steel in natural bedrock groundwater of Loviisa repository area is studied by weight loss measurements and surface analysis methods. The long-term parallel corrosion tests for non-activated and activated samples to measure corrosion rates and to evaluate the effect of microbiological behaviour on corrosion of a pressure vessel steel are going to be finished in summer 2020. The tests will give information on the effect of activity of the steel on the corrosion rate.

### *Microbes*

Corrosion of carbon steel in anoxic groundwater is strongly affected by microbial biofilms and their metabolic activity. Corrosion induced by microorganisms is mainly localized corrosion (Rajala, 2017). The effect of microbes on corrosion of steel in groundwater has been studied in several investigations at VTT and even a Doctoral Thesis has been made on the subject (Rajala, 2017). Formation of biofilms and the risks of microbiologically influenced corrosion (MIC) to the metallic decommissioning waste material in Finnish disposal environment has been evaluated through experiments in the laboratory and on the site. Several corrosion measurement methods have been used together with microbiological and material characterization techniques to study the properties of corrosion products, biofilms and microbe-metal interactions in bedrock groundwater from the repository area. Laboratory and *in situ* experiments, gravimetric and electrochemical methods, were performed for durations from 3 months to 15 years (Carpén et al., 2012b).

Microbiological activity on the surfaces accelerates the corrosion rate of steel in oxygen free water. At the Olkiluoto site the corrosion behaviour of carbon steel in groundwater simulating repository conditions has been studied continuously since 1998. Carbon steel specimens are situated in oxygen free groundwater in bedrocks of Olkiluoto Island. The test site is in the underground tunnel of operational waste repository of the power plant that is in operation. The specimens immersed in 1998 are placed together in the same drill hole as concrete specimens. In 2007, new specimens were immersed in another drill hole in the bedrock at the same site without concrete specimens. After 33 months and 136 months the immersed carbon steel specimens from both drill holes were investigated. In these cases, increased corrosion rates of carbon steel have been detected (Carpén et al., 2012b).

A testing environment where corrosion of decommissioning metal waste can be investigated reliably in natural bedrock groundwater environment was created in the project KYT-CORLINE. A large laboratory test set-up was built and simultaneously an *in situ* test with a novel field measurement system together with a water sampler collector (OsmoSampler) was set up in the final repository cave. Several corrosion measurement methods were used together with microbiological and material characterization techniques to study the properties of biofilms, corrosion products and microbe-metal interactions.

In laboratory tests, adding nutrients to the water changed the composition of the microbial community and accelerated corrosion of carbon steel in electrochemical measurements. Adding microbial enrichments (SRB, metanogens, acetogens) accelerated the corrosion of steels in all tests. In the abiotic environment, the corrosion rates of the studied steels were relatively small. The highest weight losses indicating highest average corrosion rates ( $19.2 \mu\text{m yr}^{-1}$  as an average of three samples varying from  $6.4 \mu\text{m yr}^{-1}$  to  $33.2 \mu\text{m yr}^{-1}$ ) were recorded for carbon steels in the acetogen enriched environment. The electrochemical measurements agreed with this finding, since also the highest momentary corrosion rates were recorded in the same environment. Even though having a smaller general corrosion rate (average  $10 \mu\text{m yr}^{-1}$ ) by weight loss measurements, the natural groundwater enriched with SRB together with acetogens caused localized corrosion which could be also detected by electrochemical measurements (multi array sensors). These results were confirmed by visual observations after the exposure.

The deep groundwater microorganisms benefit from carbon steel. In the presence of carbon steel the microbial community in anaerobic groundwater was found to be more diverse and abundant than in the same environment without carbon steel (Rajala et al., 2015). Černoušek et al. (2019) found that in natural granitic water in anaerobic conditions at laboratory temperature, the corrosion rate of carbon

steel was accelerated due to biofilm formation. However, the formation of biofilm inhibited the corrosion rate at 35 °C. The microbial community of the environment was dominated by sulphate-reducing bacteria.

*Gas generation*

A large-scale *in situ* Gas Generation Experiment (GGE) was started in 1997 to simulate the gas generation under final repository conditions. A significant observation from the GGE was that the pH conditions were heterogeneous (pH 11 to 6), providing optimal neutral pH niches for microbiological activity from the outset of the experiment. The results demonstrate that LLW is converted to methane and carbon dioxide by a succession of anaerobic processes within a complex microbial consortium. In addition, microbial groups with potential to metabolize formed saccharides to acetate, hydrogen and volatile fatty acids were detected. Hydrogenotrophic methanogens dominated after one year of operation, which was related to the utilization of hydrogen generated by anaerobic corrosion of steel and metallic waste. Sulphate reducers were the most significant microbial group competing with methanogens for electron donors and their relative ratio compared to methanogens decreased considerably during the operation of the GGE (Vikman et al., 2019; Small et al., 2017).

*Field experiments on corrosion of low and intermediate level decommissioning metal wastes*

A long-term field exposure experiment was started in the bedrock in 1998 in one drill hole and 2007 in another drill hole to measure quantitatively the corrosion rate of carbon steel in the environment that simulates the final repository conditions. The analysis of the waters is presented above in Table 7-1. The corrosion rates calculated from the weight loss measurements varied from 7 to 63 µm yr<sup>-1</sup> after three years exposure and from 10.1 to 12.4 µm yr<sup>-1</sup> after 11 years of exposure. Since corrosion proceeded not uniformly these corrosion rates do not very well represent the actual situation. The localized corrosion rates were much higher and at the end in some areas of the 11 years specimens, the whole wall thickness was lost. Large differences in corrosion rates were found not only in the specimens immersed in different drill holes but also between parallel specimens in the same drill hole. The results indicate that the conditions in different drill holes in the same bedrock as well as on the metal surfaces may differ a lot from each other. All carbon steel coupons were covered with black deposits that consisted mainly of iron and oxygen and sulphur (10 wt%) but contained also small amounts of silicon, aluminium, sodium and magnesium. The large variations in the measured corrosion rates are believed to be cause of variations in the microbiology and chemistry of the water (Carpén et al., 2012b).

When test specimens from the same drill holes were examined again after 15 and 6 years, the specimens were covered by black or brownish deposits. The analysis of the black deposit was, on the average, 53 wt% iron, 21 wt% oxygen, and 20 wt% sulphur, and also small amounts of calcium, carbon, magnesium, silicon, aluminium and sodium were detected in EDS analysis. In the brown deposits the main components were 50 wt% of iron and 40 wt% oxygen. The chemical composition of the water is given in Table 7-2 (Rajala et al., 2019).

The corrosion rates determined from the weight loss were up to 29 µm yr<sup>-1</sup>. The specimen in drill hole B was partly vanished. The high corrosion rates can be explained only by microbes producing corrosive products or affecting the local microenvironments to favour corrosion. Sulphate reducing bacteria and methanogenic archaea were found enriched on the surfaces of the specimens although they were found to be in minority in the groundwater (Rajala et al., 2019).

*Table 7-2 – Water composition in the long-term exposure experiments (Rajala et al., 2019).*

Drill hole	pH	Cl mg/l	SO <sub>4</sub> mg/l	HCO <sub>3</sub> mg/l	Ca mg/l	Conductivity mS/cm	Alkalinity mmol/l-	O <sub>2</sub> ppb
A	7.9	530	128	311	71	2.37	5.07	<10
B	7.90	1830	250	214	250	6.18	4.59	<10

### 7.3 Application of conceptual and mathematical models

The redox conditions in a LLW and ILW repository have been modelled by Duro et al. (2014) They found that the system will be kept under reducing conditions for a long time because of corrosion of steel-based materials. The simulations have been done both in presence and absence of microbial activity. As mentioned in the previous section, Small et al. (2017) and Vikman et al. (2019) have modelled the conditions for corrosion although the corrosion reactions have not been modeled.

### 7.4 Resume

Corrosion of steel/iron in contact with granitic water is affected by many factors including pH, redox and composition of water. High pH tends to decrease corrosion rates of steel whereas high chloride and sulphide contents in groundwater induce localized corrosion. The presence of concrete in groundwater alters the corrosion behaviour of carbon steel because it changes the environment and hinders biofilm formation, but in certain cases can induce localized corrosion. The role of microbes on corrosion of steel in anaerobic conditions is important and has to be taken into account in bedrock environments. The effect of radiation on corrosion of steel is not known yet. The effect of steel corrosion to granite is negligible and can be ignored.

The data of all the VTT references mentioned here is available for the project. The articles and presentations are written in English, but the KYT projects VTT Research Reports are written in Finnish.

### 7.5 References

Ahn, T.M., Soo, P., 1995. Corrosion of low-carbon cast steel in concentrated synthetic groundwater at 80 to 150 °C. *Waste Management* 15, 471-476.

Carpén, L., Vepsäläinen, M., Rajala, P., Bomberg, M., Itävaara, M., 2012a. Mikrobiologisen korroosion riskit Suomen loppusijoitusolosuhteissa (REMIC) – Vuosiraportti 2011. Tutkimusraportti: VTT-R-00473-12. VTT, Espoo, Finland.

Carpén, L., Maukonen, J., Salo, S., 2012b. Accelerated corrosion of carbon steel and zinc in oxygen-free groundwater - due to the microbiological activity? NACE-2012-1397. CORROSION 2012, 11-15 March, Salt Lake City, UT, United States.

Carpén, L., Vepsäläinen, M., Rajala, P., Bomberg, M., 2013a. Mikrobiologisen korroosion riskit Suomen loppusijoitusolosuhteissa (REMIC) – Vuosiraportti 2012. VTT Tutkimusraportti: VTT-R-01485-13. VTT, Espoo, Finland.

Carpén, L., Rajala, P., Bomberg, M., 2014a. Mikrobiologisen korroosion riskit Suomen loppusijoitusolosuhteissa (REMIC) – Vuosiraportti 2013. Tutkimusraportti: VTT-R-01000-14. VTT, Espoo, Finland.

Carpén, L., Rajala, P., Bomberg, M., 2015a. Mikrobiologisen korroosion riskit Suomen loppusijoitusolosuhteissa (REMIC) – Loppuraportti 2011-2014. Tutkimusraportti: VTT-R-00739-15. VTT, Espoo, Finland.

Carpén, L., Rajala, P., Bomberg, M., Huttunen-Saarivirta, E., 2016. Matala- ja keskiaktiivisen jätteen mikrobiologinen korroosio (CORLINE) – Vuosiraportti 2015. Tutkimusraportti: VTT-R-00868-16. VTT, Espoo, Finland.

Carpén, L., Rajala, P., Bomberg, M., Huttunen-Saarivirta, E., 2017. Matala- ja keskiaktiivisen jätteen mikrobiologinen korroosio (CORLINE) – Vuosiraportti 2016. Tutkimusraportti: VTT-R-01118-17. VTT, Espoo, Finland.

Carpén, L., Rajala, P., Bomberg, M., Huttunen-Saarivirta, E., 2018a. Matala- ja keskiaktiivisen jätteen mikrobiologinen korroosio (CORLINE) – Vuosiraportti 2017. Tutkimusraportti: VTT-R-01739-18. VTT, Espoo, Finland.

Carpén, L., Rajala, P., Kinnunen, T., 2018b. Real-time corrosion monitoring system under in situ conditions of crystalline groundwater. 114552. European Corrosion Congress, EUROCORR 2018, Krakow, Poland.

Černoušek, T., Kokinda, J., Vizelková, K., Shrestha, Ševců, A., 2019. Anaerobic microbial corrosion of canister material. MIND-Deliverable 2.13 ([www.mind15.eu](http://www.mind15.eu)).

Duro, L, Domènech, C., Grivé, M., Roman-Ross, G., Bruno, J., Källström, K.. 2014. Assessment of the evaluation of the redox conditions in a low and intermediate level nuclear waste repository (SFR1, Sweden). *Applied Geochemistry* 46, 192-205.

Liu, C., Wang, J., Zhang, Z., Han, E-H., 2017. Studies on corrosion behavior of low carbon steel canister with and without  $\gamma$ -irradiation in China's HLW disposal repository. *Corrosion Engineering, Science and Technology* 52, 136-140.

Rajala, P., Carpén, L., Vepsäläinen, M., Raulio, M., Sohlberg, E. & Bomberg, M., 2015. Microbially induced corrosion of carbon steel in deep groundwater environment. *Frontiers in Microbiology* 6, 647.

Rajala, P., 2017. Microbially-induced corrosion of carbon steel in a geological repository environment. VTT Science 155; PhD Thesis. ISBN 978-951-38-8545-8.

Small, J., Nykyri, M., Hovi, U., Sarlin, T., Itävaara, M., 2008. Experimental and modelling investigations of the biochemistry of gas production from low and intermediate level radioactive waste. *Applied Geochemistry* 23, 1383-1418.

Small, J.S., Nykyri, M, Vikman, M., Heikinheimo, L., 2017. The biogeochemistry of gas generation from low and intermediate level nuclear waste: modelling after 18 years study under in situ conditions, *Applied Geochemistry* 85, 360-373.

Smart, N.R., Blackwood, D. J., Werme, L., 2001. The anaerobic corrosion of carbon steel and cast iron in artificial groundwaters. SKB Technical Report TR-01-22, SKB, Stockholm, Sweden.

Tunturi, P.J., 1988. Korroosiokäsikirja, Suomen korroosioyhdistys, Hangon kirjapaino. ISBN 951.99916-7-0.

Vikman, M., Marjamaa, K., Nykyri, M., Small, J.S., Miettinen, H., Heikinheimo, L., Haavisto, T., Itävaara, M., 2019. The biogeochemistry of gas generation from low-level nuclear waste: Microbiological characterization during 18 years study under in situ conditions. *Applied Geochemistry* 105, 55-67.



## 8. Concluding remarks

This deliverable describes the existing knowledge on relevant processes and transients occurring at the interfaces between various near field materials relevant for the chemical evolution ILW and HLW disposal cells in European repository concepts. Based on an extensive literature review, a structured overview on i) existing experimental data on relevant processes occurring at the interfaces, ii) information on natural/archaeological/industrial analogues that provide insight/data for long-term processes relevant to the chemical evolution at the interfaces not accessible in short-term (laboratory) experiments, and iii) conceptual and mathematical models used to describe the processes occurring at the different interfaces is provided. The information compiled in this deliverable can be used as basis for conceptualisation of the chemical evolution at these interfaces in the ACED tasks 2 to 4 and will be employed to support model validation and parametrisation of models.

It can be seen that, so far, the attention received by the different interfaces addressed here, namely, glass-steel, cement/mortar-granite, cement/concrete-clay, steel/iron-bentonite, steel/iron-cement/concrete and steel/iron-granite is rather diverse. For example, while a relatively large number of experimental studies from the laboratory to the field scale (URL scale), natural analogue studies and (reactive transport) modelling studies can be found that address the interface between cementitious materials and clay/clay rocks or the interface between iron/steel and clay materials/bentonite, distinctively less studies are devoted to interfaces with granitic rocks. The interface between (waste) glasses and steel has been investigated in a number of experimental studies. Phenomenological models describing glass dissolution and specific models that address the influence of steel corrosion on glass dissolution accounting for silica sorption or precipitation of iron silicates have been developed; however, coupling of these specific models to reactive transport models has so far been rarely performed.